UNIVERSITY OF
BIRMINGHAM

EXPERIMENTAL INVESTIGATION OF CAST IRON CORROSION ON CLAY SOIL AND GPR PERFORMANCE

by

TARA MOGHAREH ABED

A thesis submitted to
The University of Birmingham
For the degree of
DOCTOR OF PHILOSOPHY

School of Civil Engineering
Collage of Engineering and Physical Sciences
The University of Birmingham
August 2014

ABSTRACT

Cast iron water distribution pipes exist widely in UK and elsewhere. As these cast iron pipes were traditionally directly buried into local soil, where the soil is chemically aggressive (as in the case of some clays) corrosion of the pipes often occurs due to an electrochemical process, which both changes the pH environment and releases iron ions into the clay. This can cause chemical alteration to clay minerals and 'corrosion products', such as iron oxide, hydroxide and aqueous salts, to form in the soil. These chemical interactions are complex and time dependent, and can result in failure, and thus the conditions under which they occur need to be understood. Ground Penetration Radar (GPR) has been proposed for routinely detecting, assessing and monitoring buried cast iron pipes, and thus it is important to know how these chemical changes affect the electromagnetic properties of soil.

A bespoke set of laboratory experiments was devised to simulate and accelerate (using electrokinetics) cast iron corrosion and ion migration processes in two types of clay: a relatively inactive Kaolin Clay and Oxford Clay, which has a mixed mineralogy. Tests were conducted for periods of up to 3 months using both inert electrodes and with a cast iron disc as the anode, and changes in the geotechnical (undrained shear strength, moisture content and Atterberg limits), geophysical (permittivity) and geochemical (iron content, pH and conductivity) properties were monitored. The conductivity and permittivity results were used in GPR simulations to investigate reported difficulties in detecting corroded cast iron pipes.

The control tests using inert electrodes demonstrated the expected behaviour of the development of a pH gradient across the consolidated clay samples, increased conductivity at the anode and cathode, and concomitant changes in Atterberg limits and undrained shear strength. The introduction of a cast iron anode caused large iron ion concentrations to be generated (via anode degradation) and migrate towards the cathode, more intense pH gradients,

a greater tendency for clay mineral dissolution (for Kaolin Clay near the cathode, and for Oxford Clay at both electrodes), far higher conductivities (especially near the electrodes, but with time in the body of the Oxford Clay also) and progressive increases in undrained shear strength. The highest strengths at 3 months for the Kaolin Clay occurred in the upper half of the sample adjacent to the anode, while this was both replicated in the Oxford Clay and accompanied by an even stronger zone in the lower half of the sample nearest the cathode. The strength gain in the Kaolin Clay was attributed to the combined effects of cation exchange and precipitation, whereas the additional strength gain in the Oxford Clay was attributed to clay mineral dissolution at high pH near the cathode and the formation of CAH, CSH and/or CASH amorphous gels that crystallised to create clay cementation. Normalisation of the undrained shear strengths with water contents emphasised the effects of these chemically-induced changes, while the physical appearance of the cast iron anodes at 3 months emphasised the far greater aggressiveness of the Oxford Clay.

The GPR simulations demonstrated that the chemically-induced changes to Kaolin Clay did not materially affect the performance of GPR in detecting corroded cast iron pipes, whereas in Oxford Clay the (greatly accelerated) chemically-induced changes were sufficiently advanced after approximately 7-8 weeks to cause GPR to be unable to detect the corroded pipes.

DEDICATION

To my parents- Mohammad Hossein Moghareh Abed and Mania Akhavan Sharif and my sister Vala Moghareh Abed for your incredible love, support and guidance, you truly are inspirations beyond comprehension.

None of this would be possible without your encouragement.

ACNOWLEDGEMENTS

I want to thank my family and friends, for their patience, support and kindness over the last 4 years.

To my parents, Mohamad Hossein Moghareh Abed and Mania Akhavan Sharif.

To my sibling- Vala Moghareh Abed

To Professor Christopher Rogers and Dr David Chapman for their support, kindness, supervision, guidance and tolerance. None of this would be possible without your belief in my ability.

To Unyime John, special thanks for your assistance, support and sharing your knowledge.

To Professor Ian Jefferson and Dr. Gurmel Ghataora for their opinion and advice.

To laboratory staff and fellow researches, thanks for helping during laboratory testing. Thanks to Mr. Mike Vanderstram, Mr. Jim White, Mr. Sebastian Ballard, Mr. David Cope and Mr. Bruce Reed for their support.

Finally, friends in Birmingham and postgraduate members in room F59A and F59B for their help and support.

TABLE OF CONTENTS

LIST OF FIGURES

LIST OF TABLES

LIST OF ABBREVIATIONS

ABC	Absorbing Boundary Condition
BSI	British Standards Institution
c	Speed of Light in Free Space
CEC	Cation Exchange Capacity
CEN/TS	European Committee for Standardisation / Technical Standards
CMP	Common Mid-Point
c_u	Undrained Shear Strength
D	Distance
DAFD	Distance Away From Disc
dB	decibels
DDL	Diffuse Double Layer
DW	Distilled Water
e	Void Ratio
EC	Electrical Conductivity
EK	Electrokinetic
EO	Electroosmosis
f	Frequency
FDTD	Finite Difference Time Domain
FV	Flocculation value
g	Acceleration due to Gravity
GPR	Ground Penetrating Radar
G_S	Specific Gravity
h	Distance

HDPE	High Density Polyethylene
I	Current
IAEA	International Atomic Energy Agency
i	Penetration Depth
i_c	Chemical Potential Gradient
ICP	Inductively Coupled Plasma
i_h	Hydraulic Gradient
IHP	Inner Helmholtz Planes
J_i	Flow Rate K Potassium
K	Cone Tip Angle
K_e	Electroosmotic Conductivity
K_h	Hydraulic Conductivity
K_p	Probe Constant
kPa	Kilopascal
L	Length
LG	Lamellar Graphitic
L/A	Liquid / Surface Area ratio
L/S	Liquid / Solid Ratio
L_a	attenuation loss
LDH	Layered Double Hydroxide
L_{ii}	Conductivity Coefficient for Flow
LL	Liquid Limit
m	Weight of the Cone
MDPE	Medium Density Polyethylene
Mol	Molarity

Mpa	Mega Pascal
MTU	Mapping The Underworld
NDT	Non-Destructive Technologies
OHP	Outer Helmholtz Planes
pH	Acidity / Alkalinity of system / -$\log_{10}$ of hydrogen ions activity
PL	Plastic Limit
PVC	Polyvinyl Chloride
PVCU	Unplasticised Polyvinyl Chloride
Pzc	Point of Zero Charge
q_c	Cone Resistance
q_h	Hydraulic Flow
R	Electrical Resistance
rpm	Revolutions Per Minute
SG	Spheroidal Graphitic
SRB	Sulphate Reducing Bacteria
T	Temperature
t	Time
TDR	Time-Domain Reflectometry
USS	Undrained Shear Strength
v	Velocity
VNA	Vector Network Analyser
V_p	Signal Propagation Velocity
WARR	Wide Angle Reflection and Refraction
XRF	X-ray Fluorescence
Z	Impedance

α	Attenuation Coefficient
ε	Dielectric Permittivity
ε_a	Apparent Permittivity'
ε_r	Permittivity of a Material
μ	Magnetic Permeability
ν	Velocity
σ	Electrical Conductivity
$\tau_{f,}$	Undrained Shear Strength

CHEMICAL ABBREVIATIONS

$5Fe_2O_3.9H_2O$	ferrhydeite
Al, Al^{3+}	Aluminium, Aluminium ion
$Al(OH)_3$	Aluminium hydroxide (Gibbsite)
Al_2O_3, AlO_4^{5-}	Alumina (Aluminium oxide), Aluminium oxide ion
$Al_4Si_4O_{10}(OH)_8$	Kaolinite
Ba, Ba^{2+}, BaO	Barium, Barium Oxide
Ca, Ca^{2+}, CaO	Calcium, Calcium ion, Calcium Oxide
CaCl	Calcium Chloride
$CaCO_3$	Calcium Carbonate
Cd	Cadmium
Cl^-	Chloride ion
CrO_4^{2-}	Chromate ion
Cs^+	Cesiumion
Cu^{2+}	Copperion
Fe, Fe^{2+} ,Fe^{3+}	Iron, Ferrous ion, Ferric ion
$Fe(OH)_3$	ferric hydroxide
Fe_2O_3, $Fe(OH)_3$	Iron (III) oxide, Iron hydroxide
H^+, OH^-	Hydrogen ion, hydroxide ion
$H4SiO_4$	Silicic acid
HNO_3	Nitric acid
K, K^+	Potassium
K_2O	Potassium Oxide
Li^+	Lithium ion

Mg, Mg^{2+}, MgO	Magnesium, Magnesium ion, Magnesium Oxide
Mn	Manganese
Na, Na^{+}, Na_2O	Sodium, Sodium ion, Sodium Oxide
Na_2SO_4	Sodium silicate
Na_4SiO_4, Na_2SiO_3	Sodium orthosilicate, Sodium silicates
NaOH	Sodium hydroxide
Ni	Nickel
P_2O_5	Phosphorus Pentoxide
Pb, Rb^{+}	Lead
Rb_2O	Rubidium
S	Sulphur
Si, Si^{4+}, Sio_2	Silica , Silicon ion, Silicon oxide,
SrO	Strontium oxide
Th^{4+}	Thoriumion
TiO_2	Titanium oxide
V_2O_5	Vanadium
Zn, Zn^{2+},ZnO	Zinc, Zinc ion, Zinc Oxide
ZrO_2	Zirconium Dioxide

CHAPTER ONE

1.0 Introduction

Water is essential to life. Potable water is often transferred to the user through pipes that are buried in the ground. These pipes are widely made of cast iron, which, although first recorded as having been used in Versailles in 1664, were first introduced into routine use in the early 1800s (e.g. in the USA, see Jason Consultants, 2009) and extensively used to build water distribution systems in the UK and elsewhere from the early 1890s until ductile iron pipes were introduced in the 1970s. Unplasticised Polyvinyl Chloride (PVCU) water pipes were introduced in Europe and North America during the 1970s, and more recently medium- and high-density polyethylene (MDPE and HDPE) have become alternative materials for the renewal of existing water mains. Most of the mains installed during the first half of the last century were made of cast iron, and now have an age of 50 to 100 years (Rajani et al., 1996). There has been a progressive movement towards modern materials; for example, it was reported by Kirmeyer et al. (1994) that water utilities in the United States of America (USA) were replacing approximately of 0.6% of their water mains each year, yet they noted that 48% of water pipes at that time (in 1992) were made of cast iron and hence they still exist in enormous volumes. In Australia, there are around 260,000 km of pipelines used, of which more than 70% are in the form of ferrous metal, and the most common corrosion failure mechanism for buried cast iron pipes is localized corrosion, which leads to leakage (WSAA, 2008-09). In the UK, cast iron pipes were manufactured in various ways from 5 to 150 years ago, therefore the properties of these pipes are different. London water mains are the oldest in the UK (44% over 100 years old). As these pipes need to be replaced, companies have carried out detailed investigation using computer modelling to find the best way of renewing the old pipe network.

This investigation helps to prevent unnecessary digging and effectively the cost. So far over 1,600 miles of old pipe network replaced (Thames Water, 2013).

Cast iron has a tendency to corrode in an aggressive environment, which leads to pipe degradation (Rajani et al., 2000). It has also been found that cast iron pipes have a very high failure rate in some soils, i.e. in soils that are particularly aggressive such as London Clay (Schmidt, 2007). Therefore, failures of these pipes are not only mechanical, but can also be induced by the prevailing environmental conditions.

Cast iron water pipes were designed to be sufficiently strong to resist mechanical loading, and to resist predicted environmental conditions, as they transfer clean water to users. However, the problem of cast iron water pipe breaks and leaks in distribution systems is relatively common globally (Atkinson et al., 2004). When these pipes are in direct contact with active or chemically aggressive soil, chemical degradation due to corrosion may be induced. Corrosion is the degradation of metal due to a reaction with its environment (Bradford, 2000). These chemical degradation processes are complex, time dependent and costly. Cast iron corrosion in soil occurs due to electrochemical processes and results in the formation of pitting, converting metal substrates to oxides, hydroxides and aqueous salts (in anode-cathode systems). Buried pipes are in direct contact with the soil, and obviously different types of soil have different physical and chemical properties. Therefore, the level of aggression in the environment can even change over the length of a pipe: it can induce graphitic corrosion of the iron pipe or the precipitation of salt on the pipe and, given sufficient time and oxygen, the pipe may be completely corroded. Corrosion products, such as iron oxide and hydroxide, are released into the surrounding soil, so that the chemical, geotechnical and geophysical properties of the soil change, although these interactions are not well understood. If the condition of these buried pipes can be routinely assessed and monitored, the consequences of deterioration in the utility network can be effectively reduced. Therefore, intrusive or, ideally, non-intrusive

assessments via geophysical techniques such as Ground Penetrating Radar (GPR) are needed. GPR has been developed to locate and map cast iron pipes (Pennock et al., 2010) and is being developed to provide condition assessments (Hao et al., 2012; Rogers et al., 2012), yet as these papers testify chemical alteration of fine-grained soil by cast iron corrosion products inhibits GPR's abilities to achieve both of these goals. This provides the context of the research.

1.1 Background

The nature of the corrosion of metal pipes depends on the soil in which it is buried, the surrounding groundwater properties and the chemical composition of the metal. Cast iron pipe corrosion occurs readily in saturated or partially-saturated zones of clays, where electrochemical oxidation takes place in the presence of oxygenated water – this is graphitic corrosion due to the creation of a galvanic cell between the cast iron (the anode, where the pH is lowered) and the surrounding high-conductivity clay (the cathode; see Freeman, 1999). Given sufficient time and oxygen, the cast iron pipe will corrode and corrosion products such as ferric oxide, ferric hydroxide and aqueous salts will be released and will react with the soil. Furthermore, the rate of corrosion increases with the increase in the electrical conductivity of soils (Ekine & Emujakporue, 2010). The release of corrosion ions from buried iron pipes is expected to increase the rate of pipe corrosion due to an increase in concentrations, hence concentration gradients. These released ions contaminate the surrounding soil, elevating the iron/cation contact and creating a diffuse plume zone around the source (the cast iron pipe). The plume zone is where ion diffusion and migration occur, and this can ultimately lead to modification of the soil, with the concentration of these ion contaminants decreasing away from the source (the cast iron pipe) as they form precipitates or complexes with the surrounding soil (Yong et al., 2003).

However, the level and scale of these interactions differ. The released ions are not chemically inert, and therefore they typically react with clay minerals in the soil and modify its physical and chemical properties. Different clays have different selectivity for ions they can sorb or complex with (Yong et al., 1996), usually dependent on the valency of cation in the lattice for substitution, the ease of substitution (Mitchell & Soga, 2005) and the reactive components contained. Depending on the type of ions present in soil, different interactions take place, such as dissolution, precipitation, ion exchange and complexation. Clay tends to strongly sorb cations through cation exchange and complexation, thereby reducing cation mobility (Yong et al., 1996).

Over a number of years, the soil around the corroding surface is likely to become severely altered, and this is likely to significantly modify the soil's physical and chemical properties. In some cases, cast iron water pipes have been found completely corroded with time, and the surrounding soil has become altered and found to have a hard profile, due to cementation by carbonates and silicates, so that the modified soil acts as a pipe and allows water to flow (Schmidt, 2007). All of the above makes detection of cast iron pipes using GPR a significant challenge.

1.2 Research Philosophy

Buried cast iron pipes interact with surrounding soil porewater in saturated and partially-saturated zones in the presence of oxygen, thereby undergoing electrochemical oxidation, which induces corrosion to form rust and release chemical corrosion products (ferric oxide and ferric oxyhydroxides) into the surrounding soil. These released corrosion products interact (forming complexes or precipitates) with the surrounding soil, and given sufficient time severe or complete degradation will result in an increase in the extent and effects of the interaction

with the surrounding soil. From a geotechnical perspective, it is important to understand how these released ions influence changes in the soil properties and how the extent and degree of influence changes with time. From a geophysical perspective, it is important to understand the change in the electromagnetic properties of the soil, because this affects GPR performance. This requires the adoption of a suitable controlled laboratory experimental procedure to simulate the corrosion and ion migration process, whereby the effects on the surrounding soils can be evaluated and the obtained information used to infer behaviour in the field. Changes in the chemical properties of soil have an effect on its physical properties as well, so the geotechnical properties of soil should be considered and defined in the methodology, to ensure that an effective characterisation of mechanisms and modifications is obtained within a practical and realistic method. However, given the slow rates of these interactions, it is imperative to adopt acceleration catalysts to make the work achievable. Since corrosion is an electrochemical oxidation process, increasing the acidity at the anode should accelerate the corrosion process (Reeves et al., 2006) and if sufficient water is present in the test system, advection with cathodic draining can also aid ion migration. Also, the different aspects and influences of electrolysis and hydrolysis should be considered and evaluated in relation to the behaviour of the soil, the migration of released ions and the dissociation of minerals and water during testing.

1.3 Conceptual Modelling

A conceptual model presents the complex natural process in a system, identifies any gaps in scientific understanding, and simulates the process in a non-technical way. It is a vital aspect of simulation studies, and requires accurate definition of modelling requirements, and validation against actual conditions (Robinson, 2006). In this case, it simulates the field

modification (Figure 1.1) and experimental arrangement (Figure 1.2) of soils due to corrosion of buried cast iron. As understanding emerges from the research, it will be continually modified to yield a final conceptual model at the end of the experimental processes.

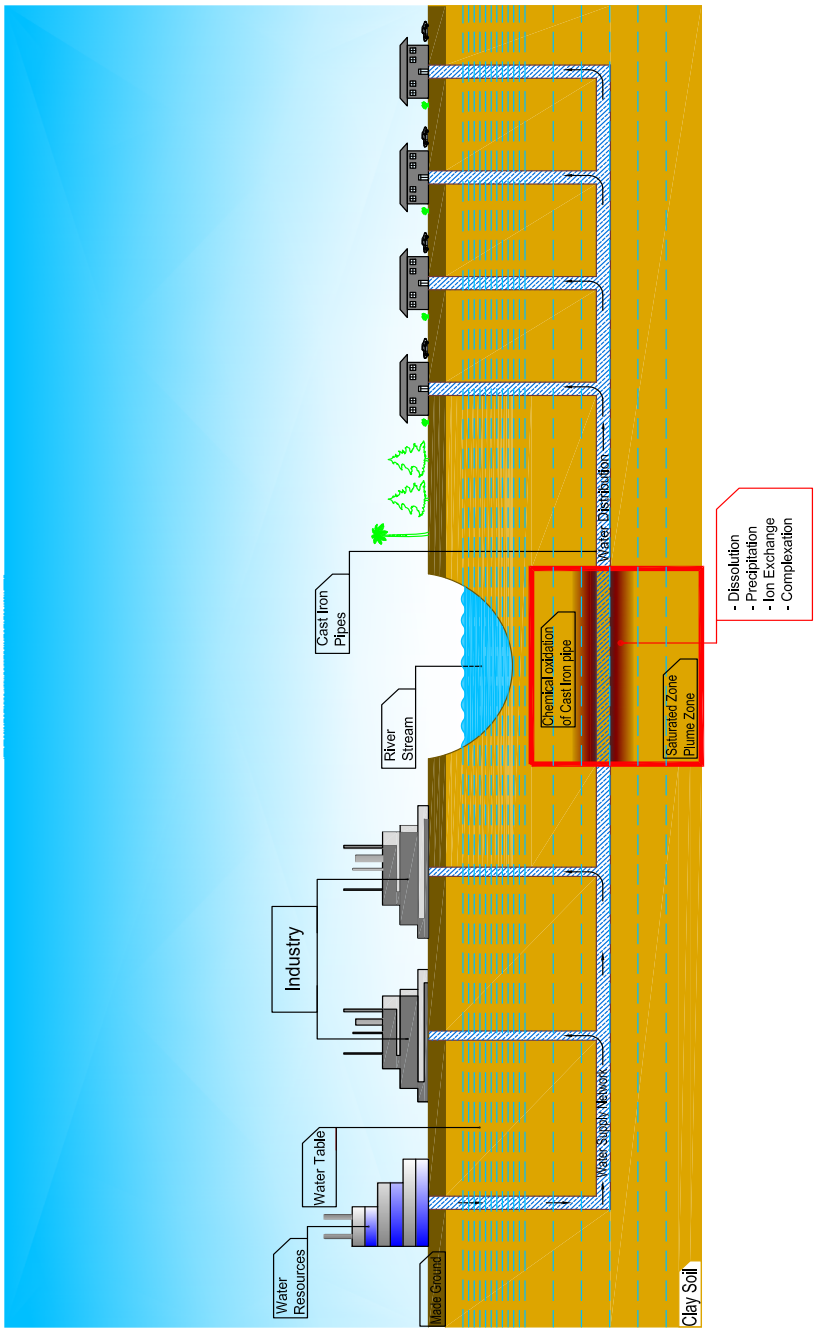

Figure 1.1 Conceptual model of site condition, migration pathway and possible implications

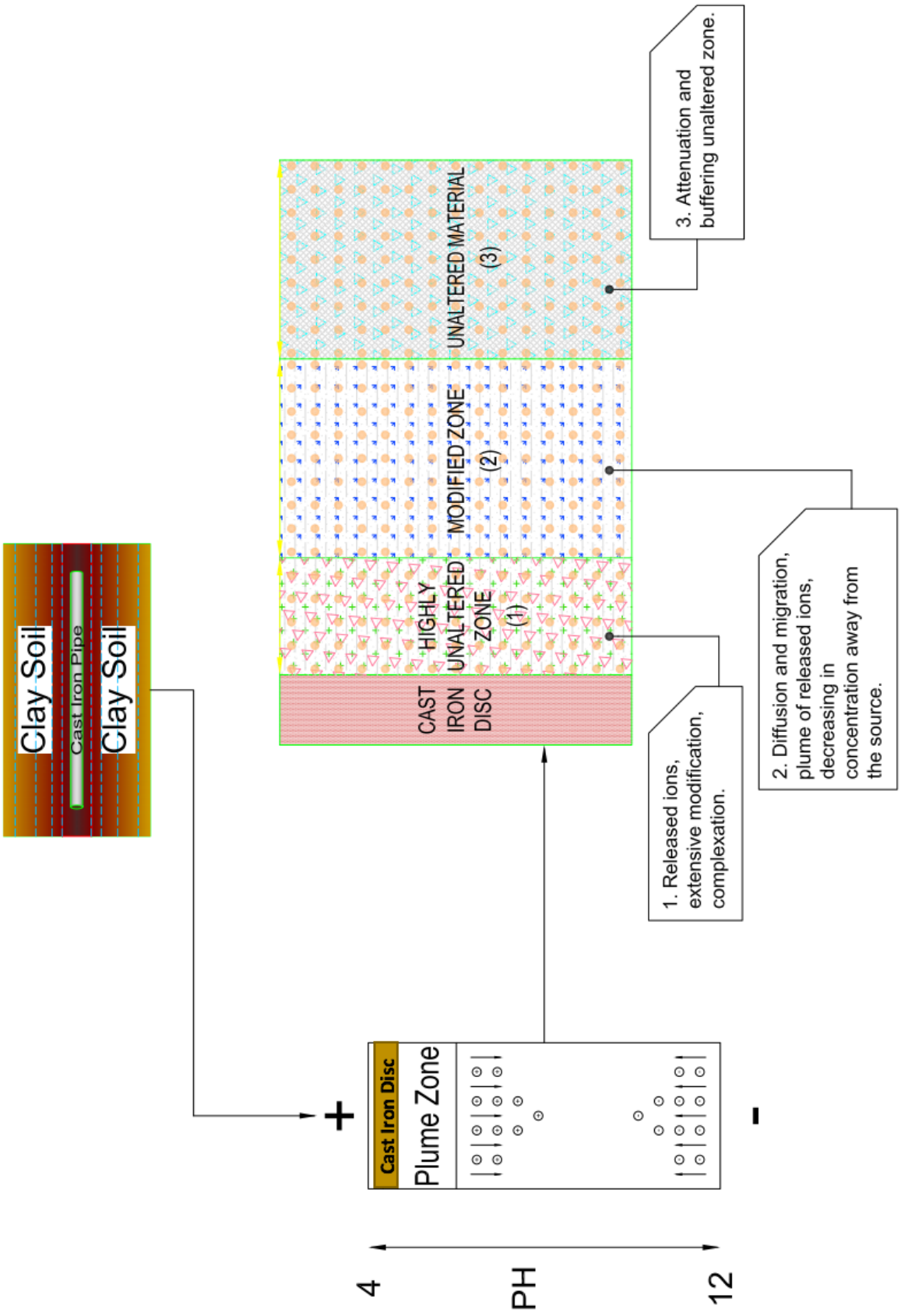

Figure 1.2 Soil modifications through ion migration

1.4 Aims, Objectives and Hypothesis

Corrosion of buried cast iron (in the form of iron oxide and hydroxide) and precipitation of salts can alter and modify the soil surrounding a cast iron pipe and create a diffuse plume of migrating iron ions around the pipe. This plume decreases in concentration away from the pipe as it precipitates or complexes with surrounding soil and increases in extent with time. Importantly, these changes can significantly modify the soil properties, i.e. mineralogy and pore water, chemical, electrical, and hence geophysical and geotechnical, properties, resulting in behaviour that deviates from those typical of the prevailing soil type.

Aim:

The aim of the study is to investigate the effects of the corrosion of buried cast iron on the physical and chemical properties of surrounding clay soils, and hence to explore the reported tendency of deteriorated cast iron pipes being harder to detect using GPR (Ground Penetrating Radar) than pristine pipes.

Objectives:

- Establish the current state-of-the-art of the corrosion of cast iron pipes in clay-based soils and their detection using Ground Penetrating Radar through conducting a literature review relevant to the geotechnical and geophysical implications.
- Develop an appropriately-designed laboratory testing regime and conduct an experimental investigation of the corrosion of buried cast iron in consolidated Kaolin and Oxford Clay soils, evaluating the release and migration of corrosion products into the clays. A weak electric field will be induced to accelerate the corrosion rate and migration of ions into the surrounding soil.
- Evaluate geotechnical and geophysical changes in the properties of the clay with time.

- Evaluate chemical modifications of the surrounding soil: measuring the changes in pH, conductivity and total soluble salt content of the clay extending radially and laterally away from the source (the corroding cast iron). The changes in conductivity due to released salts by corrosion of cast iron will be determined using time domain reflectometry (TDR).
- Using elemental analysis (x-ray fluorescence – XRF), carry out a microstructural analysis to determine changes in the composition of the clays, and hence the degree of clay modification, around and away from the corroding cast iron.

- Simulate the results of the corrosion products that have caused variable conductivity and permittivity in the experimental samples by using a finite difference time domain (FDTD) simulation (GPRMax software) in order to investigate the ability of GPR techniques to detect buried iron pipes.

1.5 Thesis Outline

This introduction is followed by a critical review of the literature (Chapter 2). It provides a short overview of the history of cast iron pipes and the different types of cast iron. The corrosion of cast iron is explained, as this is the main explanation for the failure of cast iron pipes, as are the products of cast iron corrosion. Then, a section explains the mineralogy, properties and interactions of clay. And finally, methods of non-intrusive assessment via geophysical techniques (GPR) and the simulation of GPR signals by GPRMax, using conductivity and permittivity obtained from Reflectometry (TDR), are described.

Chapter 3, which describes the creation of bespoke experimental facilities and the methodology, gives full details of the testing programme, including material characterization, the preparation of samples, how the experimental data were collected, and how the analysis of the results was carried out. In particular, the chapter describes in detail the test development and design, which involved the use of an electrical gradient to increase the rate of corrosion. The most important part concerns the tests carried out to achieve the objectives of this research, based on the results of state-of-the-art information derived from the literature review.

Chapter 4 presents the physical and chemical, and hence relevant geotechnical and geophysical, results obtained from the tests. This is followed in Chapter 5 by discussions comparing the results for the two types of soil and the FDTD simulation by GPRMax software based on the conductivity and permittivity (TDR) results. Finally, the conclusions are presented in Chapter 6, based on the discussion chapter, and recommendations for further work are made.

CHAPTER TWO

2.0 Review of Background Literature

2.1 Introduction

The underground distribution network for utilities is one of the most complex networks in the world, and this complexity has influenced the services being delivered and the material for the pipelines and conduits through which they are delivered, with due cognisance to their interconnectedness, their different ages, and their different sensitivities to disturbance. The various utility service networks in urban areas include water pipes, gas pipes and electricity cables, sewer and storm water drainage channels, and so on (Hao et al., 2012). Cast iron was the most common material used for water pipes historically (see history of cast iron pipes in Section 2.2). A large part of the cast iron pipes network was produced some 50 to 150 years ago (Thames Water, 2013). These pipes were designed to be durable under different environmental conditions. However, these buried pipes are in direct contact with soil and different types of soil, some of which are not inert, have different physical and chemical properties along the pipe network. Hence, the level of aggressive interactions with the surrounding geomedia could change over the length of pipes, potentially shortening the pipe service life from that predicted or inducing leakages and system failures. Cast iron pipes were extensively used to build water distribution system from the early 1890's, and most were installed during the first half of the last century with ages of 50-75 years (Rajani et al., 1996).

The problem of breaks and leaks in pipe distribution systems is relatively common globally, and cast iron has a relatively high failure rate in some reactive soils, such as London Clay (Schmidt, 2007). These failures include graphitic corrosion, where a galvanic cell is set up and metal loses electrons and reacts with surrounding water and oxygen. Also, clay soil properties, such as mineralogy, pH, oxygen level, moisture content, and the presence of sulphate reducing

bacteria (Schmidt, 2007), can influence how aggressive clay soils interact with cast iron pipes. The results of these interactions are complex, time dependent and may be costly. Given sufficient time for the reactions to occur, iron ions are released and react with the soil surrounding a pipe, corrosion products such as iron oxide and iron hydroxide are formed, and these processes can create a plume of diffuse ions / precipitated salts around their source (Pennock, 2014). Furthermore, it is also possible that the corrosion rate can increase with increasing conductivity or decreasing permittivity (Ekine & Emujakporue, 2010). This means that the release of corroded irons ions into the soil, which in turn increases the total dissolved salt content and thus electrical conductivity, can further accelerate the corrosion process and increase its extent.

Buried pipes cannot be inspected visually, but the monitoring and surveying of heritage buried cast iron pipes are important to assess their current condition and rate of deterioration. With this knowledge, it may be possible to organise proactive maintenance in the most cost effective manner. If the condition of the buried infrastructure is routinely assessed and monitored, it is possible to ensure that there are warnings of impending failure, and so the possibility of serious consequences from accidents caused by the deterioration of the network can be effectively reduced (Hao et al., 2012). To increase inspection efficiency, remote (non-intrusive) techniques have been developed. The techniques, such as Ground Penetrating Radar (GPR), can potentially be used to detect these corroded pipes. GPR is used to survey the buried utilities and it resolves the position of buried objects, though one open question is whether it can be used to determine the corroded state of cast iron pipes (MTU, 2013).

2.2 History of UK Cast Iron Pipelines

The growth of cities and large urban areas triggered the need for water distribution systems. As the populations increased, it became vital to bring water from its natural sources to meet end user needs at point of need. Ancient civilizations first devised aqueducts and tunnels, and created pipes and tubing out of clay, lead, bronze and wood. None of these materials was a complete success, as they were all prone to deterioration and breakdown with time. The earliest recorded use of cast iron piping was in Langensalza, Germany, in 1562, where it supplied water for a fountain (Cast Iron Pipe Soil Institute, 2006). However, the first full-scale cast iron pipe system for the distribution of water was installed in 1664 at the Palace of Versailles in France (AWWA, 2005). This system carried water for 15 miles from the River Seine to the Palace and surrounding area; and it is still working after more than 300 years of continual service. It represented a genuine pioneering effort, and at the time it was created, the cost of construction was extremely high. This was due mainly to the fact that high-cost charcoal was used as the fuel for reducing iron ore until 1738, when it was replaced by coke. Immediately following this development, cast iron pipes were installed in a number of other distribution systems in France, and in 1746 they were introduced in London by the Chelsea Water Company (Kirmeyer et al., 1994). In 1914, the spin casting method was developed in the United Kingdom (Koehl, 2000). The new production method brought an improvement in the quality of cast iron, and cast iron pipes became homogenous in terms of the quality of the material and geometry. After the 1960s, ductile iron and plastic water mains were introduced. Nevertheless, cast iron is still the most common material found for existing pipes that are in service, and is also the material that produces the highest number of bursts historically (Makar et al., 2007).

2.3 Cast Iron

Cast iron is a name given to a wide range of ferrous alloys, distinguished by a carbon content of 2 to 4%, along with varying amounts of silicon (1- 3%), manganese, and impurities such as sulphur and phosphorus (Reynaud, 2006; Melchers, 2013). The degree of control achieved in the heating and cooling processes can give a wide range of properties to different grades of cast iron (Sing, 2011). The properties of cast iron are controlled by the solidification, inoculation and cooling rate, as well as by the alloy composition.

Also, the physical form of the carbon content controls the properties of cast iron. Four main types of iron, which are classified regarding to their microstructure (depending on the carbon content, alloy and impurity content, the cooling rate and heat treatment after casting), are commonly referred to:

- **White iron,** in which all carbon is present in the metal carbide phase.
- **Grey iron,** in which most carbon is present as graphite flakes.
- **Ductile iron** (nodular iron), in which most of the carbon is present as graphite nodules that are produced during solidification in casting.
- **Malleable iron**, in which most of the carbon is present as graphite nodules and which is produced as a consequence of solidification due to the heat treatment of casting (Cast Iron Pipe Research Association, 1952).

Grey cast iron (see Section 2.3.2) was the most common iron alloy used for the production of pipes, before ductile iron was introduced (Cast Iron Pipe Research Association, 1952). In Section 3.3.3 the properties of the cast iron used in this project are given. Table 2.1 shows the typical composition of cast iron material alloys. The main difference between grey cast iron and other cast iron alloys is the high content of carbon formed in flakes, which creates grit within the iron matrix (Cast Iron Soil Pipe Institute, 2006).

Table 2.1 Compositions of cast iron alloys (Reynaud, 2006)

	Microstructure		Total carbon	Combined carbon	Silicon	Manganese	Sulphur	Phosphorus
	Graphite	Matrix Iron	[%]	[%]	[%]	[%]	[%]	[%]
Grey Cast iron	Flake	Pearlite	2.7-4	<1	0.5-3.3	0.3-1	<0.15	<1.4
White iron	None	Pearlite	1.7-3.0	100%	0.8-1.3	0.4	<0.15	<0.5
Malleable iron	Nodular	Ferrite	2.0-2.7	None	0.8-1.2	0.1-0.6	<0.15	<0.2
Ductile iron	Nodular	Pearlite / ferrite	3.3-3.9	<1	1.6-1.25	0.4	<0.01	<0.1

2.3.1 White Cast Iron

In this type of iron, the carbon is in the form of iron carbide in a matrix of pearlite, which depends on the amount of carbon in the iron. This material is hard and brittle. Alloys of white iron can be produced from the formation of alloy carbides that are even harder, and are ideal for hard and abrasion-resistant applications such as extrusion dies and cement mixer liners (Reynaud, 2006).

2.3.2 Grey Cast Iron

This type of iron is the oldest and most common form of cast iron. Grey cast iron takes its name from its characteristic fractured surface, which has a grey appearance and consists of carbon in the form of graphite flakes in a matrix usually consisting of pearlite or ferrite or a mixture of the two. The terms ‘cast iron’ and ‘grey iron’ are used interchangeably. The fluidity of the liquid and its expansion properties during solidification due to the formation of graphite (depends on the presence of sulphur in the cast iron) make this ideal for the economical

production of shrinkage-free material. These alloys are often known as lamellar graphitic (LG) cast iron.

Generally, as the combined equivalent of carbon and silicon is reduced in the matrix, the strength of the cast iron increases (Reynaud, 2006). Removing sulphur from the metal by using calcium carbides can induce the graphite to precipitate in a spheroidal shape. It is necessary to undertake the calcium treatment before adding the magnesium, because the magnesium has an affinity for both sulphur and oxygen, but its spheroid zing ability depends on it being present in solution in a liquid ion (Reynaud, 2006). Also, magnesium is frequently added as an alloy with iron and silicon (Fe-Si-Mg). However, magnesium tends to encourage the precipitation of cementite, so silicon in form of ferro-silicon is also added to ensure the precipitation of carbon as graphite (Cast Iron Pipe Research Association, 1952). For thicker sections requiring tensile strength above 350MPa, additions of chromium, nickel or molybdenum alloys are required. This material does not exhibit any plastic behaviour and fails under tension without significant plastic deformation (Reynaud, 2006). The presence of graphite flakes results in excellent machinability, damping and self-lubricating characteristics. Consequently, this in turn provides high resistance to sliding wear and it has been used successfully for sliding surface including cylinder bores, piston rings, and machine tools. Also, due to the graphite flakes, grey cast iron has high resistance to gulling and seizing and has a low coefficient of friction. It was evidenced in most materials with a high percentage of graphite flakes, resulting in the excellent capacity of absorbing vibration energy and thus damping vibrations (Reynaud, 2006). Grey cast iron has favourable long-term corrosion characteristics, particularly when it is exposed to air, as witnessed by the existence of many railway bridges in the UK and USA that are over 100 years old (Melchers, 2013). Also, ASTM Specification A-48 lists the several classes of grey cast iron

based on the tensile strength, which ranges between 140 to 420 MPa, and where strengths above 280 MPa are considered as high tensile strength iron (Reynaud, 2006).

2.3.3 Alloy Cast Iron

In both white and grey cast iron, the properties of the metal can be changed by varying alloy elements such as nickel, chromium, molybdenum and silicon. For example, an alloy containing 4-5% nickel and 1.2% chromium will have increased rigidity and better mechanical properties. Cast iron with 25-35% chromium is a 'stainless' cast iron that has good resistance to corrosion and behaves well at high temperatures. Cast irons with up to 16% silicon content have an increased rigidity and good corrosion resistance, but their mechanical properties are inferior (Reynaud, 2006).

2.3.4 Ductile Cast Iron

Ductile cast irons have the same properties as cast iron but the inclusion of alloy components such as magnesium results in a relatively low melting point, good fluidity, castability, excellent machinability and resistance to wear. However, cast iron pipes are stronger and tougher (their tensile strength exceeds 800MPa), and are easier to handle when hot.

2.3.5 Malleable Cast Iron

This type of cast iron is known as white iron, and during its manufacture it is heat-treated, which converts its carbides into graphite. Malleable irons are produced by two different processes. Depending on the process used, the result is either a ferrite or a pearlite matrix in pearlite form with a surface layer of ferrite (Reynaud, 2006).

2.4 Reasons for Cast Iron Pipe Failure

After over 100 years of use, cast iron pipes can still be found in widespread use in the UK, and they dominate water distribution systems globally. As these pipes have failed, and needed to be replaced, the critical questions are: why do they fail? And is this failure due to corrosion? Cast iron can fail for reasons that include the physical environment, the characteristic of the water supplied, internal corrosion, external stress (ground movement, frost load and so on), internal stress, pipe resilience and so on (Kleiner et al., 2001b). The design of pipes for use underground draws on the physical behaviours that give the pipe resistance capacity against expected loads (operational and environmental). When all of these factors are taken into account, the design must also include a margin of safety (Rajani et al., 2001). The quality of pipes depends on both their age and their source, and also on the methods of manufacturing (Cast Iron Pipe Research Association, 1952). One important factor in their performance is iron cathodic behaviour of existing graphite towards the iron, which is the unique way grey cast iron corrodes (Freeman, 1999). Corrosion processes can make holes and therefore can contribute to mechanical failure by weakening and therefore, in a water pipe system, with high internal pressure, the pipes start to fail. In this case, corrosion is a very important part of cast iron pipe failure.

Even though operational pressures are regulated, in some cases the stresses induced in the pipes are of such magnitude that they could be the cause the failure – external loading can in principle be of any magnitude – especially in the case of pipes whose integrity may have already been compromised by other factors such as corrosion (Baracos et al., 1955; Mordak & Wheeler, 1988; Hudak et al., 1998). Decreases in temperature during the winter can cause an increase in pipe tensile stresses, which consequently leads to a higher water main breakage rate. These cast iron pipes continue to cause problems in water distribution systems and therefore research into the corrosion of cast iron pipe still has great importance. Moreover, the pipe and soil are

working both as one system, and thus each can affect each other and the cause of failure. Therefore, it is important to analyse both systems (pipes and surrounding soil) to understand potential failures problems.

Different types of corrosion might happen depending on the situation of the cast iron pipes, such as soil condition, moisture content, oxygen concentration reaching the buried pipes and flux of any other corrosive salt (Cole & Marney, 2012).

2.5 Corrosion of Cast Iron

Buried cast iron pipe will interact with surrounding soil pore water in the saturated and unsaturated zones in the presence of oxygen, thereby undergoing electrochemical oxidation which induces corrosion to release ions (ferric oxide and ferric hydroxide) into the surrounding soil.

Corrosion of cast iron in contact with oxygenated water follows a monotonic bi-modal trend with time (see Figure 2.1). This trend has shown that for various metals (such as mild, low alloy, weathering steel and cast iron) in various environments (sea water and freshwater immersion, tidal zone, coastal and inland atmospheric exposures) (Melchers, 2011). Also, Figure 2.2 presents data for corrosion mass loss of ferrous metal (both steel and cast iron) in soils that show similar trends. Corrosion of cast iron has a similar behaviour to other metals and the most common type of corrosion is graphitic corrosion.

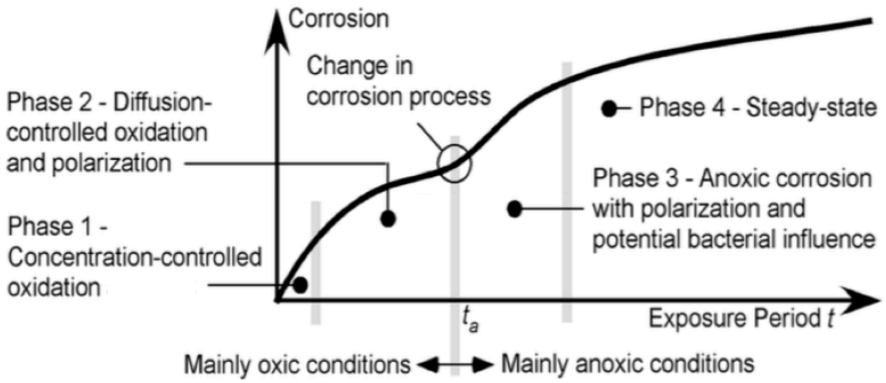

Figure 2.1 Schematic representation of the bi-modal behaviour of corrosion loss showing the principal phase (Melchers, 2011)

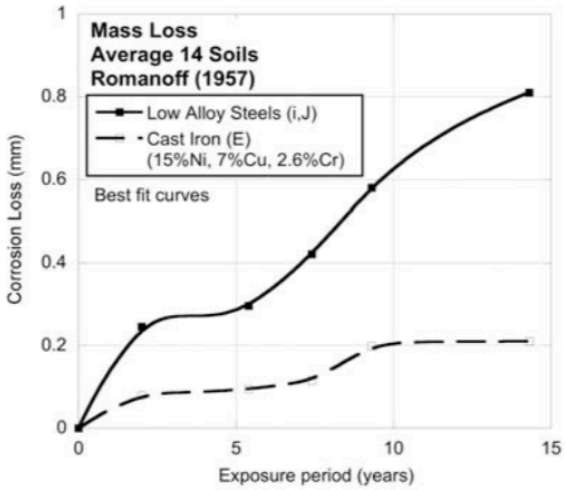

Figure 2.2 Trends for the average corrosion mass loss of pipe coupons buried in soils for two low alloys (I,J) and a high alloyed cast iron (E) (Romanoff, 1957)

As mentioned earlier, the graphitic corrosion process is an electrochemical process with an anodic reaction where metal is oxidized and a corresponding equal cathodic reduction reaction. At the anode, ferrous ions are dissolved into the electrolyte solution:

Anode: (Reaction 1.0) $Fe = Fe^{2+} + 2e^{-}$

The electrons released at the anodic site are accepted at separate, cathodic sites. The cathodic reactions are:

Cathode: (Reaction 2.0) $2H^+ + 2e^{--} = H_2$

(Reaction 2.1) $½O_2 + H_2O + 2e^- = 2OH^-$

Reaction 2.0 is most common in acid, and Reaction 2.1 is the common reaction in a pH range of 6.5-8.5. Galvanic corrosion is self-generating and occurs on the surface of a metal exposed to an electrolyte (such as moist, salt-laden soil). Differences in the electrical potential between points on the surface of the metal (pipe) in contact with the soil may occur. Differences in electrical potential may also be caused by the properties (chemical and physical) of the soil surrounding the pipe. These properties include the pH, the number and type of soluble salts, the oxygen and moisture content, soil resistivity, temperature and the presence of certain bacteria. Any of, or any combination of, these factors can result in a small amount of electrical current flowing through the soil between areas on the pipe or metal surface (Cole & Marney, 2012).

Depending on their solubilities, these rust products (from cast iron corrosion) are deposited within the graphitised zone, on the external surface of the pipe, or diffuse away into the surrounding soils (Petersen, 2012).

Regarding Figure 2.1, in Phase 1, the rate of corrosion depends on the rate of diffusion of oxygen to the surface of the metal from the surrounding environment. Thus for the cast iron buried in soil this depends on the permeability of the soil adjacent to the pipe, the moisture content and the depth of burial.

During Phase 2, the rate of corrosion decreases due to the build-up of rust products on the external surface and an increase in the depth of the graphitised zone. The rust products prevent the inward diffusion of oxygen to the surface of the metal and this reduces the rate of corrosion.

In Phase 3, the rate of corrosion increases initially but then gradually declines with time. The increased degree of corrosion is due to a change in the corrosion process from one involving oxygen reduction (controlled by oxygen diffusion) (Melchers, 2011). Hydrogen reduction is thought to occur in crack-type formations on the corroding surface. Due to non-uniform oxygen access, these cracks develop at anoxic (oxygen-restricted) points on the corroding surface. This behaviour is the same as that for corrosion in steel and cast iron. And finally, Phase 4 is the most important for the prediction of long-term rates of corrosion of cast iron in soil. This phase may be entered as late as 10-20 years after initiation (Figure 2.1).

Figure 2.3 presents the corrosion process. The corroding surface has retreated into the cast iron component leaving behind a graphitised zone. Rust products have built up on the external surface of the metal in contact with the external environment, and within the graphitised zone. In Figure 2.3 the graphitised zone has retained the original shape of the pipe.

Two corrosion processes may be active (see Figure 2.3), the first being oxygen reduction outside of the crevice (Reaction 2.1), with a corresponding anodic process within the crevice (Reaction 1.0). This separation of anode and cathode is the result of differential aeration between the inside and the outside of the crevice, thus creating a differential aeration cell. Possible rate limiting processes include the inward diffusion of oxygen and water to the cathode, and the outward diffusion of ferrous ions away from the anode. Oxygen and water must be replenished at the corroding surface, and ferrous ions need to be removed from the corroding surface to take place in the corrosion reactions (Petersen, 2012). The second

corrosion process involves hydrogen reduction at the cathode within the crevice (Reaction 2.0), with a corresponding anodic process within the crevice (Reaction 1.0). Reaction 2.0 involves the evolution of hydrogen gas, and is typically much slower than Reaction 2.1, except when in acidic condition (pH<4) (Uhlig, 1963). Possible rate limiting processes include the inward diffusion of water to the cathode (in the crevice), the outward diffusion of hydrogen gas from the cathode, and the outward diffusion of ferrous ions away from the anode (Petersen, 2012).

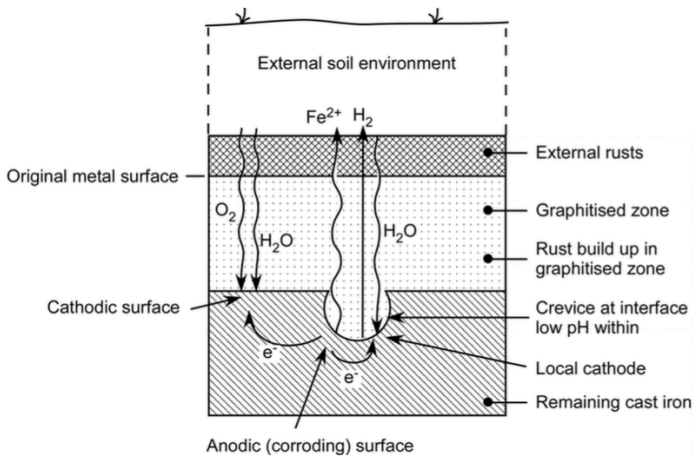

Figure 2.3 Schematic view of the corrosion of cast iron in reasonably moist, neutral, and aerated soil (Petersen, 2012)

LaQue (1958) states that the outward diffusion of ferrous ions is likely to govern since its atomic size is much larger than that of the other elements. The rate of diffusion of ferrous ions will be affected by the permeability, thickness of the graphitised zone, external rust and by the level of saturation of these layers.

The corrosion rate of cast iron in water is 0.759mm $year^{-1}$ at 28°C (Reynaud, 2006). According to Murray and Moran (1989), who monitored the moisture content of pipes buried in clay soil, corrosion the current density of corrosion depends primarily on the soil environment's moisture

content. Also, laboratory tests by Gupta and Gupta (1979) showed that the lowest corrosion rate occurred in soil with the highest resistivity. These tests were based on a 65% moisture content. Also, these researchers found that uniform corrosion was positively correlated with water content and negatively correlated with soil resistivity, and these correlations were reversed from local corrosion. A great deal of research has been done to investigate possible correlation between soil parameters and corrosion rate (Logan, 1947; Murray & Moran, 1989; Romanoff, 1957; Nicholas & Ferguson, 2005 and Cole & Marney, 2012). However, on the whole, only weak correlations have been found (Cole et al., 2012). It should be noted that often there is no relationship between the rate of iron release and the rate of corrosion (Benjamin et al., 1996).

2.5.1 Factors that Affect the Corrosion of Iron in Soil

There are many factors that influence the corrosion of iron in soil: soil type, moisture content, degree of aeration, resistivity, pore water chemistry, temperature and microbiological activity.

Soil type: The corrosiveness of a soil towards metal is affected by soil's physical properties, mineralogy and organic content (Jack & Wilmott, 2011). In engineering, soils are broadly classified into coarse-grained soils (sand and gravels), fine-grained soils (silts and clays) and highly organic soils (peats) (ASTM, 2011). Soils' physical properties, such as permeability, water holding capacity (e.g. particle size, particle distribution) and overall structure, have the strongest effects on corrosion. The soil permeability controls the rate of movement of water and air in soil. This can affect the soil moisture content next to the pipe and its variation with time and the degree of aeration. For example, coarse-grained soils have a high permeability, low water holding capacity, good drainage and good aeration; whereas fine-grained soils such as clays have a low permeability, high water holding capacity, and typically poor drainage and

poor aeration, and this causes the soil to behave corrosively next to cast iron pipes and increases the corrosion process.

Moisture content: Water is the essential electrolyte required for the electrochemical corrosion process (Roberge, 2008). The amount of water in the soil and (more importantly) in contact with the metal surface is a significant influencing factor for the corrosion of iron in soil. Practical observations and scientific investigations support this statement. Practical experience has shown that the corrosion of iron in a dry soil is much less than the corrosion of iron in a moist soil (Roberge, 2008). In a recent review of the scientific and engineering literature on iron corrosion in soils, Cole and Marney (2012) concluded that the only factor that is consistently found to control corrosion (rate and extent) is the soil moisture content. The corrosion rate of cast iron depends on the diffusion of ferrous ions away from the corroding surface. In the long term, the rate of corrosion is strongly influenced by the surrounding soil moisture content level in the vicinity of the anodic region. At a low moisture content levels (less than 25 % by weight), observations have shown that more rusts developed more quickly, resulting in a lower permeability of rust (and graphitised zone) layers and a lower corrosion rate (Tomashov, 1966; Gupta & Gupta, 1979). At high moisture content levels (higher than 25 % by weight), rust products tend to diffuse out into the external soil environment more easily, resulting in a higher permeability of rust (and graphitised zone) layers and a higher corrosion rate in the long term (Romanoff ,1957; Uhlig, 1963).

Degree of aeration: The ease of access/transport of oxygen in soil is called the degree of aeration, and this is related to the soil's physical properties and moisture content. Another related factor is the oxidation-reduction potential of the soil, which is the qualitative measure of the oxygen level at a particular level in a soil (Roberge, 2008; Jack & Wilmott, 2011). The degree of aeration reduces with increased moisture content and also reduces with soil density, and therefore burial depth (underlying soil is compressed by overlying soil layers). Also, oxygen levels typically decrease with burial depth, due to consumption by organic processes in the soil (Kreysa & Schütze, 2008). The available oxygen oxidises corrosion products into less soluble, more adherent products (Petersen, 2012). Compaction (by which the authors mean

densification, via compression) reduces the permeability of soil adjacent to the pipe and the access of oxygen (and water) to the cast iron surface is restricted (Romanoff, 1962 and Ohsaki, 1982).

Differential aeration: Variations in oxygen access to different regions of a metal pipe surface may result in the formation of a differential aeration cell across a relatively large distance. Differential aeration creates an oxygen concentration cell, where the surfaces with access to the greatest amount of oxygen become cathodic and the surfaces with restricted oxygen access become anodic (with associated metal loss). Variations in oxygen access in a soil may be the result of variations in soil type, moisture content, and degree of compaction (Petersen, 2012). Figure 2.4 shows the photograph of corrosion by a longitudinal difference in soil properties in contact with the pipe. The corroded area is located on the bottom of the pipe when the pipe was in service. Resistivity of the soil electrolyte is an important factor in the establishment of a different aeration cell (Peterson, 2012).

Figure 2.4 Corrosion caused by difference in the properties of the soil in contact with a pipe (Petersen, 2012)

Resistivity: The electrolytes dissolved in soil water carry the corrosion current between the anode and the cathode to complete the circuit required for corrosion to occur. The electric current is carried by ions in the electrolytes in the water. Soil resistivity is a measure of how strongly the soil opposes the flow of an electric current, and is the inverse of conductivity. Soil resistivity is influenced by a variety of factors including: solution ionic content, moisture content, soil type, degree of compaction, and temperature (Doyle et al., 2003; Roberge, 2008; National Highway Institute, 2009). Low values of soil resistivity are associated with: high solution ionic content, high moisture content, fine soil texture, low degree of compaction (i.e. densification), and high temperature. In general, it is believed that as soil resistivity decreases, the corrosion rate of buried iron or steel increases. Soils with resistivity values less than 2000 ohm-cm are generally considered corrosive (Jack & Wilmott, 2011; National Highway Institute, 2009; Doyle et al., 2003). Several researchers have attempted to correlate soil resistivity with corrosion (Gummow & Wakelin, 1993; Jakobs & Hewes, 1987; O'Day, 1989; Doyle et al., 2003). In general, only weak correlations between soil resistivity and corrosion have been observed (Cole & Marney, 2012). Tomashov (1966) suggests that corrosion in a soil can be divided into two different forms: a micro corrosion cell leading to general corrosion and a macro corrosion cell leading to localised corrosion. Micro corrosion cells form as a result of non-homogeneity in the composition of the metal structure. These cells are established over a short distance (of the order of 1 mm or less), with the anode and cathode located relatively close to one another (leading to general corrosion). A change in bulk soil resistivity has little effect on the rate of this type of corrosion. Macro corrosion cells form as a result of variations in the structural and chemical properties of the soil (and soil water) surrounding a metal. These cells are established over a long distance (of the order of metres), separating anode and cathode, and leading to localized corrosion. Low resistivity is considered to lead to acceleration of this type of corrosion (Tomashov, 1966; Jack & Wilmott, 2011; National Highway Institute, 2009).

Microbiologically influenced corrosion: The activity of micro-organisms (such as bacteria) in the soil may influence the rate and extent of corrosion. Several forms of bacteria have been implicated in the corrosion of ferrous metals, with the most attention given to Sulphate-Reducing Bacteria (SRB) (Roberge, 2008). There are many reports of accelerated corrosion in saturated soils in the presence of SRB (Von Wolzogen & Van der Vlugt, 1934; Jack & Wilmott, 2011; among others). Sulphate-reducing bacteria are only active in oxygen-free environments, such as in saturated soils and potentially within anoxic (oxygen-free) niches developed within rust layers. Saturated soils with high levels of organic matter and high levels of sulphates are typically considered aggressive to metals, due to the activity of SRB (Roberge, 2008; National Highway Institute, 2009).

Soil water chemistry: The pH of common soils typically varies between 5 and 8. In this range, pH has little direct effect on the corrosion rate, when compared with other factors (Roberge, 2008). However, some highly acidic or highly alkaline soils may be encountered. Acidic soils (pH of 3-6) occur in such natural environments as those containing a large amount of organic matter (Tomashov, 1966). The corrosion of iron as a function of pH increases considerably at pH values less than 4 (Uhlig, 1963; Jack & Wilmott, 2011). Under such conditions, the solubility of corrosion products increases and protective corrosion product layers are difficult to form. Both Reactions 2.0 and 2.1 occur simultaneously, uninhibited by corrosion product build-up, resulting in very appreciable corrosion rates (Uhlig, 1963).

The pH of alkaline soils (7.5-9.5) is unlikely to have a direct influence on corrosion rates. Some forms of alkaline soils (calcareous soils) contain high levels of calcium and magnesium ions in the pore water, which have the potential to form protective, carbonate deposits over cathodic surfaces (Roberge, 2008; Jack & Wilmott, 2011). The sulphate ion and the chloride ion have been identified as the most important dissolved anions in soil corrosion phenomena (Roberge, 2008; National Highway Institute, 2009; Jack & Wilmott, 2011).

Temperature: Tomashov (1996) has discussed the effect of temperature on corrosion rate. The rate of chemical reactions and diffusion processes generally increases exponentially with an increase in temperature, although the actual corrosion rate in a soil will not normally follow this trend. For example, an increase in temperature may lead to a drying of the soil, thus changing a major factor (moisture content), which complicates matters. Even though the corrosion processes are dependent on temperature, in practice, temperature is not considered a basic factor in soil corrosion. In fact, soil temperature is rarely recorded during field investigations of soil corrosion (Petersen, 2012). Tomashov (1966) states that soil temperature becomes a factor to be taken into account only when extremes in temperature are involved, such as when comparing corrosion in frozen soils with corrosion in unfrozen soils.

2.6 Flow Theories

The corrosion of buried cast iron takes a long time to occur naturally in soil (Schmidt, 2007). In order to accelerate the corrosion process, the electrokinetic method can be used. Therefore, it is important to understand the method and its effects on the clay. It is well known in geotechnical engineering that applying an electric field to clays and silt results in a strengthening of the soil (Casagrande, 1948 and 1949).

The flow of water plays an important role in the deformation, volume change and stability behaviour of clays themselves and thus can control the rates at which the process occurs. Therefore, the flow of water through soil has been extensively studied because of its essential role in geotechnical problems, which form a major part of engineering analysis and design. Mitchell et al. (2005) identified four different flows in soil (see Figure 2.5). Different flow regimes cause a flow rate flux, $J_{i,}$ in ion movements, fluids, electricity, chemicals and heat flow, and this is linearly related to the driving force, $X_{i,}$ according to:

$$J_i = L_{ii} X_i \qquad \text{[Equ. 2.1]}$$

where L_{ii} is the conductivity coefficient for flow. In the case of using a phenomenological coefficient for a cross section area, A, each flow is described with different laws, which are as follows:

Water flow	$q_h = K_h\, i_h\, A$	Darcy's law	[Equ. 2.2]
Heat flow	$q_t = K_t\, i_t\, A$	Fourier's law	[Equ. 2.3]
Electrical flow	$I = \sigma_e\, i_e\, A$	Ohm's law	[Equ. 2.4]
Chemical flow	$J_D = D i_c\, A$	Fick's law	[Equ. 2.5]

It should be noted that the corrosion of cast iron changes the chemistry and electric charge around the pipe. Heat flow does not have an important effect, and it is chemical and electrical flows that are the most important (Schmidt, 2007). These flows often occur parallel to each other in the soil.

Water flow [Equ. 2.2] (fluid flow) within soil is a function of the degree of saturation, particle size and packing arrangement, and temperature (Barker et al., 2004). The hydraulic conductivity of soils depends on the clay content, the sedimentation procedure, the compression rate and the electrolyte concentration (Mitchell & Soga, 2005).

Electric flow [Equ. 2.4] or electrical conductance is the transport of ions due to an electrical potential applied across a medium. The electrical conductivity value depends on several properties of the soil, such as porosity, degree of saturation, composition (conductivity) of the pore water, mineralogy (as it affects particle size, shape, and surface conductance), soil structure (fabric and cementation) and temperature (Mitchell & Soga, 2005). According to Barker et al. (2004), the specific factors affecting the conductivity of soil undergoing treatment

include the following:

- The solubility of the minerals present, which is a function of pH. A reduction in pH from around pH 8.0 to 7.0 causes the solubility of aluminium oxide (a predominantly clay mineral) to reduce slightly.
- The migration of ions into and out of the soil. An applied electrical current causes anions and cations within the pore fluid to migrate towards the anode and cathode, respectively. Ions are also introduced through the addition of chemical solution at the electrodes and corrosion at the anode.
- The precipitation of compounds as ions mix within the pore fluid. As the species of ions alter within the pore fluid, compounds are formed that may be more sensitive to changes in pH over the ranges observed, thus resulting in precipitation.

Chemical flow [Equ. 2.5], or diffusion, is the transport of a chemical species due to a gradient in its concentration. This net transport of chemicals from an area of high concentration to an area of low concentration is the result of random molecular motions (Mitchell et al., 2005).

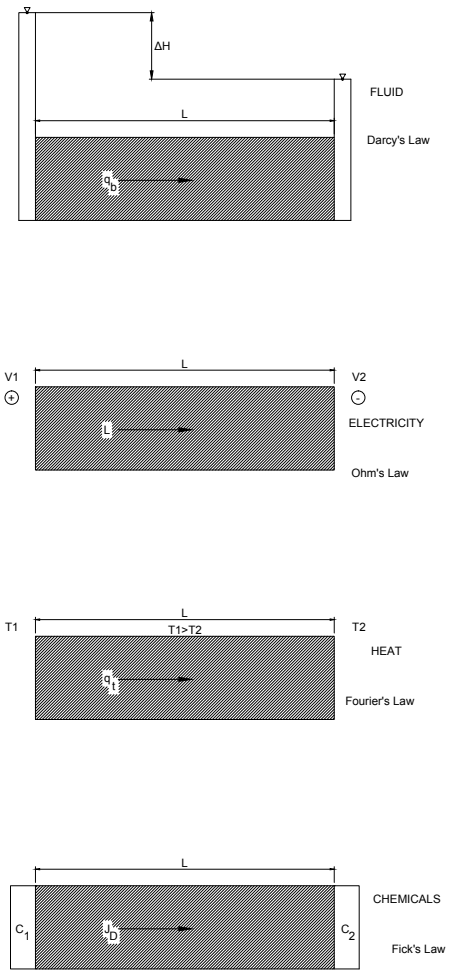

Figure 2.5 Four types of direct flow through a porous mass of soil. A is the total cross-section area normal to flow and n is the porosity (Mitchell et al., 2005)

2.7 Electrokinetic Phenomena in Soils

Electrokinetics is defined as the physicochemical transport of charge, the action of charged particles and the effects of applied electric potentials on the formation and transport of fluid in porous media.

Mitchell and Soga (2005) state that the coupling of electrical and hydraulic flows and gradients can develop four related electrokinetic phenomena in material such as fine grain soils: electroosmosis, streaming potential, electrophoresis and sedimentation potential (see Figure 2.6). A further major phenomenon reported by Acar and Alshawabkeh (1993) and Yeung (2006) that occurs when an electric field is applied to any soil sample is electromigration.

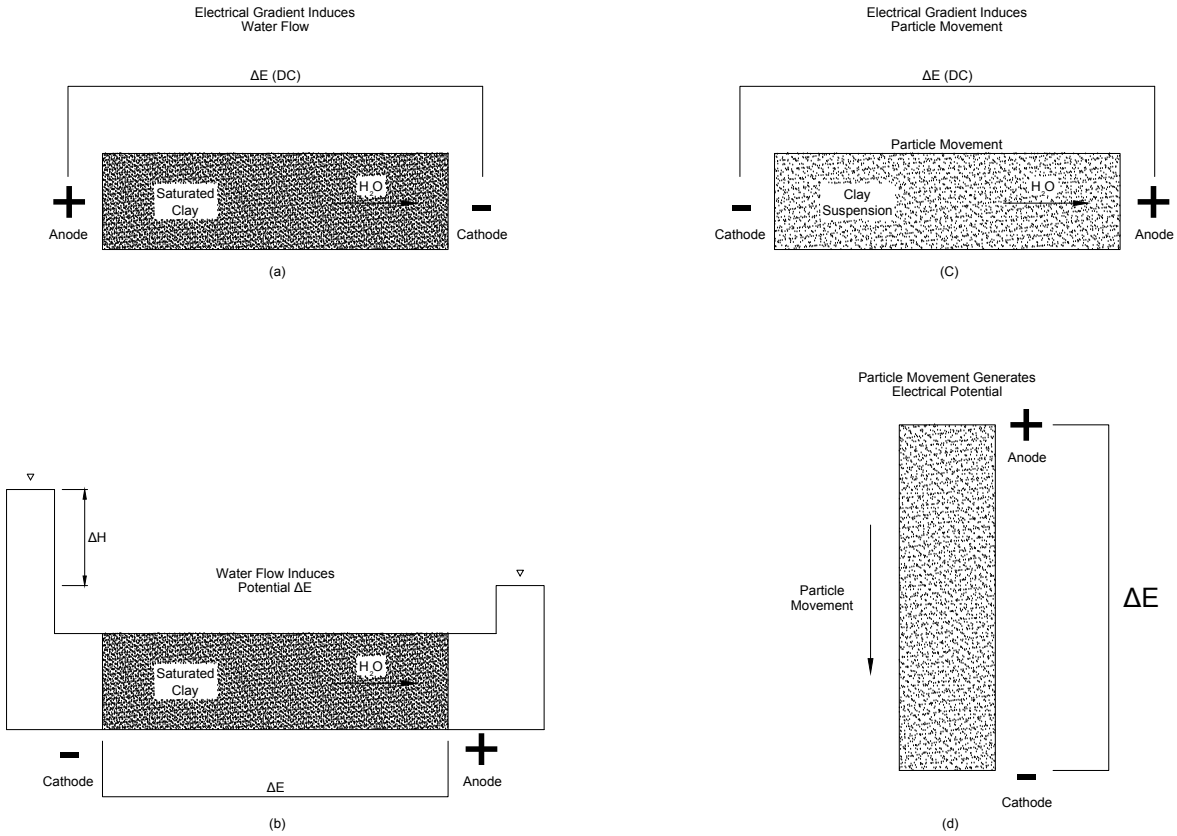

Figure 2.6 Electrokinetic phenomena: (a) electroosmosis, (b) streaming potential, (c) electrophoresis, and (d) migration or sediment potential (Mitchell & Soga, 2005)

Electroosmosis is defined as water movement as a result of an applied electric potential gradient (Figure 2.6 (a)). When an electrical potential is applied across a wet soil mass, cations are attracted to the cathode and anions to the anode. As ions migrate, they carry their water of hydration and exert a viscous drag on the water around them. Since in a negatively charged clay there is a net water flow towards the cathode, there are more mobile cations than anions. As a result, a net flow of pore water takes place in the diffuse double layer towards the cathode relative to the stationary soil particles. This motion of double layer water applies a viscous force to the free pore water. The result is that pore water moves towards the cathode in response to the applied electrical gradient (Mitchell & Soga, 2005).

Electroosmosis is a phenomenon that occurs only in soils containing particles with a charged surface. It is a function of the excess of positively charged ions over negatively charged ones,

or vice versa (in which case the direction of water flow is reversed). It therefore does not occur in sands, silts or gravels unless an appreciable amount of clay particles is present (Harbottle, 2003).

When water flows through a soil under a hydraulic gradient, the double layer charge is displaced in the direction of the flow. This develops an electric potential difference that is proportional to the hydraulic flow rate, which is called **streaming potential** (see Figure 2.6 (b)) (Mitchell & Soga, 2005).

Electrophoresis is the phenomenon that occurs when a direct current electric field is applied across a clay suspension. The negatively charged particles are attracted electrostatically to the anode, while they are repelled from the cathode, as shown in Figure 2.6(c). This involves discrete particle transport through water, while electroosmosis involves water transport through a continuous soil particle network (Mitchell & Soga, 2005).

Electromigration (see Figure 2.6 (d)) is the transport of ions in pore fluid due to electrostatic attraction. When a direct current electric field is applied across the soil, positive ions will be attracted to the cathode and negative ions to the anode. Experiments by Acar and Alshawabkeh (1993) demonstrate that when the initial ionic conductivity of pore fluid is high and when the initial soil pH is between 2 and 3, the electroosmotic process is not efficient, while the ionic species are transported efficiently by electromigration. Electromigration is the major transport mechanism for ionic species under electric fields in soils. Consequently, in a porous medium with conductive water, it seems that electromigration is the major cause of charge transport relative to electroosmosis. Furthermore, the mechanism depends mainly on ion mobility (Paillat et al., 2000). Electrical migration will increase when species ionic concentration increases (Hamnett, 1980).

2.7.1 Electrochemical Effects

There are other mechanisms affecting the electrokinetic process along with the main effects of the electrokinetic technique. These include the electrolysis of pore water molecules and the reaction of electrodes to the application of electric current.

Electrolysis takes place due to the oxidation and reduction reactions occurring at the anode and the cathode respectively. Liaki (2006) and Acar and Alshawabkeh (1993) state that electrolysis reactions dominate the chemistry at the boundaries. When an electrical potential is applied between two electrodes that are submerged into water, the oxidation and reduction take place as a results in the release of oxygen and hydrogen respectively:

At the **anode**: $2H_2O \rightarrow O_2(g) + 4H^+ + 4e^-$ [Equ. 2.6]

At the **cathode**: $4H_2O + 4e^- \rightarrow 2H_2(g) + 4OH^-$ [Equ. 2.7]

If these resulting ions are not removed or neutralised, an acid front will form around the anode, whereas a base front will develop around the cathode. Hydrogen ions that are produced at anode by electrolysis of ware are removed towards the cathode via electro migration, diffusion and electroosmosis, resulting in a low pH near the anode area. Hydroxide ions produced at the cathode are transported into the soil against the flow of water via electromigration and diffusion resulting in an area of high pH near cathode (Barker et al., 2004). These fronts will move towards each other due to the electrical gradient applied. The acid front moves more rapidly, and thus over a much greater distance, than the base front (Acar et al., 1990). These fonts migrate towards each other under the electrical gradient, with the soil being neutral where these fronts meet. The change in pH at the electrodes that occurs under an applied electric potential not only causes the development of pH gradient across the soil sample, but also influences the solubility of the electroytes. The acid front produced at the anode causes desorption, dissolution and ionization of cationic metals, which then migrate toward the cathode. Some of the

exchangeable cations on the clay may be replaced by the hydrogen ions. This, coupled with high acidity and oxidation, causes rapid deterioration of the anode, and the clays will soon tend to alter due to aluminium or iron release into the system, the form that this takes depending on the anode material. As a result, the soil is usually strengthened in the vicinity of the anode (Mitchell & Soga, 2005).

When the electric current passes through an electrode surface in one direction or the other, an electrochemical reaction always takes place. This is called an electrode reaction. The electrode reaction at the anode is always an oxidation reaction. The cathode reaction on the other hand is always a reduction (Liaki, 2006). The reactions that occur between the electrodes and pore water depend on the characteristic of the pore water and the material properties of the electrodes (Barker et al., 2004).

In geotechnical applications, electrokinetic processes have been reported by many researchers to increase the shear strength of soils (Ozkan et al., 1999; Alshawabkeh & Sheahan, 2003; Asavadorndeja & Glawe, 2005) and to change the Atterberg limits of the soil (Ozkan et al., 1999; Rogers et al., 2003; Barker et al., 2004; Asavadorndeja & Glawe, 2005; Jayasekara & Hall, 2006). Changes in the physical properties are attributed to the electrochemical effects under the influence of an electrical gradient, including electroosmosis, electromigration, electrolysis, hydrolysis, degradation of electrodes. These processes are variable across the soil samples from the anode to the cathode, which contributes to the changes in the physicochemical properties of the treated soil. The electrochemical effect can also be related to the clay-water-electrolytic system that leads to the dissolution of chemical compounds or clay minerals, ion exchange capacity, adsorption, desorption, complexation, precipitation and mineralisation. The reaction that occurs between the electrodes and pore water depends on the characteristics of the pore water and the material properties of the electrodes (Barker et al.,

2004), but the general pattern is as recorded above (oxidation at the anode to generate a lowered pH and an acid front, reduction at the cathode to create a raised pH and an alkaline front, Jayasekera & Hall, 2006). The development of this pH gradient and its effects on the species transport through soil porous medium have been investigated in detail and well documented by many researchers, including Ozkan et al. (1999), Rogers et al. (2003), Alshawabkeh and Sheahan (2003), Barker et al. (2004), Asavadorndeja and Glawe (2005) and Liaki et al. (2010).

In electrokinetic treatments, when cations such as iron or aluminium are released through the sample, the ions migrate into soils through a process of electroosmosis and electromigration. These ions improve the soil strength by cation replacement, precipitation of species in the pore fluid and mineralisation. These reactions are caused when the pH values of the soil solution are greater than 7 (Barker et al., 2004; Asavadorndeja & Glawe, 2005). According to Boardman et al. (2004) describe the solubility of some common metal hydroxides as a function of pH, as illustrated in Figures 2.7 and 2.8.

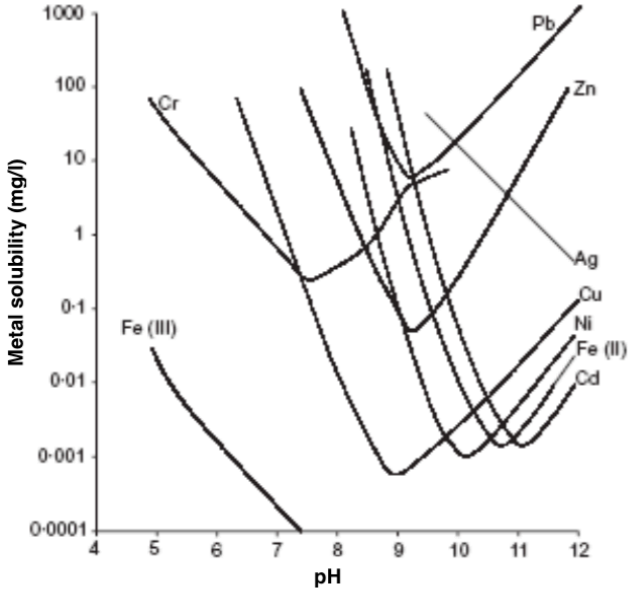

Figure 2.7 Solubilities of metal hydroxides as a function of pH (Boardman et al., 2004)

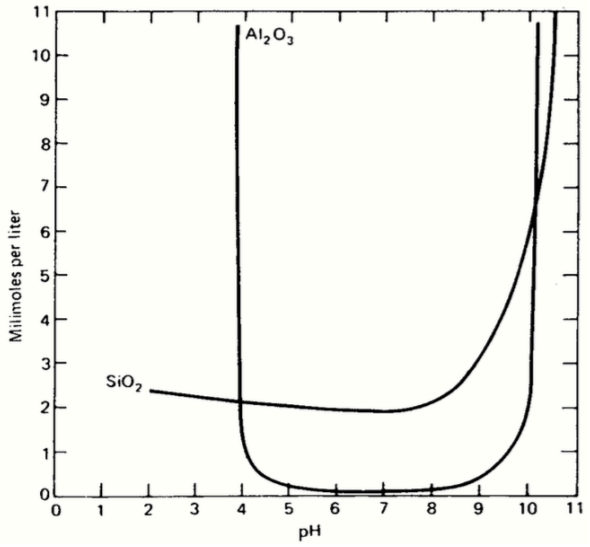

Figure 2.8 Solubility of alumina and amorphous silica in water (Mitchell & Soga, 2005)

In short test times, researchers found that at the beginning of the test, the soil is weakened at the anode due to the acidification of the soils causing dissolution of carbonates, silicates and hydroxides of aluminium and iron (depending on the solubility of the metal compounds at low pH). As the time increases and the water content can reduce (unless the water is replenished), the release of these cations from the clay surface or clay mineral lattice will be replaced by stronger valence cations, larger cations or a concentration of cations by mass action. This displacement causes a decrease in the thickness of the diffuse double layer and thus promotes the edge-to-edge attraction, closer contact of clay platelets, or flocculation, and results in improvement of the soil properties (Rogers et al., 200; Barker et al., 2004). This is also called molecular bonding and these bonds are weakened on moistening (Zhinkin**,** 1960; Adamson et al., 1966). Subsequently, stronger and more stable bonds arise between the soil particles and the strength as a whole can be attributed to a 'coagulation crystallisational' process. In some clays (such as Oxford Clay), there are metal oxides, oxyhydroxides and hydrous oxides, which may exist as discrete crystals, as coatings on phylosilicate and a humic substance, as a mixed

gel, and are collectively part of the secondary mineral (Faulkner, 2010). Naturally occurring metal oxides, oxyhydroxides and hydrous oxides in clays are listed in Table 2.2.

Table 2.2 Some naturally occuring oxides, oxyhydroxides and hydroxides found in soils (after Faulkner, 2010)

Aluminium oxides	Bayerite α-$Al(OH)_3$ Boehmite γ-AlOOH Diaspora α-AlOOH Gibbsite γ-$Al(OH)_3$
Iron Oxides	Alkagnite β-FeOOH Ferrihydrite $Fe_{10}O_{15}.9H_2O$ Feroxyhyte δ-FeOOH Goethite α-FeOOH Hematite α-Fe_2O_3 Lepidocrocite γ-Fe_2O_3 Maghemite γ-Fe_2O_3 Magnetite Fe_3O_4
Manganese Oxides	Birnessite δ-MnO_2 Pyrolusite β-MnO_2
Titanium oxides	Anatase TiO_2 Rutile TiO_2

However, under extreme alkalinic environments (high pH) cause by the electrokinetic process, this compound may disassociate and react with the other metal cations available and then re-precipitate to form a new secondary mineral, which completely changes the mineralogy of the soil. These crystalline bonds are also intensified with time and retained regardless of consequent wetting of the soils. The growth of these bonds increases the density and stability of the soils and are known to be permanent with time (Adamson et al., 1966). Therefore, these phenomena, which contribute to the soil strengthening and weakening, are a function of time. Barker et al. (2004) suggested that the alkaline environment developed at the cathode causes the dissolution of clay minerals (silica and/or alumina) and subsequent reaction with available metal cations (such as iron or calcium), which could precipitate to from amorphous aluminate

and/or silicate gels. This cementation agent will harden with time (due to the crystalline process) and consequently increases the soil shear strength. Therefore, the studies based on the electrokinetic stabilisation method that were initiated by Rogers et al. (2003) have confirmed that this phenomenon is permanent if sufficient calcium ions are introduced into the system (Barker et al., 2004) or Fe ions are introduced from the source of the anode (e.g. cast iron), with these ions migrating to the cathode area. According to Barker et al. (2004), the dissolution of alumina and silica at higher pH (pH>8) is needed for the formation of CAH and CSH gels. Therefore, the results from these studies have demonstrated the ability of the electrokinetic method to promote the precipitation of insoluble salts based on the results of pH and conductivity.

There are significant changes in the properties of the soil under the influence of an electric gradient. The most important factors to consider when using electrokinetics are shear strength, water content, Atterberg Limits, pH, conductivity and chemical concentration effects. In geotechnical engineering, the changes of physiochemical properties of the soil can be determined from Atterberg limit values, and thus these tests provide a good indication of electrochemical effects across a soil system. The introduction of ions into the system during the process of electrokinetic stabilization had been shown to cause variation of plastic and liquid limit values among different clay mineral groups (Barker et al., 2004; Liaki, 2006).

The three mechanisms that are associated with electrochemical effects to cause increases in shear strength are preliminary cation exchange, precipitation and mineralisation (Tajudin, 2012). Despite the preference for ions of high ‘replacing power’ (being a combination of valency and size), cations with lower ‘replacing power’ can still replace cations with higher ‘replacing power’ by mass action, provided that the ratio of concentrations of the cations of lower to higher ‘replacing power’ is sufficiently high (Mitchell & Soga, 2005). The cation

exchange will stop after reaching equilibrium. It has been found that most of the studies reported by Ozkan et al. (1999), Rogers et al. (2003), Alshawabkeh & Sheahan (2003), Barker et al. (2004), Asavadorndeja & Glawe (2005), Ou et al. (2009), Ahmad et al. (2011) and Tajudin (2012) are in the agreement, all observing an increase in shear strength. As electrokinetics generates a differential pH environment across the soil sample, some chemical elements such as Al and Si that are available in the pore fluid between the soil particles, adsorbed on clay surface or within clay mineral itself may be released under appropriate pH conditions and be replaced by other ions. Some of them may complex with other ions and some will be flushed out from the system under electrokinetic process (Tajudin, 2012).

Kaolin Clays have been widely used for investigation of the electrokinetic application in the laboratory, with only a few researchers using different types of soil, which include illite soils (Esrig & Gemeinhardt, 1967; Gray, 1970; Alshawabkeh & Sheahan, 2003; Ou et al., 2009). Where a high pH environment causes compound dissociation, reaction with the other metal cations and reprecipitation to form a new secondary mineral, the crystalline bonds increase with time and this increases the density of the soil, a change that is known to be permanent (Adamson et al., 1966). Thus these reactions that cause the soil to strengthen and weaken are a function of time.

In order to verify the mechanism contributing to the increase of soil shear strength, it is essential to validate the changes taking place with Atterberg limits results. Changes in Atterberg limits are responsive to the electrochemical process and chemical stabilisation through alteration made to the structure and fabric of the clay, modifications to clay mineralogy and the type of exchangeable ions (Tajudin, 2012). Mitchell and Soga (2005) stated that increasing the cation valence decreases the liquid limit values of expensive clay, such as montmorillonite, but tends to increase the liquid limit of non-expansive clays such as kaolinite. Increases in liquid limit

have been observed by many research studies due to the soil cementation in the vicinity of the cathode generated by electrochemical reactions after the introduction of chemicals at the electrodes or caused by degradation of the anode (Ozkan, et al., 1999; Asavadorndeja & Glawe, 2005; Jayasekera & Hall 2006). The factors contributing the Atterberg limits include pH, electrolyte concentration, thickness of the double layer relative to cation exchange and precipitation, types of clay mineral, secondary minerals from crystallisation processes, and the types of exchangeable ions (Schifano, 2001).

Liaki et al. (2010) have found an increase in the liquid limit at the anode and a decrease at the cathode when using steel electrodes, while liquid limits had an opposite trend when using inert electrodes (and no chemicals were introduced at the electrodes) for kaolinite Clays. This is due to the additional higher valency positive ions (such as Fe ions) coming into the system from the degradation of the steel anode and further thinning of the diffuse double layer via cation exchange. The low liquid limit occurs at the cathode due to the opposite phenomenon, i.e. a raised pH and a thickening of the diffuse double layer. Therefore, the changes in Atterberg limits are governed by the electrochemical effects, which changes across the soil sample under an electric current.

According to Barker et al. (2004), the result of cation exchange is a considerable reduction in the thickness of the diffused double layer. This allows closer contact between the clay platelets that promotes edge-to-edge attraction, or flocculation, and results in changes in the soil workability, permeability, plasticity and swelling properties. On the other hand, the precipitation of metal hydroxides can also be assessed by changes in plasticity of the soil. Again this changes the thickness of the diffuse double layer and it forms a relatively strong and brittle solid. However, these two mechanisms have opposite effects in term of the thickness of the

double layer, although interestingly both mechanisms have resulted in positive increments of shear strength. This strengthening effect could be validated by the combining strength measurements with the results from both water content and chemical tests (conductivity and pH) (Liaki, 2006).

Where the electrochemical processes cause a large pH gradient, this causes changes to the chemistry of the pore fluid and leads to alteration of the soil structure, and even soil mineralogy, especially at the anode and cathode. pH measurement, to evaluate the effectiveness of cation exchange and precipitation phenomena, can directly indicate effects on the physical properties of the soil such as shear strength and Atterberg limits (Tajudin, 2012).

The chemical concentration levels in the electrochemical system indicate which ions have migrated across the soil sample and subsequently which have been flushed out through the cathode drainage. Metals ions such as Fe and Al exist in the soil as multivalent cations, either in the pore fluid and/or absorbed on soil surface and/or within the clay mineral itself. As stated above, the release of cations from a clay soil and dissolution of the clay mineral is dependent on the pH environment – for example, dissolution of alumina can occur in small quantities at a pH less than 7 and starts to increase significantly at a pH > 8, reaching a maximum when the pH has reached 11 (Barker et al., 2004) while dissolution of silica is negligible at pH < 8 but becomes significant at pH more than 10 (see also Figure 2.7).

2.8 Clays

The term clay refers to a naturally occurring material composed primarily of fine-grained minerals, which is generally plastic at appropriate water contents and will harden when dried or fired. Although clay usually contains phyllosilicates (the group of silicate minerals that contains composite layers of tetrahedrally coordinated Si, Al and octahedrally coordinated cations, principally Fe^{3+}, Fe^{2+}, Al, Mg), it may contain other minerals that impart plasticity and harden when dried or fired. Associated phase in clay may include materials that do not impart plasticity and organic matter. Clay minerals contain about 45% of sedimentary minerals, essentially, silica, alumina and water in variable combinations, frequently with appropriable quantities of iron and alkaline earths (Reeves et al., 2006). In British civil engineering practice, clay is defined as a material made up of particles less than 0.002mm in size (BSI, 1999), although some clays might have larger particles than this. BSI (1999) defines silt by mechanical analysis as having particles between 0.06 and 0.002mm. Thus clay is defined without reference to its mineralogical composition (Reeves et al., 2006).

2.8.1 Clay Mineralogy

The clay minerals are a group of hydrous aluminosillicates that are characteristically found in clay (<0.002 mm), fractions of sediments and soil, and have a sheet silicate structure. Most clay minerals belong to the kaolinite, montmorillonite and illite groups. Their crystal structure is similar to that of mica, with strong intra and intrasheet bonding but weak interlayer bonding (Reeves et al., 2006). Clay minerals have two types of composite layer: the 1:1 type, which is one tetrahedral to one octahedral (two layers), such as Kaolin and the serpentine groups; and the 2:1 type (three layers), which is one octahedral to two tetrahedrals and is represented by the illite, mica, smectite, vermiculite and chlorite groups. In the 2:1 layer minerals, one alumina

or magnesium sheet shares oxygen atoms with two silica sheets, one on each side. The combination of an octahedral sheet and one or two tetrahedral sheets is called a layer. Most clay minerals consist of such layers, which are tacked parallel to each other (Van Olphen, 1977).

Clay minerals are usually amorphous (see Figure 2.9), and due to isomorphous substitution of Si and Al, or the dissociation of hydroxyl ions, carry a residual negative charge. This result in the attraction of cations from a solution to the clay mineral surface, forming a double layer of tightly bound ions on the clay particle surface and a dispersed layer of cations (Reeves et al., 2006).

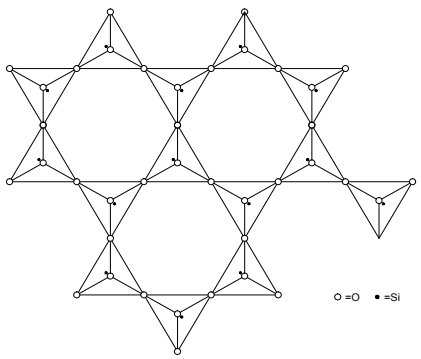

Figure 2.9 The silica sheet (Ciullo, 1996)

2.8.1.1 The Kaolin and the Serpentine Group

Kaolinite is common in humid climates, well-leached acid soil and stream sediments where there is good drainage. Kaolinite forms from weathering of potassium feldspar and muscovite mica in rocks such as granite. In conditions of high rainfall and good drainage, kaolinite is destroyed through loss of silica and becoming unstable to $Al(OH)_3$ (gibbsite). Increase of rainfall and infiltration decreases the pH of the soil, and cation and silica concentrations. As

kaolinite lacks structural cations other than relatively insoluble aluminium and silicon, it is the clay most stable under acid-weathering conditions (Langmuir, 1997). The Kaolin group are isometrical 1:1 layer silicate $Al_4Si_4O_{10}(OH)_8$ but not isostructural. They have a dioctahedral structure with no negative charge on the composite layer, and consequently no compensating interlayer cations or water layers (Reeves at el., 2006). They are non-swelling clay with interlayer spacing 7Å. Halloysite is a kaolin group mineral that contains one water layer in interlayer sites and produces 10Å in inter layer spacing ($Al_4Si_4O_{10}(OH)_8.H_2O$). The serpentine group of minerals is the trioctahedral equivalent of the Kaolin group. The most important member of the serpentine group is berthierine [$(Fe^{2+}, Mg)_{6-x}$ $(Fe^{3+}, Al)_xSi_{4-x})$ $O_{16}(OH)_8$)] (Reeves et al., 2006). Kaolinite has been shown to dissolve and precipitate reversibly and thus attain thermodynamic equilibrium at 25ºC (May et al., 1986; Nagy et al., 1991).

2.8.1.2 The Illite-Mica Group

Illite clays are result of the weathering of micas (silicates) and alkali feldspars under alkaline conditions. Their formation in soils and sediments is favoured by high K^+ and moderate silica concentrations. When smectites or mixed layer smectite/illite clay are buried in deep sedimentary basins, they are gradually transformed into more stable illites by a combination of time and temperature (Velde & Vasseur 1992, Huang et al. 1993, Cuardos & Linarres, 1996). The rate of smectite/illite reaction is thus directly proportional to K^+ and H^+, although it depends on Mg^{2+} and is influenced by dissolved silica and Na^+ (Langmuir, 1997). Illites mostly have a dioctahedral 2:1 or three-layer composite structure with the general formula ($K_{1-1.5}$ Al_4 $(Si, Al)_8$ $O_{20}(OH)_4$ and with a non-exchangeable cation of K with subordinate Na and Ca. Substitution $[Si^{4+}]^{IV}$ by $[Al^{3+}]^{IV}$ and $[R^{3+}]^{IV}$ by $[R^{2+}]^{IV}$ produces a net negative charge of 0.7-0.1 per $O_{10}(OH)_2$ formula unit. The excess negative charge result in compensated for by interlayer K^+ ions that are hold electrostatically and fairly strongly between adjacent tetrahedral

layers and lenses of water may be present in interlayer sites. Also, they have non-swelling properties. Micas are relatively hard and elastic and the potassium ions not readily exchangeable (an Al^{3+} ion substitutes for about one of every four Si^{4+} ions in the tetrahedral layer). Micas are included muscovite (dioctshedral), phlogopite (trioctahedral), and biotite, which is similar to phligopite but with Fe^{2+} substitution for Mg^{2+} in some octahedral site. The micas have a repeat basal spacing about 10 Å. Mucotive and biotite are common in igneous and metamorphic rocks. Ideal compositions of micas are (Langmuir, 1997):

Muscovite: $KAl_2(AlSi_3O_{10})(OH)_2$

Phlogopite: $KMg_3(AlSi_3O_{10})(OH)_2$

Biotite: $K(Mg,Fe)_3(AlSi_3O_{10})(OH)_2$

In biotite up to approximately 75% of the octahedral Mg in phlogopite can be replaced by Fe^{2+} (Deer et al., 1992). Because they are dominant mineral in shales, illites, and illite-smectites are the most abundant of all clays. Illites are defined as mica like material less than 2μ in size, which like the micas, have a basal spacing of 10 Å (Drever, 1988). Most illites are dioctahedral and structurally similar to muscovite, although some are trioctahedral like biotite. Illites contain less K^+ and Al^{3+} and some Si^{4+} than muscovite. They usually contain some Mg^{2+} and Fe. The irregularity of occurrence of interlayer K^+ makes bonding between the layers weaker than in muscovite. Illitic clays are usually mixed-layer clays, with illite making up perhaps 80% of the clay layers and smectite the rest. All illites contain a smectite layer of montmorillonite or biedellite composition (Deer et al., 1992) and therefore are named mixed-layer illite-smectite (I/S) clays.

2.8.1.3 The Smectite (Montmorillonite) Group

Smectite clays such as montmorillonite are formed by relatively poor drainage, alkaline pHs, high concentrations of silica and divalent cations, and low potassium concentrations. They tend to form early in the weathering of unstable Fe-, Mg-, and Ca- rich minerals in igneous or metamorphic rocks (Langmuir, 1997). Smectites are three layers or 2:1 clay minerals (similar to the basic structure of illites) that are commonly dioctahedral, although trioctahedral varieties do exist and has interlayer repeat distance expands to 17 Å. They have a layer charge of 0.2-0.6 per $O_{10}(OH)_2$ unit of structure, which is offset by hydrated interlayer cations, principally Ca and Na. The hydration of the interlayer cations causes the interlayer crystalline swelling that characterizes the smectites. The interlayer cations are adsorbed to balance the unsatisfied net charge (usually negative charge) of the clay crystal lattice caused by structural substitutions or vacancies in the octahedral and/or tetrahedral layers. They have the general formula $M^{2}/_{3}(X, Y)_{4-6}$ (Si, Al)O_{20} $(OH)_4.nH_2O$, where M = Na or Ca, X = Al or Fe^{3+}, Y = Mg or Fe^{2+}. Na and Ca are the exchangeable ions and can absorb up to three layers at 90% relative humidity, but in some instances at 100% humidity (Mitchell & Soga, 2005). Water is normally present in the interlayer space of smectites. When Mg^{2+} or Ca^{2+} occur in interlayer space, about two water layers separate the clay layers. This creates a spacing layout 14Å. When Na^{+} is the interlayer cation large amounts of water can enter the interlayer space and swelling of clay ensues. This decreases the permeability of smectite rich soil (Langmuir, 1997).

2.8.1.4 The Vermiculte Group

Vermiculite clay are formed as a results of the weathering and partial degradation of biotite or phlogopite micas or of other iron- and magnesium-rich aluminisilicates. Vermiculite have similar structure to the smectite group but have a large net negative charge on the composite

layer of 0.6-0.8 per $O_{10}(OH)_2$ due to having Mg as the principal interlayer cation. They have similar swelling properties to smectites, but to a lesser extent, due to the higher layer change. Vermiculites are trioctahedral with the general formula $Mg,Ca^{(x-y)/2}(Mg, Fe^{2+})_{3-5}(Al, Fe^{3+})Y(Si_{4-X} Al_X) O_{10}(OH)_X.nH_2O$ (Mitchell & Soga, 2005). Where Mg and Ca are the adsorbed interlayer cations and the interlayer cations in Vermiculite are diavalent. As in smectites, the vermiculites have the highest cation exchange capacities among the clays and the interlayer charge in vermiculite results from substitution of Al^{3+} for Si^{4+} in tetrahedral layer and Mg is the cation in the octahedral layer. Drever (1988) mentioned that when Mg^{2+} is the interlayer cation, two water layers occupy the interlayer space, and the basal spacing is about 14Å.

2.8.1.5 The Chlorite Group

Chlorites have a 2:1 type structure with a second octahedral layer in the interlayer sites having a net positive charge to offset the net negative charge on the 2:1 layers. They consist of a heterogeneous group of layer silicates with the general formula $(Mg,Fe)_{10}Al_2(Si,Al)_8O_2(OH, F)_{16}$. The majority of the chlorites are trioctahedral, but some dioctahedral and mixed dioctahedral 2:1 - trioctahedral (interlayer) forms are known. They are common products of alteration from ferromagnesian minerals, and may be present as mixed layer clays with illite and montmorillonite (Reeves et al., 2006; Mitchell & Soga, 2005).

2.8.2 Clay Properties

The swelling properties of clay minerals depend on the behaviour of the water sorption onto the clay surface or into the clay interlayer sites. Different types of clay have different

behaviours, so that there are swelling and non-swelling varieties. As the Table 2.3 shows, swelling clays are smectites and vermicultes and non-swelling clays are kaolinite, illite and chlorite. Clay minerals such as illite have lenses of water in the interlayer site but do not show intra particle swelling properties. All clay minerals can show interparticle swelling, governed by similar factors to those that control the intraparticle swelling that is characteristic of clay minerals, and concentrations of cations absorbed onto the clay surface in the diffuse double layer and hydration of surface cations. Interparticle association of clays controls their flocculation and dispersion in natural waters (Reeves et al., 2006).

Table 2.3 Classification of clay minerals (Reeves et al., 2006)

Sheet silicate type	Property
(1:1 type)	
Kaolinite and serpentine	Non-swelling
(2:1 type)	
Illite	Non-swelling
Chlorite	Non-swelling
Smectites (montmorillonite)	Swelling
Vermiculite	Swelling

The high surface area results from the small particle size and platy or elongate morphology of the minerals and the negative charge from ionic substitutions in the crystal structure. The charge is now through to occur as discrete charge rather than as a uniform distribution over the surface (Gillot, 1987). Kaolin ideally has neutral composite layer structures, but in reality limited cation substitution may occur producing a very small net negative charge on the composite layer offset by a small number of interlayer cations (Reeves et al., 2006).

On the edge of clay particles, the disruption of the clay structure produces broken-bond-edge sites, which may be negatively or positively charged. The nature of the charge is determined by the presence of certain ions, notably H^+, OH^-, Al^{3+} and AlO_4^{5-}, whose presence is pH

dependent, being negatively charged in acid solutions. This pH-dependent charge accounts for only a small percentage of the total charge in illite and smectite, but is more significant for Kaolin and chlorites. Also, it is possible to have anion exchange, but usually to a lesser extent than cation exchange. The ions principally adsorbed onto the clay surfaces, and to a lesser extent on the edge of clay particles, can be exchanged with other available ions. This gives rise to the phenomena of cation/anion exchange (Reeves et al., 2006).

2.8.3 Clay-Water- Electrolyte System Interaction

When the water is in contact with soils particle, the water is strongly attracted to the soil particles and sorption of water onto the surface of the soil particles influences the physical and physiochemical behaviour of the mixture (Mitchell & Soga, 2005). Ingles (1968) discussed the fact that it is due to the high degree of hydration and the energy of aluminium in clay structures that water is so strongly attracted to the surface of clay particles. Clays are lyophobic or hydrophobic colloids, even though water wets clay and is absorbed on the clay particle surface (Mitchell & Soga, 2005). Colloids characteristically have large surface areas and a strong tendency to absorb other materials. Hydrophobic colloids are the liquid dispersion of small, solid particles that are two-phase systems with a large interfacial surface area, and they have a behaviour dominated by surface forces. Also, they can flocculate in the presence of small amounts of salt (Mitchell & Soga, 2005). The colloidal activities of the clay minerals depend on their specific surface area (meters squared per gram) and the charge density expressed by their cation exchange capacity divided by their specific surface area. Kaolinite is a widespread 1:1 clay mineral with low CEC (1-15 meq/100g), low surface area (10-15 m^2/g), and low colloidal activity (Shainberg & Levy, 2005). Its clay particles are small and platy with a large surface area, and are especially influenced by these forces (Shaw, 1992). When clay mixes with water, it can form spherical peds (individual units of soil aggregates, with clay holding the

particles together) separated from each other along zones of weakness, which can result in increased pore spaces and permeability (Mirsal, 2004). Because of the uneven charge distribution and dipolar character of water molecules, they are attracted to ions in solution and cause ion hydration. Positive ions attract negative corners of water molecules and vice versa (Mitchell & Soga, 2005).

Yong and Mulligan (2003) suggest that understanding the nature and mechanism of interactions between soil particles and electrolytes in water will help to explain how the reactive surfaces of soils react with the chemical properties of water in the soil pores. Isomorphous substitution of the ions in the tetrahedral and octahedral layers of clays by lower valency ions results in the development of electric charges on the siloxane surfaces, and electric charges can also be developed on the edges of clay particles. The nature and magnitude of the charge is dependent on the basic structure of the clay and the pH of the immediate surroundings (Yong & Mulligan, 2003).

2.8.4 The Diffuse Double Layer

Adsorbed cations are tightly held on the surface of negatively charged dry clay particles, and excess cations are needed to neutralize the electronegativity of the clay particles and associated anions presented as salt precipitates. In the contact of clay with water, the precipitated salts go into solution, adsorb cations produce a high concentration near the surface of the particles, and in order to equalize the concentration, try to diffuse away. However, there is limited possibility for movement because of the negative electrical field in the particle surface and the ion surface interactions that are unique to specific cations. The tendency to escape due to diffusion and opposing electrostatic alteration leads to ion distributions adjacent to a single clay particle in suspension that are often idealized, as shown in Figure 2.10 (Mitchell & Soga, 2005). The

thermal motion of water molecules causes the layer of counter-ions to be diffuse, with the concentration of counter-ions declining exponentially as the distance from the surface increases. Since the overall charge within the solution must be maintained, the net charge on the surface is balanced by a net charge in the diffuse layer. So, basically, the electric double layer is the arrangement of the charge on the colloidal surface, and the counter-ions in the diffuse layer. To account for the finite volume of counter-ions, a Stern layer is introduced to the diffuse layer, and this can be subdivided into inner and outer Helmholtz planes (IHP and OHP), resulting in separation of the diffuse layer from the surface of the colloid by the stationary layers of dehydrated and hydrated ions (Snoswell, 2003).

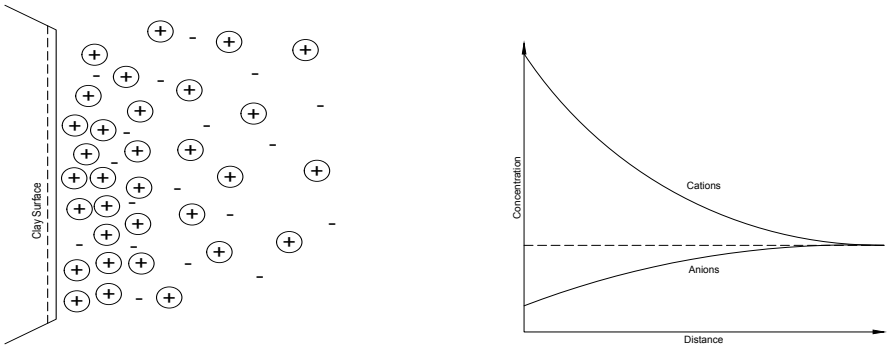

Figure 2.10 Distribution of ions adjacent to a clay surface according to the concept of the diffuse double layer (Mitchell & Soga, 2005)

Hiemenz (1977) pointed out that generally, the thicker the diffuse layer the less the tendency for particles in suspension to flocculate and the higher the swelling pressure in expensive soils. The diffuse layer become thinner when an increase in electrolyte concentration reduces the surface potential for the condition of constant surface charge and the decay of potential with distance is much more rapid. The consequence of this phenomena cause the flocculation of

particle in suspension when facilitated by an increase in electrolyte concentration. Hence swelling behaviour of clay depends on electrolyte concentration.

The most widely accepted theory of ionic distribution, and the one that accounts for the electric diffuse double layer, was developed by Gouy-Chapman, and was based on the assumption of a point charge in an electrolyte medium. It has been shown that this theory accurately describes the actual distribution of ions only for smectite particles at a low concentration (<100 mol/m^3). However, it provides a useful basis for understanding flocculation and deflocculation, and the relationships of these processes to the formation of structure and aspects of clay compression and swelling. Mitchell & Soga (2005) suggested that the theory of the diffuse double layer provides useful insight into ionic distribution adjacent to clay particles. This theory helps to predict the flocculation and deflocculation, swelling and the effect of pore fluid compositional changes. However, there is serious disagreement in many cases that consider some factors such as pH, ion size, particle interference and forces.

2.8.4.1 The Effects of System Variables on Double Layers

As the dielectric constant influences the surface potential and the diffuse layer thickness, it is important to understand the various influences on the behaviour of fine-grained soil towards the ion.

- Effect of electrolyte concentration: increase in electrolyte concentration; reduction of the surface potential for the surface charge and rapid decline of potential with distance from the surface.
- Effect of cation valence: for solutions of the same concentration and constant surface charge, a change in cation valance decreases both surface potential and the thickness of the double layer.

- Effect of dielectric constant: dielectric constant influences the surface potential and the diffuse layer thickness. In the case of clay being in contact with chemicals of different types, contaminants, oils, solvents or other organic chemicals may replace pore water.
- Effect of temperature: an increase in temperature causes an increase in diffuse layer thickness and a decrease in surface potential for a constant surface charge. However, increasing the temperature may result in increasing the dielectric constant, although a small variation in dielectric constant should not greatly influence the diffuse double layer.
- Other factors include size of ion, clay platelet associations and particle interference, and the effect of pH. Also, the effects of temperature changes on soil properties such as strength, compressibility and swelling (Mitchell & Soga, 2005).

2.8.5 Cation Exchange

The main reactions between soils and cation ions are occur due to ion exchange. Clay absorbs cations of specific types and amounts under various environmental conditions such as temperature, pressure, pH, chemical and biological composition of the water. The total amount adsorbed balances the charge deficiency of the solid particles. Exchange reactions involved replacement of a part or all of the adsorbed ions of one type by ions of another type. The types of adsorbed cations depend on the depositional environment. For example, sodium and magnesium are dominant cations in marine clays since they are common in seawater. These exchange reactions may change the physical and physicochemical properties of the soil. However, the exchange reactions do not affect the structure of clay particle themselves (Mitchell & Soga, 2005). Different samples of the same clay mineral give different values for cation exchange capacity so a range of values exists for the same mineral due to the differences in structure and composition between samples. In addition, particle size also has an important

effect (Gillot, 1987).

In clays, cation exchange is caused by the attraction of positive ions in pore water to negatively charged clay surfaces (Yong & Mulligan, 2003). Exchangeable ions are represented the amount of exchangeable cations that can be replaced by leaching with a solution containing other dissolved cations of greater replacement power than the adsorbed cations. The quality of exchangeable cation is called cation exchange capacity (CEC), and is expressed in milliequivalents (meq) per 100g of soil (Yong & Mulligan, 2003). Table 2.4 shows the CEC, specific surface area, and the source of charge for different types of clay.

There are three important source of clay exchange capacity:

1. **Isomorphous substitution** is the major source of clay exchange capacity and in crystal lattice. In clays (except for Kaolin minerals) for example, Al^{3+} replaces Si^{4+} in tetrahedral layer and Mg^{2+} replaces Al^{3+} in octahedral layer which results in an excess of O^{2-} bond and it is important for illites. Also its cause to obtain negative surface charge for smectite and vermiculites.
2. **Broken or unsatisfied bonds** is major source of second source of clay exchange at crystal plate corners and edges lead to the inonization of surface group, usually resulting in a net negative charge due to exposed O^{2-} and OH^{-}. This mechanism of charge development affects all clays. Figure 2.11 presents the CEC versus pH for Kaolinite, illite and bentonite (smectite) clay. All the curves show a slight negative slope which showing that metal adsorption decreases with decreasing pH. This is due to the H^{+} ion concentration increasing compete more effectively with fixed metal cation concentration for adsorption sites on the clay. The broken bonds are the chief source of surface charge for kaolinite but less important for illites as have a much higher surface charge than kaolinite due to the permanent charge effects. As the clay particle

size decreases, the relative important of broken bonds increases (this is more important for Kaolin and lesser important for illites).

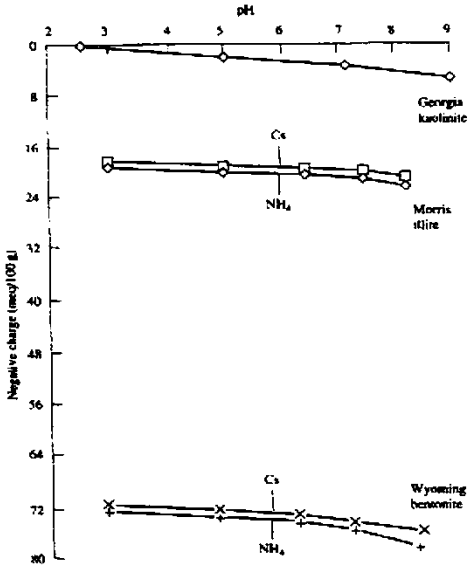

Figure 2.11 Negative surface charge of some clays between pH 2 and 9 (Van Olphen, 1977)

3. **Lattice defect**, such as deficit in octahedral Al^{3+} or interlayer K^{+} which results in a net negative charge. This is more important for smectite and less important for illites. The permanent charge of clay minerals is due to the lattice imperfection or defects, plus isomorphous substitution. The permanent negative charge of illites in mol sites/kg is 1.6 to 2.5 (Mitchell & Soga, 2005).

Thus the contributions of each of these sources depends on different environmental and compositional factors, so given clay minerals does not have a fixed, single value of exchange capacity. The capacity is directly related to the specific surface and surface charge density. Table 2.4, also presents the pH dependence for some sorbing minerals. Dependencies characterized as absent, negligible, or slight shows that the sorbent obtains its CEC chiefly due

to the interior lattice charge imbalance. Strong dependencies present that the surface charge results from reactions at sorbent-solution interface (Langmuir, 1997). The capacity is directly related to the specific surface and surface charge density.

Table 2.4 Charge characteristics and cation exchange capacities of clay minerals at pH 7 and their pH dependences (Goldberg et al., 1990; Grim, 1968; Brady et al., 1996; Mumpton, 1977; Lide, 1995)

Soil	Charge per unit half-cell		Cation Exchange Capacity $Cmol_c kg^{-1}$	pH dependence
	Tetrahedral	Octahedral		
Kaolinite	0	0	1-10	Strong
Smectite			80-120	Absent or negligible
Montmorillonite	0	-0.33	80-150	Absent or negligible
Vermiculite	-0.85	0.23	120-150	Negligible
Mica			20-40	Slight
Chlorite			10-40	Slight

The CEC values for kaolinite are a strong function of pH however, for smectite and illite, surface charge is relatively independent of pH. In some soil was observed that below pH 5, proton occupy a large fraction of clay surface site. Below pH 4 to 3, protons occupy all the sits and tend to destroy clay structure (Langmuir, 1997).

2.8.6 Ion Selectivity

Ion exchange reactions usually occur in an aqueous environment. Clays, however, can absorb ions from trace constituents that go into solution from being rather insoluble, even in very little moisture (Mitchell & Soga, 2005). Under different environmental conditions, such as temperature, pressure, pH, and the chemical and biological composition of water, clay adsorbs

cations of specific types and amounts. An exchangeable cation can be replaced by another of greater valency, and this is a mechanism that plays a significant role in heavy metal partitioning (Yong & Muligan, 2003). The cation replaceability / lyotropic series (Mitchell & Soga, 2005) is given below in order of replacing power.

$$Na^{+}<Li^{+}<K^{+}<Rb^{+}<Cs^{+}<Mg^{2+}<Ca^{2+}<Ba^{2+}<Cu^{2+}<Al^{3+}<Fe^{3+}<Th^{4+}$$

The ease with which replacement takes place depends mainly on the valance, the relative abundance of different ion types and ion size. However, it is possible to displace a cation of high replacing power, such as Al^{+3}, by Na^{+}, by mass action, if the concentration in the solution of the ion of low replacing power is high relative to that of the ion of high replacing power (Mitchell & Soga, 2005).

When Fe is presents in the system, the process involves adsorption by the clay minerals of iron ions as soon as they pass into solution. As clay immobilizes the iron ions quickly, there is further solution from the metal, the process continues, and as a result the clay soil is chemically and physiochemically altered (Yong & Mulligan, 2003). Most metals become mobile at low pH, and sorption on clay particles becomes less effective. The presence of other components, such as oxides/hydroxides and carbonate matter, enhances retention. Environmental changes may alter the retention capacities of clay, but the clay system may exhibit dynamic mechanical and rheological behaviour, due to physiochemical changes in particles and changes in pore fluid characteristics (Ouhadi et al. 2006).

The rate of exchange depends on the type of clay, solution concentration and temperature. Exchange reactions in Kaolin minerals are, on the whole, almost instantaneous. In illite it might take a few hours, due to the fact that a small number of exchange sites may be between unit layers, and a longer time is required in smectite because the major part of the exchange capacity is located in the interlayer regions.

2.9 Assessing of Buried Geotechnical Utilities

In the UK, many utilities have been installed few hundred years ago (see Section 2.2). Since then, a majority of existing underground infrastructure system or buried utility services such as cast iron pipes have become degraded and thus have been replaced. Deterioration of cast iron water mains through pitting corrosion and graphitisation was investigated by Romanoff (1962), Makar & Rajani (2000) and Makar et al. (2001). Furthermore, in UK, Thames Water is replacing more than 1600 km of iron mains in London over next five years (Costello et al., 2007).

In order to ensure that deterioration does not have serious consequences for a utility network, the condition of buried infrastructure (such as iron pipes) needs to be routinely assessed and monitored. However, buried pipes cannot be routinely inspected visually without being dug up, which is expensive. So, non-intrusive (see Section 2.10) assessments using geophysical techniques such as GPR (see Section 2.13) may be more advantageous. It is important to analyses the existing soil condition area of interest. The presence of the clayey soil, iron oxide (corrosion of buried cast iron pipes (Olhoeft, 2000), dissolved metallic ions, depth of water table, salt water intrusion and metallic ions in solution can limit or eliminate the use of GPR which means that GPR signal reflection can be attenuated. Clayey soil with high specific surface area can retain more water and therefore show greater losses due to the relaxation (specially in wet conditions). The effect of bound water depends on the soil constituents (percentage of clay particles, mineralogy), on the density and the degree of saturation, on the ions in the pore water and pH (Cassidy, 2008). Pennock (2010) examined the reduction in reflection that could occur with corroded materials. For this he used very wide estimates of permittivity and conductivity in soil modified by corrosion products, and a simple assumed variation in the permittivity and conductivity.

2.10 Non-Intrusive Methods

The existence of a strong relationship between the physical properties of geologic materials and their electromagnetic properties means that the physical structures of subsurface may be identified using electrical methods (Scott et al., 1977; Delaney & Arcone, 1982; Dallimore & Davis, 1987; Davis & Annan, 1989). Over the past 10 or 12 years, there has been development several non-destructive technologies (NDT) that facilitate the inspection of water pipes (Rajani et al., 2004). Some of these technologies exploit the specific properties of some materials used for pipes, and consequently they are not suitable for use with all pipe materials. Internal tuberculation can lead to an increase in complaints about red water, and fragments sloughed off can clog the graphitized area in cast iron pipes. Inspections caused by the problem mean that there must be disinfection, and there is an increased risk of contaminants getting into the system. For these reasons non-intrusive inspection is required (Rajani et al., 2004). NDT is also more cost effective and faster than intrusive inspection. Different methods of non-intrusive inspection exist, and the choice of which technique to employ depends mainly on the type of pipe material, the type of commodity carried by the pipe, the type of soil, and the ground surface features. Some non-intrusive techniques are shown in Table 2.5. There do exist some limitations in the use of these techniques, such as the need for physical contact (electrical, electromagnetic, magnetic density) between the target and the material being tested (Hao et al., 2012).

Table 2.5 Some non-intrusive testing methods (Hao et al., 2012)

Non-Intrusive Techniques	
Visual techniques	
	Closed-circuit television (CCTV)
	Sewer scanner and evaluation technology (SSET)
Electromagnetic and radio frequency techniques	
	Magnetic flux leakage (MFL)
	Eddy current technique
	Hydroscope technology
	Rapid magnetic permeability scan (RMPS)
	Low frequency electromagnetic field (LFEM)
	Passive magnetic fields (PMFs)
	Ground penetration radar (GPR)
	Time domain ultra wideband
Acoustic and vibration techniques	
	Sonar
	Vibro-acoustic
	Impact echo/spectral analysis of surface waves
	Correlator and listing stick for leaks
	Other acoustic techniques
RFID/Sensor techniques	
Other techniques	
	Infrared thermography
	Continuous wave Doppler sensing technique
	Laser surveys
	Combined techniques

In order to use non-intrusive methods to assess soil modification around a corroding cast iron pipe, it is important to understand the possible effects of the natural soil environment (geotechnical and geophysical properties) on assessments, since the geophysical signals need to travel through the ground.

Complexation reactions between clay and corrosion product can produce a smooth variation in the electrical parameters within a radial distance from the pipe, as a result of chemical and electrical ion transport mechanisms (Pennock et al., 2010). The performance capability of this type of radar is strongly dependent on the soil electrical conductivity. If the soil conductivity

is high, attenuation of the radar signal in the soil can severely restrict the maximum penetration depth of the radar signal. For this reason, fundamental electromagnetic parameters for example dielectric permittivity, electrical conductivity (EC) and magnetic permeability need to be identified (see Section 2.11.1). Table 2.6 is listed the electromagnetic and radio frequency technique with pointing the technical challenges.

Table 2.6 Electromagnetic and radio frequency techniques

Electromagnetic and radio frequency techniques	
Magnetic flux leakage (MFL)	• Used for metallic pipeline inspection. • Detects and characterises metal loss defect such as corrosion and cracks on interior wall of pipeline. • Good detection capabilities even for small pitting anomalies and under extremely poor conditions.
Eddy current technique	• Smaller metallic pipes (100mm). • Generally used for gas pipelines. • Problem: dimension of skin depth depends on induced frequency.
Hydroscope technology	• Based upon remote field eddy current (RFEC) technique. • Non-destructive for buried cast/ductile/steel pipes. • Assesses condition of water pipelines. • Detects general wall loss, pitting and graphite corrosion and is sensitive to internal and external wall loss. • Can be used on wet or dry pipes. • Pits of less than 3000mm^2 in size cannot be detected (Makar & Chagnon, 1999).
Rapid magnetic permeability scan (RMPS)	• Magnetic field applies strong permanent magnets to metallic pipe wall. • Used for bigger metallic pipe diameters.
Low frequency electromagnetic field (LFEM)	• Electrical signals in the frequency range of 0.5-50 kHZ. Approach of measuring non-invasively is relatively new: 1. Continuous resistivity imaging (CORIM). 2. Capacitive resistivity imaging (CRI). • Both systems are able to conduct subsurface surveys in conditions that are normally challenging for ground penetrating radars (such as high electrical conductivity soil). • Both systems are limited to operating on a single, non-variable frequency which has little impact on their effectiveness.
Passive magnetic fields (PMFs)	• Find location of underground power cable based on principle proposed by Michael et al. (1998).

Ground penetration radar (GPR)	• Environmental, agricultural and glaciological monitoring. • Buried utility detection. • Condition assessment of infrastructure. • Detects abnormally wet areas within the ground. (Leaking water pipes)
➢ **Traditional GPR**	• Look-down mode. • GPR technologies can be categorized into three main types: 1. Time domain: Impulse GPR (well stablished – most commonly available). 2. Frequency domain: frequency modulated continuous waveform (FMCW); stepped frequency continuous waveform (SFCW); and noise modulated continuous waveform (NMCW) GPR. (Comparatively new – under research for academic and industrial domain). 3. Spatial domain: single frequency GPR. (Viable). • Detection of significant ground sewer and drainage culverts and leak detection.
➢ **In-pipe GPR**	• **Look-out**: transmitter and receiver are mounted on a pig inside a pipe. Or, **Look-though**: receiver is on the surface. (Or vice versa). • Path loss due to attenuation of soil is reduced compared to traditional GPR system. • Detection of significant ground sewer and drainage culverts and leak detection.
Time domain ultra wideband	• Monitoring of pipeline for broader working frequency range and better resolution. (Sachs et al., 2007b). • For non-ferrous pipeline. • Detects voids occurring in soil envelope surrounding pipe. • Provides accurate condition assessment of predominantly non-ferrous buried pipes including presence, location, orientation and dimension of soil voids. Detection of external corrosion and measurement of wall thickness of buried pipes (Jaganathan et al., 2010)

2.11 Soil Electromagnetic Measurement Techniques

The electromagnetic methods (e.g., TDR and GPR) are usually used to measure soil water by measuring the soils permittivity. These methods, however, are also affected by other factors such as soil salinity, soil temperature, the presence of magnetic properties, soil bulk density and the frequency with which measurements are taken, which in turn depends on the instrument used and on the dispersive nature of the soil (Curioni, 2013).

2.11.1 Soil Electromagnetic Parameters

As discussed above, graphitic corrosion in cast iron pipes releases Fe^{2+} ions into the surrounding soil, with the result that the soils total dissolved salt content increases. This causes changes in the conductivity and permittivity of the soil. In GPR and TDR, these electromagnetic parameters are linked through the velocity, (m/s), and the attenuation coefficient, (Np/m) of the signal. The two properties can be measured in terms of three fundamental electromagnetic properties: dielectric permittivity (ε), electrical conductivity (EC), and magnetic permeability (μ) (Curioni, 2013).

Dielectric permittivity (ε): This refers to a material's ability to transmit an electric field. It indicates the signal energy that the material can store through the separation of charges. It is normally expressed as its ratio to the dielectric permittivity of free space (ε_0, 8.8954×10^{-12} F/m), which is why it is defined as relative dielectric permittivity (ε_r). The permittivity of a material is not constant, but varies according to variation in the frequency of the charge (Evett and Parkin, 2005). Another way of expressing permittivity in discussing GPR and TDR results is as 'apparent permittivity', ε_a, (Curioni, 2013).

Electrical conductivity (σ, EC): This is the measure of a material's ability to conduct electric current (S/m). In most soils, electrical conductivity is ionic, and so it depends on the concentration of salts in the pore water. It is also frequency dependent, and is one of the important factors affecting the attenuation of an electrical signal (Curioni, 2013). Electrical conductivity has a greater effect in the low frequency range of kHz, up to tens of MHz (Campbell, 1990).

Magnetic permeability (μ): This measures the degree to which a material is capable of being magnetised when exposed to a magnetic field. It is usually expressed as relative permeability (μ_r), and is often assumed to be equal to 1 in the TDR and GPR frequency ranges (Huisman et

al., 2003). However, this assumption does not hold for soils with high magnetic permeability. For example, it does not hold for anthropogenic soil rich in iron-oxide components, or for some natural soils that are rich in magnetic minerals (Cassidy, 2007 and 2008). EM signals effect on the soil's permittivity and bulk electrical conductivity (Curioni, 2013).

2.11.2 Soil Properties that Affect the Performance of GPR

The resolution and penetration depth of GPR are determined by antenna frequency and the electrical properties of earthen materials (Olhoeft, 2000; Daniels, 2004). Due to the high rate of signal attenuation, penetration depths reduced in soils that have high electrical conductivity. The electrical conductivity of soils increases with increasing water, soluble salt and/or clay contents (McNeill, 1980). In soils, the moist significant conduction-based energy losses are due to the ionic charge transport in the soil solution and electrochemical process associated with cations on clay minerals (Neal, 2004). These losses can seriously impact the performance of GPR (Campbell, 1990; Olhoeft, 2000).

Electrical conductivity is directly related to the amount, distribution, chemistry, and phase (liquid, solid, or gas) of the soil water (McNeill, 1980). Electrical conductivity, direct permittivity and energy dissipation increase with increasing soil water content (Campbell, 1990; Daniel, 2004). Consequently, by increasing these salts, the electrical conductivity of the soil solution increases and causes the attenuation of electromagnetic energy (Doolittle & Collins, 1995). In these soils, effective GPR penetration is restricted to surface layers and depth of less than 25cm. Lebron (2004) state that the soils with higher calcium carbonate contents have higher dielectric permittivity. Grant and Schultz (1994) observed a reduction in soils that have high concentrations of calcium carbonate. The electrical conductivity of soils is governed by, the amount of clay particles (particles <0.002mm in diameter) and the types of clay

minerals present (McNeill, 1980). Clay particles have greater surface areas and can hold more water than the silt (particles 0.002-0.005mm in diameter) and sand (particles 0.05-2.0mm in diameter) fractions at moderate and high water tensions. Due to the isomorphic substitution, clays minerals have a net negative charge. To maintain electrical neutrality, exchangeable cations occupy the surfaces of clays particles and contribute to energy losses (Saarenketo, 1998). These cations concentrate in the diffuse double layer that surrounds clay minerals and provide an alternative pathway for electrical conduction. Because of clay high adsorptive capacity for water and exchangeable cations, clays increase the dissipation of electromagnetic energy. The clay content is inversely related to the penetration depth of GPR. Olhoeft (2000), using a 100-MHz antenna, observed a penetration depth of about 30m in some clay-free sands. However, with the addition of only 5% clay (by weight), the penetration depth was reduced by factor of 2 (Olhoeft, 2000). Doolittle and Collins (1995) mentioned that depending on antenna frequency and the specific conductance of the soil solution, penetration depth ranges from 5 to 30m in dry, sandy (>70% sand and <15% clay) soils, but average only 50cm in wet, clayey (>35% clay) soils. Soils contain various proportions of different clay minerals (e.g., Kaolin, mica, chlorite, vermiculite and smectite groups). The size, surface area, cation exchange capacity (CEC), and water holding capacity of clay minerals vary greatly. Variations in electrical conductivity are attributed to difference in CEC associated with different clay minerals (Saarenketo, 1998). Electrical conductivity and energy loss increase with increasing CEC (Saarenketo, 1998). Soils with clay fractions dominated by high CEC clays (e.g., smectitic and vermiculitic soil mineralogy classes) are more attenuating to GPR than soils with an equivalent percentage of low CEC clays (e.g., kaolinitic, gibbsittic, and halloysitic soil mineralogy classes). As a general rule, for soils with comparable clay and moisture contents, greater depths of penetration can be achieved in highly weathered soils of tropical and subtropical region than in soils of temperate regions (Harry, 2009).

2.12 Time Domain Reflectrometry (TDR)

Time domain reflectrometry is a relatively new technique for the measurement of soil electrical conductivity (Jones et al., 2002; Topp et al., 1980) used TDR to determine the volumetric water content of soils with different particle size distributions and organic contents. Since 1980, further studies have been done which have helped to develop TDR methodology, bringing in the use of digital cables. As a result, TDR has become a commercially worthwhile method for monitoring soil water in the field (Robinson et al., 2003a). Currently, TDR is one of the most commonly used techniques for measuring soil water content in the field (Robinson et al., 2003a; IAEA, 2008; Herkelrath et al., 1991; Rajani & Ryden, 1992; Stangl et al., 2009). With TDR, a good standard of accuracy (<2%) can be achieved for volumetric water content estimation (Jones et al., 2002), and this technique is less affected by temperature and salinity than capacitance sensors, because it works at higher frequencies (Evett & Parkin, 2005). Also, it has minimal calibration requirements often, soil-specific calibration is not needed at all, and measurements can easily be obtained, with the technique providing continuous measurements through automation and multiplexing (Jones et al., 2002). Another important advantage of TDR is that it can measure bulk electrical conductivity and apparent permittivity in the same sample of soil. For this reason, it has frequently been used in soil science work (Robinson et al., 2003a; Jones at al., 2002; Dalton et al., 1984) were the first to investigate the measurement of permittivity and bulk electrical conductivity using TDR, and they developed a type of waveform analysis for this. The Gies-Tiemann method is now considered the standard one for calculating bulk electrical conductivity from TDR measurements (Lin et al., 2008; Huisman et al., 2008).

2.12.1 Measurement of Bulk Electrical Conductivity (BEC)

Dalton et al. (1984) were also amongst the first authors to show how useful TDR can be for measuring the bulk electrical conductivity of soil. The fact is that TDR could measure the apparent soil electrical conductivity of the sample of soil opened up new possibilities for investigating salinity and the behaviour of ionic solutes in soil. However, soil water contents play an important role in these problems as well due to the ability to measure delectrical permittivity.

TDR has been developed into one of the most advanced techniques for measuring permittivity and conductivity. Nevertheless, it is important to recognize the technologies limitations. Long cables, and poor quality connectors and multiplexers can significantly affect TDR waveforms. Logsdon (2000, 2005 and 2006) showed that TDR readings were affected by cable length and by attachments, where these were used. Each attachment caused further signal attenuation and impedance mismatches, and these produced unwanted reflection and noise. Attenuation causes the reflection coefficient to be reduced and the waveforms to be rounded, and this can complicate their interpretation. The use of attachments and long cables causes the pulse rise time to increase and the frequency bandwidth to decrease, by creating a low-pass filter (Heimovaara, 1993). In highly conductive soils, the signal can be attenuated to the point where the reflection at the end of the probe becomes impossible to detect (Jones et al., 2002). Therefore, in this kind of situation TDR cannot measure the apparent permittivity. Also, if the TDR probe is incorrectly inserted into the soil, this can produce significant errors in the results obtained (Topp et al., 1980; Ferre et al., 1996). TDR provides only a single value for apparent permittivity; and so it does not provide information on the dispersive nature of a soil sample (Thomas et al., 2008). In conductive soil, a shorter probe and cable length were a better choice, as the signal was less likely to be attenuated and TDR would still be able to achieve measurements of the apparent permittivity (Curioni, 2013).

2.13 Ground Penetrating Radar (GPR)

Radar has been used for ground sounding techniques since the 1960s (Annan, 2008). Ground penetrating radar is a safe, non-intrusive form of geophysical investigation that is suited to checking on buried utility distribution systems, and it can be used to investigate both the layout and depth of such systems (Pennock et al., 2010).

GPR can detect metallic and non-metallic, and natural and man-made underground features. For this reason, it is suitable for checking on buried utility distribution networks, storage tanks, rebar, sinkholes, voids in the ground, water tables, buried artifacts, mines and so on. The technique is currently the most widely used for shallow geophysical investigation (Rogers et al., 2007). Its main advantage is that it can survey large areas at a speed that makes something approaching real time interpretation possible. It operates on the same principle as TDR (see Section 2.12); but of the two, only GPR can send a signal in an unguided wave both up into the air and down into the ground, rather than along a coaxial transmission line (Huisman et al., 2003). GPR has been used to estimate soil water content by a number of research teams (Weiler et al., 1998; Huisman et al., 2001and 2003). It sends a high frequency electromagnetic signal (generally between to 1MHZ to 1 GHZ, see Davis & Anna, 1989) into the ground and measures the portion of the signal that discontinuities permit to be sent back. However, GPR is limited by signal attenuation, which depends on the EM properties of the ground (Davis & Annan, 1989).

Testing with GPR depends on attenuation of the signal, which is related to the depth of resolution, and this limits the range of buried items it can be applied to. Attenuation is proportional to the frequency of the signal. The higher the frequency is, the more strongly attenuated the signal will be. But high frequencies have a high spatial resolution and make possible the detection of smaller discontinuities in the ground. In the case of buried utility

distribution systems, the detection of a clear target is enough to enable the estimation of the average soil permittivity (and water content) in the ground above the target. This can be very useful for estimating soil conditions as part of surveys; but clear visible target is required.

2.13.1 Principles of Ground Penetrating Radar

As Table 2.6 shows, there are different types of GPR, the most common one being impulse GPR, which operates in a time domain and sends electromagnetic pulses into the ground. Continuous-wave GPR, which operates in a frequency domain, is another type of GPR (Koppenjan, 2008). Continuous-wave GPRs (stepped, frequency, noise modulate radar) sends a sample signal with frequency increments over a specific frequency bandwidth. These systems all have the advantage that they provide direct control of the operative frequency. However, due to the electronic complexity of their digital signal processing, few are at present commercially available (Koppenjan, 2008).

In the case of a cast iron pipe buried in clay soil, as was mentioned earlier, the reaction between the clay soil around the pipe and the corrosion products created by the pipe is complex, with the results causing changes through the permittivity and conductivity in the ground. Conductivity lessens the further it gets from the pipe (see Introduction Chapter, Figure 1.2). Iron oxide in its red rust form is relatively insulating, and it has a relative permittivity that is higher than that of most soils. As the iron pipe is the source of the iron oxide, a higher concentration of the oxide can be expected nearer the pipe. In addition, the corrosion process creates salts at the surface of the pipe, and this produces high conductivity (Pennock et al., 2010). For these reasons, the corroded cast iron pipe cannot be detected with GPR.

The characteristics of GPR mean that it works through a comprise between range and spatial resolution. The range is defined as the ratio of the maximum receivable signal to minimum detectable signal, and it is expressed in decibels (dB) for a specific frequency bandwidth in Hertz (Koppenjan, 2008) and the spatial resolution determines the dimension of the smallest detectable target (Curioni, 2013). A GPR system generally has two antennae one a transmitter that emits the electromagnetic pulse; and one a receiver that samples the reflected signals. The most common GPR system works in a reflection-profiling mode (Davis & Annas, 1989). In this process, the distance between the antennae is increased stepwise, whilst a common midpoint is maintained (Greaves et al., 1996). Alternative multi-offset configurations involve the common mid-point (CMP) and wide angle reflection and refraction (WARR) (see Table 2.6).

During a single offset survey, impulse GPR emits signals at regular steps along the direction x (see Figure 2.12). The vertical traces collected at each step are called A-Scans. A combination of A-scan produces an image called B-scan, which is common GPR data output which is presented in Figure 2.13.

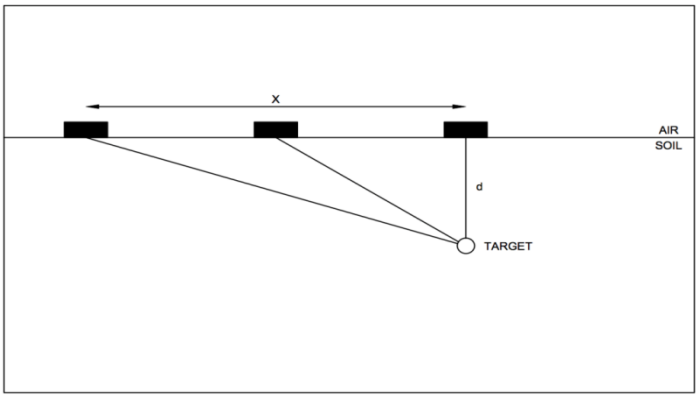

Figure 2.12 Diagram of a single offset GPR acquisition

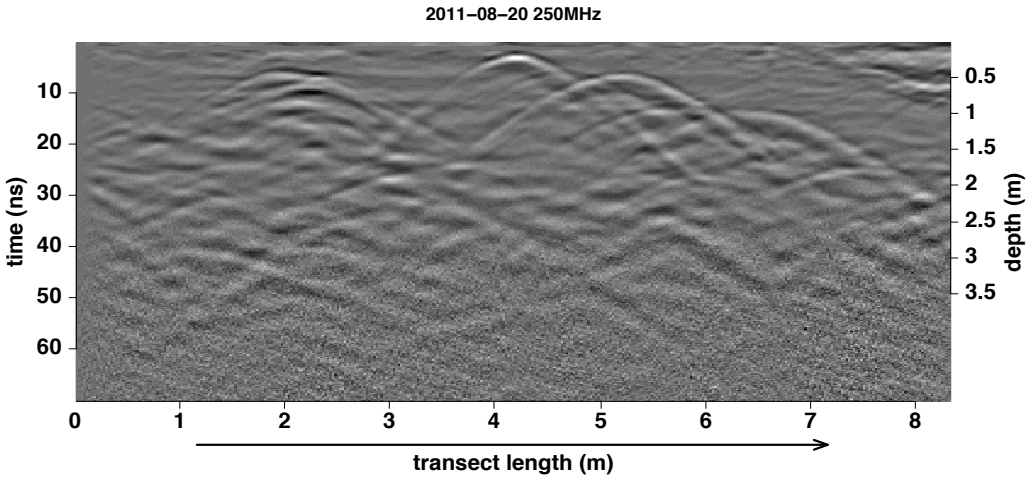

Figure 2.13 Example of a GPR image showing multiple buried pipes (Curioni, 2013)

2.13.2 Limitations of Ground Penetrating Radar

The considerable differences between the electromagnetic properties of ice, water and some sediments mean that GPR is a highly effective method for mapping permafrost structure and thermal conditions (Moorman et al., 2003). Electromagnetic soil properties can be subject to seasonal variation, which may result in anomalies not being detected. For GPR to detect anomalies, there needs to be a good contrast between the anomaly and the surrounding medium. Such contrasts vary with time as the electromagnetic soil properties change, mainly as a result of changes in the water content. Seasonal variation can effect electromagnetic soil properties and these can cause failure to detect anomalies. Finally, GPR is not effective below a certain minimum area, and so it is not suitable for small experiments in a laboratory.

2.14 Correlation between GPR and TDR

TDR works at similar frequencies to the most commonly used GPR commercial units (approximately 10MHz-1FHz), and it makes possible the measurement of both permittivity and bulk electrical conductivity. Since TDR and GPR work on similar principles, it can be beneficial to use the two together. For example, soil water can be measured on a GPR catchment scale with TDR contributing point measurements. Both GPR and TDR can be used to survey ground conditions when ground is being surveyed by remote microwave sensing techniques on a larger scale (Topp, 2003).

In this study, the state of clay modifications to soil surrounding corroded iron pipes is considered in detail, with assessment of the spatial modification of conductivity and permittivity under anode and cathode conditions at increasing distances from the corroding cast iron pipe. Regarding the details given in Section 3.6.3, GPR measurements could not be taken in this research. Therefore, conductivity and permittivity measurements were taken using TDR (see Section 3.12.1). And finally, the FDTD simulation by GPRMax software was used to simulate GPR signals' ability to detect iron pipes buried under measured soil conductivity modification induced by corrosion.

2.15 Ground Penetrating Radar Modelling with GPRMax 2D

This section is summarized and based on the 'Users' Manual' version 2.0 by Giannopoulos (2005). GPR modelling with GPRMax 2D basically means using the finite-difference time domain method (FDTD) for GPR modelling. All electromagnetic phenomena are described by well-known Maxwell's equations.

The nature of the GPR forward problem classifies it as an initial value-open boundary problem. This means that in order to obtain a solution, an initial condition has to be defined (i.e. excitation of the GPR transmitting antenna). The FDTD approach to the numerical solution of Maxwell's equation is to discretize both the space and time continua. One of the most challenging issues in modelling open boundary problems as GPR ones is the truncation of the computational domain at a finite distance from sources and targets where the values of the electromagnetic fields cannot be calculated directly by the numerical method applied inside the model. Therefore, an approximate condition known as Absorbing Boundary Condition (ABC) is applied at a sufficient distance from the source to truncate, and therefore limit, the computational space. The role of ABC is to absorb any waves impinging on it, hence simulating an unbounded space. It is usually assumed that any objects that span the size of the computational domain extend to infinity. The only reflections that will originate from their termination at the truncation boundaries of the model are the result of imperfections in the ABC; and in general these are of a very limited size in comparison with reflections from targets inside the model. All other boundary conditions that apply at the interfaces between different media in the FDTD model are automatically enforced in GPRMax 2D.

2.16 Other Researchers' studies

In order to support data analysed as part of laboratory experiments, other researchers' experiment results were used in discussion chapter (see Section 5.3.1). The Figure 5.2 was obtained from the other researchers' thesis.

Both researchers were working on proving the concepts and establishing the practical possibilities for improving weak soil condition in-situ by using the electrokinetic stabilization method. Tajudin (2012) investigated various electrochemical effects such as electroosmosis,

electromigration and electrochemical effects on the physical, chemical and physiochemical behaviour of clay soil. Tajudin (2012) and Liaki (2006) used the same test methodology. Both used a voltage gradient of 50V/m on a Kaolin Clay sample with internal dimensions of 40 x 220 x 550mm to deliver chemical stabilizer into the soil. The both sides of small compartments were filled with anolyte and catholyte solution respectively. Also, for the electrokinetic process, the electrodes were coated with conductive carbon polymer (the same electrodes were used as were used in this research; (see Section 3.6.3) in order to prevent corrosion. The final moisture content was around 50% for Tajudin (2012) and 45% for Liaki (2006). Both results show high water content at both ends after the electrokinetic process in a pure system (no chemical effects) with distilled water at the electrodes. Therefore, it can be concluded that the variation of water content in the current study is comparable to those in the previous studies, as long as the system has no chemically inert and its pure clay. In the discussion chapter (Section 5.3.1), Figure 5.2 is presented which present the pure system. It should be noted that DW stands for distilled water.

2.17 Assessment of Cast Iron Corrosion Influence on Clay Properties

The release of iron ions from a corroding cast iron pipe into clay will potentially induce modification of surrounding clay, and therefore have implications for the clay properties. Industry experiences have highlighted difficulties with locating old buried cast iron pipes using geophysical techniques, such as GPR, due to the modification of the clay which masks the pipes through changes in the soil properties. This study looks to assess the clay modification and potential implications for limiting geophysical sensing (using GPR simulation), by characterising the modified clay around the corroding source. However, due to the complex nature of environmental conditions influencing these interactions, clear and succinct

descriptions of the modified ionic environment and its behaviour is required. This would include pH dependent characterisation, conductivity influences on behaviour, ion interactions, influences of the experimental set up and variability with time. Since Kaolin Clay and Oxford Clay are to be used in the experimental programme (see Chapter 3), their properties in particular will be reviewed hereafter.

Kaolin Clay is predominantly comprised of kaolinite, which is thermodynamically stable in most soils. The predominant species for formation of complexes are dominated by alumina (as Al-OH) and silica (as silicic acid H_4SiO_4), which have a theoretical solubility in water at 25°C similar to that of $Al(OH)_3$ (gibbsite); see Figure 2.14 (Langmuir, 1997). This theoretically exhibits amphoteric solubility behaviour, where reactions and complex formation occurs with kaolinite in solution, with kaolinite having an order of magnitude lower solubility than gibbsite (Langmuir, 1997). However, it is important to understand that Kaolin Clay is stable under acidic conditions (being a product of weathering under acidic conditions), has relatively low reactivity and is the least soluble of all clays. As such, the most important factor for interactions is dissociation rather than solubility. Kaolin dissociates under alkaline conditions (above pH 12) through silica loss (as silicic acid), resulting in the formation of complexes with the released species due to low solubility of the silica species. Also, kaolinite can form solid solutions with released Fe ions up to 3% of the total kaolinite (Tardy & Nahon, 1986), in addition to lattice substitution of Fe^{3+} for Al^{3+} (Langmuir, 1997) due to mass action.

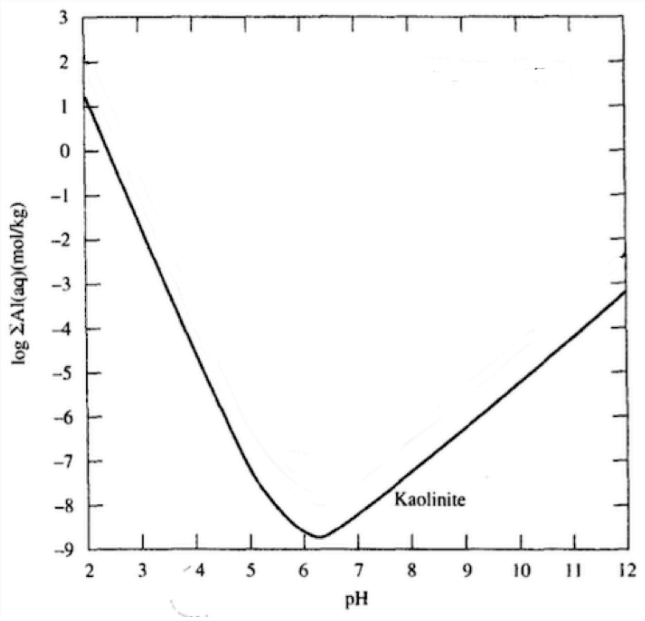

Figure 2.14 Kaolinite solubility (Langmuir, 1997)

Oxford Clay is clay with mixed mineralogy, dominated by illite with smaller proportions of other clay minerals and precipitated salts, with available interlayer cations of Al, Si, Mg and Fe. The chemical complexity of Oxford Clay influences available ions, ion migration and electrical conductivity variably, in addition to its high organic content (5%) which can complex large quantities of cations. The ease of exchange of cations is much more complicated, and the exchange pattern may also vary from the lyotropic series due to the mass-balance effects (Batchelder et al., 2007).

Different clay can sorb cations of specific types and amounts under specific environmental and chemical conditions, dependent on the selectivity of the clay for available ions. These exchange reactions may change the physical and chemical properties of the clay. Exchange reactions depend on the valance, ion size and relative abundance of available ions in aqueous solution, with higher valence cations preferentially replacing cations of lower valence and larger cations replacing smaller cations of the same valence, or exchanges due to mass action occasioned by

a large quantity of ions in solution. In Kaolin Clay, the exchange reactions are almost instantaneous, while in illite, this would take longer, due to exchange occurring at the interlayer clay sites of the 2:1 clay (Mitchell & Soga, 2005).

MacDonald (1994) investigated the precipitation of cations in aqueous solution, and indicated that the pH at which cations transmit from soluble form to precipitate forms varied for the different metals investigated. It was also discovered that the presence of other cations in solution affected the precipitation behaviour of the individual cations and their salts. As such, it is important to understand the solubility conditions for different cations; see Figure 2.7, which shows the theoretical solubility of metals (after Bone et al., 2004b). This precipitation/solubility behaviour will significantly influence the behaviour of ions released from cast iron corrosion, and, ultimately, the fate of released ions during mass transfer and ion migration.

Since corrosion naturally occurs slowly in soils, reaction acceleration has traditionally, and in this study will be, undertaken by inducing an electrical potential across the clay in contact with cast iron, using the principles of electroosmosis and electromigration (electrokinetics). This electrokinetic modification induces the migration of H^+ (formed at the anode) and OH^- (formed at the cathode) towards the oppositely charged electrodes, which generates acid (at the anode) and alkaline (at the cathode) fronts across the test specimens, and hence a pH variability (ranging from acidic pH 2 to alkaline pH 12). These fronts will migrate towards each other under the electrical gradient, with the clay being neutral where these fronts meet (Tajudin, 2012). The acid front produced at the anode causes desorption, dissolution and ionisation of cations, which migrate towards the cathode. However, due to the low solubility of iron ions released during corrosion of cast iron, the majority of the initial reactions will be highly localised at the anode, with significant precipitation of salts and increases in both conductivity

and strength of the clay. At the cathode (alkaline environment) where OH^- is generated, the cations released at the anode combine with OH^- and other anions to form hydroxides and other salts. The high pH induces dissolution of silica and/or alumina from the clay minerals, which can complex with available cations such as calcium to form Calcium Silicate Hydrate (CSH) and/or Calcium Aluminate Hydrate (CAH) amorphous gels that would crystallise and induce cementation.

2.18 Summary

The literature review has outlined the important subjects related to the corrosion of cast iron pipe, clay mineralogy and its properties, and techniques that could assess the condition of cast iron pipes. The review includes a brief history of cast iron pipes, what makes up cast iron, its corrosion process and the manufacture of cast iron pipes. In addition, it was highlighted that using electrokinetic techniques can help to accelerate the corrosion process and hence help to understand the corrosion effects within a fine-grained soil environment (based on the research by, for example, by Pugh, 2002; Ou et al. 2009; Bjerrum et al., 1967; Wade, 1976; Soderman & Milligan, 1961; Milligan, 1995; Boardman et al., 2004; Lamont-Black & Weltman, 2010). Furthermore, it was important to understand non-intrusive methods of detecting pipes, such as GPR, and methods for simulating GPR in the laboratory, via the use of techniques such as TDR, and this has been achieved via a review of the basic concept of GPR, a review of GPR limitations and a review of TDR. This also included a review of the soil properties which might have an effect on the measurements made by these techniques and, finally, how GPR can be simulated using FDTD with respect to its ability to detect buried iron pipes using measured soil conductivity.

In conclusion, the key findings of the review are as follows:

- Most investigations of cast iron pipe failure in the past have focused on the mechanical behaviour of pipes, such as corrosion-induced failure and fracture of cast iron pipes, which is now well understood (e.g. Rajani et al., 2000). Therefore, it is important to understand the chemical interactions between the corrosion products of the cast iron pipe and the fine-grained soil around the pipe.
- Corrosion process of cast iron pipes were explained and discussed with factors that could affect this process. Also, it has explained that release of these iron corrosion products (such as iron oxides) deposited within graphitised zone diffuse away into the surrounding soils, and that this is dependent on their solubilities.
- In order to accelerate the corrosion process by using electrokinetic methods, it is important to understand the effect of this treatment on the clay soil in relation to the corrosion process of cast iron. There has been much previous research in relation to soils, but not specifically in relation to fine-grained soils and cast iron. For example, although Schmidt (2007) used this method for the purpose of accelerating the corrosion process of cast iron, the effect of this system on the clay soil was not fully investigated. Also, clay mineralogy and the physico-chemistry of clay-water-electrolyte was discussed here in order to understand the effect of the electrokinetic system on clay soils.
- Cast iron pipes buried in particular soils (e.g. fine-grained soils) can be hard to detect with GPR. The literature suggests that as a result of the corrosion process, a varying conductivity and permittivity profile may be established around the pipe. Hence this needs further investigation.
- Even though much research has been conducted into GPR applications, there is still a lack of knowledge on a use of GPR to assess the location (and in particular the condition) of buried utilities in specifically fine-grained soils, with very little literature related to this

subject. Thus further research is needed with respect to the ability of GPR to assess the condition of cast iron pipes in fine-grained soils, and in particular this should aim to fully understand the problem of poor detection of cast iron pipes in fine-grained soils.

- The resolution and penetration depth of GPR signals are determined by the antenna frequency and the electrical properties of the soil. Therefore, the properties of the soil, such as moisture content, electrical conductivity and permittivity, might be expected to affect the performance of GPR. For example, clay particles have a greater surface area and can hold more water than silts and sands. It is important to understand the additional effects of these materials once they are chemically altered by corrosion products from the cast iron and understand their effects on GPR performance.
- The limitations of GPR have been demonstrated in the review, and therefore other techniques such as TDR were also introduced as they work at similar frequencies to GPR and work on similar principles. Both GPR and TDR can be used to measure conductivity and permittivity of soils. This potentially allows TDR to act as a replacement for GPR in laboratory situations.

CHAPTER THREE

3.0 Methodology

3.1 Introduction

Building on the arguments in Section 2.18 regarding the gaps in knowledge, it is evident that an experimental programme of research to explore the effects on fine-grained (i.e. clay-based) soils of cast iron degradation is needed, and for this to be effective it is important to use electrokinetic techniques to accelerate the corrosion process. While such research could be conducted via field experiments, the lack of control offered by such work demands that laboratory tests in a controlled environment should be undertaken to develop the fundamental understanding prior to application in the field. Moreover, it has been shown that laboratory experimentation requires bespoke equipment development and associated testing procedures for specimen preparation, monitoring and sampling, alongside programmes of geotechnical and geophysical testing (Sections 2.11 and 2.12 established that TDR is appropriate for this) to determine the effects of corrosion on the properties of the soils. A natural limitation on the number of tests that can be carried out demands that the results be extrapolated using numerical analysis, and the use of GPRMax was identified in Section 2.15 as being most appropriate.

It has been shown in the literature that it is important to understand the fundamental processes in simple soil systems and, following the lead of many researchers working in the field of electrokinetics (e.g. Barker et al., 2004; Liaki, 2006), it was decided to use a relatively pure form of kaolinite (termed herein Kaolin Clay). However, for translation of the results to practice, while retaining the ability to compare results with previous researchers and therefore

aid in extrapolating the results (e.g. Barker et al., 2004; Schmidt, 2007), a clay of mixed mineralogy (Oxford Clay, which is illite-rich) was chosen to act as a comparator.

This chapter therefore provides details of the materials, apparatus and methods employed in the experimental design and testing. The final experimental design was developed based on preliminary and modified designs. For better understanding the results of tests simulating cast iron corrosion in clays, a testing programme was developed to identify the properties of clay. These tests were divided into three different categories, i.e. geotechnical, geochemical and geophysical. The required physical and chemical properties of the clay soil were determined according to the appropriate British Standard. The overall process of the research methodology is summarised in Figure 3.1.

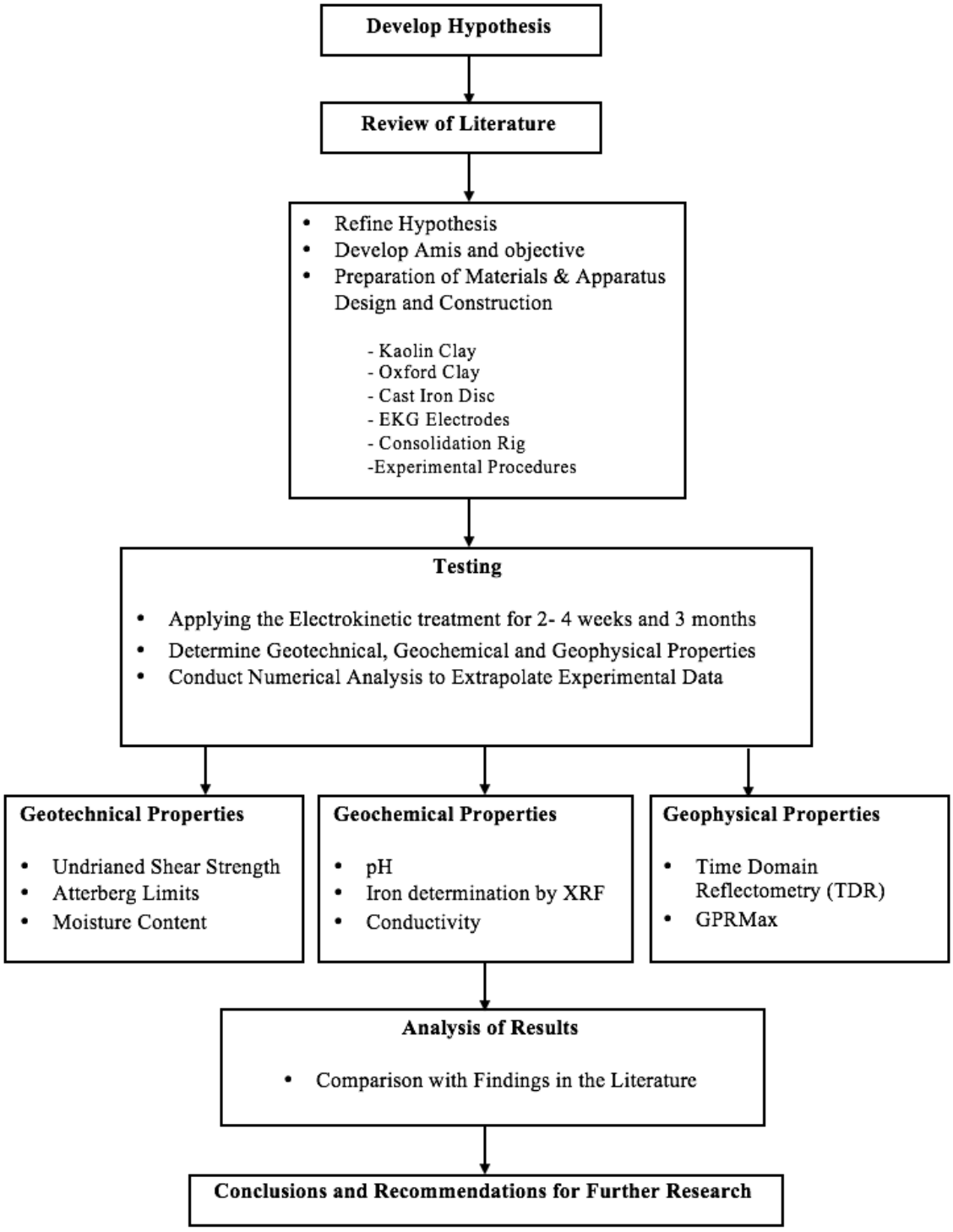

Figure 3.1 Flowchart of research methodology

3.2 Research Philosophy

The literature review established that corrosion of cast iron pipe releases ions into the surrounding soil and modifies the soil's physical and chemical properties. However, most investigations to date have been focused on the mechanical behaviour of the associated pipes, which is now well understood (Rajani & Kleiner, 2001). This chapter describes a laboratory-based test programme devised to meet the aim of this research, i.e. to help understand how the released ions influence changes to the soil properties and the extent and degree of influence these changes have with time or increasing corrosion. An experimental methodology was therefore designed to characterise and evaluate the modification of the surrounding clay, and hence assess the implications of the release of ions from the corrosion of cast iron. Consequently, the methodology was designed to focus solely on the modified clay associated with a single corrosion source: cast iron. This meant that it had to be designed to prove the accuracy (by preliminary design – see Section 3.6.1), to ensure that the required parameters (as established from the literature review – see Sections 2.7.1, 2.9 and 2.17) for critical evaluation of soil modification were obtained (by the geophysical and chemical tests – see Section 3.4), and that the modified soil was characterised (by the geophysical and chemical test results – see Sections 4.2 and 4.3).

A series of experimental testing arrangements were designed to help understand the complex interactions occurring when buried cast iron pipes corrode within soils. The focus of the experimental process was on the effects of cast iron corrosion on the physicochemical properties of clay, including novel geophysical assessments. The experimental process was designed to ensure reliability and repeatability (e.g. the system was tested regularly to ensure that it was performing the same for each test, and that the tests were repeatable – see Section

3.7), including the use of replicates and controls (e.g. ensuring external factors that might affect the system were minimised – see Section 3.7) for each testing approach to ensure consistency. Due to the very slow timescales for natural corrosion processes for cast iron, a catalyst for acceleration (a weak electric field) was employed to drive corrosion and migration of released ions. Control samples (samples without a cast iron disc) were also created and tested to assess the implications of this acceleration on the natural behaviour of the test clays, i.e. tests were carried out with and without cast iron discs. Two clay (Kaolin Clay and Oxford Clay) were tested to provide a platform for comparison of behaviour, due to the clays' different natures (predominantly single and mixed mineralogies) and properties.

3.3 Material Specification and Characterisation

The primary soil used for this study was Kaolin Clay, due to its low chemical complexity and ease of understanding of any induced modifications, i.e. the induced physicochemical modifications of the clay could be clearly delineated, from which comparisons could then be drawn with the behaviour of more complex clays. Oxford Clay (a mixed-mineralogy, though predominantly illitic, clay) was used for comparison, as stated in Section 3.1.

A simple schematic of the experimental arrangement that was finally adopted for the testing is shown in Figure 3.2. A cast iron disc was used in the accelerated corrosion tests that had similar properties and composition to old pipelines, in order to help relate the test results to field conditions. The only difference was that phosphorous was not included in the composition of the disc, due to health and safety considerations (kidney damage). The cast iron was used as a source of ions, which were released through the soil due to the application of an electrokinetic field across consolidated soil samples, i.e. between the cast iron disc (the anode) and a cathode created from graphite-coated electrodes (or Electrokinetic Geosynthetic, EKG; the coating

prevented corrosion of the electrodes and hence any ions being released from the electrodes). In the control experiments EKG was used for both the anode and cathode. EKG has been used by many researchers (Barker et al., 2004; Liaki, 2006; and Ahmad et al., 2011) for the same purpose and has shown no evidence of corrosion or release of other ion products.

Consolidation, rather than compaction, was chosen as the means of soil sample creation in order to avoid the possible creation of air voids and non-uniformity across the diameter of the sample, both of which could adversely affect the results. A consolidation rig was consequently designed and constructed for this project (see Section 3.7.1); the consolidation equipment was made of steel. Demineralised water with a purity of 0.056 μs/cm, was used during all the tests to prevent any significant quantity of additional ions coming into the soil. The materials' specifications used in this study are explained in subsequent sections. Furthermore, when testing the soil after electrokinetic treatment, all the plates and equipment used were washed with 1.0ml of nitric acid (acid wash) to make sure that no further ions (especially iron ions) entered the soil while it was being tested.

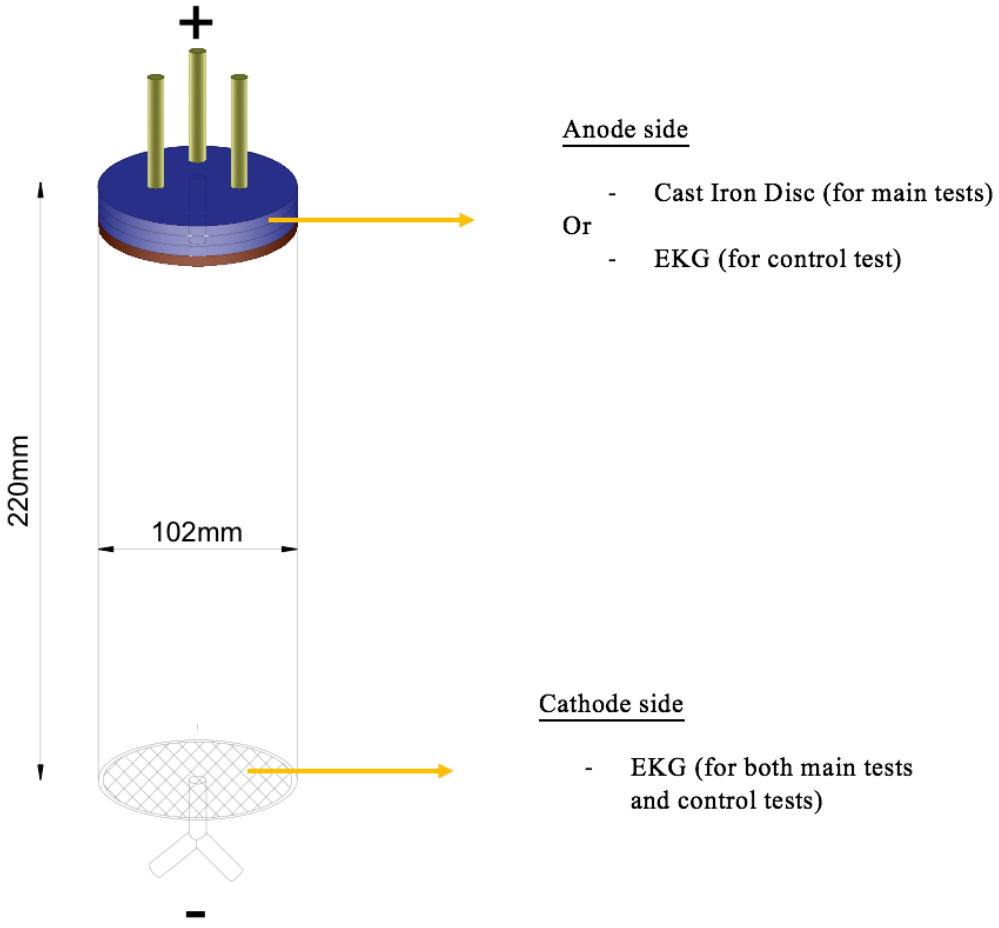

Figure 3.2 Anode and cathode sides of the cell arrangement

3.3.1 Clay

Kaolin Clay was selected due to its widespread usage in similar research and consequently its relatively well-known physical and chemical properties, including low activity, low adsorptive capacity and high electro-osmatic transport efficiency (Tajudin, 2012). The precise product used was PolWhite E English China Clay, supplied by Sibelco Minerals Ltd of Cheshire, UK. This is a high quality Kaolin product (Sibelco, 2012) with a fine particle size (<2m).

The mineralogy of the Kaolin Clay and Oxford Clay (the table for which is likely to be representative of the clay that was used in this tests, but do not necessarily present the exact proportions as it was not possible to do such percentage determinations) is given in Tables 3.1 and 3.2 respectively, while Tables 3.3 and 3.4 present the properties of the Kaolin Clay and Oxford Clay. The Oxford Clay sample was collected from Hanson Brick Quarry (in Peterborough, England) at ground level. Oxford Clay consists of a marine sedimentary rock formation from the Jurassic period and underlies much of southeast England, around Oxford, Peterborough and Weymouth. All the clay used in this research was from the same batch, and was mixed before any tests were carried out in order to homogenise the soil.

Table 3.1 PolWhite E bulk mineralogical composition provided by Sibelco, Ltd.

Mineral	**Content %**
Kaolin	≈ 66
Feldspar	6
Quartz	1
Mica	≈ 23
Montmorillonite	2

Table 3.2 Oxford Clay mineralogical composition (Batchelder et al., 2007)

Mineral	**Content %**
Near-illite	21
Illite-smectite	15
Quartz	28
Calcite	12
Kaolinite	7
Feldspar	4
Gypsum	3
Pyrite	2
Chlorite	3

The undisturbed Oxford Clay was packed and sealed in a bag and stored in a storage room with a temperature of 21°C. Given the difficulty of accessing Oxford Clay, it was decided to use soil already available in the laboratory and reanalyse its chemical and physical properties before starting any sampling. The soil's chemical compositions were quantified by using X-ray fluorescence.

Table 3.3 Kaolin Clay properties

Kaolin Clay Physical and Chemical Properties			
Liquid Limit	55.6%	Specific Gravity	2.6
Plastic Limit	23.6%	Conductivity	37.6 µs/cm
pH	5.63		

Table 3.4 Oxford Clay properties

Oxford Clay Physical and Chemical Properties			
Liquid Limit	65.1%	Specific Gravity	2.6
Plastic Limit	35.2%	Conductivity	25.2 µs/cm
pH	7.31		

The chemical composition of the Kaolin Clay and Oxford Clay is given in Tables 3.5 and 3.6 respectively. Kaolin Clay has a high amount of silicate and aluminate, is a non-reactive clay with a low cation exchange capacity, and is an acidic clay with a low specific surface area compared to other clays (Reeves et al., 2006).

Table 3.5 Compositional results from analysis of the Kaolin Clay provided by Sibelco Ltd.

Chemical Composition	Typical value (%)
SiO_2	48.30
TiO_2	0.04
Al_2O_3	36.30
Fe_2O_3	0.80
CaO	0.06
MgO	0.40
K_2O	2.60
Na_2O	0.10
Loss on Ignition at 1000℃	11.60
H_2O moisture content	0.80

Table 3.6 Compositional results from analysis of Oxford Clay, as reported by Batchelder et al. (2007)

Chemical Composition	Typical value (%)
Al_2O_3	17.44
Na	0.28
K	2.42
CaO	7.40
$FeO+Fe_2O_3$	6.46

3.3.2 Composition Evaluation of Clay

Elemental compositional analyses were undertaken using X-ray fluorescence (XRF), which provided information on the quantitative elemental composition (%). The elements present (with atomic numbers greater than 16) may be identified and quantitated by counting the number of photons of each energy level emitted from a sample. The XRF measures the total concentrations of all elements in the chemical form of oxides. This method is suitable for the determination of metals in soil samples. However, XRF analysis cannot distinguish ions of same element in different states. The accuracy of XRF depends on factors such as quantity of

material available for analysis as well as its form and geometry. The analysis was undertaken using a Bruker S8 Tiger instrument at the School of Chemistry, the University of Birmingham. Samples were prepared as explained in Section 3.10.3. Table 3.7 presents the oxidic elemental composition of the Kaolin Clay and Oxford Clay as obtained from the XRF analyses.

Table 3.7 Elemental composition of Kaolin Clay and Oxford Clay obtained via XRF (%)

Kaolin Clay		**Oxford Clay**	
SiO_2	42.2	SiO_2	34.9
Al_2O_3	30.8	Al_2O_3	12.6
K_2O	2.85	CaO	9.68
Fe_2O_3	1.11	Fe_2O_3	7.11
MgO	0.28	SO_3	5.05
P_2O_5	0.13	K_2O	3.09
Rb_2O	0.119	TiO_2	1.23
TiO_2	0.082	MgO	1
SrO	0.045	Na_2O	0.27
MnO	0.034	P_2O_5	0.27
ZrO_2	0.024	BaO	0.15
CuO	0.017	ZrO_2	0.071
As_2O_3	0.01	V_2O_5	0.061
		SrO	0.06
		ZnO	0.029
		Rb_2O	0.021

3.3.3 Cast Iron

As the purpose of this research was to understand the effect of cast iron corrosion products on clays, and due to the difficulties of producing consolidated samples in contact with cast iron pipes, it was decided to use cast iron discs instead of cast iron pipes. It was felt that this would not affect the aim of the research.

The cast iron discs were an important aspect of this study as they were the main source of the corrosion products in the tests. The cast iron used for the study was in the form of cylindrical discs (99 mm in diameter and 10 mm thick), and was cast by James W Shenton Ltd., UK. This company uses vertical sand moulds for producing cast iron when small quantities of the material are required. The moulds leave a rough surface to the material induced by the sand grains. Similar cast iron materials have been used previously for experimental testing by other researchers (for example Schmidt, 2007). The company reported that the cast iron was produced using similar casting techniques to those used for the old water-bearing cast iron pipes, and this gave the cast iron discs similar properties to those old pipelines, in terms of surface roughness and density. Table 3.8 presents the chemical composition of the cast iron used for this study.

Table 3.8 Composition of cast iron (Numbers from James W Shenton Ltd.)

C	3.2-3.4%	Ni	~0.2%
Si	1.8-2.2%	Cu	~0.2%
Cr	0.1-0.2%	Ti	~0.01%
Mn	0.5-0.7%	Sn	0.02-0.6%
P	~0.07%	Pb	0.005%
S	~0.1%	Fe	~96%

The cast iron is composed of iron alloyed with relatively small amounts of carbon and silicon. This helps to keep the iron fluid enough during casting to fill moulds with large or complicated shapes (Makar & Rajani, 2000). The difference between this material and the original cast iron used for making water pipes is that it has a lower phosphorus (P) content. A high amount of P content improves abrasion resistance and casting properties, due to the lower melting

temperature (Makar & Rajani, 2000). However, it was difficult to find a company using iron with a higher P content because of health and safety issues. The properties of cast iron are influenced firstly by the form in which carbon is presented, as graphite flakes, and secondly, the matrix material, which is ferritic (Reynaud, 2006). The amount of silicon (Si) has little effect on the corrosion resistance of cast iron and, in general, as the combined carbon and silicon content is reduced, the strength of the cast iron is increased (Reynaud, 2006).

3.3.4 Water

Demineralised, or deionised, water was used for the preparation of the clay slurry, as well as all the processes involved in the physical and chemical tests and the analytical processes undertaken as part of the experimental study. Demineralised water is defined as water that is almost or completely free of dissolved minerals, as a result of distillation, deionization, membrane filtration, electrodianalysis or other technologies (Kozisek, 1992) and it has a conductivity of 7.5 μS/cm at a temperature of 25ºC. For this research the demineralised water was created using a Elga Prima machine (MEDICA-R 7/15) and achieved a conductivity of 0.056 μS/cm at a temperature of 25ºC. It should be mentioned that the term 'water' in this thesis will be used to refer to demineralised water throughout. The demineralised water was created and stored in a temperature-controlled room at 21±2°C.

3.3.5 Electrodes

Due to the need to accelerate the rate of corrosion during the experimental testing, an electrokinetic process was employed. This process involved applying a weak electrical current across the soil specimens to drive the corrosion process of the cast iron disc, and hence ion migration into the soil, when this was used as the anode in the experiments examining the effect

of corrosion products on the clay. In cases where ion release from electrodes needed to be prevented during testing (a non-corrosive electrode was used as the cathode in all tests, and at the anode in place of the cast iron disc in control tests), it was necessary to use electrodes that were non-corrosive. The type of electrode used for this study was the Electrokinetic Geosynthetic (EKG) made at the University of Newcastle. This electrode consists of a geonet extruded from a Cabot Cabelec3892 polymer, which is a specially formulated conductive compound based on conductive carbon black dispersed in a modified high density polyethylene resin, and therefore a carbon polymer (Pugh, 2002).

The geonet consisted of horizontal ribs intersected by diagonal ribs (Figure 3.3(a)). Monofilament stainless steel wires ran through the centre of alternate horizontal ribs to act as current distribution stringers. This was done to achieve a more efficient distribution of current through the length of the EKG, as the electrical conductivity of wire was significantly higher than that of the conductive polymer. The electric current would otherwise have selected the path of least resistance and the majority of the current would have been passed where the EKG entered the conductive medium to be treated, i.e. the soil, resulting in high localised current densities with possible adverse durability implications (Pugh, 2002). Prior to use, the EKG material was cut along its length and expanded. The EKG was then cut to the required length, which was approximately 80x55 mm (see Figure 3.3(b)). A stainless steel wire was twisted and attached tightly at the centre of the EKG material (see Figure 3.3(b)). The stainless steel wire was attached to one of the wires within the EKG. This helped to distribute the current while the EKG was in direct contact with soil. During the electrokinetic process no evidence of corroded stainless steel wire was observed.

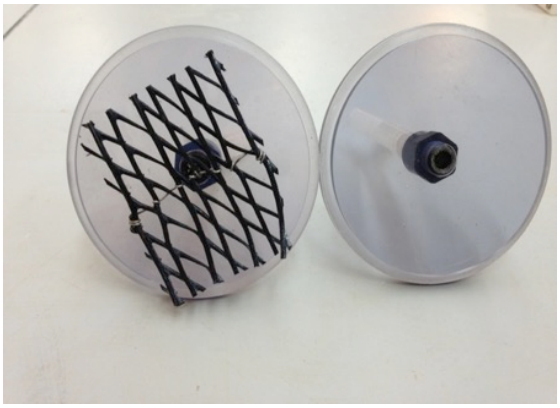

Figure 3.3 (a) Electrokinetic geosynthetic used as the anode in control tests

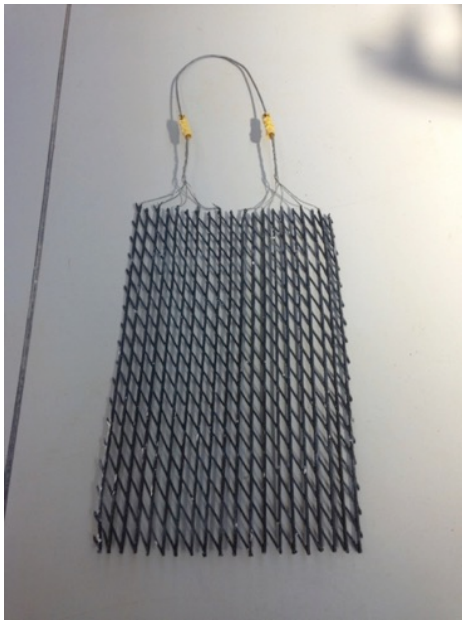

Figure 3.3 (b) The EKG used for the geosynthenic bottom section of sample (the cathode)

3.3.6 Current Supply

The power supply equipment used to induce the potential difference across the test samples was a TS3022S instrument, produced by Thurlby Thandar instruments (TTi, Huntingdon, UK). The electrical gradient used was 10V/cm length DC (between electrodes), based on the results of preliminary tests, which are explained in Section 3.8.

3.4 Laboratory Experimentation

To assess the modification of the clay samples by ion transmission (from the corroding cast iron) and the interaction of the ions with the soil, experimental methods were identified and/or developed to determine the physical, chemical and geophysical properties of the soil. The chemical assessments were essential to determine component release, and assess how the surrounding soils were chemically modified due to the cast iron corrosion. Corrosion of cast iron pipes naturally causes rust in the form of ferric oxide and ferric hydroxide to form at the external surface of the pipe, and importantly to release iron ions into the surrounding soil, which themselves can form iron oxyhydroxides in the soil. These oxyhydroxides have a low solubility (Schwertmann, 1991). Therefore, the parameters controlling this needed to be evaluated, as follows.

To evaluate the solubility properties of the iron oxyhydroxides, and the amount of iron that could be sorbed by the clay in addition to the precipitated salts, ion leaching assessment (to determine the pH-dependency of ion solubility, complexation or precipitation; see Section 3.10.1) and compositional analysis (X-ray fluorescence method, see Section 3.10.3) were carried out, and these were validated by pH modification assessment showing what was changed throughout the sample due to the acceleration of the corrosion rate via electrokinetics.

Therefore, the solubility of the ions within the treated soil was evaluated to give an indication of the ion migration plume (see Section 2.17), which could be correlated with the total ion content to identify the solubility condition using the pH-dependent leaching behaviour as validation. This provided a better understanding of the behaviour of the released ions within the pH domain.

When soil is modified chemically, it is important to evaluate the physical changes in the soil properties. These modifications may be tightly bound and localised to the immediate area surrounding the corroding source. Physical changes such as undrained shear strength and Atterberg limits were established, as were changes in the moisture content. The undrained shear strength showed the differential changes in shear strength within the sample induced by the electrochemical treatment and the migration of ions. In order to define the boundaries of pipe detection using GPR, it was essential to measure the geophysical and geochemistry parameters of clay soil. Parameters such as Atterberg limits (e.g. liquid limit) have an influence on the results of GPR imaging, for example. Moreover, it is of interest not only to understand the implication on visibility to GPR, but also in appreciating how the physical properties could have implications on managing such assets.

Geophysical measurement can provide an indication of the spatial variability of properties across a sample both before and after treatment. The choice of which geophysical tests to use depends on the parameters to be examined. In this study it was essential to evaluate the changes in properties such as resistivity, permittivity and conductivity; therefore, time domain reflectometry (TDR) was chosen for this measurement, particularly in view of the size of the sample being used.

From the corrosion of cast iron, the released iron ions readily form iron oxyhydroxides and are theoretically expected to have low solubility, which therefore mandates an evaluation of the solubility conditions within the experimental clays, as well as the maximum amount of iron ions that can be sorbed or complexed by the clay, in addition to co-precipitation of ions (Schwertmann, 1991). To evaluate the solubility properties of iron oxyhydroxides and the amount of iron ions that could be removed from the soluble fraction by the clay soils in addition to insoluble or precipitated salts, iron solubility tests were adapted and undertaken. Electrokinetics was used to increase the electric potential across the soil samples and accelerate the corrosion rate of cast iron in contact with the clay soils. However, this method induces a variable pH modification within the soil, due to ion migration between the anode and cathode. This necessitates an understanding of the solubility and precipitation behaviour of the released ions (of interest) within the pH domain (pH 2-12 expected from the anode to the cathode). Therefore, a pH-dependent solubility evaluation was required (see Section 3.10.1) to assess the maximum soluble availability of the ions of interest (iron), as well as the solubility behaviour across the pH range. For repeatability and validation of the results, it was decided to prepare four samples at the same time with the same properties and conditions.

3.4.1 Chemical Parameters

In order to better understand chemical interactions and make an ion leaching assessment, it was essential to obtain information on the chemical properties that influenced the behaviour of the clay soils. These chemical parameter measurements were pH and conductivity. The pH of a solution measures its acidity or alkalinity, defined as a negative, base 1 logarithm of hydrogen ion activity, and it controls, or is involved in controlling, most chemical reactions in the

solution (Langmuir, 1997). Based on the BSI 1990 part 2.2, as the pH is sensitive to temperature, all measurements were taken in a temperature-controlled room (21±1°C), with heat release calibrated to 20°C. An Orion Bench-Top pH Meter, model 520A, was used for the measurements. Each measurement took 5 seconds on a sample, and after every 10 measurements, recalibration was undertaken using three standard calibration buffers (pH 4.00, 7.00 and 12.58).

The electrical conductivity (EC) of a solution is the measure of its ability to conduct electricity and serves as an estimate of the total amount of dissolved salt or of dissolved ions. EC is measured in microsiemens per centimetre (s/cm), and the measurements were conducted in a temperature-controlled room (21±1°C) as the solubility level is sensitive to temperature. A Hanna Hi 9033 multi-range meter was employed for elute measurements during testing and the test was carried out in accordance with the British Standard (BSI 1990 part 2.2; BSI, 1990a).

After chemical characterisation of the modified soil, it was important to evaluate, using a method suitable for the prepared samples, the physical modifications induced by precipitation and other ion interactions from the corroding cast iron. However, it was important to consider that due to the potentially high insolubility of the released ions, the zone of influence was likely to be highly localised and tightly bound around the corroding source.

3.4.2 Geotechnical Parameters

Taking physical parameter measurements was important for evaluating the soil properties and involved using methods compatible with the prepared samples. As water is a key parameter,

because it affects the propagation of EM signals and permittivity of soil and bulk electrical conductivity, therefore one of the essential parameters included the Atterberg limits (since it affects in turn the balance between free and bound water). Moreover, Atterberg limit tests are feasible for small sample volumes using methods based on the Casagrande method in BS1377 Part 2 (BSI, 1990a). Also, it was important to know the moisture content of the sample, which could be validated (Liaki, 2006; Tajudin, 2012) by the undrained shear strength test proposed by Hansbo (1957; described in Section 3.11.1). This method was chosen due to the small volume of the soil samples used and the subtle changes in shear strength likely to occur throughout the samples. Therefore, small-scale laboratory equipment was needed. This method also allowed evaluation of the differential changes in shear strength caused throughout the samples by ions released as a result of corrosion of the cast iron discs. During the electrokinetic process, the cast iron in the test cell (see Section 3.6.3) caused it to become a galvanic cell, driving the release and migration of ions from the cast iron disc at the anode through the clay.

Due to the electrochemical treatment, and the released ions migrated through the soil, the clay properties were expected to change extensively and variably throughout the sample. Geophysical measurements were taken to determine the changes in properties such as permittivity and conductivity by using Time Domain Reflectrometry (see Section 3.12.1), while taking note of the factors that affect this measurement, such as the soil salinity, temperature and the presence of magnetic material (see Section 2.11.1). Therefore, by bringing together the changes in these properties and combining them with changes in chemical properties, it was possible to make an evaluation of the modifications to the clay around the corroding cast iron.

3.5 Rationale behind the Test Arrangements

The focus of this project was to investigate the effect of cast iron corrosion on the chemical and physical properties of clays and investigate these changes on the geophysical properties of the clay soil. In Section 2.1 of the literature review, it was noted that the corrosion rate could increase with increasing conductivity or decreasing permittivity of the soil. Since corrosion of cast iron releases iron ions into the surrounding soil, which increases the total dissolved salt content and so increases the electrical conductivity, this can further accelerate the corrosion process and increase its extent.

Since the corrosion process is very slow under natural conditions, acceleration is unavoidable and therefore controls must be put in place to ensure that any changes induced by the experimental process (i.e. changes that differ from natural processes) are clearly characterised and understood. One method of achieving this acceleration is to induce an electrical field (the creation of a galvanic cell) to drive the flow of ions and fluids through the test clay. However, this has the potential to create a material with different properties to those observed in the field. Therefore, the laboratory test arrangement for the clay and cast iron had to be prepared in a way that would simulate the release of corrosion products (ions) from the cast iron and cause them to migrate into the clay, while allowing for a draining of fluids due to the electrokinetic processes. Electrochemical oxidation induces corrosion to release iron ions into the surrounding soil, which modify the physical and chemical properties of soil. Depending on the type of ions present in the soil prior to experimentation, different interactions take place, such as dissolution, precipitation, ion exchange and complexation. However, these modifications are not well understood. The methodology was therefore designed in such a way as to help understanding of how these released ions influenced changes in the soil properties, and the extent and degree to which these changes occurred with time, and affected corrosion. Also,

geophysical techniques were used in this work, and these measured the electrical properties of the clay soil, although they needed to be related to the geotechnical properties, such as moisture content and undrained shear strength (see Section 5.4). To avoid unwanted additional physical and chemical changes in the sample, a geophysical method was needed that would not require boreholes; moreover, geophysical equipment had to be chosen that was suitable for the size of the sample. Therefore, time domain reflectometry was used.

3.6 Experimental Design

3.6.1 The Preliminary Design

The first test cell design utilised cast iron discs at both the anode and cathode. These had 24x4mm diameter holes drilled through both platens to allow fluids to drain through them during the consolidation process, as well as during the ion migration and electroosmotic processes which would form part of the electrokinetic process. This also prevented gas generation or build-up within the sample. The initial soil samples were consolidated in a small 1D consolidometer to a final height of 200 mm and a diameter of 159 mm. The test arrangement was constructed to include three main parts, as shown in Figure 3.4. The top section was a water reservoir and contained a cast iron disc; the centre part contained the clay sample; and the bottom section consisted of the second cast iron disc. The whole arrangement was placed in a container to catch the water passing through the sample due to the electroosmotic flow (Schmidt, 2007). The external diameter of the discs used as the cathode and anode were 158mm and 185mm respectively. The location of the holes drilled in the discs is shown in Figure 3.4. The cable to carry the electric current to the top cast iron disc and drive the electrokinetic process was fixed in a loop and attached through one of the holes in the cast iron disc, and then soldered to the disc. The cast iron discs were placed in such a way that they had direct contact

with the clay soil. The top cast iron disc was designed to be of a slightly smaller diameter than the plastic cylinder in which the clay soil was consolidated, in order to allow it to serve as the consolidation plate. The edges were smooth and trimmed to allow ease of movement within the plastic cylinder during consolidation and to facilitate any expansion or contraction of the soil under the influence of the electroosmotic flow through the clay. The bottom cast iron disc had a greater diameter than the test cylinder to act as a bearing plate. It contained four drilled holes to connect the test cell together by four nylon rods, nylon being a non-corrosive, non-conductive material and strong enough to keep the test apparatus sections together (Figure 3.5). However, the precipitation of salts within the drainage pores in the disc caused clogging, which prevented cathodic drainage during current injection and highlighted the limitations of the experimental design. The initial design was created with a view to the potential development of larger diameter samples (300mm) and, potentially, the use of GPR as part of geophysical assessment. However, this was deemed impractical in view of a number of issues, including the preparation of samples of a dimension that would support a GPR survey (300mm was subsequently found to be insufficient), as well as the impractically long consolidation times due to the large sample size (consolidation time is related to the square of the length of the drainage path) and final moisture content.

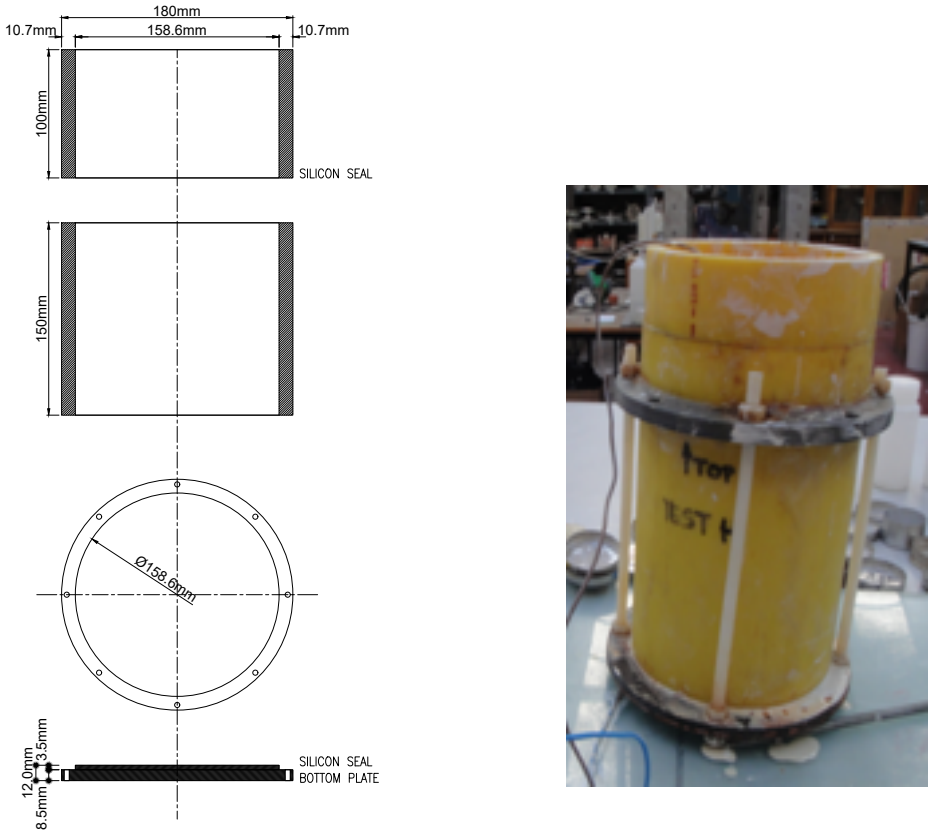

Figure 3.4 Sample dimensions and general arrangement of the preliminary test cell

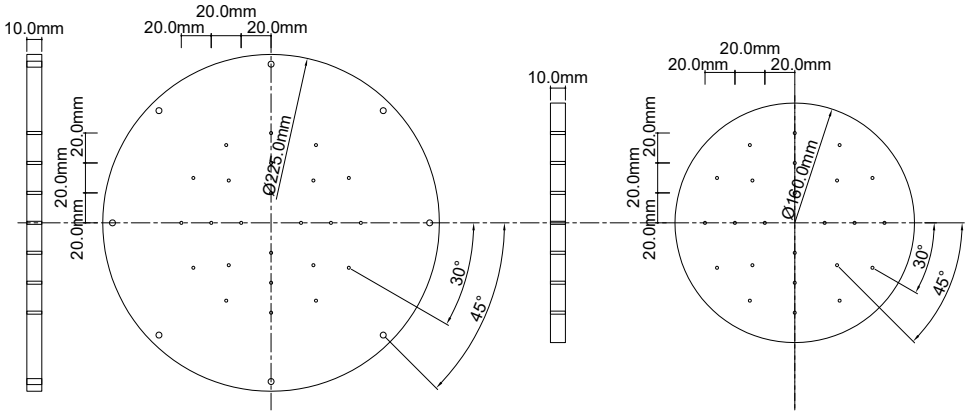

Figure 3.5 Bottom (left) and top (right) cast iron discs showing dimensions and the arrangement of holes

3.6.2 The Modified Design

The next phase in the development of the experimental design involved modification of the preliminary design to incorporate an embedded cast iron rod within the consolidated clay. This method was designed to simulate the corrosion of a buried pipe within a clay soil. A 100mm diameter x 200mm (initial) high cylinder filled with Kaolin Clay consolidated to a moisture content of 45% (due to ease of workability) was used. The cylinder contained a 180mm long cast iron rod, which was embedded within the sample before consolidation. The Kaolin Clay with 85% moisture content was poured into the cylinder and the 180mm long cast iron rod was then embedded within the sample before consolidation took place. The rod was placed in close proximity to the electrodes and between the top and bottom PVC plates to which were attached EKG electrodes (see Figure 3.6). After consolidation, a 10V/cm voltage difference was applied across the sample. After 7 days the sample was extruded and assessed. From observation, only localised corrosion and precipitation products were observed around the cast iron rod, with no evidence of migration through the sample. Also, the potential for precipitation of corrosion products on the cast iron rod itself made the design unsatisfactory. In addition, there was a need for a higher voltage gradient within time scale required (7days, in order to establish the cathode and anode area – compared to the preliminary design) and extended experimental testing times to allow corrosion and migration of ions into, and formation of corrosion products in, the surrounding claysoil. In addition, vertical measurement of the modifications or alterations to the clay soil was needed, and this required extrusion of the sample to measure the various parameters. This proved impractical with the embedded rod and the very localised nature of the soil modification.

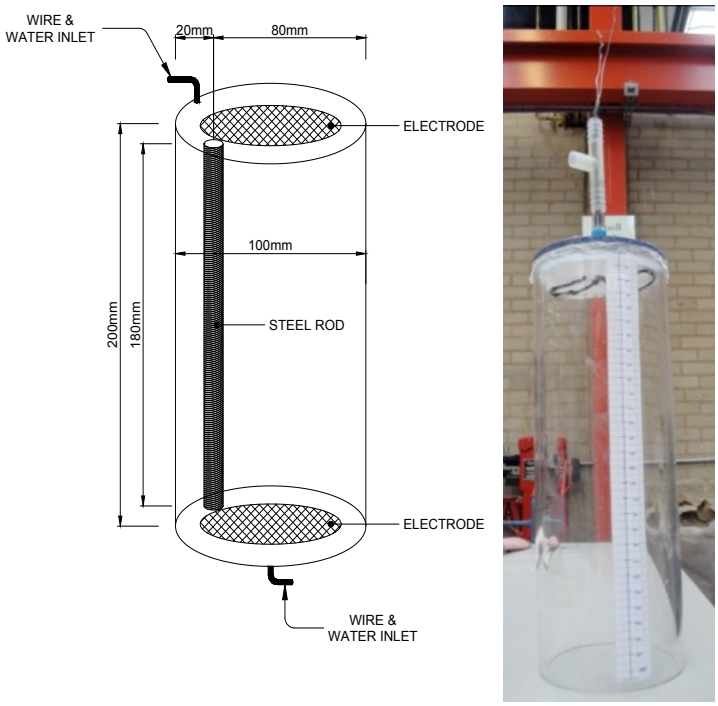

.

Figure 3.6 Modified cell design and arrangement using a vertically placed steel rod

3.6.3 Final Experimental Design

Having considered the preliminary and modified designs, lessons from these were incorporated into the design of the final test arrangement. The method was designed to be practical (i.e. practical in terms of size and ease of assembly) and accurate (no more than 5% variation in results; see Section 5.2.1) in terms of the expected parameters to be measured for characterisation of the clay soil modification. It was quickly established that it was impractical to design small experimental processes within the laboratory that would support a GPR survey, and hence this was ruled out of the scope of the work for the design of laboratory testing. Therefore, the primary focus of the experimental study was shifted to evaluating the conductivity and permittivity, i.e. the electromagnetic properties, of the clay soils via TDR, as well as the physicochemical characterisation of the test specimens. The results from TDR can

be used as a surrogate for the likely performance of GPR due to underlying principles being analogous.

The final experimental cell design utilised a Perspex cylinder for consolidating the clay samples, with dimensions of 210 mm height and 100 mm internal diameter. The Perspex material was chosen as it could resist the loads imposed during the consolidation process, as well as for its non-reactive properties. Also, the transparent Perspex material allowed observation of the changes to the clay soil during testing.

The final test arrangement is shown in Figure 3.7 and consisted of four parts. Part 1 consisted of three PVC plates with a diameter of 99mm and 10mm in thickness, which were combined together by a rod which passed through a drilled hole in the centre of these discs, when the top plate was fabricated, as shown in Figure 3.8, to improve stability (i.e. provide sufficient rigidity during loading and provide support to the cell). These plates were connected by a central rod through the middle of the plates (see Figure 3.7), which was attached to the lever arm of the consolidation device to transfer the load, and hence produce a uniform applied stress, to the samples during the consolidation process. Three 6mm diameter holes were drilled through the top plates to allow drainage (two holes) and insertion of the wire carrying the current (one hole; see Figure 3.8).

In the top platen arrangement (Part 1) used for the main experiments, there was no EKG used and the wire was directly connected to the cast iron disc to induce the potential difference across the system and accelerated corrosion. In order to keep the wire attached to the cast iron disc in place, silicon sealant was used to fill the hole in the top platen through which the wire passed. This also prevented any water draining from this hole. Plastic tubes (6mm external

diameter and 4mm internal diameter) were fed into the other two holes in the top platen, which were made to facilitate water drainage, and these were also sealed using the silicon sealant in order to keep the pipes in place and make the joint watertight. A filter paper (a glass microfibre Whatman 0.20 μm membrane filter) was placed between the PVC plates and the cast iron disc to facilitate to two-way consolidation drainage. The wire was passed through the filter paper to the cast iron disc.

Part 2 is the 99 mm diameter, 10 mm thick cast iron disc (the source of corrosion – anode section), (Figure 3.5) and wire attached to its upper surface, was placed below the filter paper.

Part 3 is the experimental cell containing the consolidated soil specimens. It was constructed from non-reactive Perspex and had dimensions of 210mm long, 102mm internal diameter with a wall thickness of 3mm. The cell housed the top platen (Parts 1 and 2) and was attached to the bottom platen (Part 4) by silicon sealer.

Part 4 is the bottom plate arrangement that housed the cathode. The cathode was created from EKG, with a glass microfibre filter paper (of the same specification as at the anode, i.e. Whatman 0.20 μm membrane filter) placed between the clay sample and the EKG in order to prevent clogging. The bottom platen (see Figures 3.9 and 3.10) consisted of a 101mm diameter, 10mm thick PVC disc and was designed with a single outlet, which had the combined function of allowing drainage and housing the wiring to the graphite-coated EKG cathode. This had a Y shaped splitter to separate the wiring from the drainage outlet. A steel wire (Figure 3.10) was bonded to the EKG to facilitate current flow through the sample. The wiring outlet was sealed with silicon sealer to prevent water drainage. The cathodic drain fluid was routinely collected

and the pH measured during tests to ensure that alkaline conditions were being generated at the cathode, which indicated that a successful electrokinetic process was being generated, and to monitor progress.

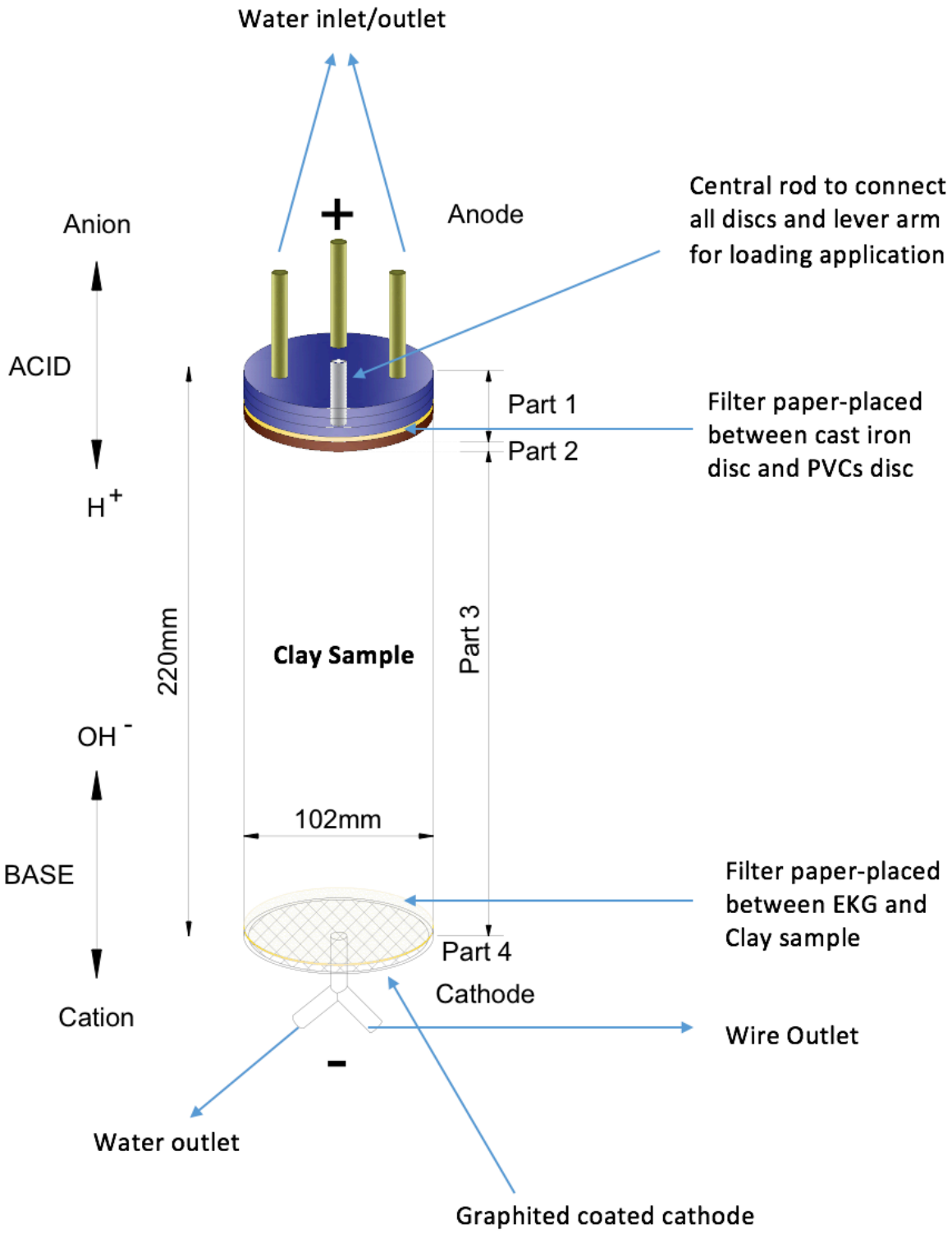

Figure 3.7 Cell arrangement set up

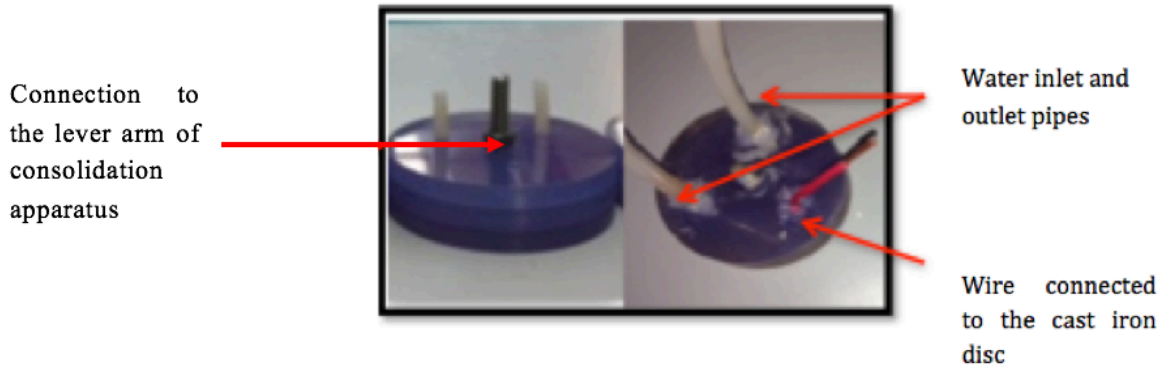

Figure 3.8 Arrangement of the top consolidation plate

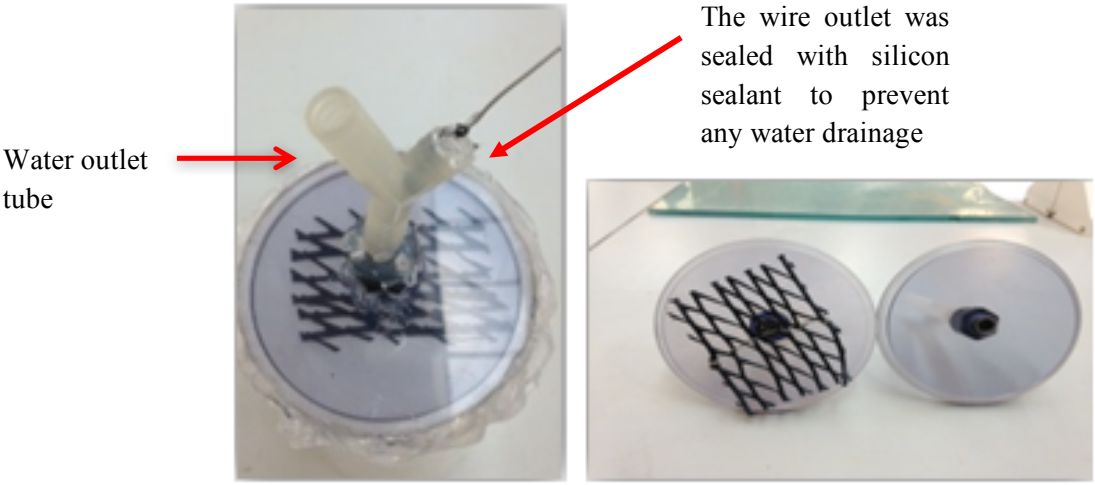

Figure 3.9 Arrangement of the bottom plate

Figure 3.10 The graphite-coated electrode used in the bottom plate of the test cell

The control tests without the cast iron disc were constructed in the same way, the only difference being that the cast iron disc was replaced by EKG (which was connected in an identical manner to the cathode) to form the anode; the electrode position, wires and set up was otherwise the same.

The time periods for the main experimental tests using the cast iron disc were 2 weeks, 4 weeks and 3 months, while periods of 2 weeks and 4 weeks were used for the control tests without the cast iron disc. These tests were repeated for both clays (see Table 3.9). There were no control tests (i.e. without a cast iron disc) of 3 months' duration due both to time constraints (the time involved in sample preparation and testing required that a focus was placed on testing the samples with the cast iron disc for as long a period as possible), but also because control tests of up to 1 month duration using EKG electrodes have been demonstrated to reach a steady-state (Liaki, 2006).

Table 3.9 Test durations for Kaolin and Oxford Clay

	With Cast Iron Disc			**Without Cast Iron Disc**		
Duration of tests	**2 weeks**	**4 weeks**	**3 months**	**2 weeks**	**4 weeks**	**3 months**
Kaolin Clay	✓	✓	✓	✓	✓	-
Oxford Clay	✓	✓	✓	✓	✓	-

An additional 'blank' base plate was designed for use as the bottom plate for the cell while the clay was placed prior to consolidation. The clay was poured into the cell as a slurry (the initial moisture content for the Kaolin Clay and the Oxford Clay was 75% and 85% respectively; see Section 3.7) after mixing under low vibration (estimated as 5Hz), which prevented the accumulation of excessive air voids during loading. After the vibration, the blank base plate

was removed carefully and the cathodic plate fitted and sealed with silicon. This was allowed to dry for 24 hours at room temperature to ensure that the cell was suitably watertight. The clay was separated from the EKG electrodes in both the top (control tests) and bottom platens by a glass microfibre filter paper (Whatman 0.20 μm membrane filter), while the cast iron disc in the main experimental series was in direct contact with the clay and the glass microfibre filter paper was positioned immediately behind it. The complete cell arrangement prior to the loading of the clay and fitting of the top platen is shown in Figure 3.11. Before the fitting of the top platen used during consolidation of the clay within the test cell, the cast iron disc (10mm thick, 99mm diameter) was placed on top of the clay sample. The thickness of the disc was chosen based on previous research test arrangements (Schmidt, 2007) and also based on the preliminary experiments conducted as part of the current research (see Section 3.6.1). The glass microfibre filter paper was then placed over the cast iron disc to prevent the flow of sediment during consolidation, and the top consolidating platen was placed over the filter paper (see Figure 3.7). The test cells were then loaded into the consolidation rig (Figure 3.12) and the consolidation process was undertaken (7 days for the Kaolin Clay and 9 days for the Oxford Clay), with the aim of achieving 40% moisture content at a height of 100mm for each clay sample. The 40% moisture content was chosen so that the soil was in a useable state (i.e. it could be handled and tested) and it also more closely related to the field condition than wetter specimens.

After completing the consolidation process, the cells were clamped to prevent any clay rebound and a current was injected to drive the electroosmosis. The samples were kept hydrated over the period of current injection by maintaining a water feed with a nominal pressure head at the anode to compensate for cathodic draining due to the electrokinetic processes. This helped to prevent the sample drying out and any potential thermal flux forming at the anode, while clamping the samples prevented the clay from taking in more water than was required to keep

the samples hydrated. In order to establish repeatability of the main experimental series, four samples tested in parallel: 3 replicates of the main experiments and one control sample using EKG electrodes with no disc.

A current (using a voltage density of 10 Volt/cm) was injected over different time durations as required for the experimental process, i.e. for 2 weeks, 4 weeks or 3 months. Two weeks' was chosen as the shortest period due to the practicalities of the electrokinetic treatment: preliminary experiments demonstrated that it took a week to develop a stable anode-cathode system. An extra week was given to demonstrate the changes within the system. The 4 weeks time period allowed for the effects to develop with the aim of showing more intensive results, while the longest period, 3 months, was the longest practical period that the timeframe of the work allowed for these treatments and aimed to show the state of corrosion effects when well advanced.

All the samples were prepared, consolidated and tested under similar conditions (including the same temperature of 20±2°C). At the end of testing, samples were extruded and kept in controlled temperature room (20±2°C) prior to geophysical and geotechnical assessments, after which extractions were undertaken for chemical and compositional analysis. These analyses are explained in Section 3.9, while the experimental processes and monitoring are described in Sections 3.7 and 3.8 respectively.

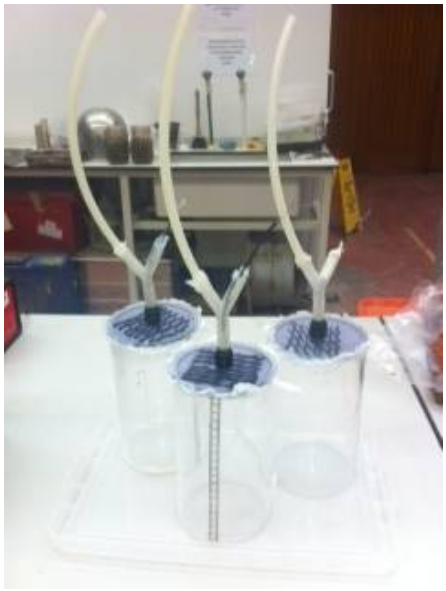

Figure 3.11 Test cells showing the base plate

3.7 Sample Preparation

The Kaolin Clay and Oxford Clay were mixed with 75% and 87% demineralised water respectively prior to consolidation to minimise the presence of air voids. Burland (1990) suggests using a clay slurry at a moisture content of 1.5 times the Liquid Limit (LL). Many other researchers, such as Schmidt (2007) and Tajudin (2012), have used moisture contents of 2.0 times the Liquid Limit for their slurry preparation to improve the homogeneity of the prepared sample.

As mentioned in Section 3.3.1, Kaolin Clay was supplied by Sibelco Minerals Ltd of Cheshire, plc. The clay was processed in their factory and was supplied 'dry' and sealed in a paper bag. The Kaolin Clay was supplied crushed and sieved (<2μm) so there was no need for any further preparation of the material. The company also provided the chemical properties of soil and compositional information is given in Tables 3.1 and 3.5.

The Oxford Clay was packed and sieved as part of a previous research project, however there was no information available relating to the crushing or sieving the soil (wet or dry). The Oxford Clay was sealed in a plastic bag, and during testing immediately resealed after every use, and kept in a temperature-controlled room (under the same conditions as the Kaolin Clay, i.e. at a temperature of 20±2°C).

It was important to minimize the time of consolidation due to the timeframe available for this work. Also, the final moisture content (after consolidation) of the sample needed to be low enough for the sample not to fall apart when it was extruded from the cell and to provide a suitable material for the further testing, e.g. for measuring conductivity/permittivity by TDR (the samples needed to be extruded out of the container in order to take a measurement). Therefore, a slurry moisture content of twice the Liquid Limit (LL) was deemed too high and a value of 1.5 times the LL was adopted. The goal was to have a moisture content as low as 40%, which was a value between the LL and the Plastic Limit (PL) of untreated soil, which were 55.6% and 34.6% respectively for Kaolin Clay. In order to achieve the goal for the Kaolin Clay slurry, 5.5 kg of dry Kaolin Clay powder was mixed with 4124ml of water, which was added gradually to the clay soil in the mixing bowl and mixed in a mechanical mixer for 20 minutes, or longer if any large lumps were evident. The same procedure was followed for the Oxford Clay, which had a LL and PL of 65.1% and 35.2% respectively: 5.6 kg of dried Oxford Clay was mixed with 5655ml of water to achieve a moisture content of 1.5 times the LL. The mixer was operated at a reduced mixing speed to prevent splashing and was stopped occasionally to allow material sticking to the sides of the mixing bowl to be scraped back into the mix.

The slurry was poured into the prepared (100mm diameter, 230mm long) cells up to a height of 161mm and these were then placed on a vibrating plate for 5 to 7 minutes (after which there was no evidence of any air bubbles) to remove any air voids prior to consolidation. It was important to ensure similarity and comparability of the sample preparation process as well as of the materials used; therefore, all the clay used for each replicate test and for all different time durations of the tests was collected from the same batch. Also, all the clay slurries were prepared in an identical way, including the mixing, vibrating and consolidation conditions. After application of the vibration, the samples were fitted with the base plates required for consolidation and the silicon seals used were applied and allowed to harden for 24 hours prior to load application.

3.7.1 Consolidation Equipment

In order to consolidate the clay slurry to the desired moisture contents for testing, it was necessary to design and build bespoke consolidation equipment that would meet the requirements of the research. Figures 3.12 and 3.13 present the overview and side view of the consolidation system respectively, which was designed based on the experimental requirements of sample size and minimal sample disturbance. The rig was designed to transmit loads through the central load transfer extension onto the top plate of experimental cell (see Figure 3.14). The consolidation rig was designed with two arms, each fitted with a splitter device to transmit the loading onto two experimental cells (see Figure 3.14). This design was deemed the most practical option that could safety be used within the constraints of laboratory operation, and that would ensure the testing process was consistent and reliable.

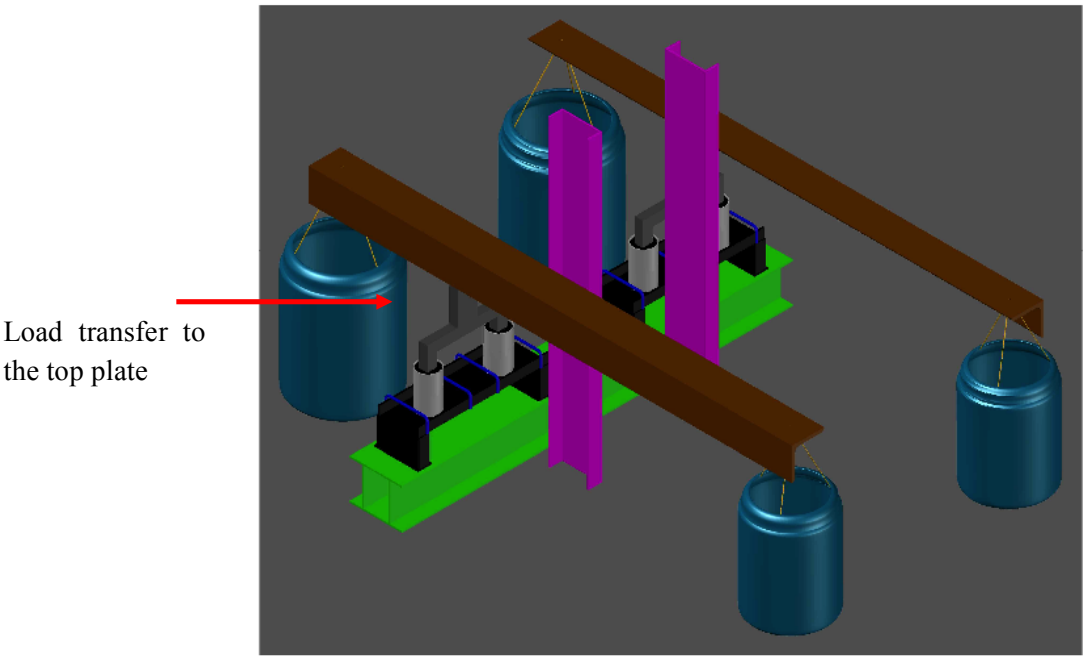

Figure 3.12 Consolidation system

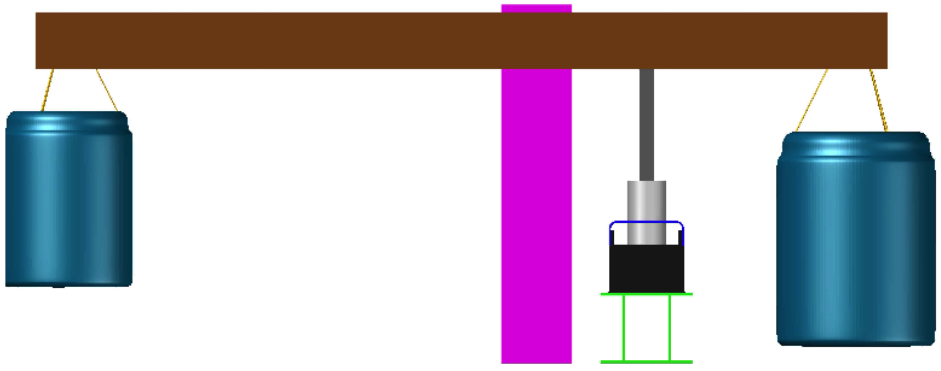

Figure 3.13 Consolidation rig – side view

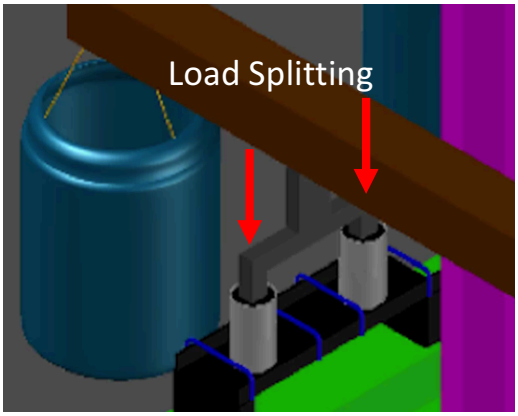

Figure 3.14 Consolidation system – detail of arm

Prior to consolidation, the samples were positioned and clamped on both sides (see Figure 3.15) in order to avoid any translational sliding during consolidation (and keep samples safely secure) and then the load splitters were located on the central rod of the top platen, which had previously been located firmly onto the top of the samples (i.e. with the cast iron disc or filter paper-covered EKG on the top of slurry).

Figure 3.15 Slurry samples placed ready for consolidation

Figure 3.16 Consolidation equipment showing the sample location and the loading machanism using water tanks

The consolidation system (see Figure 3.12 and 3.16) used in this research works by removing/adding the required amount of water to ensure the correct stress is applied to the soil samples. Figures 3.17 and 3.18 demonstrate how the loading system works for the consolidation process. In Figures 3.17 and 3.18, F_1 and (a larger tank) F_2 are the tanks of water that are used to apply the load and they hang at either end of a beam. The starting position of the beam is such that no load is applied to the sample (P_2) and by adding load gradually (adding water to tank F_2), the required amount of load (hence stress) will be applied to the sample. $P_2 = \frac{W[D_2+D_3-\left(\frac{D_1+D_2+D_3}{2}\right)]+F_2(D_2+D_3)-F_1\times D_1}{D_2}$ This method of applying the load helped to minimize any disturbance to the samples by applying the loads to them gradually. During the consolidation process, evaporation of water was checked (by marking the level of water inside the tank) and it was determined that no measurable evaporation had occurred during the consolidation process. Although all the tests took place in winter, the laboratory temperature remained approximately constant (at a temperature of 20 ± 2^{o}C).

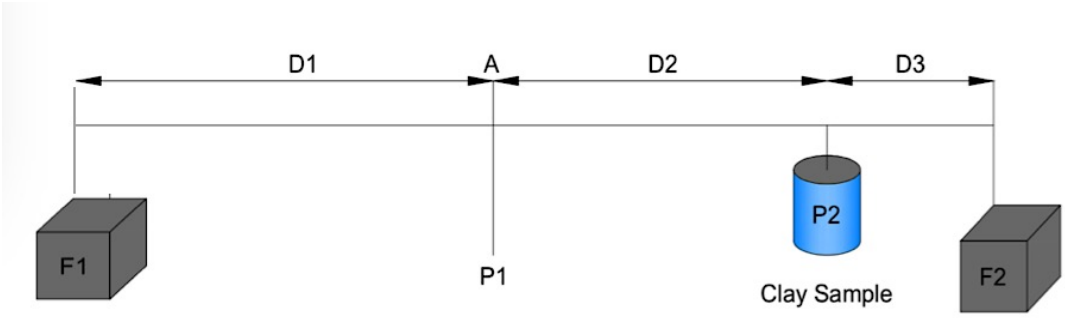

Figure 3.17 Consolidation rig at the start point (beam in equilibrium and no load applied to the sample)

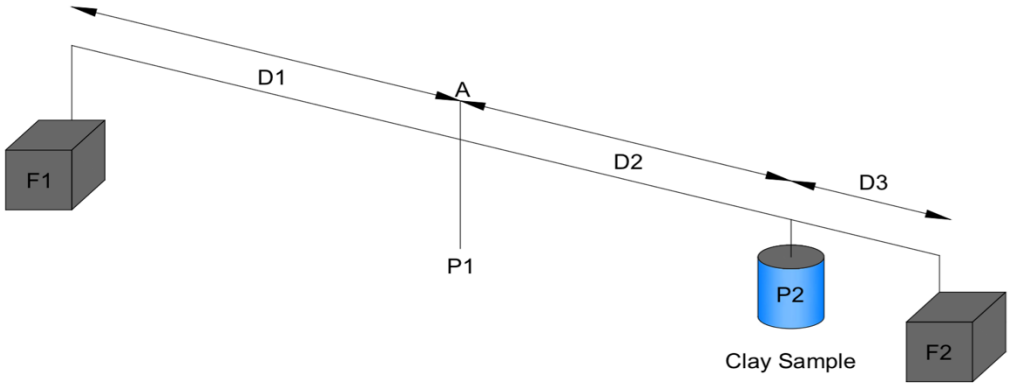

Figure 3.18 Consolidation rig during loading of the sample

Prior to the main experiments, trials were undertaken to determine the time and load requirements for consolidation, in order to achieve the desired sample and moisture properties for testing. As stated above, the system worked by gradually increasing the load (i.e. stress) on the clay sample. The stress started from zero and ended with 64.2 kPa and 72.2 kPa on samples for Kaolin Clay and Oxford Clay respectively (the load was spread over the area of the sample, which was 7.8×10^{-3} m^2). Stress increments of 10.4 kPa, 20.6 kPa, 40.2 kPa, 61.3 kPa and 64.2 kPa were used to reach the maximum stress level for the Kaolin Clay, with an additional

increment being required to reach 72.2 kPa for the Oxford Clay sample. Each loading step took 24 hours to complete and so the total loading took 5 days for the Kaolin Clay and 6 days for the Oxford Clay. This was designed based on the final moisture content that was required for the clay samples. Table 3.10 presents the results after the consolidation process.

Table 3.10 Final conditions in the consolidation process

Sample	Unit Weight (kg/m^3)	Moisture Content (%)
Kaolin Clay	17.54	40.3
Oxford Clay	17.10	47.0

To enable drainage to occur, 10 mm diameter holes were drilled in both the top and bottom platens – two holes in the top platen and one in the centre of the bottom platen (with one single hole drilled in the bottom platen the consolidation process took longer, but was more convenient for the particular design used). This enabled two-way consolidation drainage to occur and increased the speed of the process. An industrial glass microfibre filter paper (Whatman 0.20 μm membrane filter) was used to avoid any sediment flow through the drainage holes of the plate during the consolidation process.

3.7.2 Electrokinetic Treatment

At the end of consolidation, the loading was removed from the consolidated samples by draining the water from the tanks. These samples were then clamped, having reached the desired sample height of 100mm, to prevent any rebound or swelling. The wiring and electrodes were incorporated into the top and bottom plates as discussed in Section 3.6.3. The

external wiring was connected to the power supply to provide a constant voltage of 10 Volt/cm across the samples.

Figure 3.19 Samples undergoing electrokinetic treatment

The magnitude of 10 Volts/cm was chosen based on preliminary experiments (trial and error), which proved enough to bring the cell into equilibrium and modify the soil within 7 days, and this was confirmed by measurements of the pH and conductivity at the cathodic drain from the sample over the 7-day period. Electrokinetic treatment of both types of clay samples was undertaken for periods of 2 weeks, 4 weeks and 3 months to establish the degree and nature of the soil modification with time.

3.8 Monitoring

The samples were monitored both during the consolidation process and the electrokinetic treatment period on a 24-hour basis to establish any need for corrective action. During the consolidation process, it was necessary to check the water level in the tanks (evaporation

control) and observe the condition of the samples. However, there was no evaporation found during the tests. Short-term checks were undertaken during the early stages and at two and four hours after the initiation of the electrokinetic treatment to ensure that treatment was progressing as required by assessing the voltage gradient fluctuations. The voltage gradients showed a high fluctuation at the start of treatment for the different test samples, but these decreased with time and were almost constant after 24 hours, and hence for the majority of the treatment periods. A water tank with a nominal hydraulic head was positioned over the samples to maintain water feed to the top (anode) of the test cell and prevent drying during testing, while cathodic drainage was collected at the bottom of the test cell with a collection beaker. The beaker was changed every 24 hours and measurements made of the pH and conductivity of the collected cathodic drainage fluid. A reading of the voltage gradient was also taken at the same time. The samples were kept at a constant laboratory room temperature of 20 ± 2ºC. Table 3.11 presents the pH measurements for 7 days of electrokinetic treatment process, which proved that 7 days was enough time for the cathode-anode system to develop, i.e. so that acidic and alkalinic environments were generated at the top (anode) and the bottom (cathode) parts of the sample respectively, due to the electrolysis reactions at the electrodes (see Section 2.7.1), yielding the expected development of a pH gradient across the soil samples.

Table 3.11 pH measurements of cathode drainage fluid for Kaolin Clay and Oxford Clay for the first 7 days of electrokinetic treatment

Days	Kaolin Clay	Oxford Clay
	pH[-]	pH[-]
1	5.93	7.97
2	6.34	8.57
3	7.86	9.86
4	8.62	10.43
5	9.67	11.21
6	11.21	12.07
7	12.76	12.86

3.9 Testing after Sample Extraction

After the electrokinetic treatment was completed for the required time duration, the samples were unclamped and the clay soil was extracted from the cylinder for chemical and physical tests. The clay soil was extracted from the upper (anode) end, i.e. the end that had the cast iron disc in the main experiments. This was done to ensure less disturbance of the clay soil than if the sample excavation had taken place from the cathode side of the sample. Three replicate samples were available to carry out the physical and chemical tests. The first test undertaken was for undrained shear strength, which was measured through all three samples at different depths (the method, and its limitations, are explained in Section 3.11.1), while TDR measurements (measuring the conductivity and permittivity of the soil) were taken for each 10 mm layer of soil after the undrained shear strength tests had been conducted (these needed to be conducted first as they require undisturbed soil). It was necessary to take the TDR measurements while the sample was undisturbed by further tests (as the sample needed to be cut) to avoid any air voids around the rod as this would affect the conductivity and permittivity results obtained (see Section 4.3.3.2 and 4.3.4).

After the undrained shear strength and TDR measurements were taken, the Atterberg limit (Liquid and Plastic Limits) tests were completed in order to prevent any changes in the soil properties due to storage. The Atterberg limit tests were repeated on all three replicate samples to test the repeatability and hence reliability of the results. In addition, for the geochemical testing, the clay samples were sliced into 10mm thick layers, placed in airtight bags and stored in a temperature-controlled room at 20 ± 2ºC. Subsequently, pH dependency (described in Section 3.10.1) and iron solubility assessment tests (described in Section 3.10.2) were conducted on these samples. It was a prerequisite for these tests that the soil should be dried at laboratory temperatures to prevent any thermal modification in the soil chemistry, and this

usually took 3 to 4 days to complete. The clay samples were weighed to ensure that they were completely air dried. At the end of each measurement, all the tools and equipment used for the test were washed in a washing machine with hot water and after that were washed with a low concentration of acid, before finally being rinsed with demineralised water.

Tables 3.12, 3.13 and 3.14 present the geochemical, geotechnical and geophysical tests respectively that were undertaken on the Kaolin Clay and Oxford Clay, both with and without the cast iron disc. [In these tables, where a cast iron disc was used it is referred to as "disc", whereas for control tests without a cast iron disc it is referred to as "no disc".]

Table 3.12 Chemical tests for Kaolin and Oxford Clay with/without the cast iron disc

Chemical Tests	Kaolin Clay						Oxford Clay					
	2 Weeks		4 Weeks		3 Months		2 Weeks		4 Weeks		3 Months	
	Disc	No Disc	Disc	No Disc	Disc	No Disc	Disc	No Disc	Disc	No Disc	Disc	No Disc
pH Dependence Leaching Test	✓	✓	✓	✓	✓	-	✓	✓	✓	✓	✓	-
Iron Solubility Assessment	-	-	-	-	-	-	-	-	-	-	-	-
Determination of Soil Composition XRF	✓	✓	✓	✓	✓	-	✓	✓	✓	✓	✓	-

Table 3.13 Geotechnical tests for Kaolin and Oxford Clay with/without the cast iron disc

Geotechnical Tests	Kaolin Clay						Oxford Clay					
	2 Weeks		4 Weeks		3 Months		2 Weeks		4 Weeks		3 Months	
	Disc	No Disc	Disc	No Disc	Disc	No Disc	Disc	No Disc	Disc	No Disc	Disc	No Disc
Undrained Shear Strength	✓	✓	✓	✓	✓	-	✓	✓	✓	✓	✓	-
Moisture Content	✓	✓	✓	✓	✓	-	✓	✓	✓	✓	✓	-
Atterberg Limits (Liquid Limit)	✓	-	✓	-	✓	-	✓	-	✓	-	✓	-
Atterberg Limits (Plastic Limit)	✓	-	✓	-	✓	-	✓	-	✓	-	✓	-

Table 3.14 Geophysical tests for Kaolin and Oxford Clay with/without the cast iron disc

Geophysical Tests	Kaolin Clay						Oxford Clay					
	2 Weeks		4 Weeks		3 Months		2 Weeks		4 Weeks		3 Months	
	Disc	No Disc	Disc	No Disc	Disc	No Disc	Disc	No Disc	Disc	No Disc	Disc	No Disc
Time Domain Reflectometry (TDR)	✓	✓	✓	✓	✓	-	✓	✓	✓	✓	✓	-
GPRMax 2D	✓	✓	✓	✓	✓	-	✓	✓	✓	✓	✓	-

The sample layout, as shown in Figure 3.20, allowed for a variation in the ion migration and an alteration in the precipitation behaviour within the clay to be determined throughout the sample, i.e. from the anode to the cathode. The layers of soil were cut carefully with a sharp metal (stainless steel) knife. The chemical testing conducted is described in the next section (3.10), with subsequent sections 3.11, and 3.12, describing the geotechnical and geophysical testing, respectively.

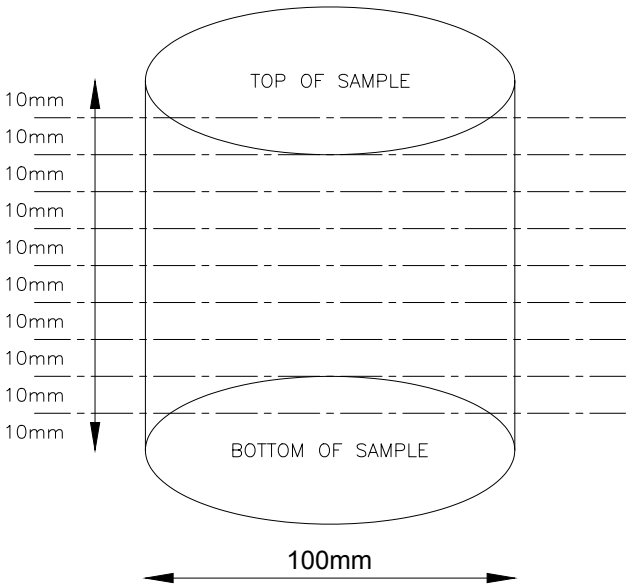

Figure 3.20 Soil samples were cut into 10mm thick layers for the chemical testing

3.10 Chemical Testing

3.10.1 pH Dependence Leaching Test

Accelerating the corrosion of cast iron and the migration of ions into the soil using an electrical field causes the pH to vary within the soil, due to ion migration between the anode and cathode (e.g. via electroosmosis and electromigration). For a better understanding of ion interactions such as migration, dissolution, precipitation and complexation, and as there was an uneven distribution of ions in the sample (caused by non-uniform corrosion of the cast iron disc and electrokinetic treatment), there was a need to undertake chemical assessment for ion behaviour within the samples, particularly for the ions of interest (i.e. iron – Fe^{3+}, Fe^{2+}). To facilitate this process, the most suitable method for assessing the ion leaching was to use a pH-dependent leaching test method (CEN/TS 14429:2008) that would allow assessment of the solubility and complexation or precipitation behaviour under the variable pH conditions induced within the samples during electrokinetic treatment. Thus pH-dependent leaching tests were undertaken to

determine the solubility properties for a variety of iron oxyhydroxides in the Kaolin Clay and Oxford Clay, based on variations in the prevailing pH. These changes were largely due to changes in solubility influenced by the speciation of the available ions under the prevailing test conditions, which presented changing solubility properties from acidic to alkalinic, as well as providing information on the maximum available soluble content for the ions. The procedure involved taking 1kg of Kaolin Clay and mixing this with 28g of Fe_2O_3 at a moisture content of 35%. The soil was mixed and sealed in a plastic bag and stored at 20ºC for 3 days. Ten grammes of the dry soil (after air-drying the sample) was then taken from the mix sample and leached with 200ml of leachant to give a (Liquid/Solid) L/S ratio of 20 ± 1:1, as recommended in CEN/TS 14429:2008. Leachants were prepared in a 200ml volumetric flask by putting in the required amount of base/acid to obtain end pH values for different fractions and making this up to 200ml using demineralised water. The amount of acid required was determined through a trial and error approach by making extra samples. The first trial for Kaolin Clay proceeded as follows: adding 1, 2 and 4ml of 0.1ml NaOH presented pH results of 6.7, 7.5 and 9.45 for the Kaolin samples. Each test required 12 fractions (nine test positions and three blanks), covering a pH range of 3 to 12, with a maximum pH variation of 1.5 pH units between successive fractions. However, it was not possible to provide a maximum pH variation of 1.5, given that the acid/base requirements were determined by preliminary titrations and test trials, and the samples exhibited significant buffering over the test duration (48 hours). However, no observed pH variation exceeded 2.0 units. In order to increase acidity, 0.1 and 2.0-mol nitric acid (HNO_3) solutions were used, while to increase alkalinity 0.1 and 1.0-mol sodium hydroxide (NaOH) solutions were used. The test procedure required end-over-end agitation at 28 ± 2 revolutions per minute (rpm), at a constant temperature.

The leachant was added to the soil in three steps (i.e. three different time periods). Wide mouth polyethylene bottles of 200ml capacity were used for the samples, and were washed with water and rinsed with HNO_3 and with de-ionised water prior to the tests. The test procedure required a sample with a maximum particle size of ≤2mm (80% passing 2mm sieve), and this was achieved by hand crushing air-dried samples in a porcelain bowl to prevent excessive alteration (thermal) or contamination (from using crushers). Leachants were prepared in 200ml volumetric flasks by putting in the required amount of base/acid to obtain the required end pH values for the different fractions, and made up to 200ml by adding de-ionised water. After weighing 10g of the sample into test containers, and preparing the leachants to obtain the end pH values of interest, the tests were started at t_0 (time zero). The first fraction of the leachant, which was one third of the total volume, was added to the test specimens at t_0. The samples were then run in the agitator for 30 minutes and a second 1/3 of the leachant was then added to the sample at t_{30} minutes. Heat and gas generation could have been problematic for some samples that may have reacted with the utilised leachant, but for the Kaolin samples this was not an issue, and the remaining leachant was added at t_{2hours}. The agitation was continued after each addition of leachant and pH values were measured at t_4, t_{44} and $t_{48hours}$, where $t_{44hours}$ was a measure to validate the equilibration at $t_{48hours}$. It should be mentioned that it was important that the difference in pH values for t_{44} and t_{48} should not exceed more than 0.3 pH units. Eluates were allowed to settle for 5 minutes and chemical measurements for pH and conductivity were taken before the samples were filtered and the eluates preserved for analysis. This criterion was achieved in all samples tested. The variation in pH was largely because of the acid and base used. Therefore, three buffer solutions were used to calibrate the meter (4.0, 7.0 and 12.58 at 20ºC). An Orion 720 pH Meter with a fitted glass electrode was used to measure the pH.

3.10.2 Iron Solubility Assessment

It was important to understand the behaviour of iron solubility during the release of iron ions from the buried cast iron discs and the formation of corrosion products such as iron oxides/hydroxides. This was required to assess the solubility conditions of the iron oxyhydroxides and determine, as a guide, the maximum amount of iron that could be sorbed by the clays of interest. This assessment was undertaken by adapting the 24-hour batch measurement for contaminants sorption, following the guidelines for the ASTM D4646–03 (2008) rapid batch extraction assessment method. This test was originally designed to determine the sorbable amount, or the sorption affinity, of specific contaminants by unconsolidated geomedia, and requires agitation (end-over-end) for 24 hours in non-reactive (polyethylene) containers under a constant temperature (20 ± 2°C). Chemical analysis showed that Kaolin Clay contains a small percentage of iron (1.11% Fe_2O_3, see Table 3.7) and so it was important to assess how much additional iron could potentially be sorbed by the clay.

The soil was dried and tested at L/S of 20:1. For each kilogramme of clay, 28g of Fe_2O_3 was used. Ten grammes of soil were mixed with 200 ml of demineralised water and 28g of Fe_2O_3 was added. The test method specified agitation (end-over-end rotation) for 24 ± 0.5 hours at 29 ± 2 rpm at room temperature of 22 ± 5^{o}C. Upon completion of this mixing, the elute solution needed to be separated from the suspended soil by filtration through a 0.45μm pore size membrane filter. The test determined the ratio of iron sorbed by the clay, based on a comparison of the initial and final amounts in solution, which were verified against a blank test. The distribution coefficient K_d was reported with pH and conductivity and compared to the original amount in the solution (Equation 3.1).

$$K_d = \frac{(A-B)V}{(Ms)B} \qquad \text{[Equ. 3.1]}$$

Where: A = Initial concentration of solute, μg/mL.

B = Final concentration of the solution after 24 hour contact, μg/mL.

V = Volume of solution, mL.

M_s = Mass of soil expressed on an oven dried basis, g.

K_d = Distribution coefficient, mL/g.

K_d represented the non-equilibrium 24-hour distribution coefficient of the element of interest, and required that both the initial and final concentrations should be reported along with the extraction pH values during testing.

3.10.3 Determination of Soil Composition – XRF Analysis

As the clay samples had high concentration of elements such as Al, Si, Ca, Na and Fe (in the case of using cast iron disc in clay samples), it was important to choose the suitable method to determine the soil composition. Methods such as Atomic Absorption Spectroscopy (AAS) and ICP-AES are useful for quantitative analysis of elements in soil (Nandy et al., 2008). However, in these methods the soils have to be dissolved into an acid solution, which might not be accurate enough due to the high concentration of elements inside the clay samples which required large dilutions. Using XRF required minimal preparation and it takes seconds to conduct an analysis of the elements (5-10 minutes per sample, depending on mass). Therefore, the most reliable and accurate method was considered to be X-ray fluorescence (XRF). Moreover, the other techniques are time consuming and costly.

XRF spectrometers are X-ray instruments routinely used for relatively non-destructive chemical (compositional) analyses of soils, minerals, sediments and fluids. Moreover, XRF is the most common method used to identify fine-grained soil minerals (Atanassova & Kerestedjian, 2004). X-ray fluorescence analyses, which determine the concentration of major and trace elements, were consequently undertaken to provide information on the quantitative elemental composition (%) of the test samples. It should also be noted that XRF measures total ion in all forms of oxides.

There are different methods of sample preparation for XRF analyses, and these depend on the type and amount of material available for testing. The method chosen for sample preparation in this study was the briquetting press pellet die approach. This is a common method involving the preparation of powdered samples. The soil was ground and pelletized at high pressure. A 10gr sample of the air-dried soil was ground to a 2μm particle size (reduced particle size) and then mixed with 0.2gr of SpectroBlend 44μ powder (a type of dry non-reactive wax) to make the briquettes for the XRF analyses. The homogeneous mixture of powder was placed carefully into the O-ring sealed briquette (see Figure 3.21) and this was positioned between the two parts of a press designed for exerting hydraulic pressure. The powder was compacted using a 15-tonne hydraulic press. XRF analysis was undertaken for the total composition of the soil. An initial programme of analysis was based on measurements taken at three different times: 5, 10 and 20 minutes. The 5-minute analysis was called a fast analysis, and was not as accurate as the longer ones. The 20-minute analysis did not show any significant difference in elemental composition compared to the 10-minute analysis, and therefore all subsequent samples were run for 10 minutes. Samples for analysis were prepared from clay sample taken from the test specimens at 10mm intervals away from the corroded cast iron discs, to assess compositional

modifications post-testing. The analyses were undertaken using a Bruker-S8 TIGER instrument in the School of Chemistry laboratories at the University of Birmingham, UK.

Figure 3.21 Required equipment for the preparation of the XRF samples

In case of clay samples, XRF intensities depend on the soil's grain size (or particle size) and the water content of the soil. However, the grain-size only does not affect the XRF intensity for high-energy X-rays (Pb, Cd), which is related to the fact that high energy X-rays generated in a deep soil layer were detected without serious absorption. In general, the clay grain size should be <2µm to detect the elements required. As the water content influences the XRF intensity, therefore the soil should be dried before using the analysis. [Low energy X-rays are absorbed by water much more strongly than high energy X-rays and therefore, the water content is related to X-ray energy. If the samples are not dried, the water content should be evaluated and then XRF intensities have to be corrected in accordance with the water content (Wada & Kakuto, 1995).] It should be noted that XRF analysis cannot distinguish ions of the same element in different valence states.

3.11 Geotechnical Testing

3.11.1 Undrained Shear Strength

Chemical changes such as cation replacement and iron compound precipitation induce changes in the physical properties of soil that potentially have implications for the undrained shear strength of the soil. The tests showed that, due to the ready reaction of iron ions to form iron oxyhydroxides and the low solubility of iron oxide and iron hydroxide, the iron migration into the clay soil modified the soil very close to the cast iron disc (the origin of the iron ions). Therefore, the measurements needed to be precise and use as small a piece of equipment as possible. Different methods such as a pocket penetrometer and a mini-vane test were investigated as potential methods for assessing shear strength. However, these test methods needed a relatively large test area, whilst the expected clay modification caused by migrating ions was expected to be highly localised. Therefore, the fall cone test described by Sven Hansbo of the Research Department of the Royal Swedish Geotechnical Institute (Hansbo, 1957) was selected because of its suitability for the test sample dimensions, its easy test set up, and its accurate results (based on the experiences of other researchers, e.g. Schmidt, 2007). The test is built on experimental and theoretical investigations of a cone penetration test, which establishes a relationship between the undrained shear strength, $\tau_{f,}$ and the depth of penetration, *I*.

The accuracy of penetration measurement by cone equipment is 0.01mm. This method is used in soft clay testing for Norwegian and Swedish standards; and it has been used by other researchers (Schmidt, 2007; Liaki, 2006; Barker et al., 2004). The fall cone test gives values of τ_f (see Equation 3.2) which agree remarkably well with the values of the τ_f obtained from the field vane test, except where the clay is extremely sensitive (a clay whose shear strength is reduced to a very small fraction of its former value on remoulding at constant moisture content) (Hansbo, 1957).

However, this test is not a standard method in the UK and it was merely carried out as a comparative measure to indicate changes in strength after the electrokinetic process.

$\tau_f = Kmg / i^2(1+h / i)$ [kPa] [Equ. 3.2]

K = Depends on the cone tip angle β (constant magnitude, see Figure3.22)

m = Weight of the cone (gr)

g = Acceleration due to gravity (m/s^2)

i = Penetration depth (mm)

h = Distance between the cone apex and the soil surface when the cone is dropped; normally h = 0 (mm)

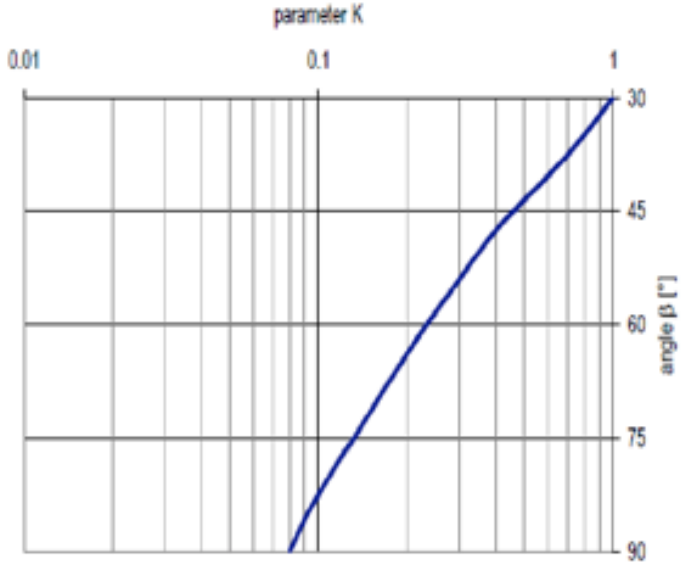

Figure 3.22 Relationship between cone tip angle β and parameter K (Hansbo, 1957)

From Equation 3.2, it can be seen that the relationship between the cone penetration and the undrained shear strength is quadratic. This causes problems with the reliability of the results at very small intervals of penetration, i.e. a change of ± 0.1mm in penetration can cause very large differences in shear strength. Hansbo (1957) solved this problem by using different tip angles (30° and 60°) and cone weights (100g and 400g). He published different tables for each type of cone and always started at a penetration of 4mm (this value was a minimum value). This resulted in the relationship between cone penetration and shear strength being close to a linear relationship.

For this application, it is important to consider the effect of cone penetration on the clay. Hansbo (1957) states that the only visible effect is heave in the immediate vicinity of the cone, which, however, is evidently far less in volume than the hole in the clay made by the cone. The total disturbance of the clay must therefore be much more extensive than that observed. If we consider the forces acting upon the surface of a cone element, these are shear stress (τ) and normal stress (σ), which are shown in Figure 3.23. The stresses have different values at different depths below the soil's surface, with their magnitude depending on the degree of deformation of the surrounding clay. In addition, Hansbo (1957) mentions that with the depth of penetration common in practice, the stress near the surface only reaches a fraction of the failure stress for undisturbed clay, that is τ_f compared to σ_f, so that the plastic state is unlikely to occur at the clay surface. The deformation of the clay around the cone increases with the increasing cone angle, as does, consequently, the tangent angle, α. There is, however, another factor that has a greater influence on the shape of the disturbed region and this is the movement of the soil. This movement happens in three ways: firstly, an upward flow of the clay takes place along the cone surface and produces heave; secondly, the clay surrounding the plastic region, being elastic, is strained horizontally; and thirdly, the pressure increase may produce a slip on the surface. Therefore, the influence of the cone on the clay soil causes limitations for

this measurement. For this reason, it was decided to measure the cone penetration at different depths, and three samples were made to prevent any limitations in these measurements. The fall cone test was carried out on all test samples and a comparison of the results was undertaken with and without the influence of the corroding cast iron. Figure 3.24 presents the location of cone penetration test for each 30mm layer away from each other.

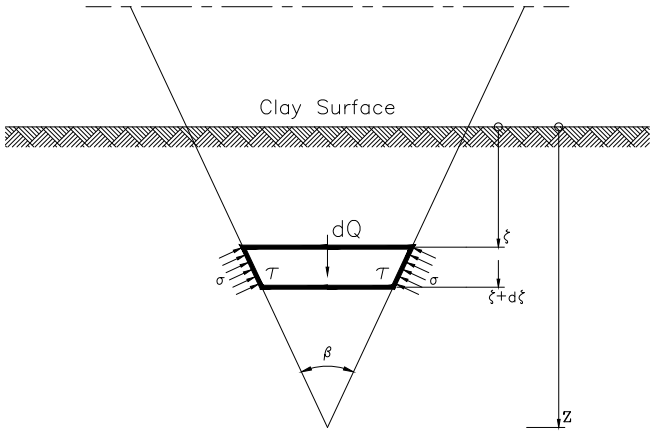

Figure 3.23 Force acting on a cone element during penetration

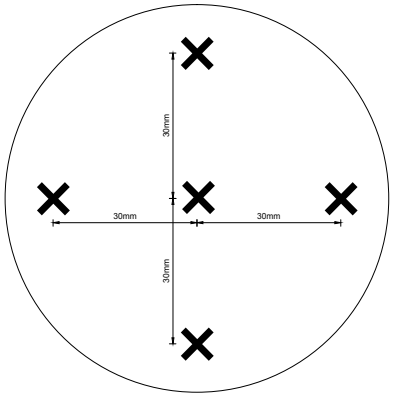

Figure 3.24 Locations of the undrained shear strength measurements for each 30 mm in depth away from the disc

Hasbo (1957) published graphs comparing the shear strength values obtained from the fall cone test with those obtained from other laboratory tests and from the field vane test. The results from these graphs show that the fall cone test gives values of τ_f which agree with the values of τ_f obtained from the field vane test. He mentioned in the report that this is true for most clays, the exception being sensitive clays (a clay where the shear strength is reduced to a very small fraction of its former value on remoulding at constant moisture content; based on BS 1377:1990), which presented different results and are not suitable subjects for this method.

3.11.2 Moisture Content

The moisture content of the sample was determined following British Standard methods (BSI 1377-2:1990). The moisture content was measured to show changes in the water distribution inside the sample. The weight of the soil was measured before being placed in an oven for approximately 24 hours at 105-110°C. The weight of the dried soil was then determined after being removed from the oven. The difference in weight allows the amount of water in the soil to be determined.

3.11.3 Atterberg Limits

Tests for determining Liquid Limits and Plastic Limits (the Atterberg limits) are the most commonly performed index tests for clays. Atterberg limit tests have been used widely to describe and classify clay soils. These limits are defined by the soil moisture content and provide data for the identification and engineering classification of clays. The clay fraction and clay mineral constituents of soils influences their properties, and the Atterberg limits can reflect some of these properties. In relation to this research, as the iron migrates through the soil and

modifies the soil's properties, this can affect the Atterberg limits and therefore show the influence of iron on the clay minerals. This is because the adhesive force between the clay minerals and water will change after cations have been exchanged, and consequently the Atterberg limits will change (Shackelford, 1994). The Liquid and Plastic Limits were determined according to BSI 1377-2:1990-3/4/5. The one-point Casagrande method was adopted for the Liquid Limit measurements, as only small amounts of soil were available for testing (BSI 1377: part 2: 4.4).

3.11.4 Correlation Between the Hand Vane and Cone Penetration Test

As explained in Section 3.11.1, the measurement of undrained shear strength for Kaolin Clay and Oxford Clay samples needed a small piece of equipment to provide sufficient accuracy of this measurement. In order to ensure the accuracy of these results, it was needed to compare the results with other available and suitable method(s). Therefore, the small vane shear test (chosen regarding its size and suitability) was used to measure the undrained shear strength of the soil. The miniature vane used had diameter of 14mm and height of 30mm, and was rotated at one degree per second (based on ASTM D2487-11). Hansbo (1957) correlated fall cone test results with values from laboratory vane tests and his results from the shear strength measurement using fall cone apparatus (Geonor, 2005b).

Two samples of both Oxford Clay and Kaolin Clay were created using with the same methods described in Section 3.7. After consolidation the samples were tested. It should be mentioned that due to the timeframe of this research it was not possible to test also samples that had been

subjected to electrokinetic treatment for this correlation, therefore these tests were carried out only on untreated consolidated clay samples.

The measurements of Kaolin Clay (moisture content of 40.3%) and Oxford Clay (moisture content of 47.0%) samples are presented in Figures 3.25 and 3.26. Due to the limitation of using cone penetration (see Section 3.11.1) measurements were done at different depths in the samples which are 0 (at the surface of the sample), 30mm and 60mm away from the top of sample. These results show that the shear vane and cone penetration tests produce very similar results, and therefore proved that the cone penetration method has adequate accuracy for the research.

In order to prove the repeatability of these results, different samples with different moisture content (30%, 35%, 40%, 45%, 50%, 55%) were prepared using the same process as when preparing the samples for the main experiments (see Section 3.7) and the vane and cone penetration methods were used. The results of these measurements are presented in Figure 3.27.

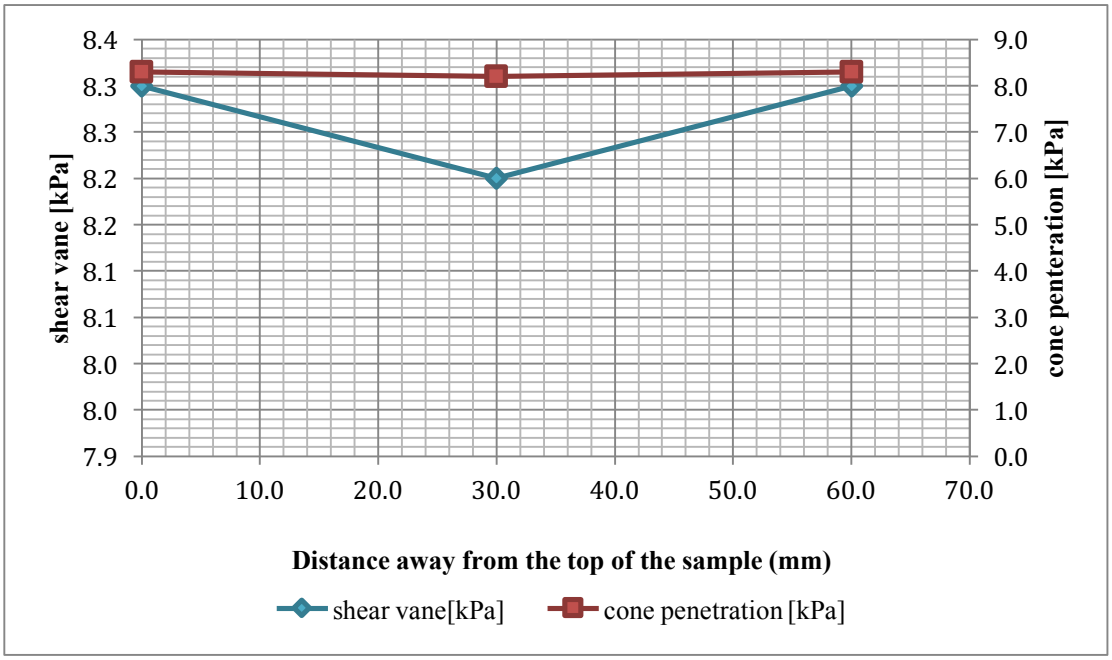

Figure 3.25 Shear strength measured by shear vane and cone penetration method for Kaolin Clay with 40.3% moisture content

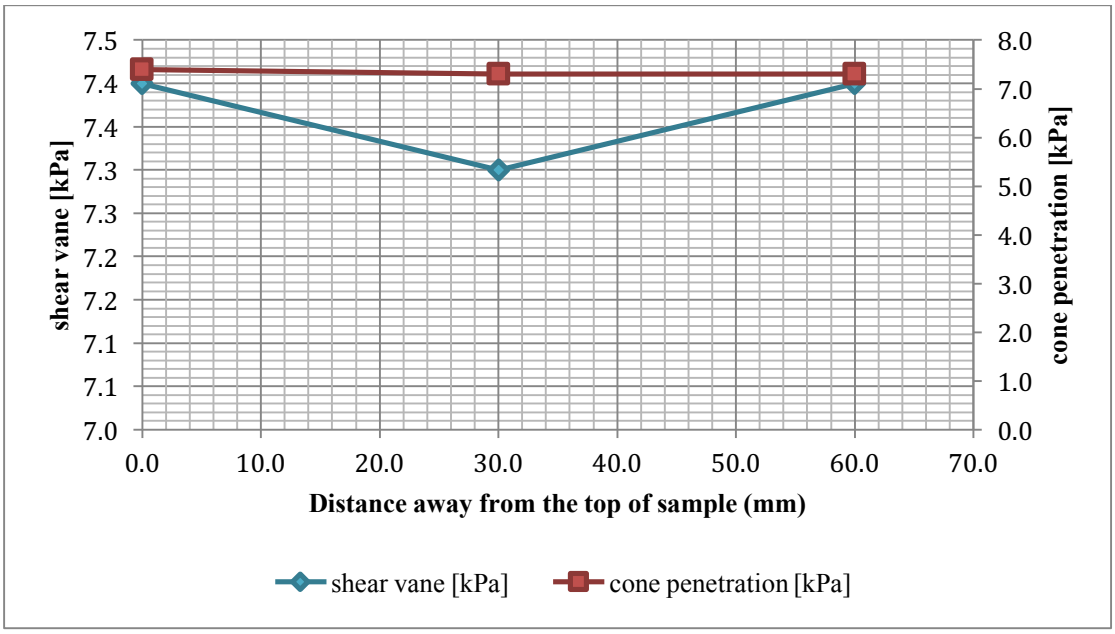

Figure 3.26 Shear strength measured by shear vane and cone penetration method for Oxford Clay with 47.0% moisture content

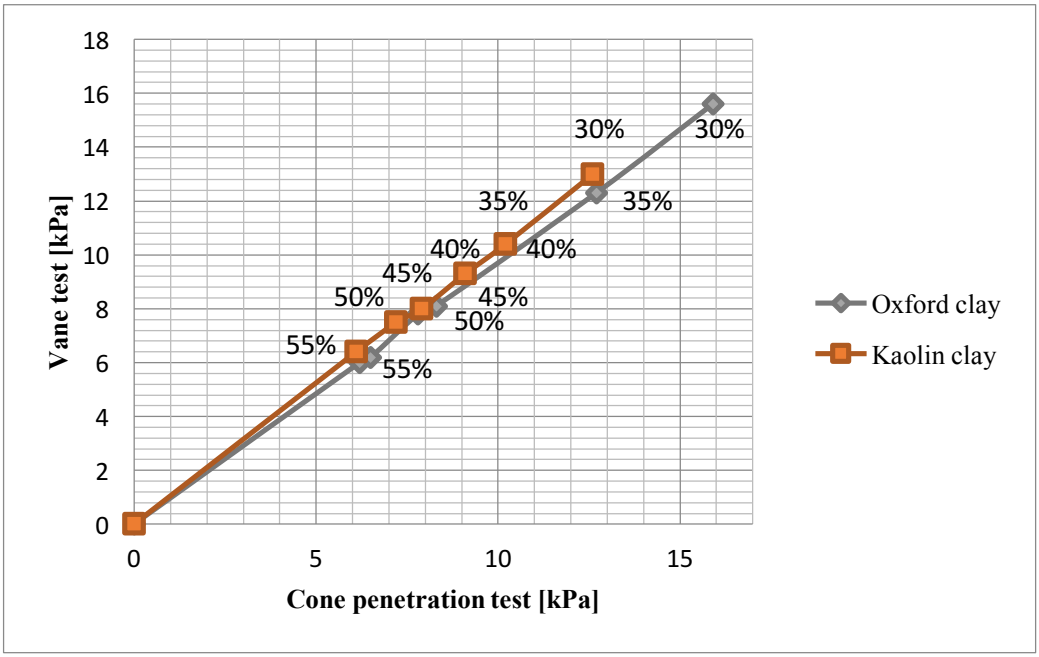

Figure 3.27 Relationship between the vane shear and cone penetration test for moisture contents ranging from 30% to 55%

3.12 Geophysical Testing

3.12.1 Determination of Electrical Conductivity Using Time Domain Reflectometry (TDR)

Time domain reflectometry (TDR) is an accurate method used to determine bulk soil electrical conductivity (σ_a) (Jones et al., 2002). Cast iron pipes release ions into the surrounding soil, which modifies the physical and chemical properties of the soil around the pipe. It is therefore important to know the salinity and the behaviour of the ionic solution in the soil. The method involves an electrical wave being transmitted through a cable into the sample and then being reflected back to the generator. From an analysis of the travel time or signal propagation velocity (V_p, a function of the cable dielectric constant), it is possible to determine the bulk electrical conductivity of the soil (Castiglione et al., 2006). A fast rise time electromagnetic pulse is injected into a waveguide inserted into (as in this research), or buried in, the soil. The

time required for the pulse to travel along the metal rods of the waveguide is determined by the bulk electrical permittivity of the soil (Curioni, 2013). The ions in the soil provide a path for electrical conduction between the TDR and probe rods (Jones et al., 2002). The conductivity and resistivity values indicate the relative capacity of the soil to carry an electric current. It was important to make sure that when the TDR probe was inserted into the samples to take measurements, it was completely covered by the soil, thereby minimising contact with air, which can yield erroneous results. Figure 3.28 shows a clay sample with a TDR probe inserted into it. After each measurement, the probe was washed with demineralised water and dried with a clean tissue to prevent cross contamination between the layers. Measurements for conductivity and permittivity were undertaken at intervals of 10mm within the sample, to minimise the influences of the insertion of the probe on the measurements. These measurements were taken after the cone penetration test was carried out (see Section 4.3.3.2).

Figure 3.28 TDR probe inserted into a clay sample

3.12.2 TDR Calibration and Calibration for Bulk Electrical Conductivity (BEC)

This section provides a summary of the calibration of the TDR probes for apparent permittivity. It should be mentioned that the following section is based on the work of Curioni (2013).

To calculate the permittivity values using TDR it is necessary to calibrate the equipment and use the same arrangement of equipment when taking the actual measurements, i.e. even a change in cable length or different TDR unit can affect the accuracy of the results. This calibration is called basic calibration, and is performed in a material with known permittivity. In the case of soils, the bulk permittivity can be considered as a combination of the permittivity of the air, water and soil components. For this application of TDR, it is suggested that a calibration should be performed in air and distilled water as these are where the extremes within which the soil bulk permittivity normally lie (Heimovaara, 1993; Robinson et al., 2003b). Air has a value of ε' very close to 1, and the values for soil components generally range between 3 and 10 (Huisman et al., 2003). The value of ε' for distilled water varies from 88 at 0°C to 78 at 25°C, with a reference value for water of 80.10 at 20°C (Weast, 1972). The measurement for each probe was conducted in air and distilled water at 20°C in a temperature-controlled room. For the air calibration, two levels of multiplexers were used with approximately 4m of cable and a 75mm long probe. Measurements were performed in air with rods short-circuited with aluminium foil, which allowed the end reflection point accurately identified. In addition, a few measurements were taken without multiplexers to verify the reliability of this approach. In addition, the measurement process was repeated four times in distilled water in a 1L conical beaker with the temperature strictly controlled and kept at 20°C by putting the beaker in an incubator at a constant temperature. The measurements were taken immediately afterwards in the temperature controlled room of 20°C, and each time the temperature were measured with a thermometer.

The calibration for Bulk Electrical Conductivity (BEC) was different to that for apparent permittivity, since in recent years an improved calibration methodology had been defined (Heimovaara et al., 1995; Lin et al., 2008; Huisman et al., 2008; Bechtold et al., 2010). The calibration was based on the methodology suggested by Huisman et al. (2008), which allows the accurate determination of BEC with TDR, based on the original method proposed by Giese & Tiemann (1975).

Every day a calibration was performed and every solution was tested three times by both the TDR and the conductivity meter HI 9033, and these tests were used to obtain the average reference BEC. The measurements were taken at a constant temperature of 20°C, which was maintained with the use of an incubator. The start and end length parameters defining the dimension of the waveform plot were set to 0m and 200m of apparent length respectively.

3.13 GPRMax 2D/3D Modelling and Programing

GPR modelling was used to extrapolate the experimental results. In order to ensure that the computational resources required by the model remain at a manageable level, and that the important features of the GPR response to a target can be studied without the solution being cluttered with too many details, there are some assumptions that it is important to observe when constructing GPR models. These assumptions for GPRMax 2D (Giannopoulos, 1997) are as follows:

- All media are considered to be linear and isoropic.
- In GPRMAX2D the transmitting antenna is modelled as a line source, which is a consequence of the assumption of the invariance of the problem in one direction.

Using permittivity and conductivity data obtained from TDR measurements on test samples after induced corrosion at different periods of treatment, simulations were performed using the GPRMax software (Giannopoulos, 2005). In addition, the compositional (see Section 3.10.3), geotechnical (see Section 3.11) and geochemical (see Section 3.10) characterization results were used to undertake FDTD simulations for GPR response.

A model was created that simulated a cast iron pipe with a radius of 0.1m buried at a depth of 0.5m and surrounded by homogenous clay (see Figure 3.29). A number of different permittivity and conductivity layers, which were obtained from the TDR measurement on the test samples where the soil was most affected by the corrosion products (i.e. taken from the 3 top layers – closest to the cast iron disc – see Tables A32 and A33 in the Results chapter- Appendix), were used in order to simulate the enrichment of ions due to corrosion. Values for permittivity and conductivity were input based on TDR measurements for both affected and control samples (samples without a cast iron disc). Magnetic permeability was not measured and assumed equal to 1 during inputs for simulation. Although, it is important to note that soil close to the cast iron disc is iron enriched, the magnetic permeability is relatively small compared to the conductivity and was not assumed to substantially influence the simulation outcome.

Results simulated a GPR antenna, with a centre frequency of 700MHz, run along the ground surface, with readings taken every 25mm along a transect. TDR readings were taken using the TDR100 cable tester and CS645, 75 mm probes supplied by Campbell Scientific, Logan, UT. The standard travel time analysis was used to determine permittivity (Jones et al., 2002) and zero frequency bulk electrical conductivity (BEC, S/m) was measured using the Giese and Tiemann method (Giese & Tiemann, 1975). A discrezation step of dx=dy=1 was used.

Two-dimensional FDTD simulations were used using GPRMax software at the University of Birmingham. Figure 3.30 presents the input file command for GPRMax 2D software. The ABC command, which allows the customization and optimization of the absorbing boundary conditions, was used for the program commands.

The essential commands that represent the minimum set of commands required to run GPRMax 2D are:

- #domain: The command domain should be used to specify the size in metres of the sample in 'x' and 'y' directions respectively.
- #dx_dy: This command is used to specify the discretization of space in the 'x' and 'y' directions respectively, (i.e. Δx, Δy). It is important to note that the smaller the values of Δx and Δy, the more accurate the model will be.
- # time_window: This command specifies the total required simulated time.

After processing of general commands, the required size is initialized to simulate free space (air). Using the #medium command helps to introduce other media and objects in the model.

#medium: f1 f2 f3 f4 f5 f6 str1

- f1: Static relative permittivity of medium (measured by for each 10mm layer away from each other)
- f2: Relative permittivity at the theoretically infinite frequency (zero)
- f3: Relaxation time of medium (in seconds)
- f4: Static conductivity of the medium (Siemens/metre, measured for each 10mm layer away from each other)
- f5: Relative permeability of the medium (zero)

- f6: Magnetic conductivity of the medium (assumed to be 1.0, which is a wrong assumption; it was not possible to measure this parameter, but its influence is small).
- str1: Medium identifier (in this case the four top layers close to the cast iron disc were used (i.e. layer 1, layer 2, layer 3, layer and layer 4) which are the most iron affected.

#box command was used to introduce a rectangle of specific properties in the model. The command is **#box: f1 f2 f3 f4 str1**

- f1 and f2 are the lower left (x, y) coordinates of the rectangle in metres (0,0).
- f3 and f4 are the upper right (x, y) coordinates of the rectangle (5.0, 0.5).
- Str1 is a medium identifier with a #medium command or in a medium currently in use. Figure 3.29 is the simulation model used for GPRMax2D software.

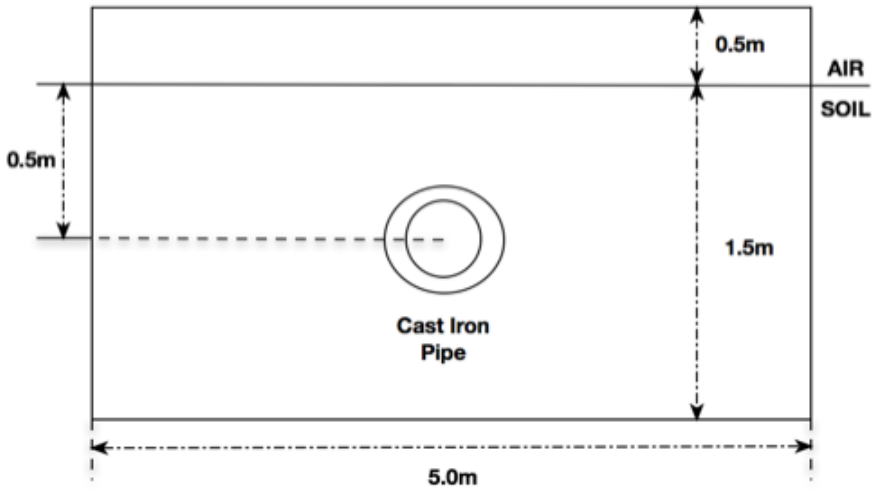

Figure 3.29 Dimensions of model used for the simulation

Free_space is used if the rectangular area is to represent a free space region on a perfect conductor. With the help of the #cylinder command, a circular disk in the 2D model (physical model) is introduced. The syntax of command is: **#cylinder: f1 f2 f3 str1**

- f1 and f2 are the (x, y) coordinates of the centre of the circular disc in metres.
- f3 is the radius in metres and str1 is a medium identifier (see #box), hence the command i.e. #cylinder: 2.50, 1.10, 0.140 layer 4.

(In this case study the length of pipe is 2.5m with diameter of 0.2m)

In GPRMax-2D, the characteristic of at least one source using the command is **#line_sorce: f1 f2 str1 str2**

- f1 and f2 are the amplitude in amperes of line source current and the frequency in Hertz of the source's excitation waveform respectively.
- str1 controls the type of the excitation waveform. In this case the ricker, which is the first derivative of the Gaussian waveform, was chosen.
- str2 is user ID which is subsequently used to relate the specification of the source with its application in the model. #line-source: 1.0 700e6 ricker MyLinesource.

After source types are introduced, then placing source and output points in GPRMax 2D is accomplished using a new command **#analysis: i1 file1 c1**.

- i1 is the number of the new run of the model.
- file1 is the name of the file where all the results for this #analysis are going to be sorted and the parameter
- c1 is a single character either 'a' or 'b' denoting that the format of the output file.

The commands #tx are used together in order to introduce a source position (#tx) and output points (#rx and #rx-box). **#tx: f1 f2 str1 f3 f4**

- f1 and f2 are the (x, y) coordinates in metres of the source in the model.
- str1 is the source ID that has been specified.

- f3 is a delay in the source's initiation. Greater than zero then the source will be active after that time delay has passed.
- f4 is the time of source removal.

When i1 is greater than 1 then the model will run again to calculate a new step in current analysis. Therefore, the following command was used: #tx-step and #rx_step.

#tx_step: f1 f2

- f1 and f2 are increments in metres of the x and y coordinates accordingly.

#rx_step: f1 f2

- f1 and f2 are the increment in metres of the x and y coordinates, accordingly in this case the #tx-step: 0.025 0.0, #rx-step: 0.025 0.0 is used. And finally, at the end of an analysis section, the #end_analysis command is used, which has no parameter.

```
      %note: see gprmax manual to know what these parameters are. Medium is:
static perm, infinite perm, relax time, BEC, magnetic perm, magnetic cond.
      %if relax time is 0, no relaxation is accounted for. If magnetic perm is 1
and magnetic cond is 0, material is considered non-magnetic.


%%% select only media that are used in the simulation!

#medium: 21.57    0.0    0.0    0.44196     1.0    0.0    layer1
#medium: 21.57    0.0    0.0    0.39357     1.0    0.0    layer2
#medium: 21.57    0.0    0.0    0.21534     1.0    0.0    layer3
#medium: 19.00    0.0    0.0    0.21521     1.0    0.0    layer4
#medium: 22.44    0.0    0.0    0.23567     1.0    0.0    OXC_matrix


      %targets (permittivity values taken from wikipedia):
      %#medium: 2.25 0.0 0.0 0.0 1.0 0.0 polyethylene                %%%choose
this if I use a plastic pipe


-------------------------------------------------------------
      %domain must be divided by tx and rx steps
      %to know number of cells: domainx/dx x domainy/dy

#domain: 5.0 2.0
#dx_dy: 0.001 0.001
#time_window: 80e-9

#abc_type: pml                %use perfect matched layers for best results
#pml_layers: 32               %the more the layers the better the results.
Default is 8 cells (e.g., 8*dx_dy = 0.04 m if dx_dy=0.005)

-------------------------------------------------------------


%%% check boxes:


#box: 0.0 0.0 5.0 0.5 free_space

      %homogeneous soil
#box: 0.0 0.5 5.0 2.0 OXC_matrix   %%%

#cylinder: 2.5 1.10 0.140 layer4
#cylinder: 2.5 1.10 0.130 layer3
#cylinder: 2.5 1.10 0.120 layer2
#cylinder: 2.5 1.10 0.110 layer1
#cylinder: 2.5 1.10 0.100 pec            %%% top of target (20cm diam) is 0.5m
deep


-------------------------------------------------------------
#line_source: 1.0 700e6 ricker MyLineSource

-------------------------------------------------------------
      %number of new scans (e.g. number after #analysis: ) must be ( domainx -
[rxx - txx] - 1.0)/txstep    [NOTE: rxx-txx is the antenna separation!]
      %it's better to place the transmitter after 0.50 m from the left boundary
and finish the scan 0.50 m before the end (right boundary)


      %so that I can use more safely pml instead of abs, and I leave some extra
 space in the domain near the boundaries.
      %for this purpose subtract 1 from domainx - rxx (if I want 0.50 on both
 boundaries) and increase the domainx of 1 m compared to the transect length.
      %(e.g., domainx = 5 m, transect = 4 m, with tx = 0.5 and number of new
 scans = (domainx - [rxx - txx] - 1)/txstep)

 #analysis: 146 3months_700MHz_OXC.out a       %%%

 #tx: 0.50 0.5 MyLineSource 0 8e-9 %transmitter after 0.5m from left boundary
 and on soil surface (0.5m in domainy)

      %it's easier to keep tx=rx

 #rx: 0.85 0.5                %the antenna separation (i.e., the distance between
 transmitter and receiver) is assumed to be 0.35 m
 #tx_steps: 0.025 0.0
 #rx_steps: 0.025 0.0
 #end_analysis:

 -------------------------------------------------------------
 #geometry_file: 3months_700MHz_OXC.geo        %%%

 #title: 3months_700MHz_OXC              %%%
 #messages: y
```

Essential commands

Figure 3.30 GPRMax2D input file commands

3.14 Summary

The literature review chapter described the corrosion of cast iron and the products of this corrosion, as well as the mineralogy of Kaolin Clay and Oxford Clay, and finally introduced the GPRMax2D software, which is able to simulate the geophysical results obtained from the TDR (conductivity and permittivity) measurement, as important considerations in the programme of research to study GPR signal ability to detect buried iron pipes.

In the methodology chapter, based on the literature review chapter, a series of experiments were designed and trialled before the final experimental design was considered to develop a better understanding of the effects of cast iron pipe corrosion on the physiochemical properties of Kaolin Clay and Oxford Clay. For evaluating these changes, suitable chemical and physical assessment methods were designed to provide the required information for critical evaluation of soil modification. These are described in the chapter, and the limitations of the testing methods were explained and addressed. The experimental process was designed to ensure the reliability and repeatability (using replicate testing and control samples).

The next chapter – describing the laboratory results – presents the chemical and geotechnical results obtained from the testing and presents the repeatability of the results.

CHAPTER FOUR

4.0 Laboratory Results

4.1 Introduction

The results from the laboratory experimentation are presented in this chapter, which additionally aims to demonstrate their replicability and validation. Validation of results is the process of verifying data that has been produced from tests, a process that is supported by checks on the degree of error when the same tests are repeated. Also, comparison of the results of samples from the same batch helps to indicate the reliability of results. The next chapter presents a discussion of the results.

This chapter presents the results from the geotechnical tests (undrained shear strength, moisture content and Atterberg limits), and the chemical results (iron content, pH and conductivity) obtained from the laboratory tests described in the methodology chapter (Chapter 3). In addition, conductivity and permittivity measurements by TDR are presented. All the tables mentioned in this chapter are placed in Appendix A.

4.2 Geotechnical Tests

The first tests that were undertaken were the geotechnical tests, which were done on material extruded from the cylinder immediately after the end of each experiment. The physical test results that are reported here are: undrained shear strength (obtained using the cone penetration test), Atterberg limits, and moisture content.

4.2.1 Undrained Shear Strength – Cone Penetration Test

After electrokinetic treatment, samples were disconnected from the electrical supply and the top and bottom sections of the experimental cell arrangement (PVC disc) were removed prior to the sample being extruded to allow the undrained shear strength measurements, via the cone penetration method (see Section 3.11.1), to be obtained. This test was the first to be undertaken, which, due to the measurement processes, caused some disturbance to all the samples. For the repetition of results, the soil left in the cylinder after these measurements had been taken was used for additional measurements (tests). The location of these initial measurements is shown in Figure 4.1, each cone penetration being done at a distance of 30mm from the next closest to avoid undue influence from prior testing. Tables A1 and A2 present the results for Kaolin Clay with and without (i.e. the control tests) the cast iron disc respectively and Tables A3 and A4 present the results for Oxford Clay with and without the cast iron disc respectively. [The results for where a cast iron disc was used are termed 'with disc', and the results without a cast iron disc are called 'no disc'.] In the figures (e.g. Figure 4.2), there is a 'Natural' (or neutral) value for some data, which presents the results of tests without any electrokinetic treatment of the sample – i.e. a baseline measurement to judge the effects of all of the electrokinetic treatments. These natural values are based on the final water content when consolidating the samples of 40.2% for Kaolin Clay and 48.0% for Oxford Clay.

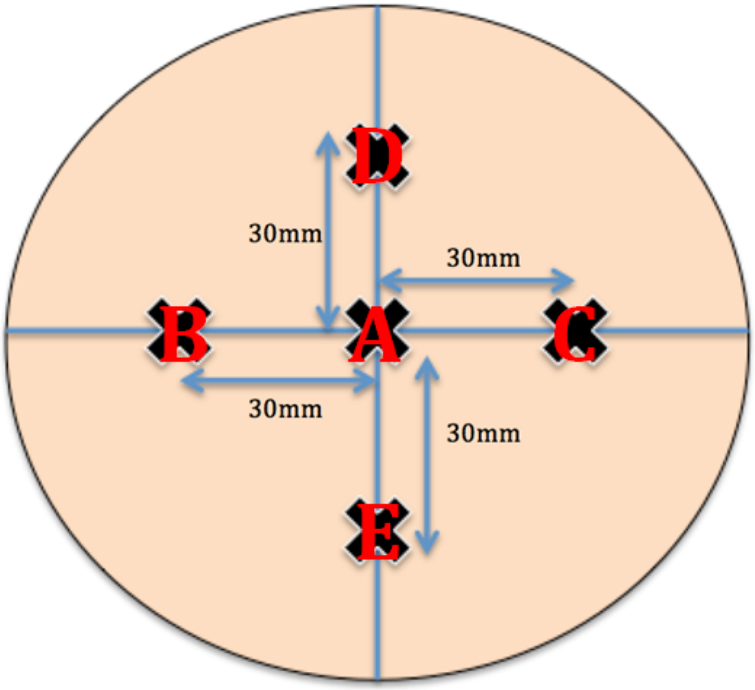

Figure 4.1 Plan location of the cone penetration tests in the samples

Tables A1 and A2, and Figure 4.2(a) and 4.2(b) in which the average data for points A to E are plotted, show that the undrained shear strength of the soil increased in samples where a cast iron disc was included. This was attributed to releasing of iron ions into the sample and a consequent decrease in the thickness of the diffuse double layer due to the iron ions lattice substitution for Al^{3+}, which brings the clay particles into a closer association and as a result the undrained shear strength increases. The effect of cast iron corrosion is strongly demonstrated in Figure 4.2(a). The electrokinetic treatment increased the shear strength of the soil compared to the 'natural' samples (i.e. samples subjected to electrokinetic treatment without any cast iron disc compared with the untreated samples) from 8.2 kN/m^2 to 14.5 kN/m^2 (4-week sample) close to the anode. Interestingly, the 2-week sample with no disc exhibited no change from the 'natural' sample at the anode, and registered a marginal reduction at all points away from the

anode. These 4-week changes were obvious for the whole sample, with the strength increasing by approximately 1.7 times relative to the 2-week sample.

For samples with a cast iron disc, this amount increased for the 2-week sample and the 4-week sample from 8.2 kN/m^2 (the baseline, 'natural' value) to 14.9 kN/m^2 and then to 30.6 kN/m^2 at the anode respectively. The increment in these values was more obvious near to the anode, while the strength increase close to the cathode was attributed to the precipitation of Fe oxides (measured by XRF – see Section 4.3.1). At the cathode, the shear strength increased from 8.2 kN/m^2 (the baseline, 'natural' value) to 9.8 kN/m^2 for the 2-week sample and then to 17.7 kN/m^2 for the 4-week sample, although the value 10 mm away from the cathode was notably higher at 25.1 kN/m^2. The highest undrained shear strength of all the samples was that of a 3-month sample, which reached 74.4 kN/m^2 (see Figure 4.2(b) with an expanded scale to include the 3-month data), with the strength remaining high until the midpoint of the sample (where the strength measured 28.5 kN/m^2 and was only marginally raised above the value for the 4-week sample of 24.1 kN/m^2) before increasing again in the lower half of the sample.

The strength increment close to the cathode in a mixed mineralogy clay soil might be attributed to dissolution of alumina and/or silica from the clay mineral at high pH, which reacts with calcium released from the clay minerals to create calcium aluminate hydrate and/or calcium silicate hydrate and crystallise, therefore causing the undrained shear strength to increase. However, for Kaolin Clay there is no ready source of calcium ions (see Table 3.5) and thus the strengthening mechanism was attributed to Fe oxides precipitation, as noted above. The water contents from the positions where the undrained shear strength were measured are reported in Section 4.2.2, this being another strong influencer of undrained shear strength. A more detailed discussion of the combined results is presented in Chapter 5.

Figure 4.3 shows the undrained shear strengths results for points A to E for the test with a disc at 2 weeks to demonstrate that the measurements were consistent across the diameter of the specimen, and that the measurement technique is also repeatable due to the closeness of the values achieved.

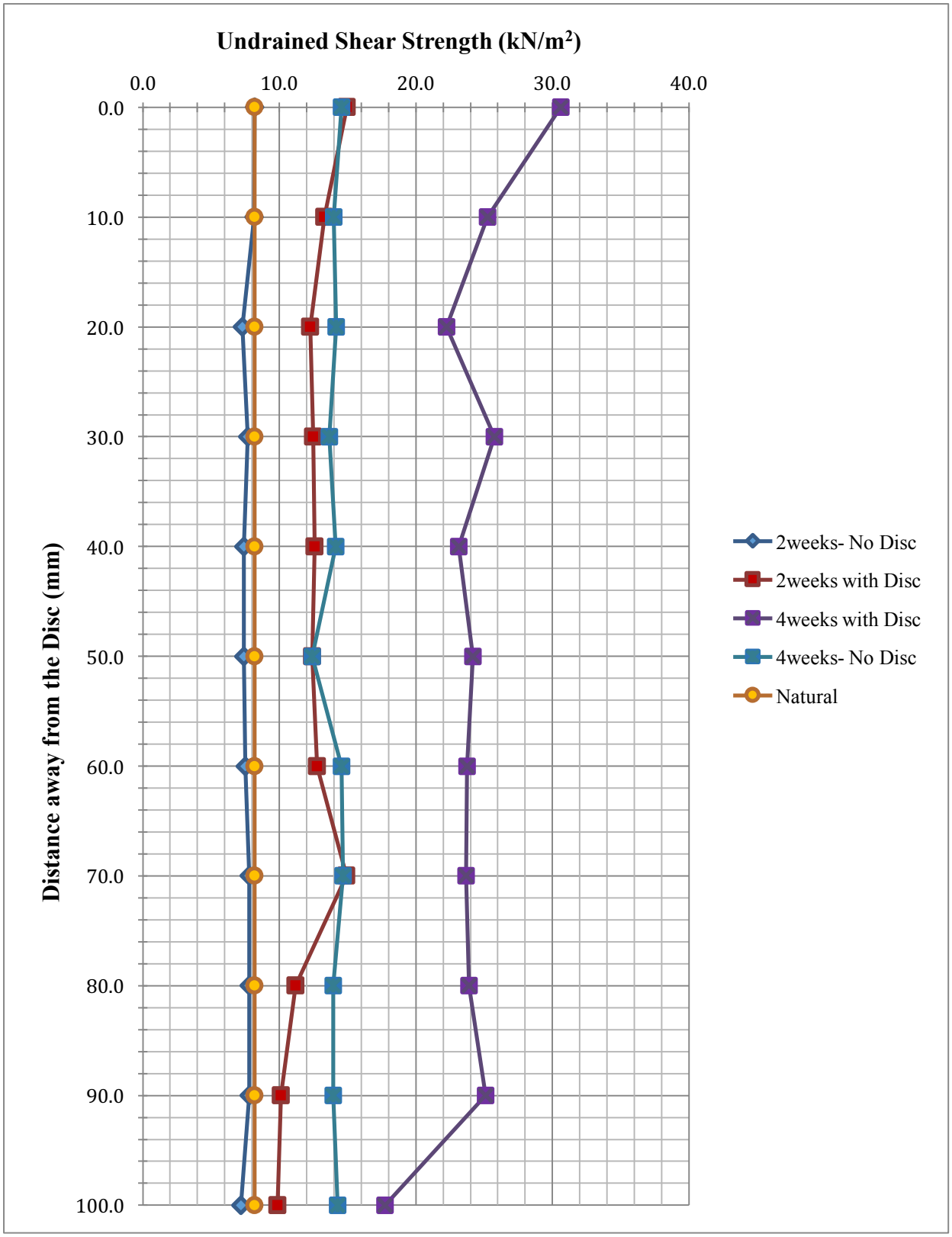

Figure 4.2(a) Undrained shear strength of Kaolin Clay for 2- and 4-weeks samples

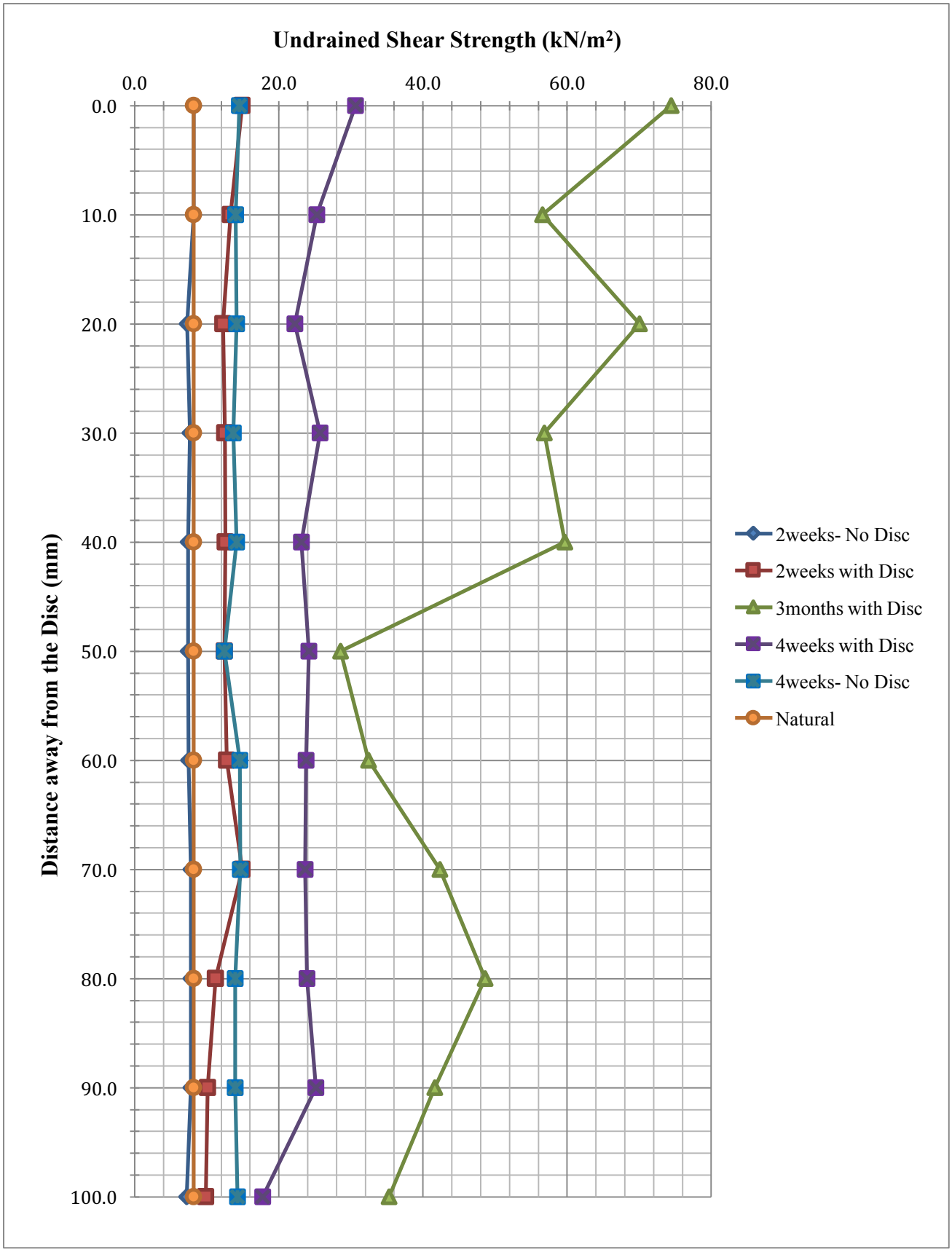

Figure 4.2 (b) Undrained shear strength of Kaolin Clay samples

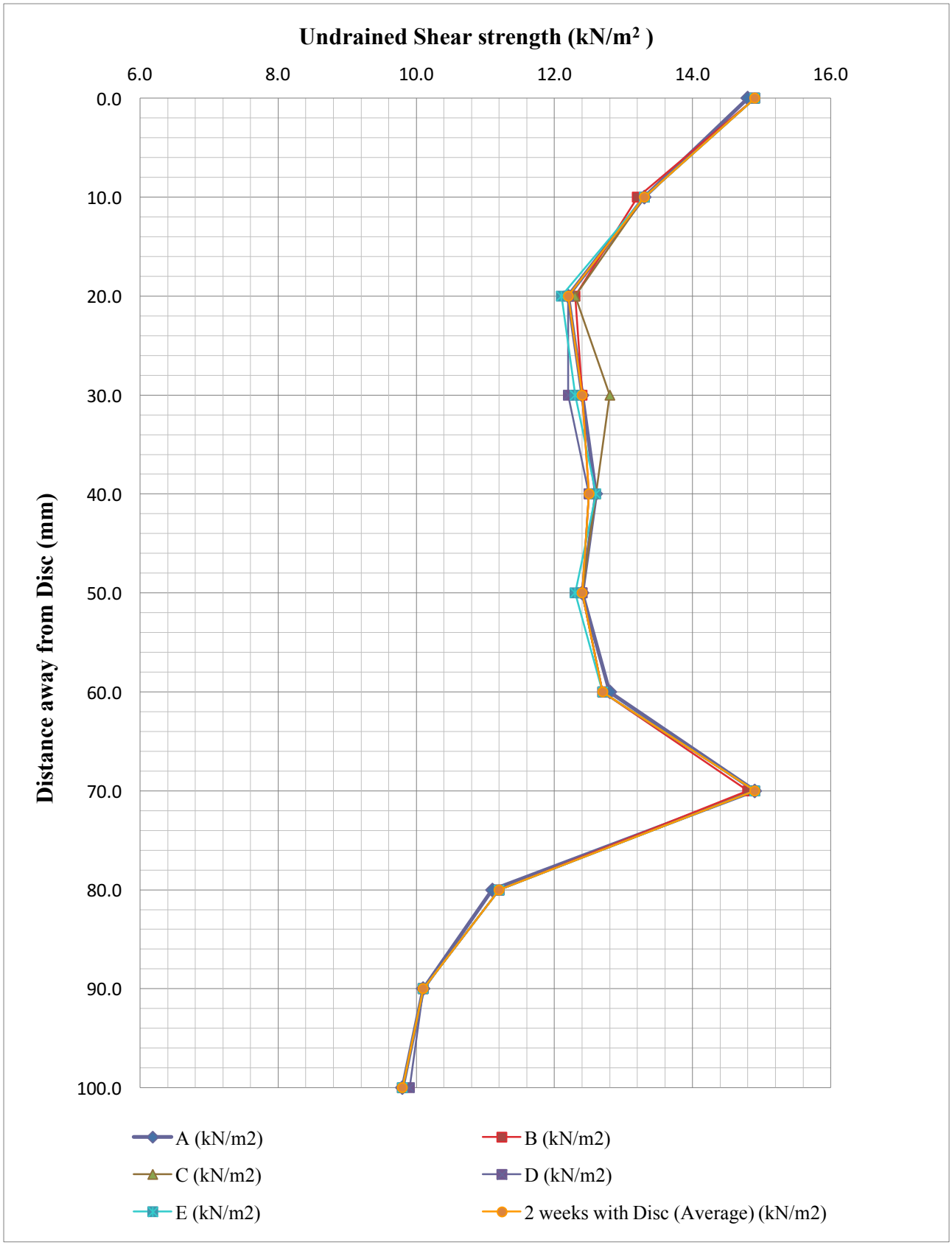

Figure 4.3 Undrained shear strength repeatability for 2 weeks with disc for Kaolin Clay sample

Figures 4.4(a) and 4.4(b) present the averaged results for the Oxford Clay samples for 2- and 4-week, and the 3-month sample respectively, and shows that near the cathode and the anode the undrained shear strength was significantly higher than in the middle of the sample (for both tests – with and without cast iron disc). The natural undrained shear strength of Oxford Clay (i.e. the value measured without electrokinetic treatment) is 7.2 kN/m^2. Tables A3 and A4 show that the undrained shear strength for the sample without a cast iron disc increased slightly from 10.2 kN/m^2 to 12.2 kN/m^2 at the anode and by somewhat more from 9.4 kN/m^2 to 14.6 kN/m^2 at the cathode from the 2-week to the 4-week sample. This showed that the electrokinetic effect increased the strength by 1.1 times at the anode and 1.5 times at the cathode under these experimental conditions. This was attributed to the expectation that the higher concentrations of high valency cations at the cathode (due to electromigration of cations to cathode) will react with dissociated minerals to cause cementation (due to ion exchange and complexation). Complexation typical involves the interaction between an available cation and an anion or a molecule, to form a more stable material, i.e. a more stable salt. (As described by Langmuir, 1997, a complex is formed due to the central coordination of a cation and an anion or neutral molecule (a ligand, which is an anion or neutral molecule that can combine with a cation to form a complex), to form a new material which is more stable than the original components.) The formation of these salts and cementitious products increases the undrained shear strength of the soil in these regions.

In the samples with a cast iron disc the undrained shear strength increased from 7.3 kN/m^2 (the 'natural', baseline reading) to 17.9 kN/m^2 and then 29.3 kN/m^3 at the anode, and to 18.6 kN/m^2 and then 25.2 kN/m^2 at the cathode, for the 2-week and 4-week samples. The strength increased further to 96.2 kN/m^2 at the anode and 99.4 kN/m^2 at the cathode after 3 months. This

confirmed that the electrokinetic treatment time has an important effect on the soil strength. When the cast iron disc was involved, the effect of Fe ion release into the system and the associated reactions increased the strength of the soil by 5.4 times at the anode and 5.3 times at the cathode for the 3-month sample (Figure 4.4(b)).

Samples without a cast iron disc showed a greater increment in strength at the cathode compared to the anode (see Figure 4.4(a)). This was different from what happened in samples with a cast iron disc (see Figure 4.4(b)), where greater strength was found at the anode (close to the cast iron disc). The increase in strength near the cathode for the 4-week specimen might be attributed to dissolution of alumina and/or silica from the clay mineral at high pH and a reaction with calcium released from the clay (which is present in a significant quantity in the case of Oxford Clay, see Table 3.6) to create calcium aluminate hydrate and/or calcium silicate hydrate, which crystallises to cause the undrained shear strength to increase. Whatever the mechanism, it is evident that the strength increase is due to chemical effects since the water content is shown to rise above the 'natural' value for all but the 3-month samples (Figure 4.8).

Figure 4.5 shows the replicability of the test data across the sample for the tests at 3 months with the cast iron disc. The agreement is again good, thus providing confidence in the test methodology.

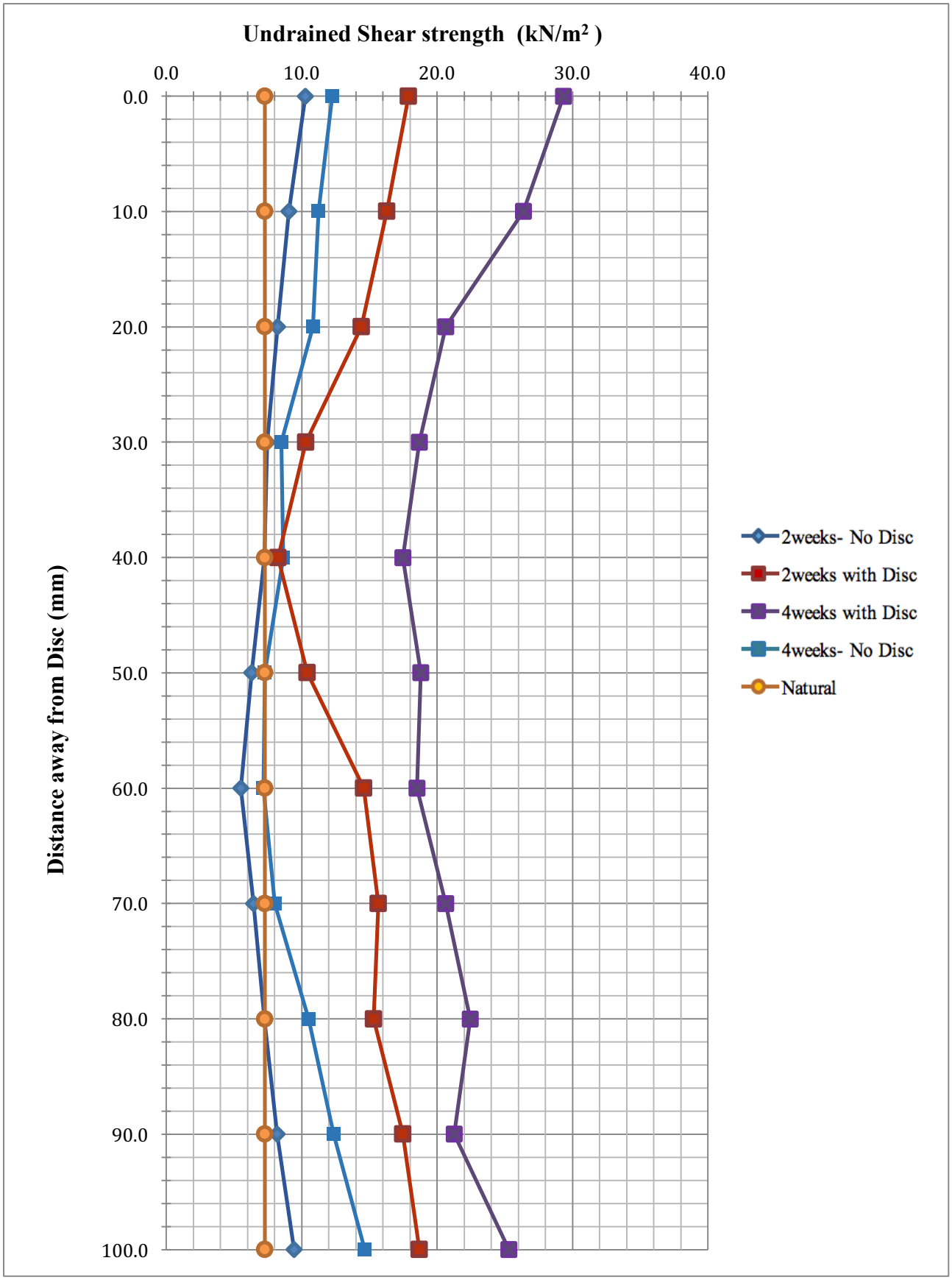

Figure 4.4 (a) Undrained shear strength for Oxford Clay for 2- and 4-weeks samples

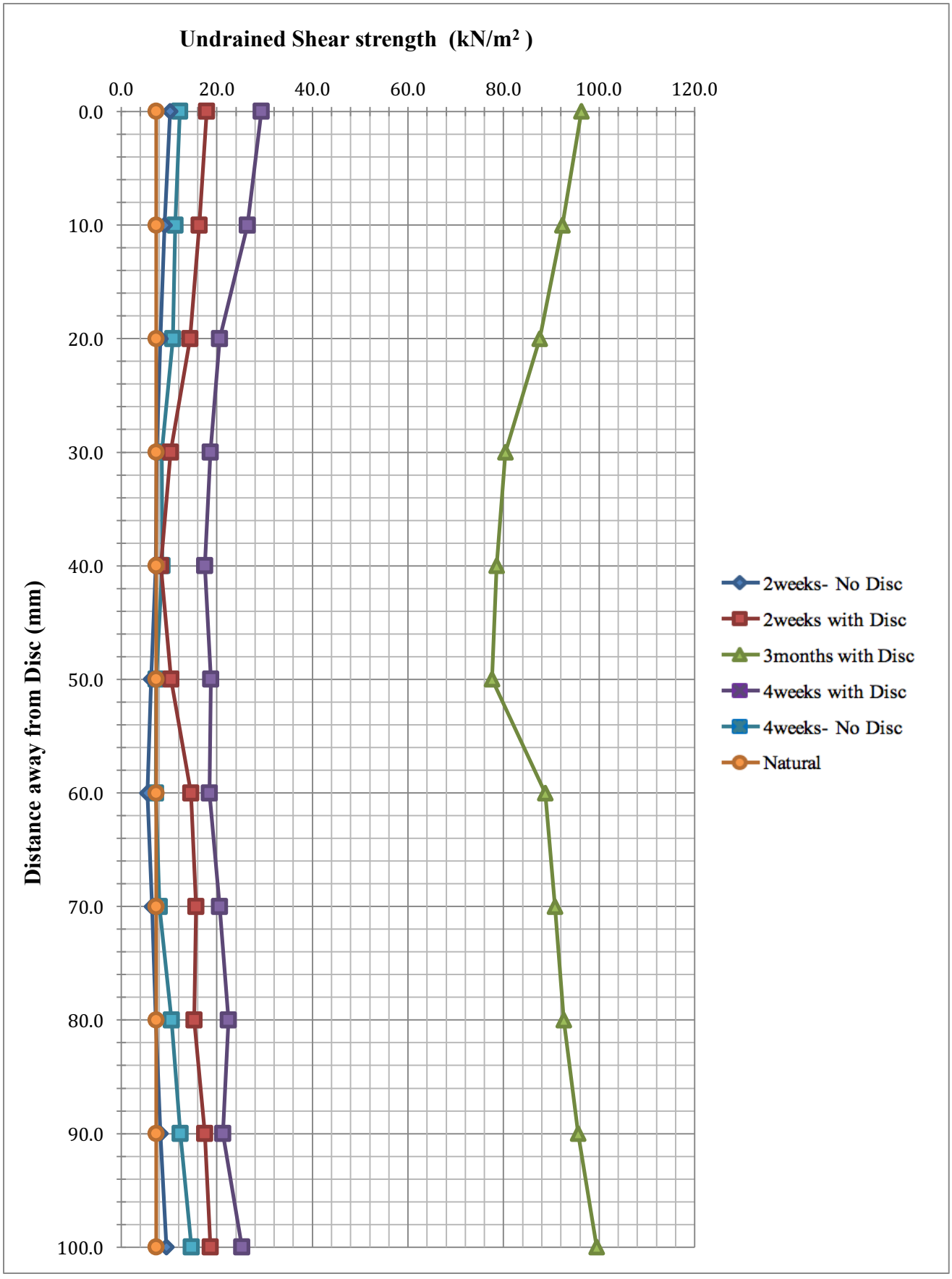

Figure 4.4(b) Undrained shear strength for Oxford Clay samples

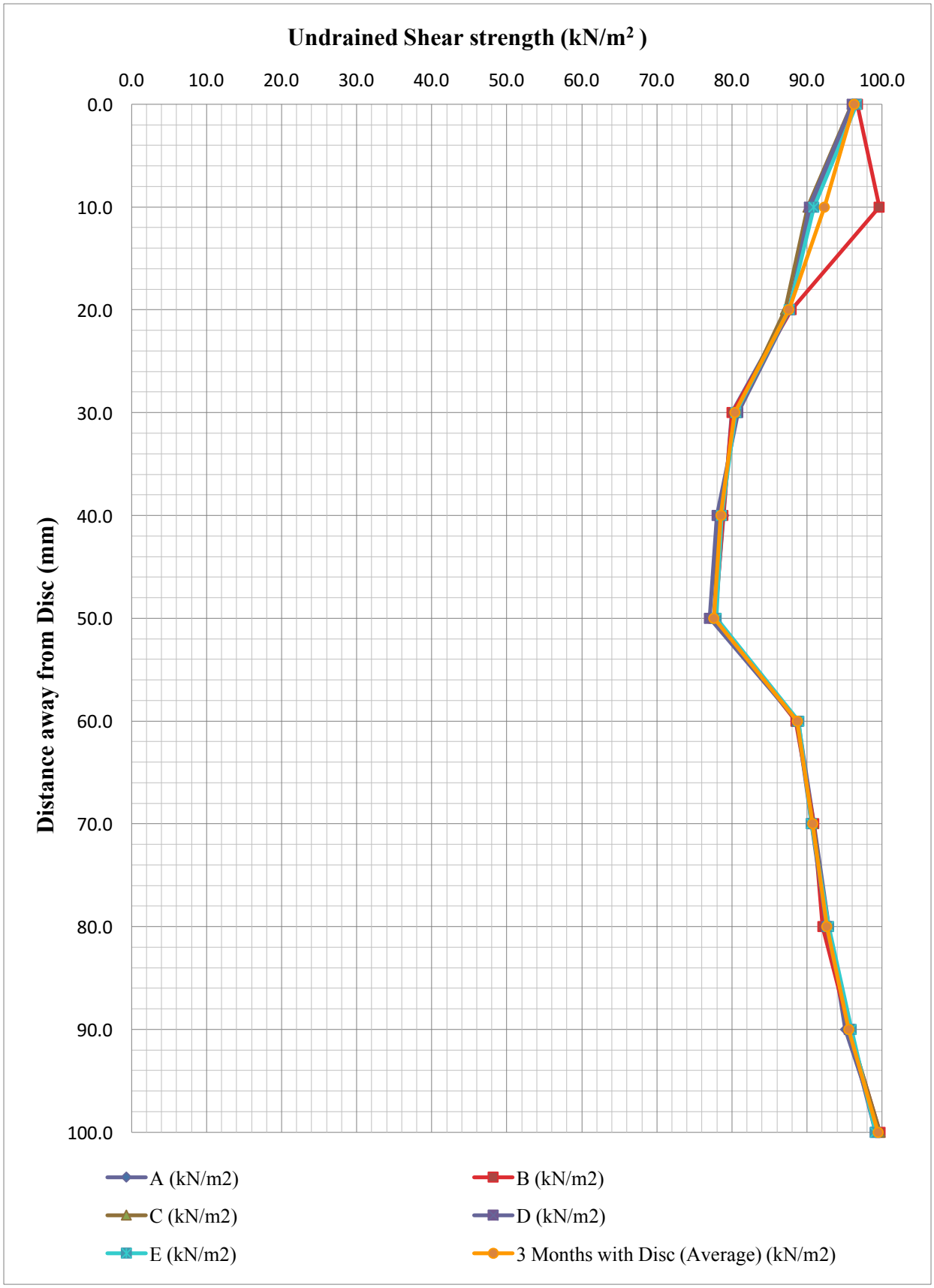

Figure 4.5 Undrained shear strength repeatability for tests at 3 months with disc for the Oxford Clay sample

4.2.2 Moisture Content

One of the significant changes over time in the test took place with respect to the moisture content. Samples were taken at a distance of 10mm away from each other along the length of the samples. The moisture content was measured before the consolidation process (to check the initial moisture content of the sample) and after the electrokinetic process. Generally, the results were found to lie between approximately 41% and 58% moisture content for Kaolin Clay and approximately between 50% and 58% for Oxford Clay. Tables A5 to A6 present the moisture content results.

As shown in Figure 4.6, the moisture content of some samples, such as at 3 months, is lower at the bottom of the sample where the cathode was located (i.e. farthest from the disc, i.e. the anode), where a clay experienced more activity within its diffuse double layer and the net flow of iron ions and water was towards the cathode (due to the electrokinetic treatment). Also, the sample was kept moist on its upper side (anode) during the experiment by providing it with access to water. The raised moisture content seen at the anode was attributed to this effect. The results showed that the water content for samples at the anode was generally higher than at the cathode and decreased over time. The moisture content in samples without a cast iron disc decreased from 49.3% to 45.7% at the anode and 47.8% to 46.9% at the cathode for the 2-week and 4-week samples (see Table A6), having risen from 40.3% for the 'natural' sample. In addition, the moisture content decreased from 58.9% to 56.9% at the anode and 54.9% to 48.9% at the cathode for 2-week and 4-week samples with a cast iron disc (Table A5).

The 3-month sample showed that the moisture content reached 45.1% and 44.8% at the anode and the cathode respectively. This indicated that when Fe was released through the system, the water content decreased by approximately 0.7% at the anode and 0.8% at the cathode (compared with the tests in which no cast iron disc was used). This was expected since when iron ions are released through the system, the changes in (i.e. thinning of) the diffuse double layer cause the solid particles to become closer together, and hence the moisture content decreases. The repeatability of the measurements for the 4-week sample with a disc is presented in Figure 4.7.

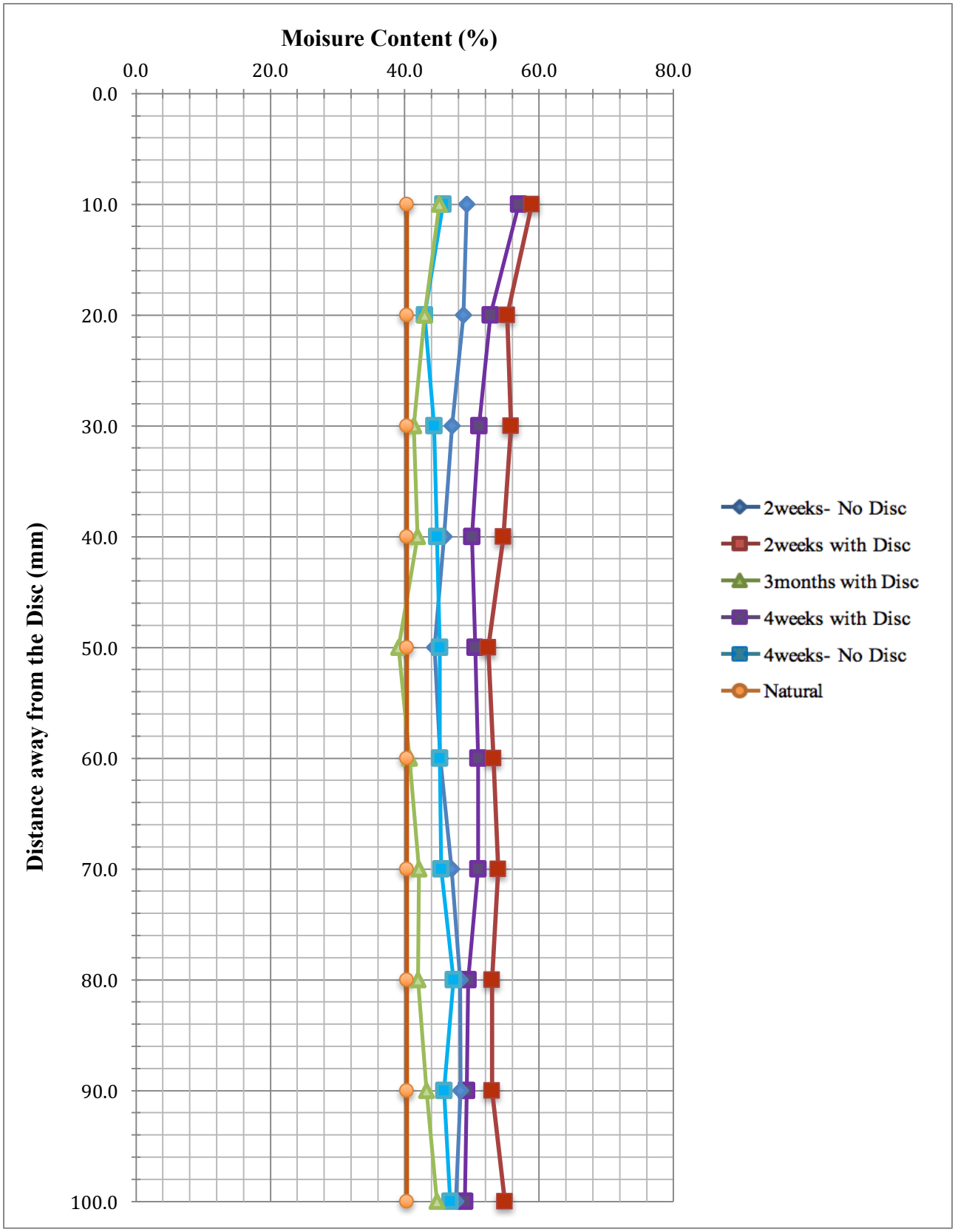

Figure 4.6 Moisture content for Kaolin Clay samples

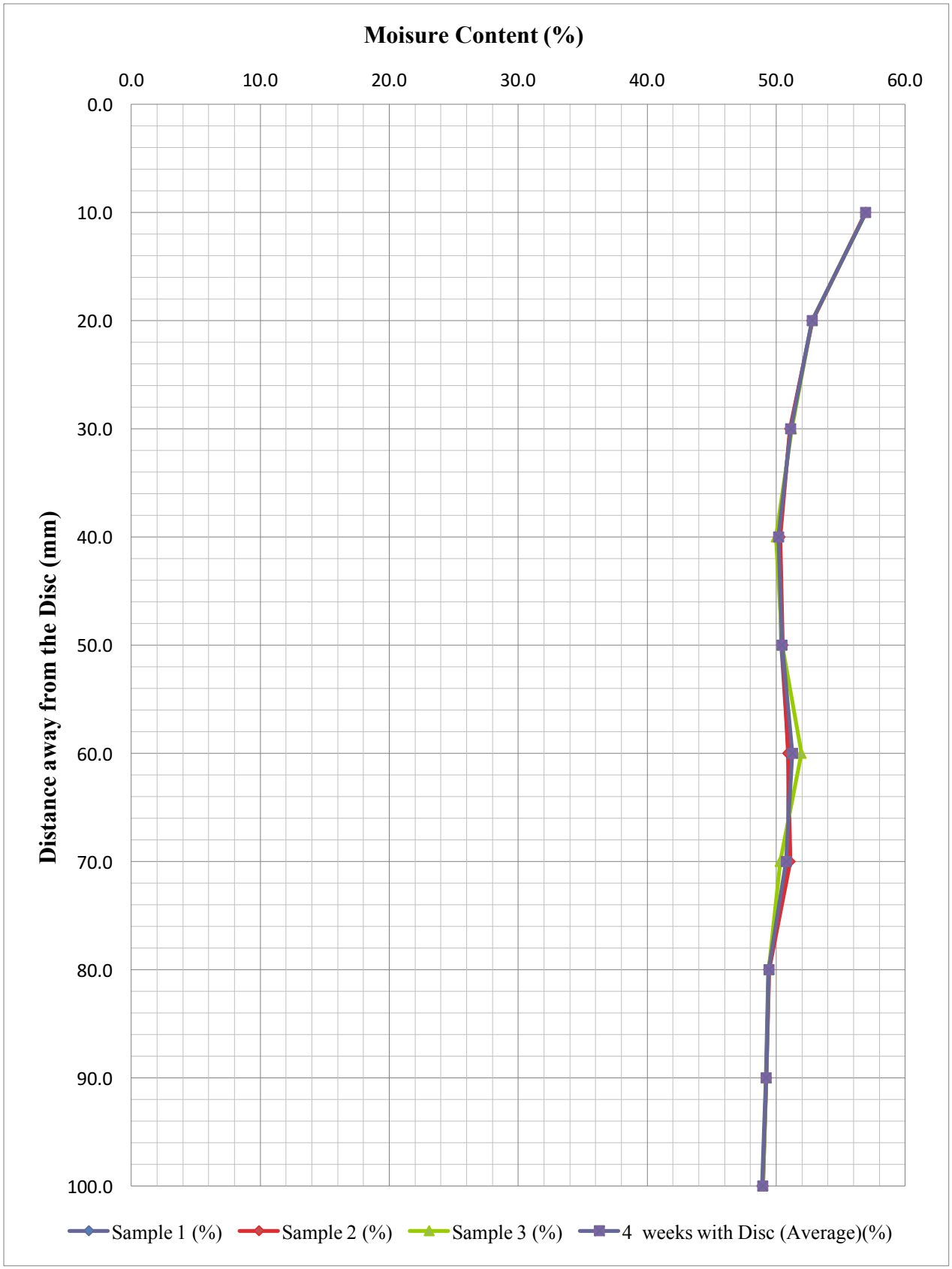

Figure 4.7 Moisture content-repeatability of 4-weeks sample with a cast iron disc for Kaolin Clay

Tables A7 and A8 show that the moisture content generally decreased for the Oxford Clay samples as the tests progressed beyond 2 weeks, except for the 4-week sample with a cast iron disc, where it increased at the bottom of the sample (cathode) from 48.9% to 53.7%. Figure 4.8 shows that the moisture content for Oxford Clay exhibited similar behaviour in the data for 2- and 4-week samples with a cast iron disc, with the one exception noted above. The moisture content for 2-week, 4-week and 3-month samples at the anode, having risen from the 'natural' value of 48.0%, decreased from 52.8% to 50.5% and 45.2% respectively. This was attributed to the release of iron ions from the corrosion of cast iron disc causing substitution on clay mineral cation exchange sites for lower valency ions and a reduction in the thickness of diffuse double layer, thus bringing the particles together and lowering the moisture content (a result that correlates with shear strength results, see Figure 4.4(b)). In the 3-month sample it significantly decreased to 45.2% and 43.3% at the anode and cathode respectively, although importantly the pattern across the length of the sample showed that the water content was depressed further in the middle section so that the water content was raised relative to this middle section at both the anode and the cathode, with a notable consistency in the patterns close to the cathode for the 4-week and 3-month samples. The repeatability of the measurements for the 4-week sample without a disc for Oxford Clay is presented in Figure 4.9.

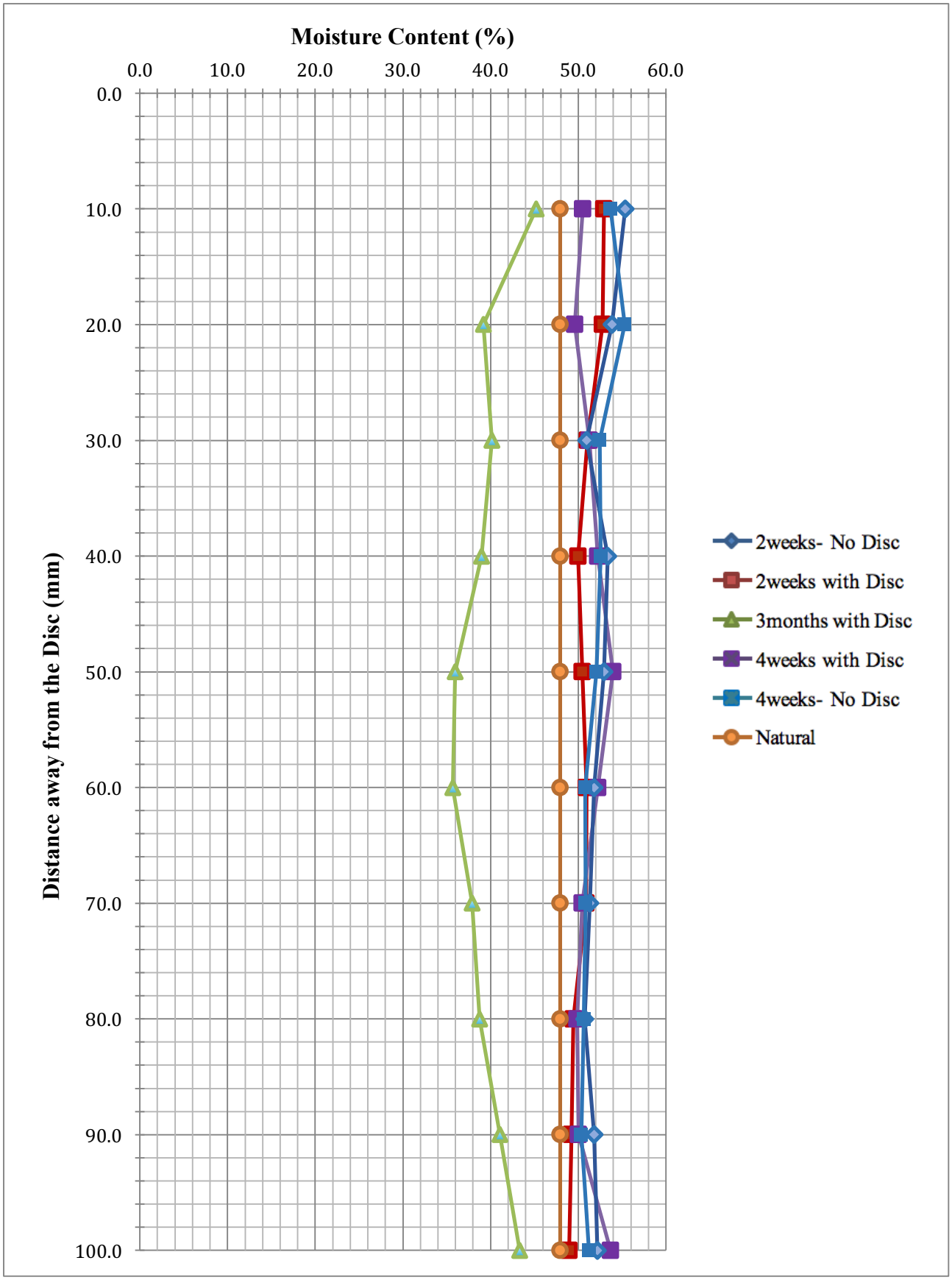

Figure 4.8 Moisture Content for Oxford Clay samples

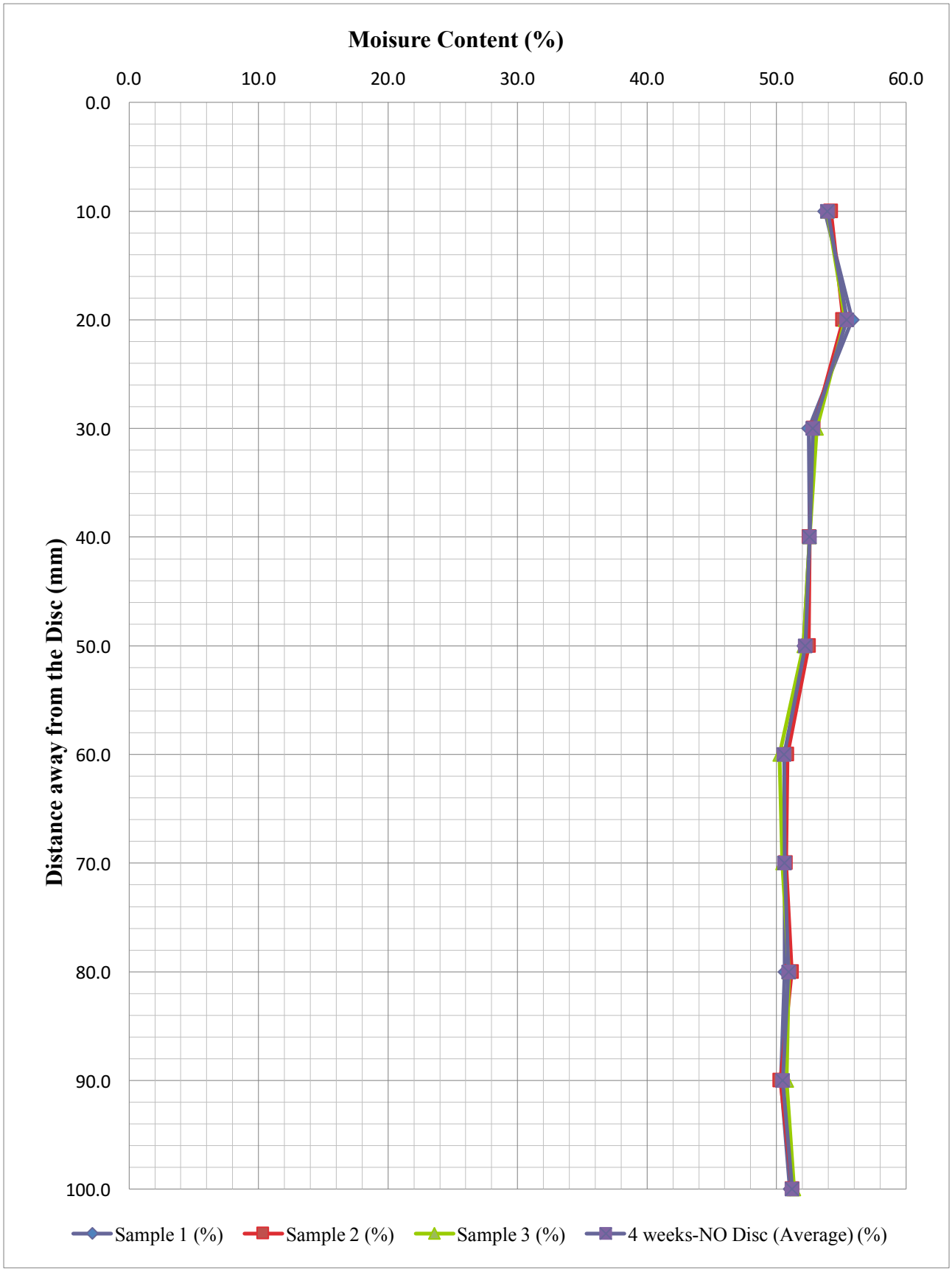

Figure 4.9 Moisture content-repeatability of 4- weeks sample without a cast iron disc for Oxford Clay

4.2.3 Atterberg Limits: Liquid Limit and Plastic Limit

After extrusion, the soil samples were placed in a plastic bag so that they would not be exposed to the air, and the soil was tested for moisture content using the wet material immediately after the cone penetration measurements. These tests were conducted in accordance with BSI 1377 Part 2 for Liquid and Plastic Limits. In Chapter 5 the plasticity properties of the Kaolin Clay and Oxford Clay are discussed. Factors such as pH, electrolyte concentration and thickness of diffuse double layer are related to cation exchange and precipitation, and these together with the type of clay minerals, secondary mineral from crystallisation processes and the type of exchangeable ion can affect the Atterberg limits.

4.2.3.1 Liquid Limit Results

The Liquid Limit of the Kaolin Clay samples increased generally over time from 2 weeks to 3 months, as shown by Figure 4.10. The 'natural' value for the Liquid Limit of Kaolin Clay was 55.6%. Tests with a cast iron disc and electrokinetic treatment showed the values were above the natural value close to the anode and, while they were depressed in the region away from the anode at 2 weeks and from approximately midway to the cathode at 4 weeks, a significant rise above the natural value occurred at all points after 3 months. The trend at 3 months remained higher at the anode and with a reducing trend as the cathode was approached. As shown more specifically in Table A9, the Liquid Limits were found to be higher at anode and decrease towards the cathode for each time period, showing a strong inverse trend with pH (Figure 4.22). This was attributed to the higher valency (iron) ions coming into the system from corrosion of the cast iron disc (the anode) and further thinning of diffuse double layer via cation exchange as the treatment period became longer (although the iron ion concentrations increased only marginally; see figure 4.18), along with a marked increase in conductivity at the anode (Figure 4.26) that was attributed to a fall in pH at the anode to values significantly below 4.0

(Figure 4.22). Conversely in the alkali environment at the cathode (pH>11.5), the opposite phenomenon occurs where the diffuse double layer thickness increases and, combined with conditions in which salt precipitation is encouraged, therefore a reduction in Liquid limit was observed.

The values close to the anode increased from 55.6% to 65.0%, 68.9% and 69.2% for 2-week, 4-week and 3-month samples respectively. Although the Liquid Limit at the cathode initially reduced from 55.6% to 53.9% and 53.4% for the 2-week and 4-week samples, the value increased to a value above the 'natural' value once sufficient time had elapsed (i.e. beyond 4 weeks) to reach 60.7% after 3 months. By increasing the time of treatment from 4 weeks to 3 months, there were marginal increases in pH (Figure 4.22) and Fe ions (Figure 4.18), which had migrated to the cathode and then precipitated as $Fe(OH)_2$ under an alkaline environment, there was a very large increase in conductivity (Figure 4.26) and this appears to have caused the increase in the Liquid Limit close to the cathode. This deduction is reinforced by the observation that the conductivity measurements of the samples for 2 and 4 weeks remained approximately the same, as did the Liquid Limit results. Figure 4.11 presents the repeatability data of the 4-week sample with the cast iron disc and electrokinetic treatment for the Kaolin Clay sample.

The main contributory factors to the increasing shear strength values (the accumulation of precipitates and modification of the mineralogy via cation exchange) as a result of the electrochemical reactions, are thus reflected in the results of the Liquid Limit tests, and are linked to the pH gradient and Fe concentration; this is discussed in greater detail in Section 5.4.2.2.

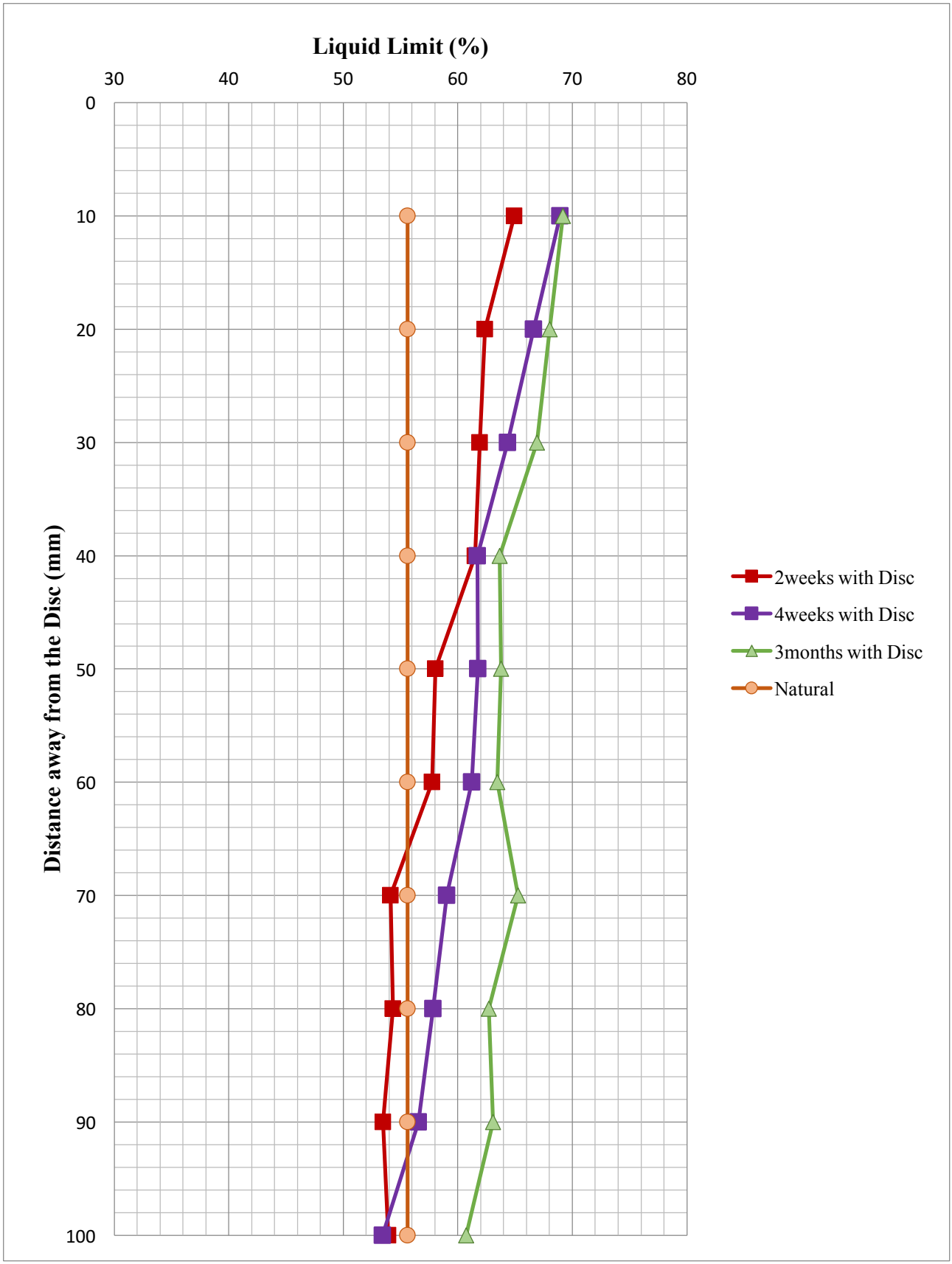

Figure 4.10 Liquid Limits of Kaolin Clay samples

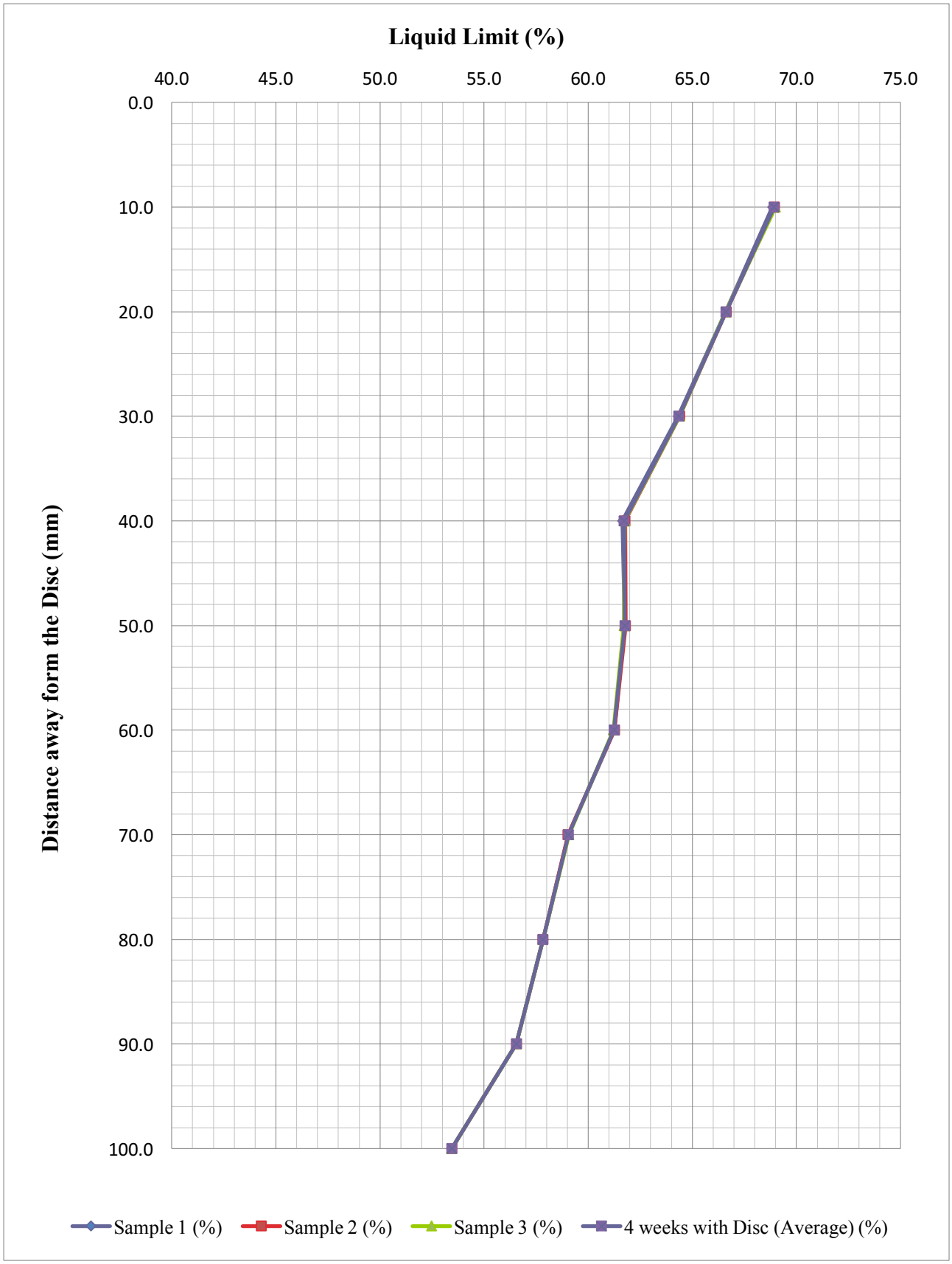

Figure 4.11 Liquid Limit repeatability for tests conducted at 4 weeks with a cast iron disc for Kaolin Clay

The results for the Oxford Clay samples produced similar findings. The Liquid Limit 'natural' value (no electrokinetic treatment) for Oxford Clay was 65.1%. Regarding Table A10, the values increased when the cast iron disc and electrokinetic treatment was involved, changing from 65.3% (2-week sample) to 73.9% for the 3-month sample close to the anode. The values decreased away from the anode, reaching markedly lower values at the cathode side for all three-treatment periods. Although near the anode the Liquid Limit increased marginally, the values decreased below the 'natural' value away from the anode at 2 weeks and, although there was an approximately uniform increase in Liquid Limit at the two later time periods a treatment period of more than 4 weeks was needed before the depressed value at the cathode increased above the 'natural' value, as shown in Figure 4.12. The repeatability of the results for the 2-week sample with a cast iron disc is showed in Figure 4.13(a).

It was observed above that the pH behaviour affects the Atterberg limits. Figure 4.13(b) demonstrates this effect by showing that trends of increasing pH away from the disc are accompanied by similar trends of Liquid Limit decreases.

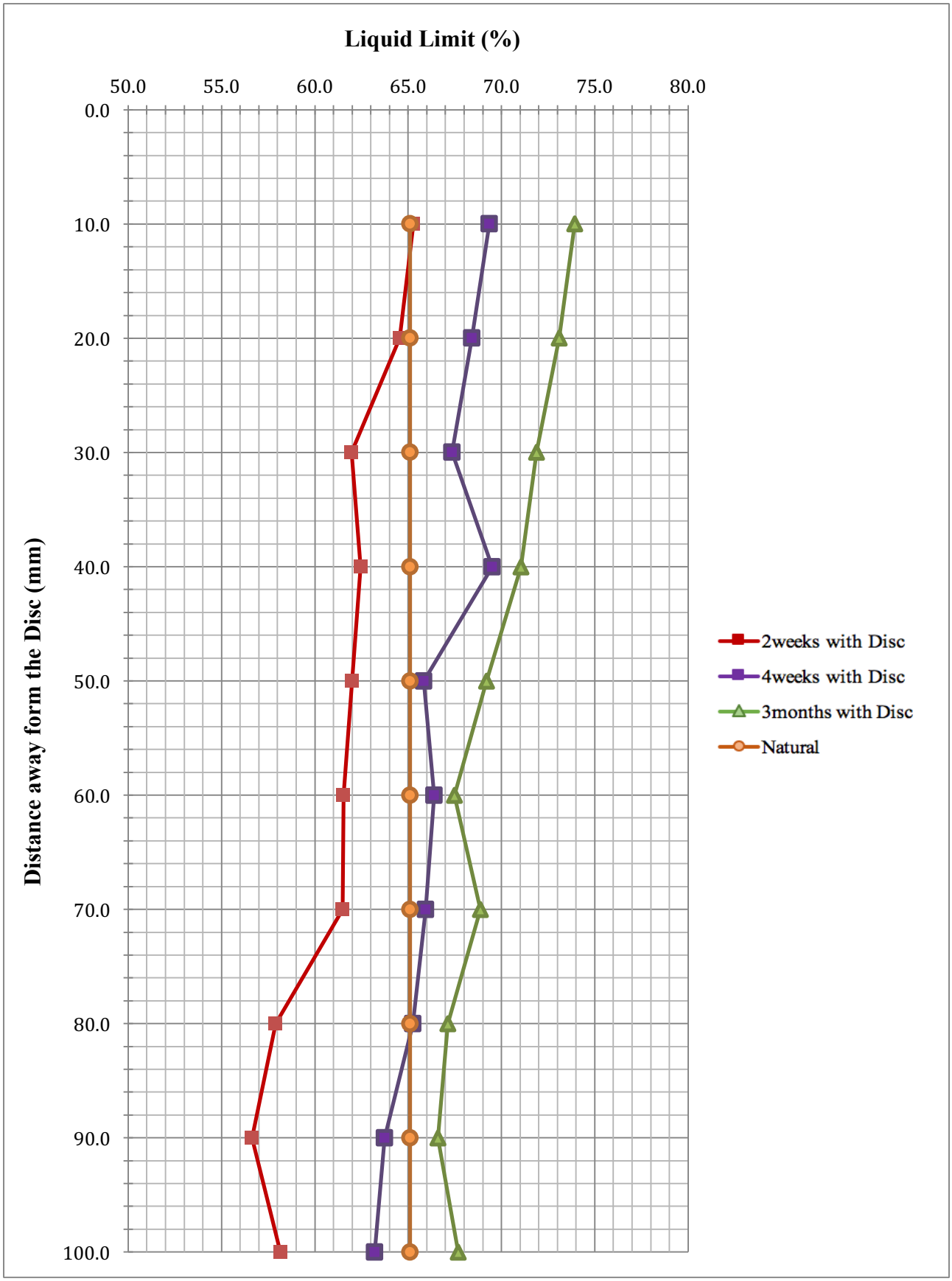

Figure 4.12 Liquid Limits of Oxford Clay samples

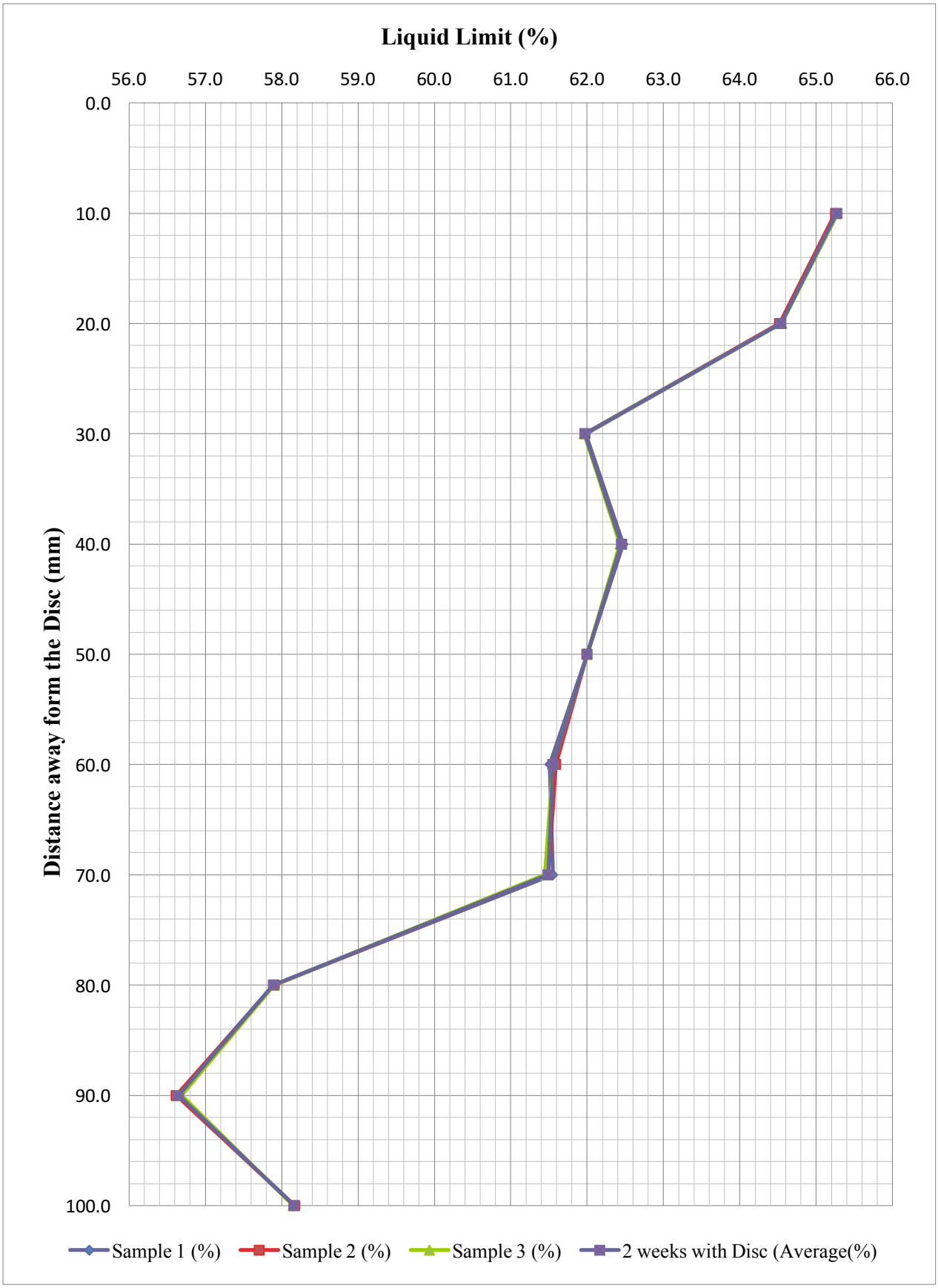

Figure 4.13(a) Liquid Limits repeatability of 2-weeks sample with disc for Oxford Clay

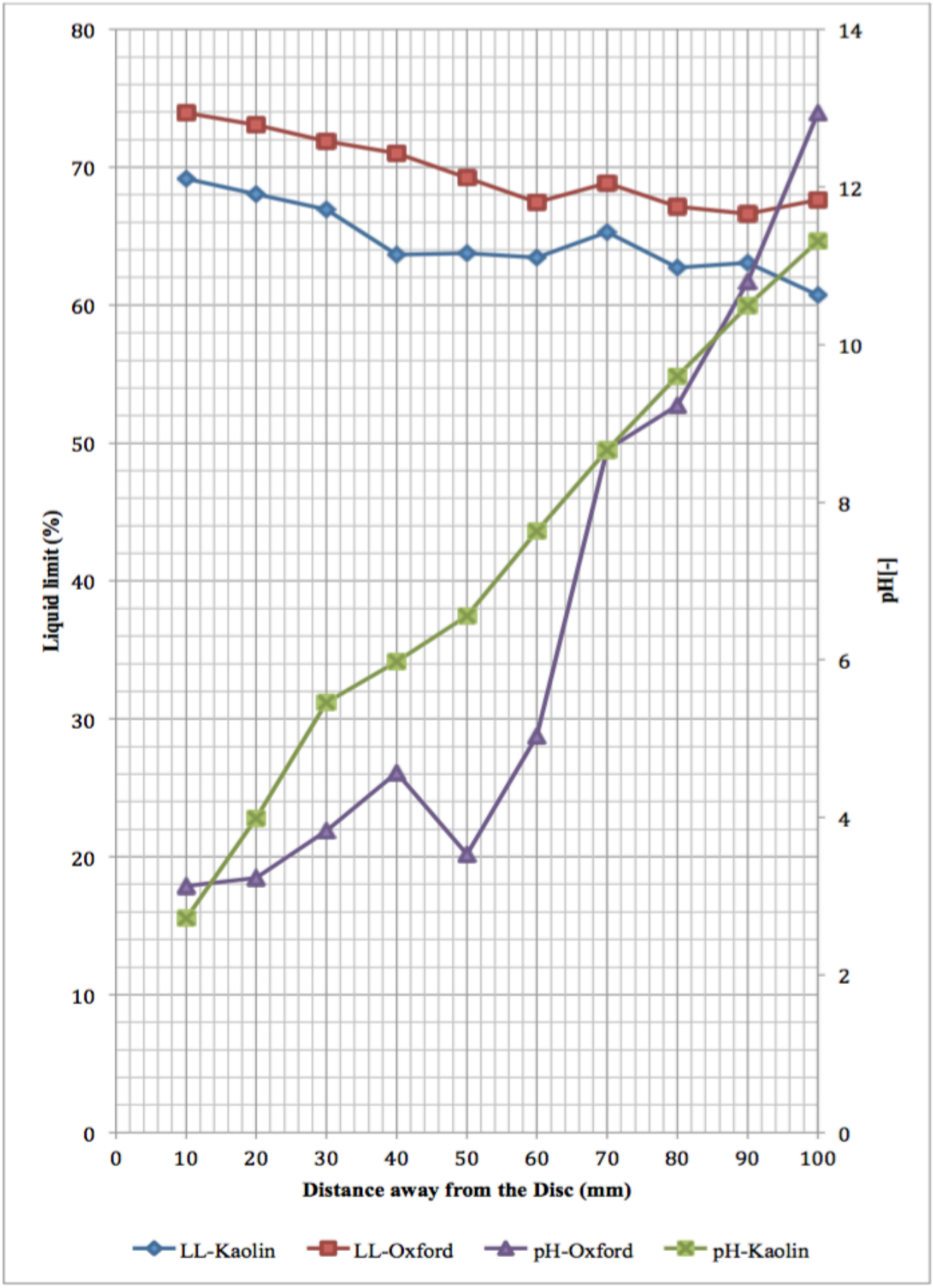

Figure 4.13(b) Liquid Limits and pH of 3-months samples of Kaolin Clay and Oxford Clay

4.2.3.2 Plastic Limit Results

Figure 4.14 illustrates that after an initial rise from the 'natural' value of 23.6%, the Plastic Limits decreased generally over time for Kaolin Clay soil between 2 weeks and 3 months, although the data for the 2-week and 4-week tests were approximately similar throughout the sample and it was only after 3 months that a significant fall occurred. Regarding Table A11, tests with a cast iron disc and electrokinetic treatment showed values above the 'natural' Plastic Limit for all three-treatment durations. The 2-week and 4-week samples with a cast iron disc have Plastic Limits of 34.2% and 32.9% close to the anode, and these values increase to 34.4% and 35.6% at the cathode. For the 3-month sample the Plastic Limit decreased (compared to the 2- and 4-week samples) to 26.4% at the anode and to 28.4% at the cathode. Figure 4.15 presents the 3-month sample results with a disc for Kaolin Clay to demonstrate the repeatability of the data sets.

Bohn *et al.* (2001) stated a low pH (pH < 4.7; see Section 4.3.2) in general caused multivalent cations of Al, Fe and Mg to be released from degradation of the clay minerals into the pore fluid. These multivalent cations are strongly attracted by the negatively charged clay surface and contribute to thinning of the diffuse double layer, hence raising of the Plastic Limit.

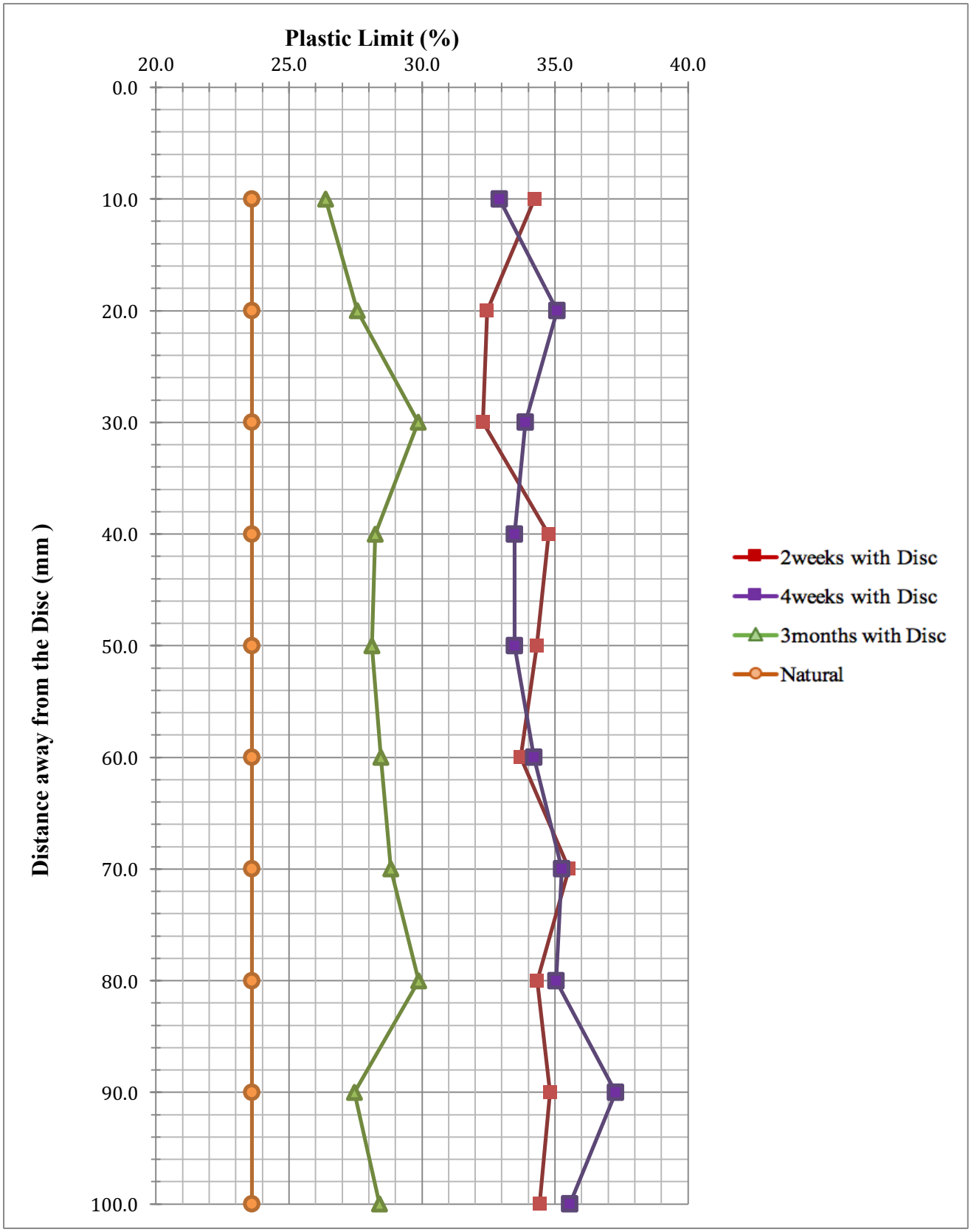

Figure 4.14 Plastic Limits of Kaolin Clay samples

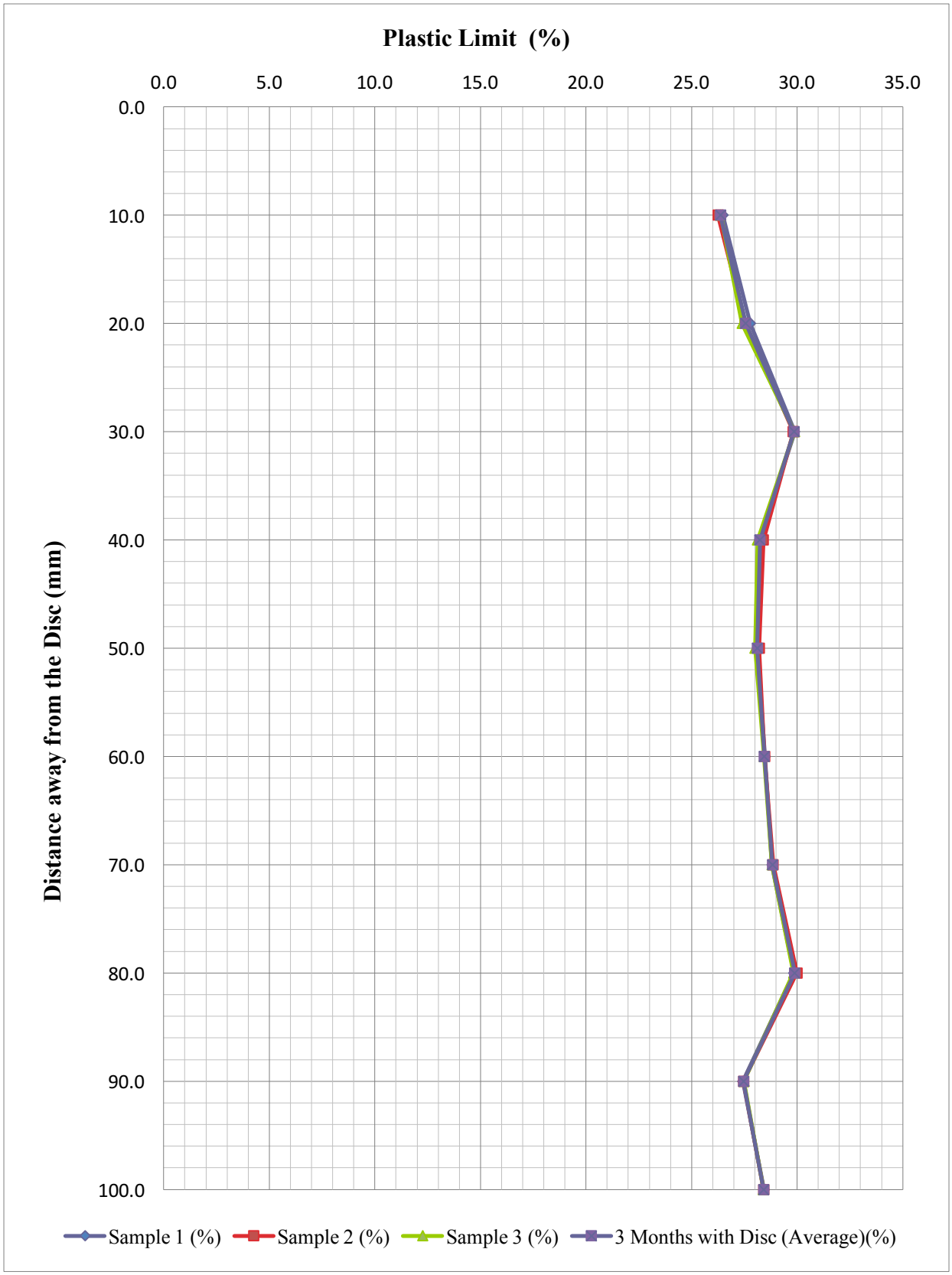

Figure 4.15 Plastic Limits repeatability for 3-months sample with a cast iron disc for Kaolin Clay

The ‘natural’ Plastic Limit of Oxford Clay was 35.2% (see Figure 4.16). Table A12 shows that the Plastic Limit increased for the 2-week and 4-week samples with a cast iron disc and electrokinetic treatment to 36.6% and 37.9% at the anode, and increased at the cathode initially to 35.6% for the 2-week sample followed by a small rise to 35.8% after 4 weeks. For the 3-months sample the Plastic Limit remained approximately constant at 37.6% at the anode and 36.9% at the cathode, with all points in between above the ‘natural’ value. Comparing the 2-week and 4-week results to the ‘natural’ Plastic Limit of Oxford Clay, the Plastic Limit increased at anode area and generally decreased away from the anode towards cathode. Figure 4.17(a) demonstrates the repeatability of the Plastic Limit measurements.

Figure 4.17(b) presents the Plastic Limit data of Kaolin Clay and Oxford Clay plotted together with pH for the 3-month samples. While there is a slight inverse trend for the Kaolin Clay, the Oxford Clay shows no obvious dependency, although the same slight inverse trend would be expected for the 2-week and 4-week Oxford Clay results in light of the discussion above referring to the Plastic Limit decreasing towards the cathode.

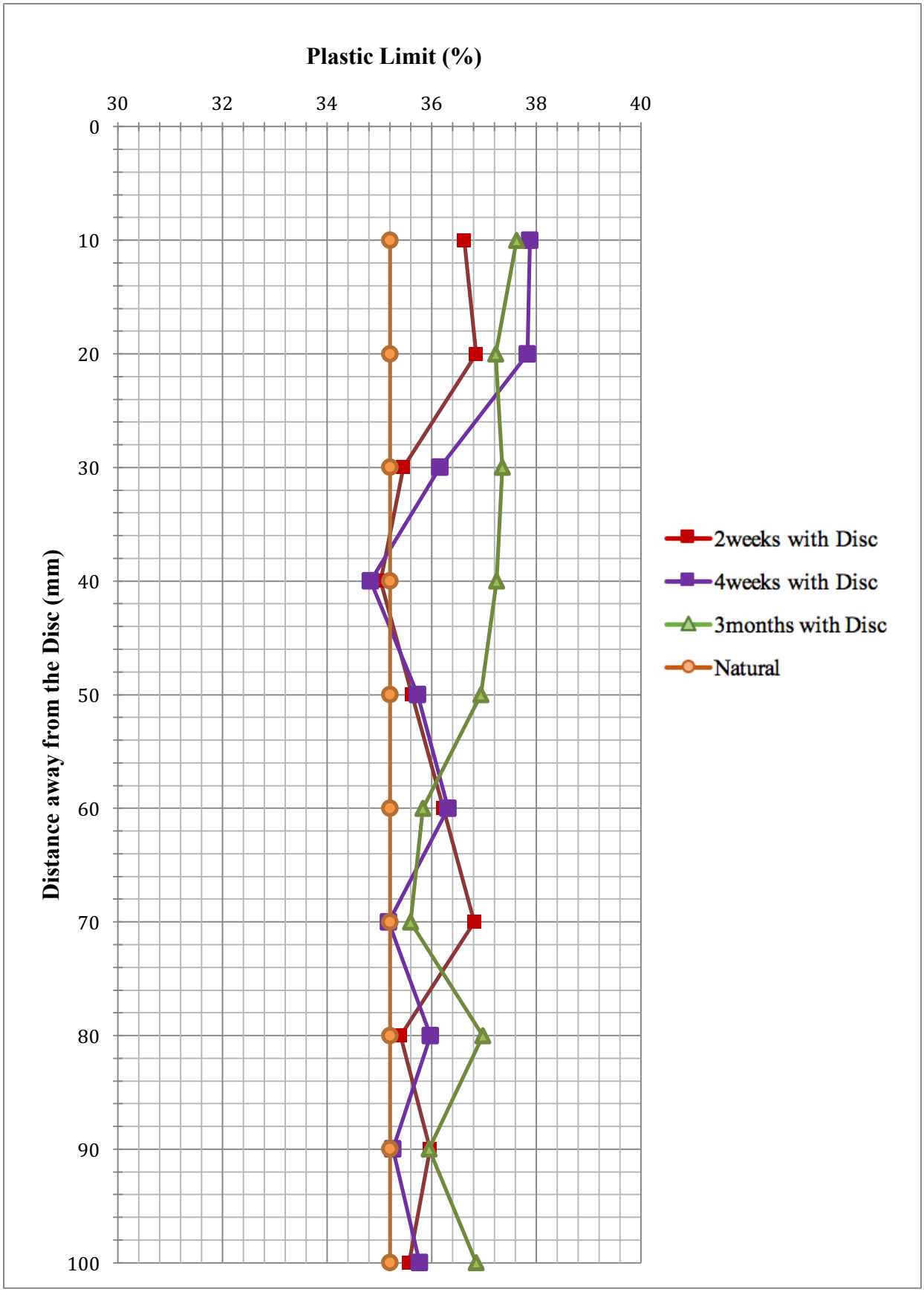

Figure 4.16 Plastic Limits of Oxford Clay samples

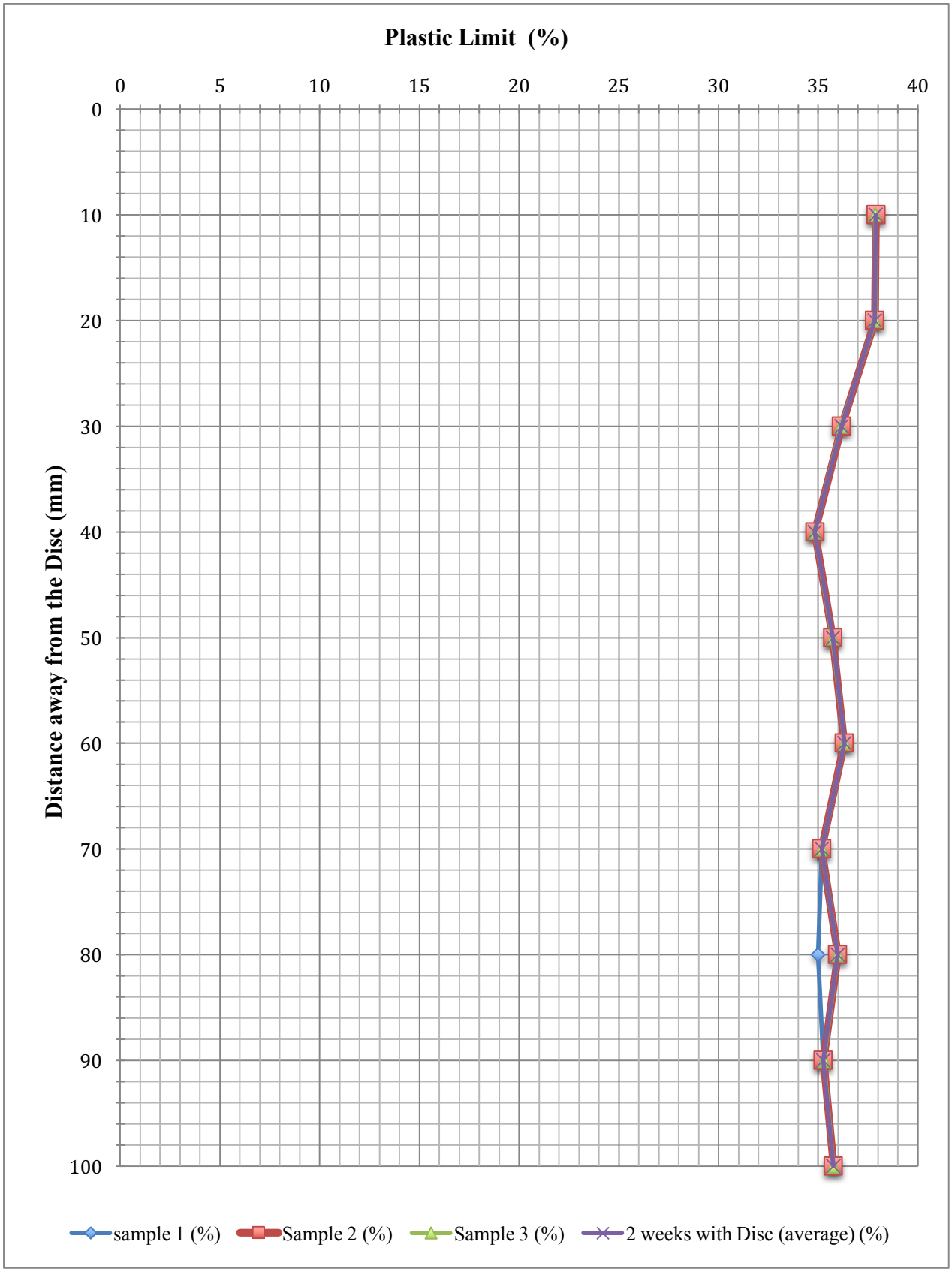

Figure 4.17(a) Plastic Limits repeatability for 3-months sample with a cast iron disc for Kaolin Clay

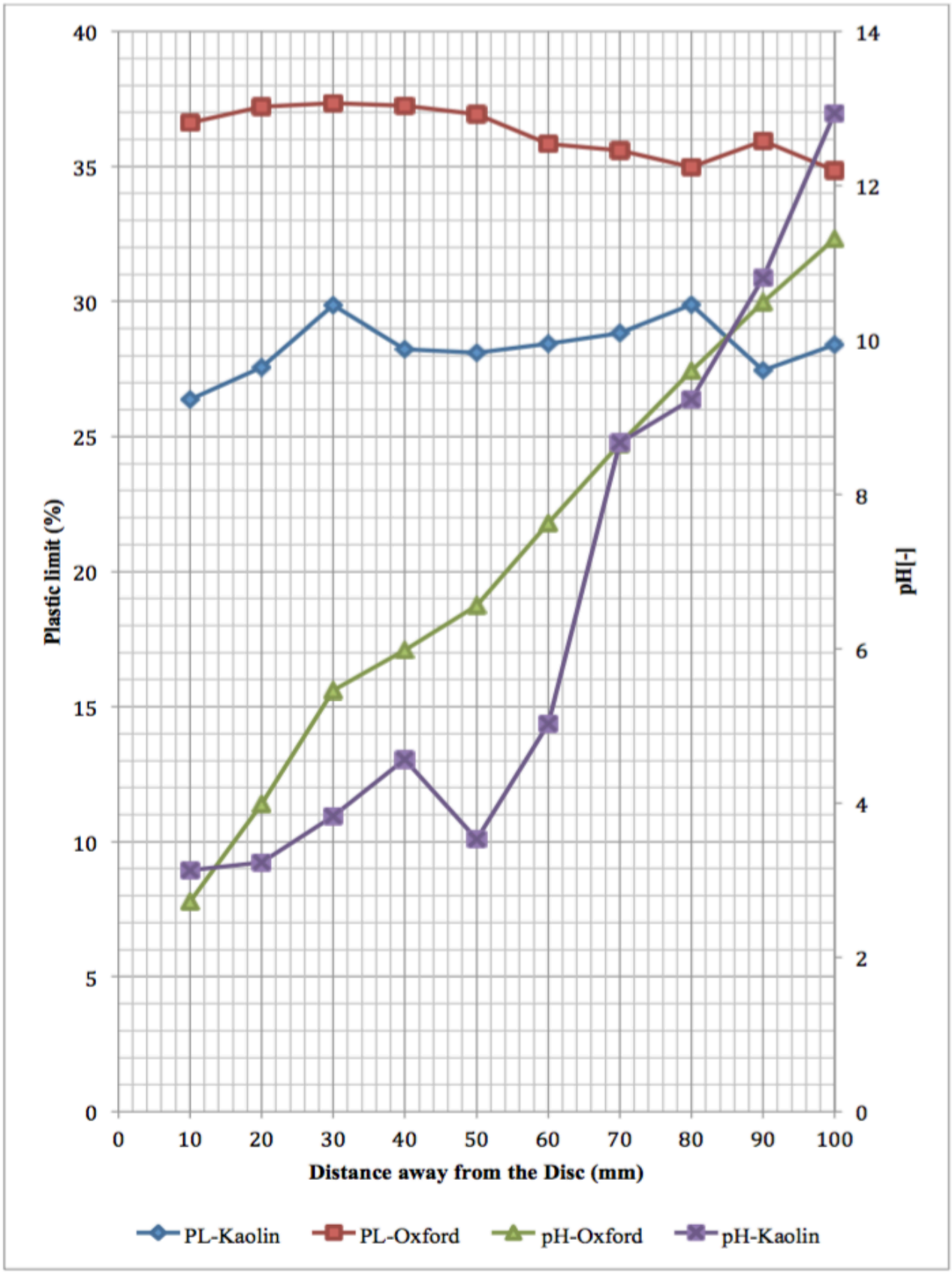

Figure 4.17(b) Plastic Limits and pH of 3-months Samples of Kaolin Clay and Oxford Clay

4.3 Chemical Tests

Chemical tests were carried out to determine the cast iron corrosion effects on Kaolin Clay and Oxford Clay chemical properties, such as pH and conductivity. In particular, it was important to evaluate the pH development as the iron migrated as well as the electrokinetic effects on the soil from the anode to the cathode. The samples were air dried for several days and then crushed to 2μm before the chemical tests were carried out (see Section 3.10).

4.3.1 Iron Content Concentration

This section provides compositional information for the different layers of the samples using a chemical pH dependency test. It was necessary to determine the amount of iron (as an oxide element) in each layer of the samples, working from the anode to cathode, in order to compare the different behaviours through the layers of the samples. Elemental compositional analyses via XRF were undertaken to show trends in iron content concentrations and variations – the main purpose of the evaluation of the iron content was to find trends of how these iron ions move through the sample. Analyses were done after each period of treatment and the compositional results are shown in Tables A13, A14, A15 and A16. To ensure the repeatability and reliability of the results, three replicates were examined.

Figure 4.18 shows that the concentration of iron in Kaolin Clay samples without a cast iron disc did not change to any significant extent as no Fe was released into the sample from the electrodes. In this case, the Fe behaviour depends on the pH, as the dissolution of the clay minerals is dependent on the pH environment and the only source of Fe is from the clay mineral, although the quantity of Fe in the Kaolin Clay is relatively very small (Table 3.6).

Only small changes were seen around the anode area – that is 1.38% and 1.41% for the 2-week and 4-week samples respectively, an increase from the 'natural' value of 1.10% – and these decreased marginally towards cathode. When the cast iron disc was used in the tests with electrokinetic treatment, due to the release from the anode and migration of Fe in the clay samples, these values increased considerably to 8.54%, 8.98% and 9.58% for the 2-week, 4-week and 3-month samples at the anode (i.e. close to the cast iron disc). The iron concentration decrease rapidly away from the anode and more generally towards the cathode, due to the low solubility of the iron oxyhydroxides released from the cast iron disc, but the concentrations through the clay profile remain higher than those without any Fe introduced from the cast iron, the concentrations in the central portion of the 3-month sample being particularly raised (Figure 4.18). There is also an increased iron concentration at the cathode, due to electroosmotic migration from the iron ions introduced at the anode, with the concentration at the cathode increasing with time from 2 weeks to 3 months. Added to this pattern of iron oxyhydroxides migration, dissociation of the Kaolin Clay at the cathode will also induce the complexation of migrated iron to form stable precipitates towards the cathode. The repeatability of 4-week 'with disc' sample is shown in Figure 4.19.

These results are presented in % weight (from XRF measurements). The weight of the powder sample used as described in the methodology chapter (see Section 3.10.3) was 10 gr. Unfortunately, it was not possible to measure the weight of the disc at the end of the test as it was caked in cemented soils and needed to be polished aggressively to remove this before it could be used again. This meant that weighing the disc at the end of the test would not provide a realistic measurement of the loss in weight.

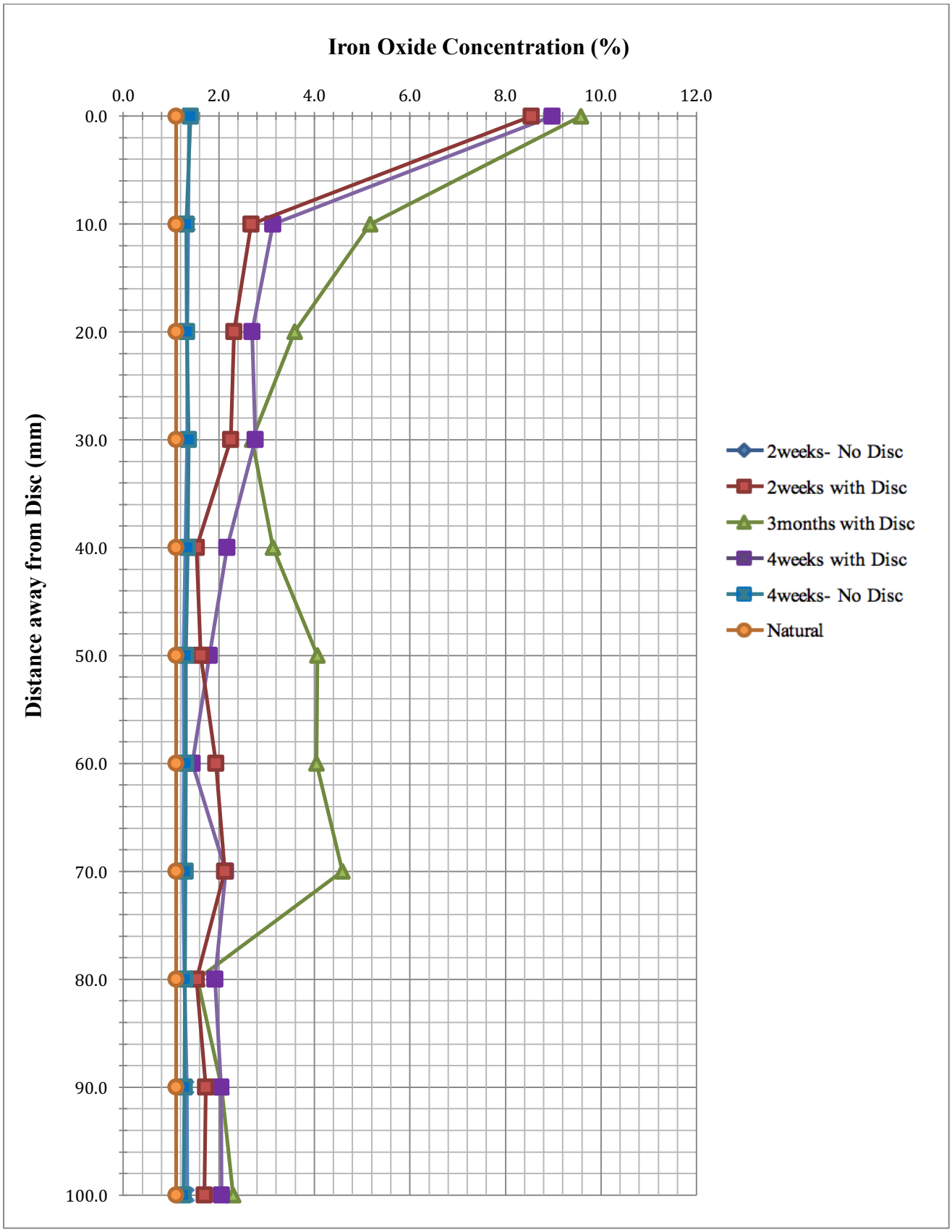

Figure 4.18 Iron concentration for Kaolin Clay samples

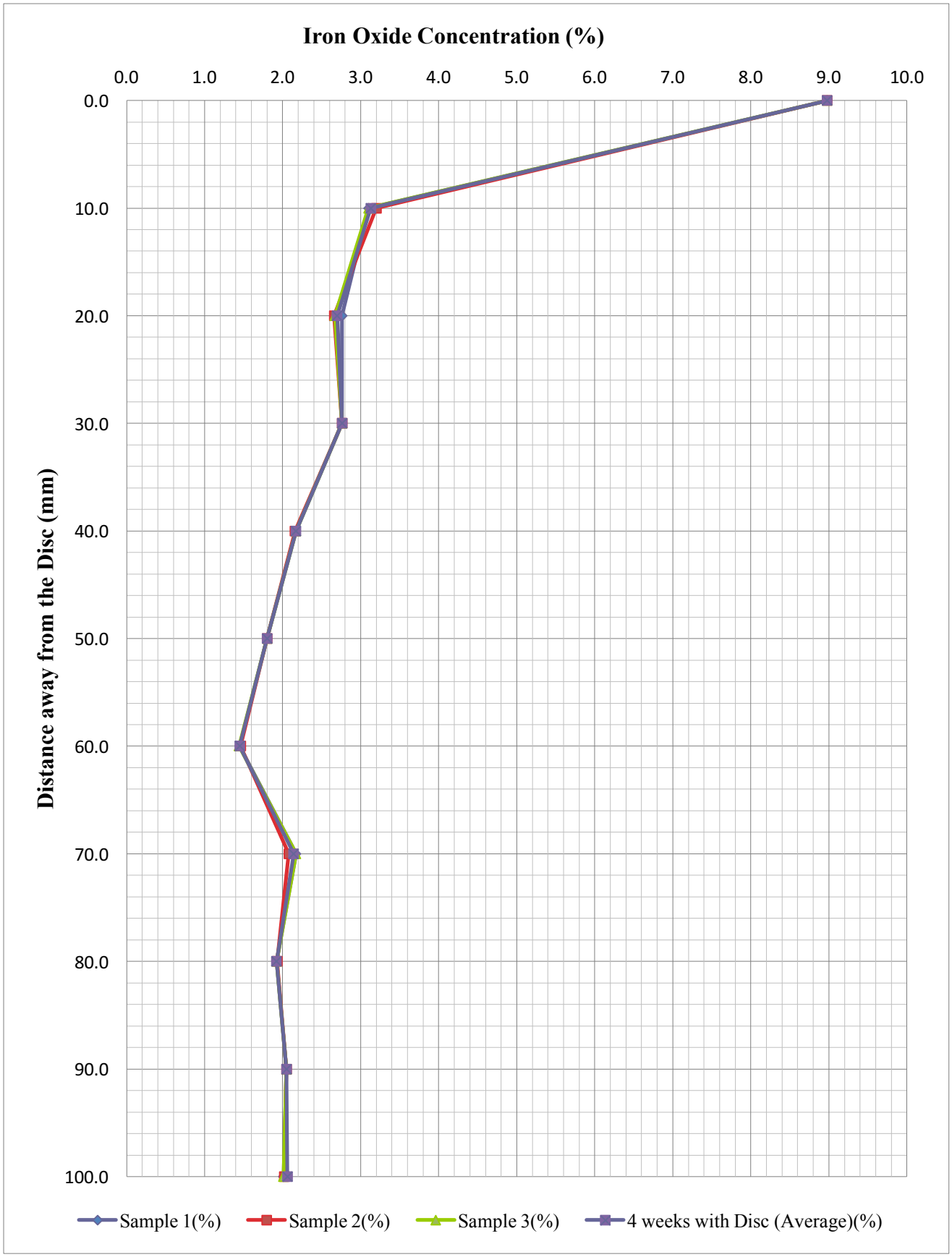

Figure 4.19 Iron concentration repeatability for 4-week sample with a cast iron disc for Kaolin Clay

Figure 4.20 shows that the amount of iron already existing in Oxford Clay was 7.11% (the 'natural 'value). Regarding Table A16, for the samples that had no cast iron disc (only EKG), electrokinetic treatment increased this amount to 7.33% and 7.36% after 2 weeks and 4 weeks respectively, and the amount decreased toward the cathode, reaching 7.09% and 7.07% (2 weeks and 4 weeks respectively) at the cathode side. Table A15 shows that when a cast iron disc was involved in the tests, the amount of iron increased to 10.76%, 29.39% and 32.98% for 2 weeks, 4 weeks and 3 months respectively, i.e. after 3 months the value of the iron oxide concentration increased to 3 times that of the 2-week sample and nearly 5 times that of the 'natural' measurement. In the 2-weeks sample, i.e. the initial phase of cast iron disc degradation, almost all introduced Fe complexes and there is minimal movement through the sample as there is enough exchangeable ion in Oxford Clay sample. Thus, the amount of iron in the clay away from the anode (i.e. at 10mm from the anode at 2 weeks and 20mm from the anode at 4 weeks) did not increase until the treatment had been applied for 3 months, where evidence of iron (possibly as precipitation as oxyhydroxides, though the pH will govern whether or not precipitation has occurred) in the middle of the sample was found: it reached a maximum of 18.69% 50mm from the anode and, although reducing towards the cathode, the concentration remained elevated at all points until the cathode is reached. The repeatability of the 4-week sample with the cast iron disc is presented in Figure 4.21.

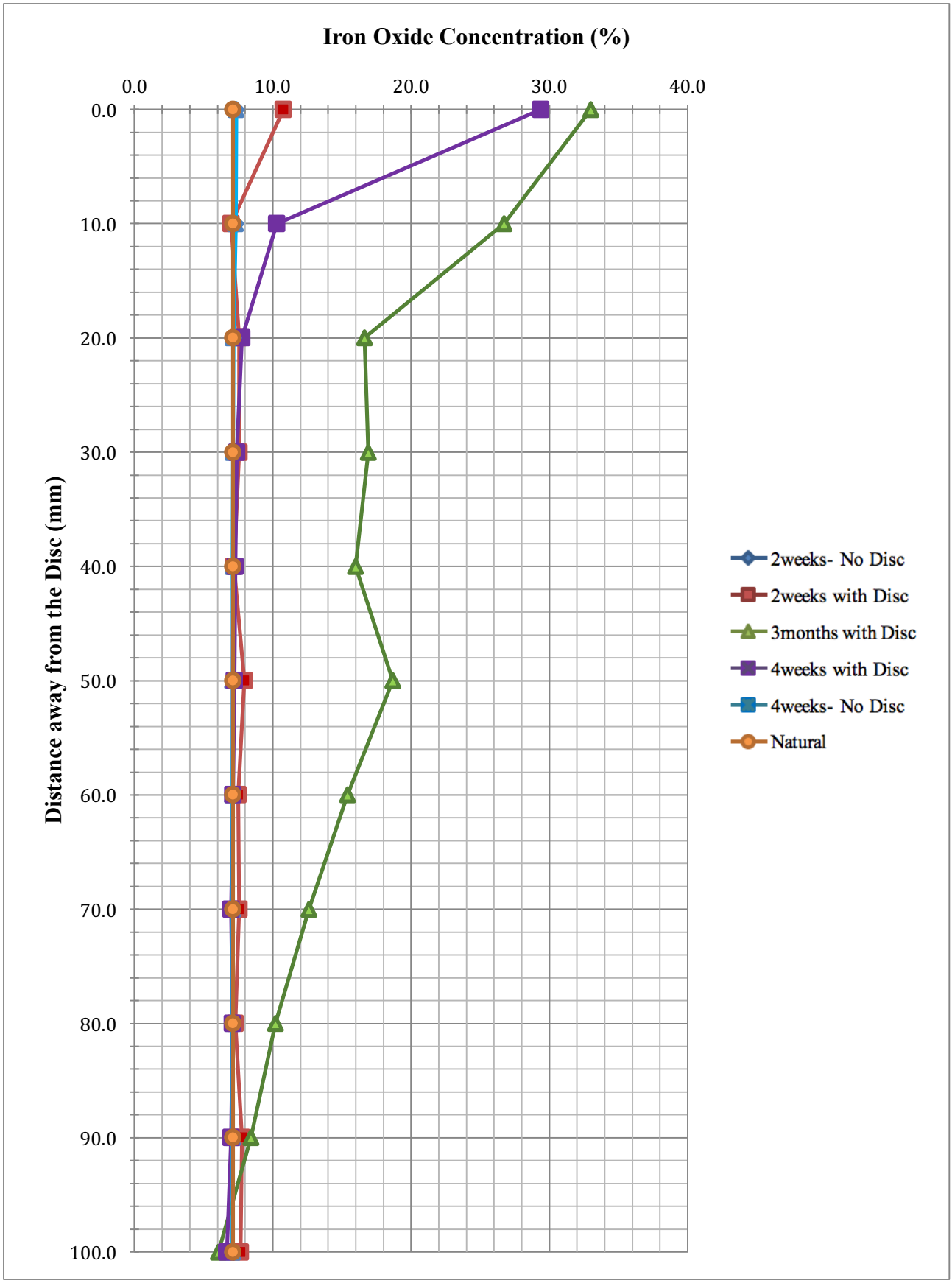

Figure 4.20 Iron concentration measurements of Oxford Clay samples

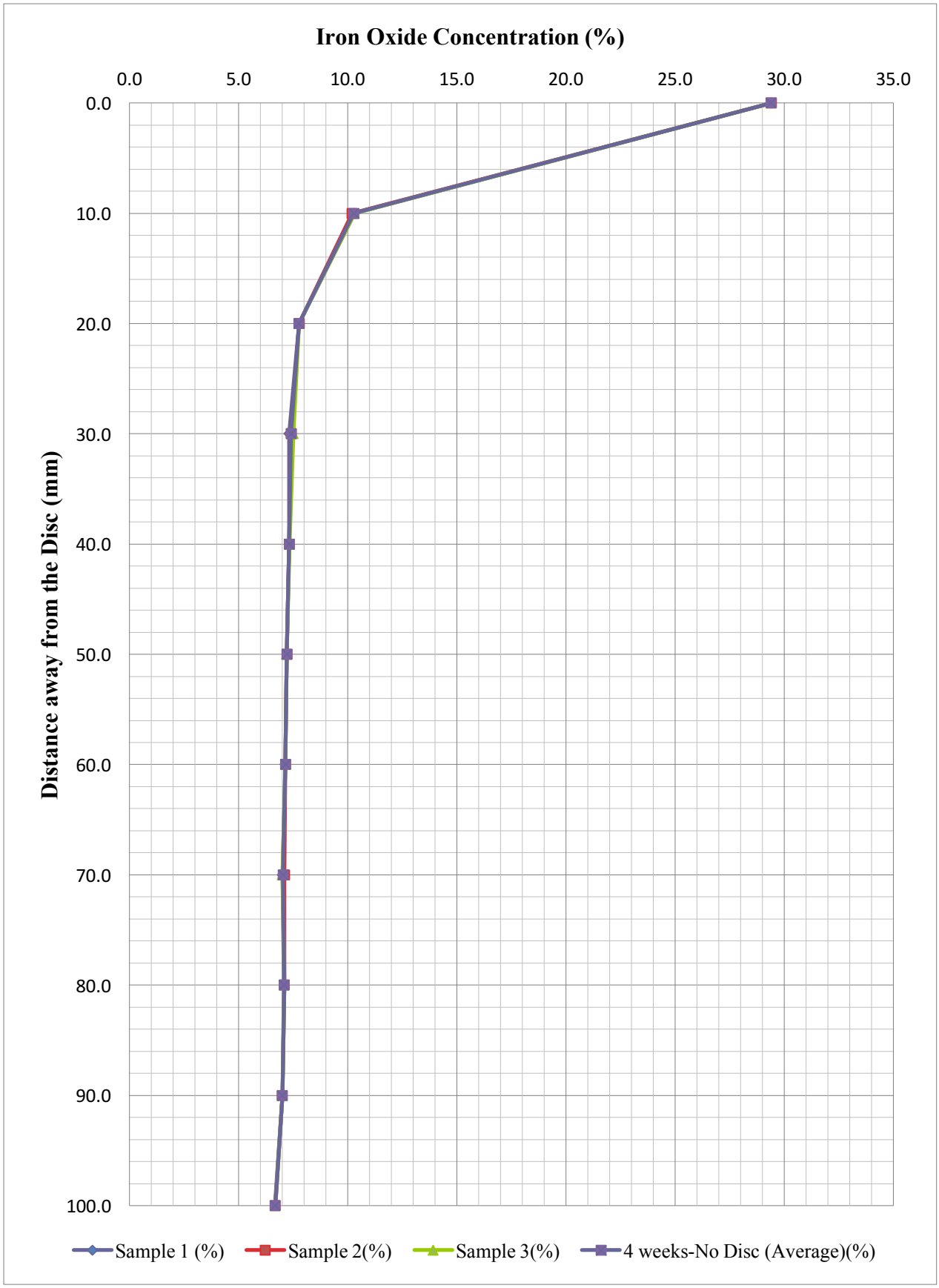

Figure 4.21 Iron concentration repeatability of results for the test at 4 weeks with a cast disc for the Oxford Clay sample

4.3.2 pH

pH measurements were taken throughout the length of the samples at the end of each test, and for each batch the test was replicated 3 times.

The natural pH for the Kaolin Clay was 7.31. Table A18 shows that the pH of Kaolin Clay soil was changed due to electrokinetic treatment alone (i.e. when no cast iron disc was involved in the tests) to 4.01 (anode) and 11.47 (cathode) after 2 weeks, and it decreased to 3.87 (anode) and increased to 11.60 (cathode) after 4 weeks. When a cast iron disc was involved (Table A17), the anode area became more acidic and the cathode area became more alkaline. Figure 4.22 shows that the pH decreased at the anode to 3.33, 3.30 and 3.15 for 2 weeks, 4 weeks and 3 months respectively. At the cathode, the values for 2 weeks, 4 weeks and 3 months increased from 11.63 to 11.93 to 12.94 respectively. The graph shows that, for samples with a cast iron disc, there was a lowering of pH at the middle of the sample. The pH suddenly, at the middle of sample (50mm away from the anode) and showing a consistent pattern, decreased to 4.63, 4.13 and 3.53 for 2 weeks, 4 weeks and 3 months respectively. More detail is given in the next chapter. The pH repeatability for the 2-week sample without a cast iron disc is presented in Figure 4.23.

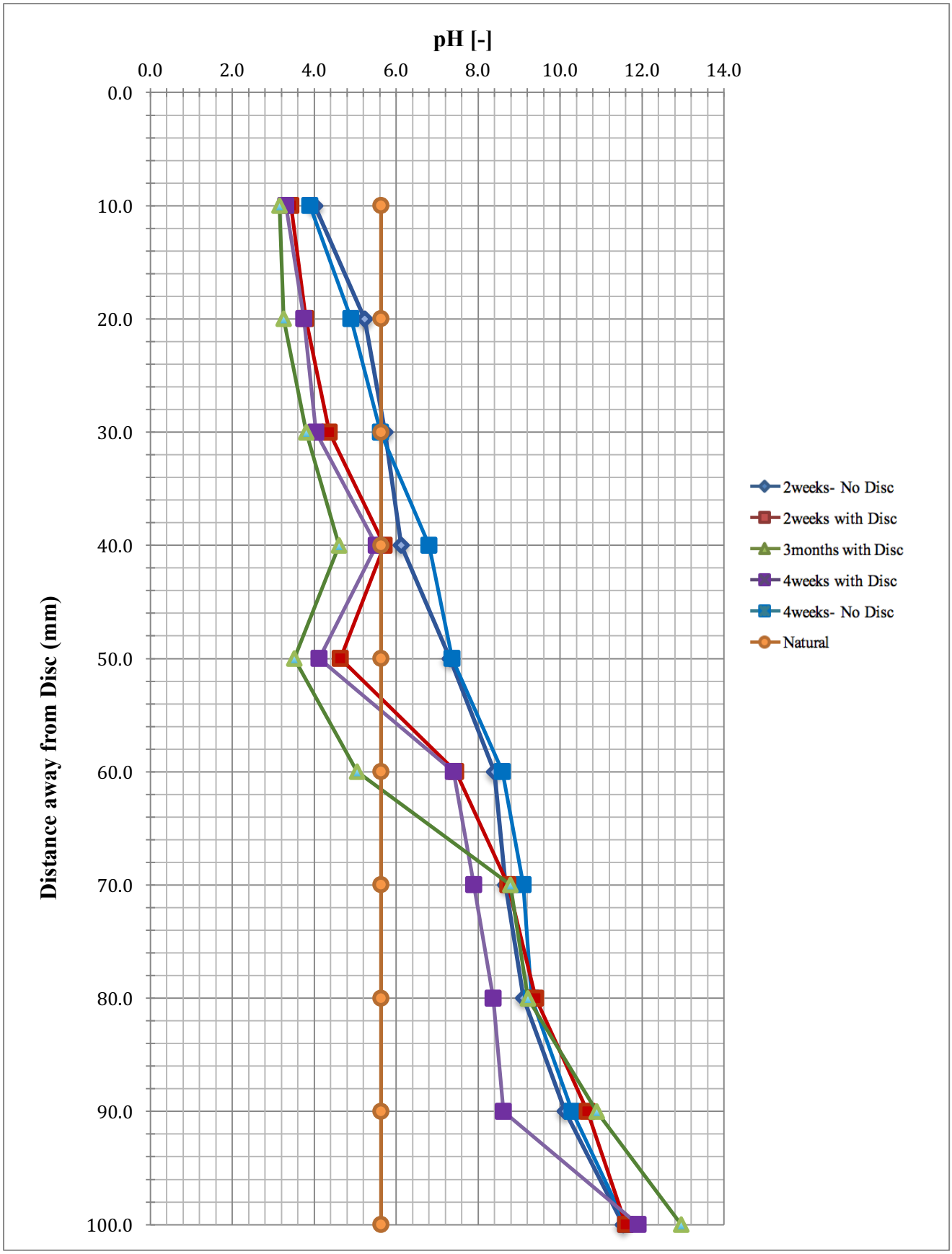

Figure 4.22 pH for Kaolin Clay samples

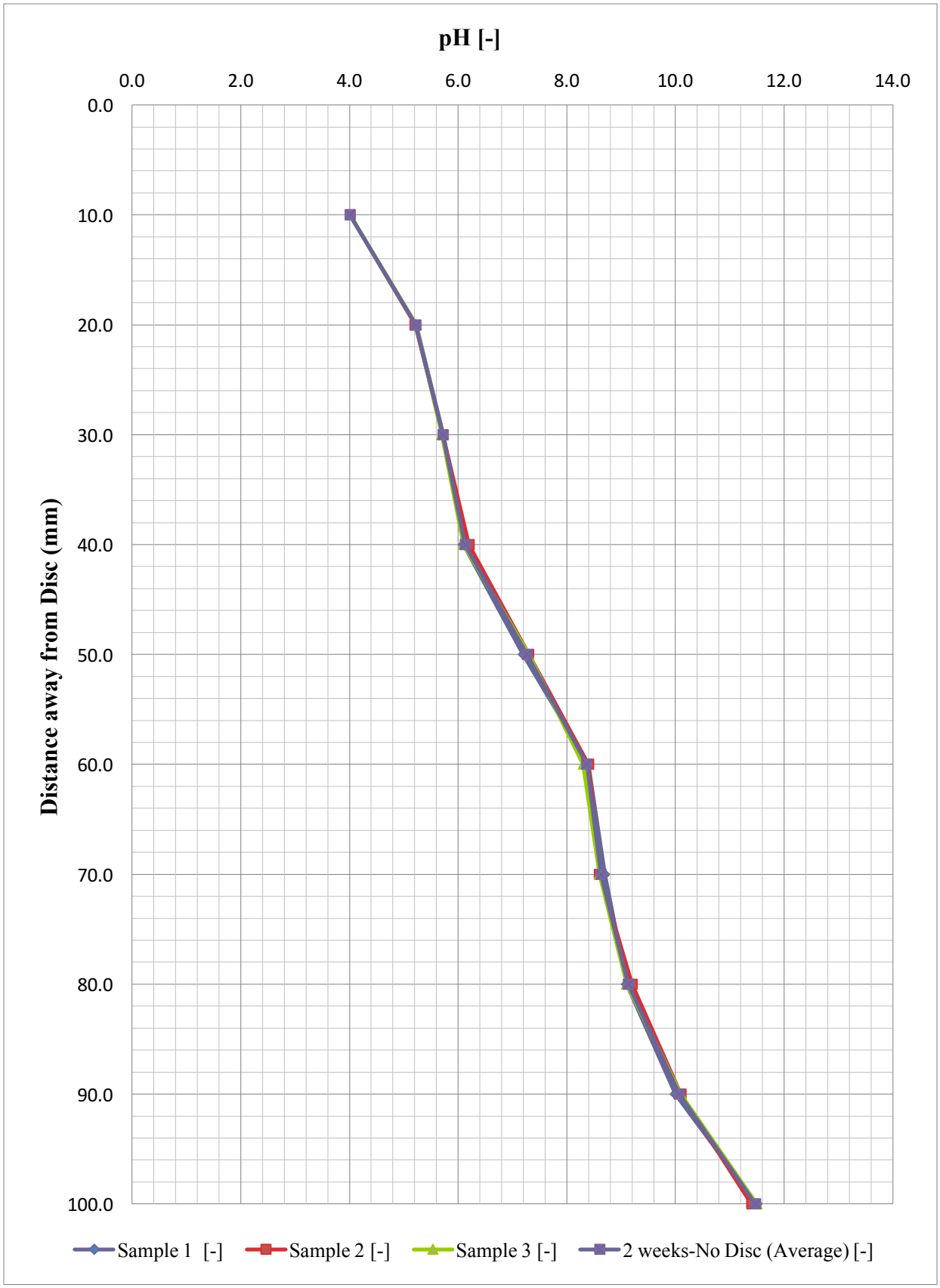

Figure 4.23 pH repeatability for test at 2 weeks without a cast iron disc for Kaolin Clay sample

Figure 4.24 presents the pH results for Oxford Clay. Oxford Clay has a natural pH of 7.31 (natural), and the electrokinetic treatment changed this pH throughout the sample. Table A20 (without cast iron disc) shows that the pH at the anode decreased to 5.67, and at the cathode the pH increased to 12.00, for the 2-week sample. The 4-week sample shows that the pH decreased further at the anode to 5.47, and increased at the cathode to 12.17. The pH at the anode deceased with increasing the treatment time due to the formation of more H^+ and OH^- ions and more ion migration with treatment.

When a cast iron disc was included in the experiment (see Table A19), the pH at the anode decreased to 4.87, 4.47 and 2.72 for the tests at 2 weeks, 4 weeks and 3 months respectively. It appeared that the more iron that was released through the system, the more acidic the environment became. At the cathode side of the 2-week and 4-week samples, the values increased to 12.15 and 12.35. However, for the 3-month sample the value at the cathode decreased to 11.31; the reason for this effect is unclear, though it is interesting to note that the curve for this test shows a more acidic pattern throughout. The repeatability of 3-month sample with a cast iron disc is presented in Figure 4.25.

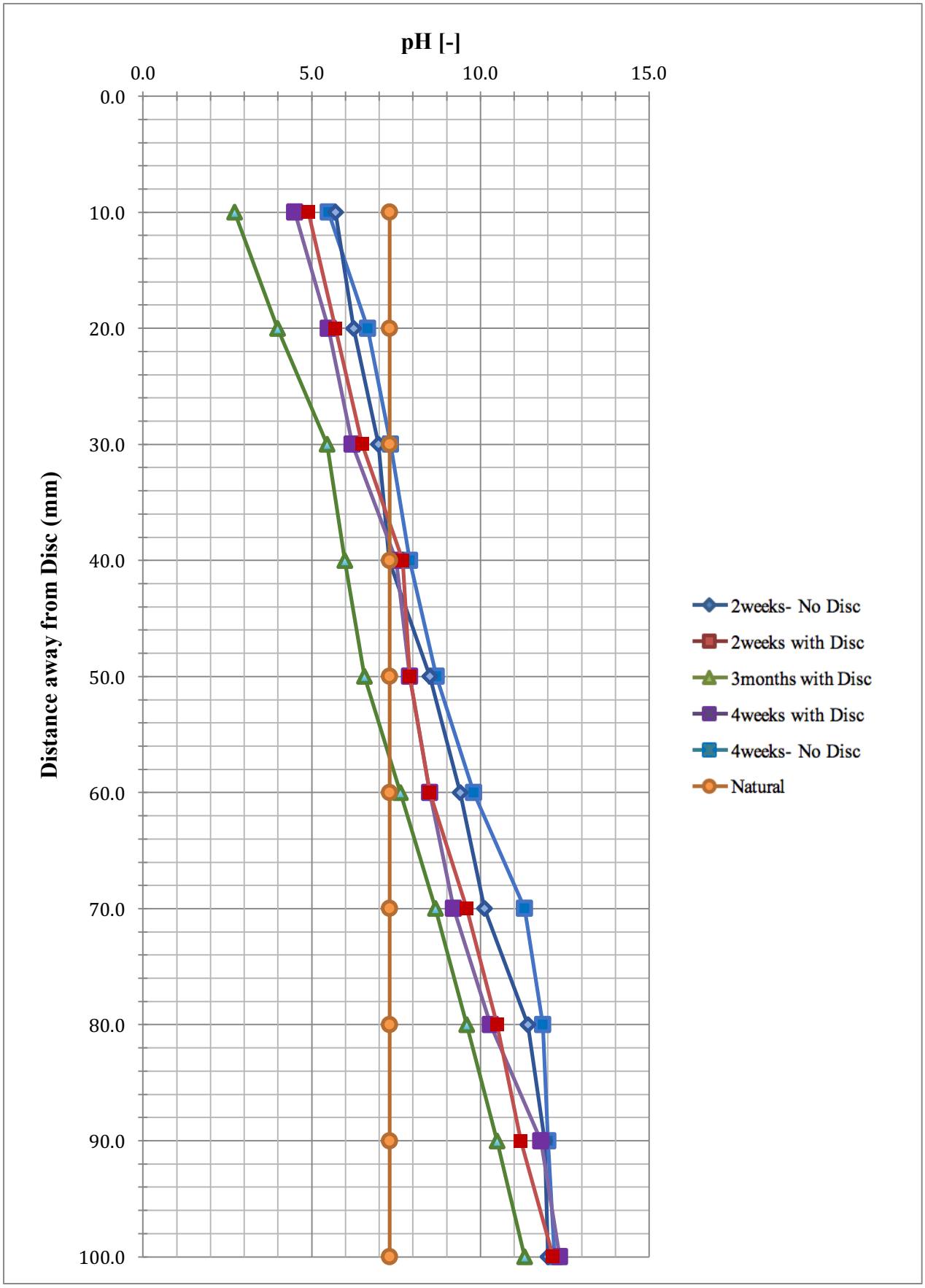

Figure 4.24 pH for Oxford Clay samples

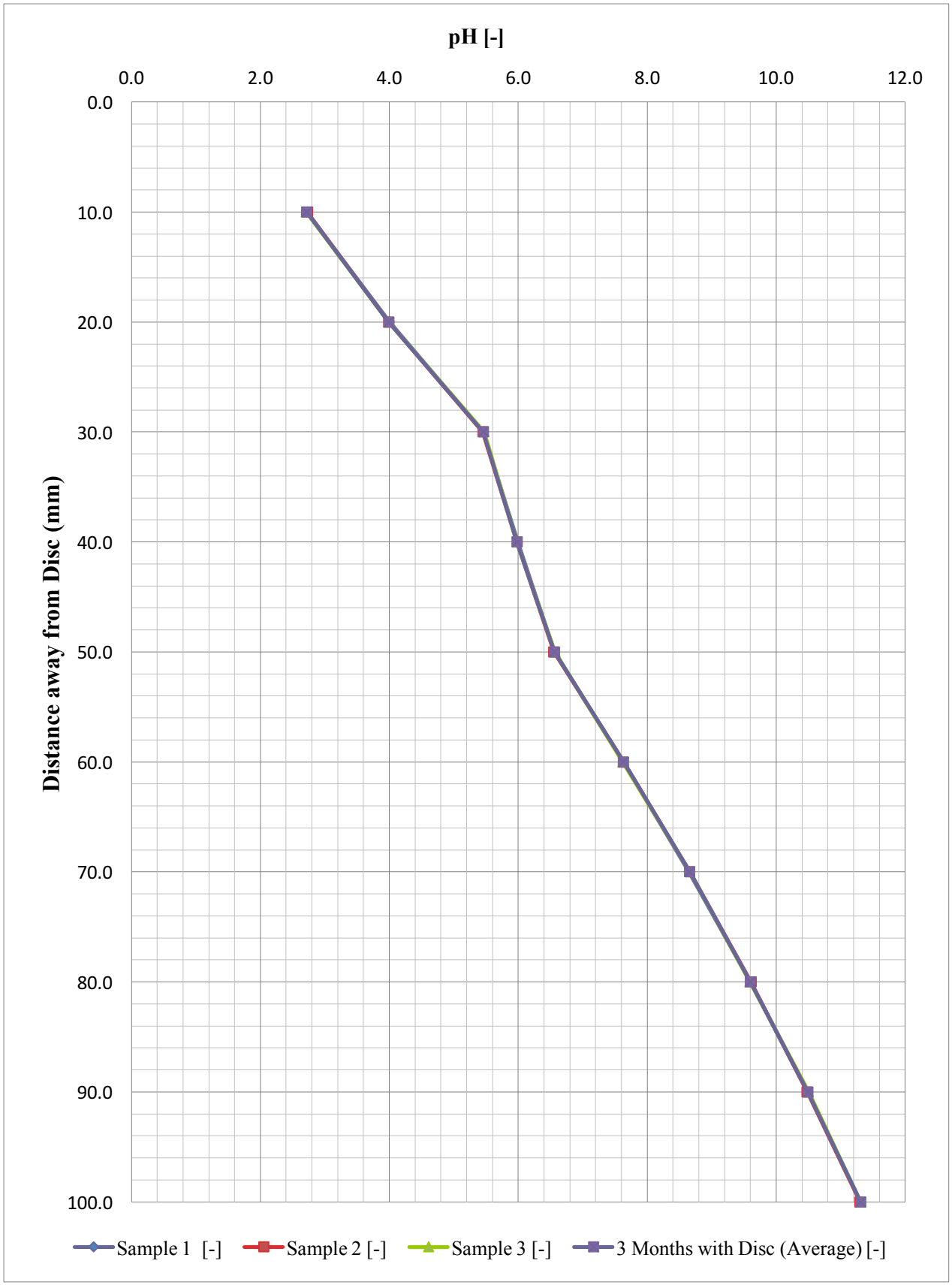

Figure 4.25 pH repeatability for 3-month sample with a cast iron disc for Oxford Clay

4.3.3 Conductivity

4.3.3.1 Conductivity Measurement Using Conductivity Meter

Conductivity was measured by two different methods. The first measurement was conducted using TDR and involved inserting a probe into the soil directly, while the other measurement was taken using a conductivity meter (HANNA-HI 9033), which was used on the same samples as the pH was measured on. The conductivity results presented in Tables A21, A22, A23 and A24 were obtained from the conductivity meter. Conductivity measurement by TDR could not be replicated because of the air gaps caused by inserting the probe into the soil, which causes an error in subsequent readings. Sampling was undertaken at 10mm intervals, and the measurements taken were assumed to be representative for that 10mm region. Therefore, it was possible to obtain one measurement every 10mm distance. The conductivity results obtained by TDR are presented in Tables A25 and A26 for Kaolin and Oxford Clay respectively.

Figure 4.26 presents the conductivity for Kaolin Clay. The conductivity in Kaolin Clay was found to increase near the anode and cathode over time due to the release of more ions from the cast iron disc and also the high solubility of ion content at anode and cathode due to the theoretical cation solubility at low and high pH. At the anode, when the cast iron disc is involved, there is an additional source of ions and the conductivity was found to be higher. In addition, H^+ ions migrated through the system and some cation exchange in the clay will have occurred. The conductivity value reduces at the centre of the samples (i.e. below the 'natural' value of 37.6 mS/m)) due to the low solubility of the ions away from the extremes of pH. As the pH increased towards the cathode, where the pH reached approximately 11.5-12.0 for the 2-week and 4-week tests, dissociation of the Kaolin (which is unstable in a high pH environment) was expected to occur releasing silica and alumina, which complexes with any

available cations in the clay soil. This appears to have occurred such that the conductivity is raised (to approximately 56-58 mS/m). However, at 3 months, the pH was raised to 13.0 and the conductivity reached 175.44 mS/m, indicating that greater solubility had occurred.

The conductivity without using a cast iron disc increased slightly from 73.21 mS/m (2 weeks) to 77.54 mS/m (4 weeks) at the anode and from 48.78 mS/m (2 weeks) to 51.58 mS/m (4 weeks) at the cathode. Once the cast iron disc was involved in the test, releasing 8.54% of iron in 2 weeks, the conductivity increased to 114.25 mS/m at the anode, and it thereafter increased to 147.23 mS/m and 189.34 mS/m for 4 weeks and 3 months respectively. At the 3-month measurement point, 9.58% iron oxide was released into the sample from the anode. The conductivity increased from 58.04 mS/m (4 weeks) to 175.44 mS/m (3 months) at the cathode, where the iron concentration increased from 2.06% (4 weeks) to 2.30% (3 months). The conductivity repeatability of the 3-month sample is illustrated in Figure 4.27.

Generally, the electrical conductivity values of the tests with cast iron are higher than those without the cast iron disc at the two ends of the samples, and these are higher in turn than the natural value. Elevated values at the anode relate to ion release into the system at this point, while elevated values at the cathode are attributed to both the migration of ions towards the cathode as well as water flow, i.e. coupled flow of electroosmosis and electromigration in that direction, combined with pH-related mineral dissolution effects. Interestingly, all samples show depressed values in the central portions of the samples away from the electrodes due to the decreased solubility of ions in this region. Considering the amphoteric (high solubility at anode and cathode, but low solubility under neutral conditions) solubility behaviour of most cations, as well as the electroosmotic migration of ions towards the anode and cathode, then this behaviour is expected.

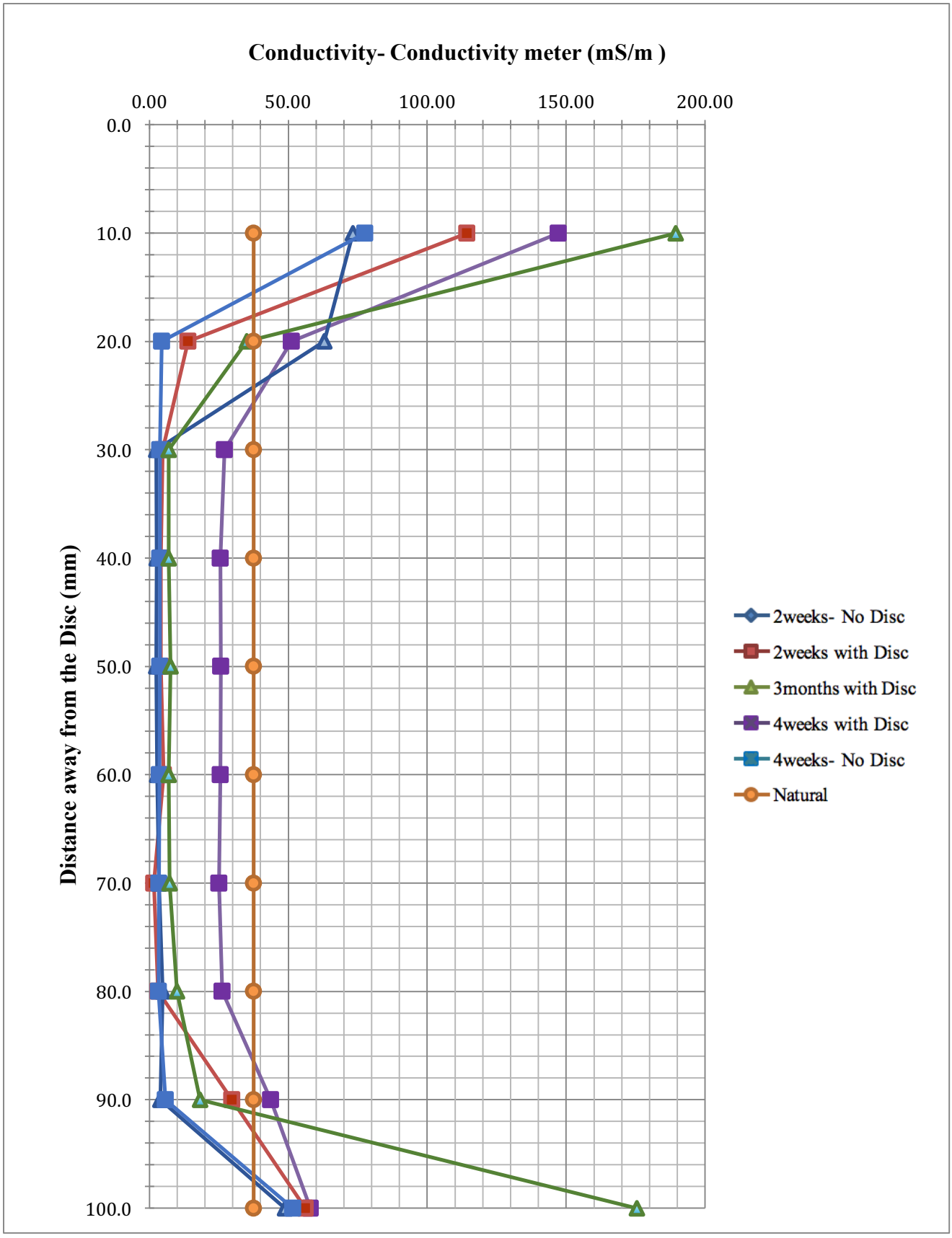

Figure 4.26 Conductivity measurements for Kaolin Clay samples using the conductivity meter

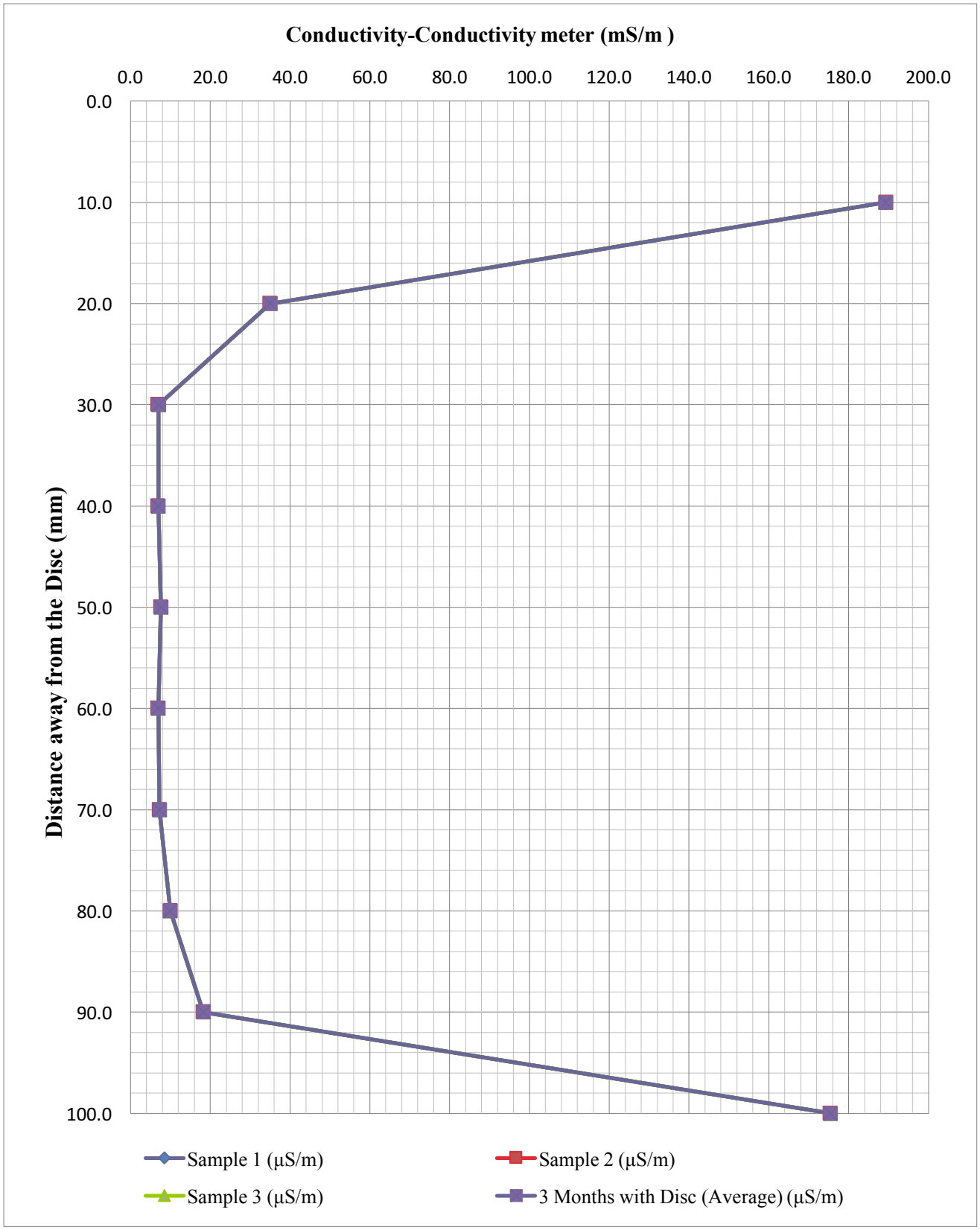

Figure 4.27 Conductivity measurements repeatability for 3 months with a cast iron disc for Kaolin Clay samples using the conductivity meter

Figure 4.28 presents the conductivity results of Oxford Clay. Table A23 shows the conductivity of Oxford Clay in tests with a cast iron disc had similarly raised values at the anode and cathode as Kaolin Clay except for the 3-month sample with a cast iron disc, which although showing a large increase at the anode did not show any significant change beyond 4 weeks at the cathode (there was a marginal reduction). Table A24 demonstrates that the 2-week and 4-week samples without a cast iron disc showed a modest increment in conductivity from 45.33 mS/m to 63.17 mS/m at the anode, while at the cathode the conductivity changed from 23.07 mS/m to 42.00 mS/m (the 'natural' value being 25.2 mS/m). When a cast iron disc was involved, the conductivity increased for the 2-week sample to 171.33 mS/m at the anode and 141.07 mS/m at the cathode; and it increased for the 4-week and 3-month samples to 253.17 mS/m and 429.00 mS/m respectively at the anode. This was while the total iron ion concentration released from corrosion of the cast iron disc reached high values (of 29.39% and 32.98%) and migrated through the sample from the anode and equated to 6.67% and 6.07% total iron ion concentration at the cathode. This reduction in iron ion concentration (from a high value at the cathode of 7.66%) corresponded with the observation that the conductivity at the cathode did not change significantly (it changed from 169.63 mS/m to 163.86 mS/m for 4-weeks and 3-months samples respectively); this was attributed to the formation of salts and precipitation in the cathode area at a raised but not exceptionally high pH (12.35 at 4 weeks and 11.31 at 3 months, see Figure 4.24).

Conductivity increased at the anode by 2.5 times from the 2-week sample to the 3-month sample with a cast iron disc, while in contrast to the Kaolin Clay results (which were depressed in the middle of the samples), only the results for the 'no disc' case showed this tendency; where a cast iron disc was present the values, although lower in the body of the samples than at the anode and cathode, were elevated significantly above the natural value. Figure 4.29 presents the repeatability of 2-week sample with the cast iron disc.

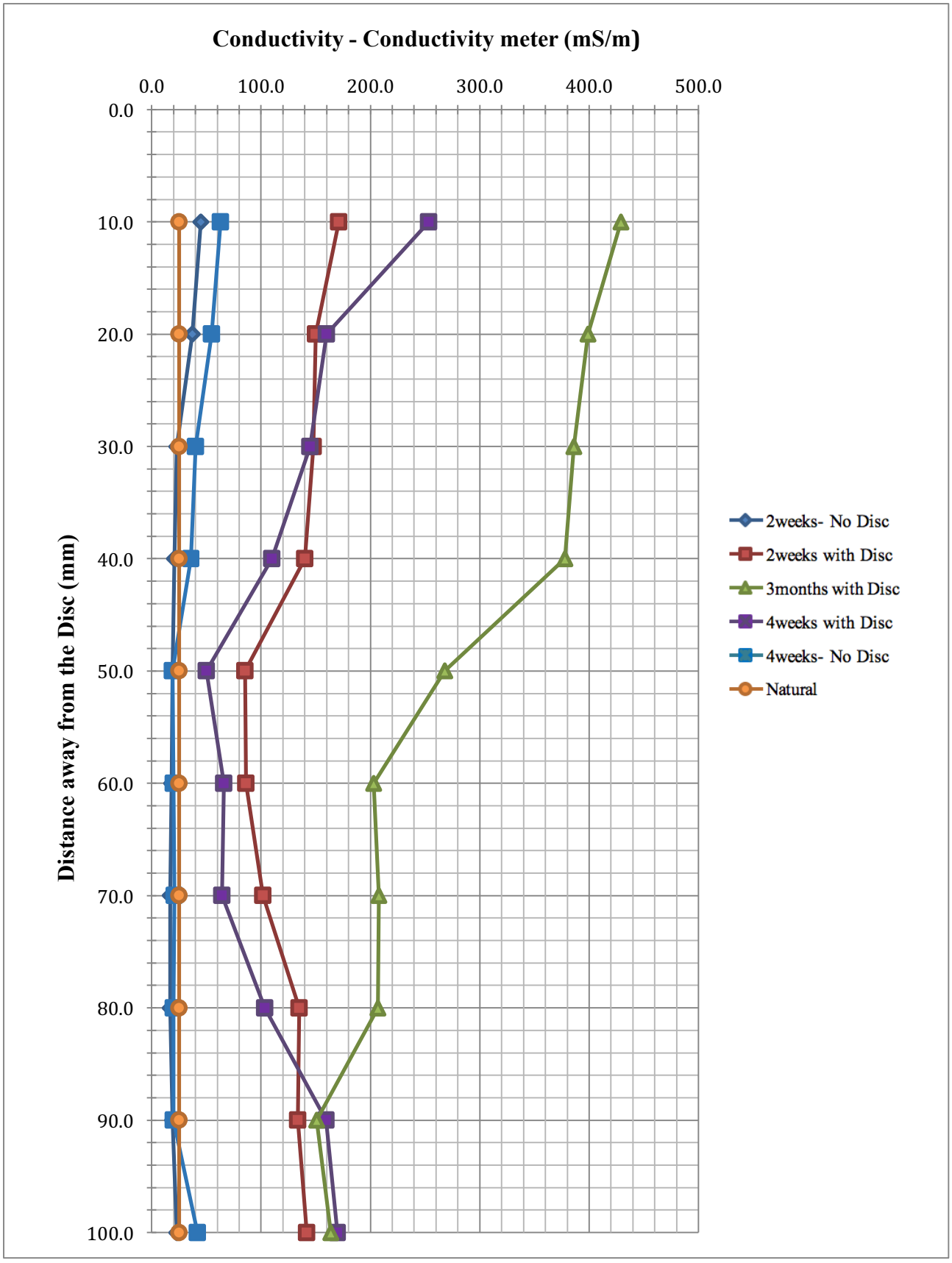

Figure 4.28 Conductivity measurements for Oxford Clay samples using the conductivity meter

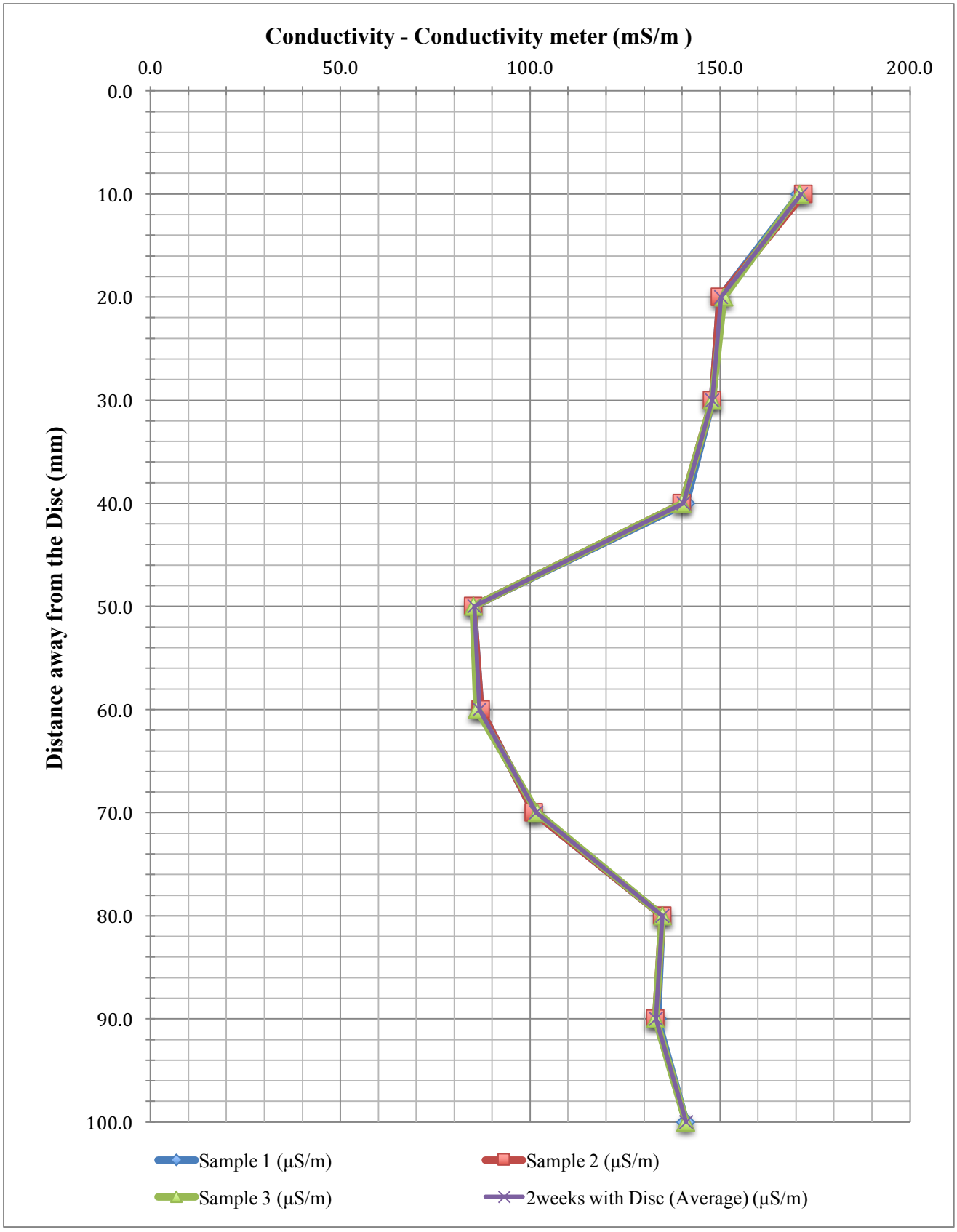

Figure 4.29 Conductivity measurements repeatability for 2 weeks with a cast iron disc for Oxford Clay samples using the conductivity meter

4.3.3.2 Conductivity Measurement Using TDR

Unfortunately, it was not possible to repeat the test (due to the probe insertion and air gaps) in order to find out the variance and repeatability of conductivity measurements taken by TDR. Therefore, there was only one chance to measure these results, as explained in Section 3.12.1. The results for Kaolin Clay are presented in Table A25 and the results for Oxford Clay are presented in Table A26. Figure 4.30 shows the conductivity of the Kaolin Clay sample increased at the anode over the time of treatment with a cast iron disc (i.e. from the 'natural' value of 37.6 mS/m, see Figure 4.26) to reach a maximum of 409.50 mS/m after 3 months, and increased greatly at the cathode between 4 weeks (69.00 mS/m) and 3 months (333.90 mS/m). For the samples without a cast iron disc, the conductivity did not show such significant changes, the values changing from 85.33 mS/m (2 weeks) to 87.27 mS/m (4 weeks) at the anode and from 61.43 mS/m (2 weeks) to 74.77 mS/m (4 weeks) at the cathode. The presence of the cast iron disc increased the conductivity at the anode to 127.40 mS/m, 154.15 mS/m and 409.50 mS/m for the 2-week, 4-week and 3-month samples, showing that the recorded concentrations were somewhat greater than those measured using the conductivity meter at 2 weeks (114.25 mS/m) and 4 weeks (147.23 mS/m), and very much greater at 3 months (189.34 mS/m). The correlation at the cathode exhibits a similar pattern, values at 2 weeks, 4 weeks and 3 months using TDR (67.00, 69.00 and 333.90 mS/m) being greater than those using the conductivity meter (56.12, 58.04 and 175.44 mS/m). In both cases, it is the 3-month values that are recorded as being far higher by the TDR method (by a factor of approximately 2). One reason that TDR might produce higher values is that TDR measures the 'bulk electrical conductivity' comprising both pore fluid conductivity and the influence of the solid particles, while the conductivity meter measures only the conductivity of the solute extraction so it is missing the solid to solid conductivity. However, the more likely explanation is that the TDR measurement occurs effectively at a discrete point (rather than taking an average of the upper

10mm of the sample, as occurred with the conductivity meter measurement), and the reaction between the corrosion products from the disc and the clay near the anode for the Kaolin Clay was particularly intense (and this effect was far more evident than for the Oxford Clay – see below).

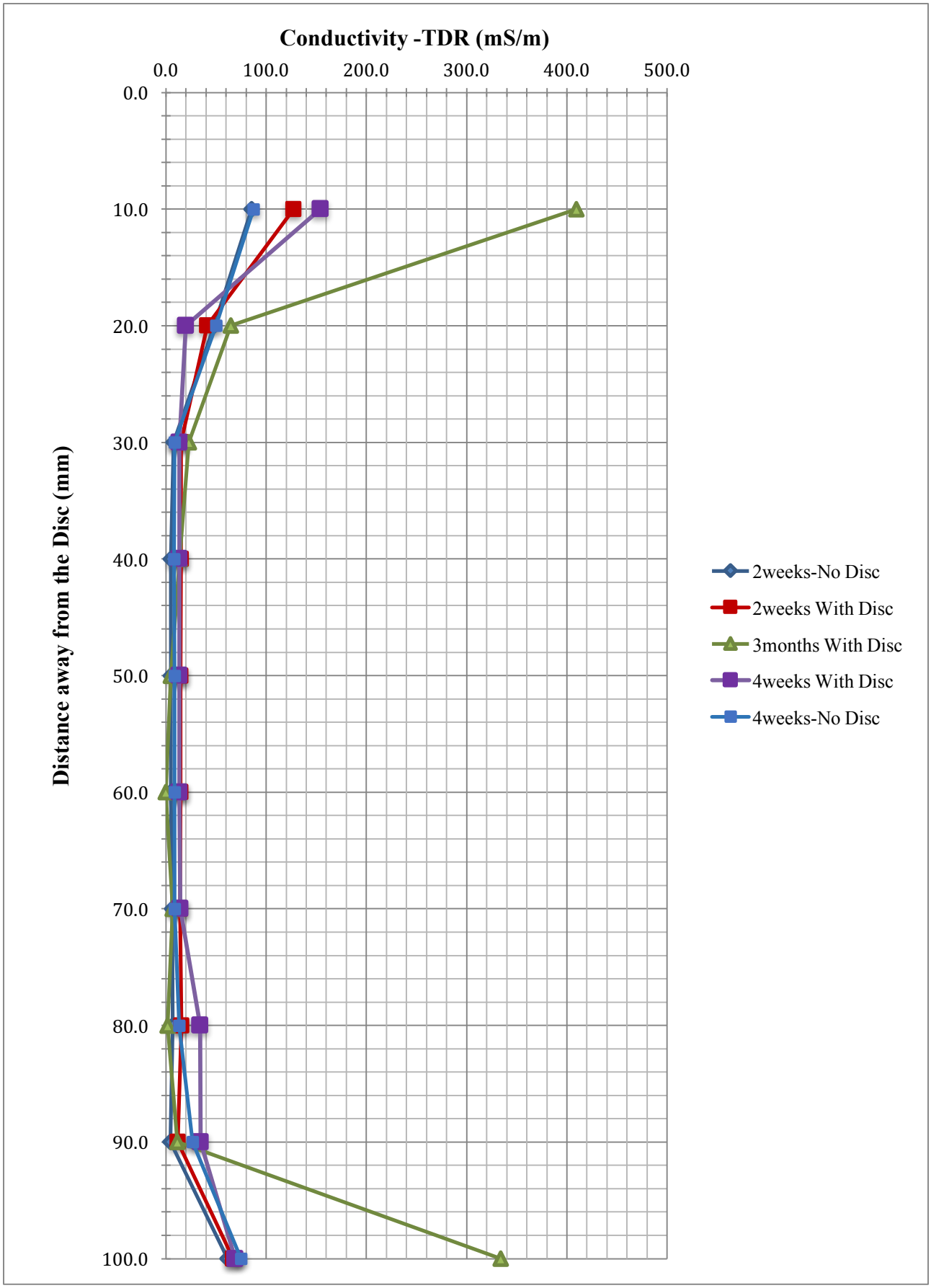

Figure 4.30 Conductivity measurements for Kaolin Clay using TDR

The conductivity of Oxford Clay measured using TDR (see Table A26 and Figure 4.31) presents a similar trend to the conductivity measured by the conductivity meter. The conductivity increased (from the 'natural' value of 25.2 mS/m, see Figure 4.28) through the electrokinetic treatment with no cast iron disc from 54.07 mS/m to 66.75 mS/m at the anode for 2 weeks and 4 weeks respectively. The sample with a cast iron disc showed that the conductivity at the anode increased to 179.99 mS/m, 276.79 mS/m and 441.96 mS/m for 2 weeks, 4 weeks and 3 months. These values correlate well with those measured using the conductivity meter (45.33 and 63.17 mS/m without a cast iron disc, and 171.33, 253.17 and 429.00 mS/m with the cast iron disc). The conductivity for 2- and 4-week samples without a cast iron disc measured using TDR were 46.06 and 58.51 mS/m at cathode, while the conductivity meter values were 23.07 and 42.00 mS/m. The conductivity at the cathode with a cast iron disc increased to 153.32 mS/m, 180.82 mS/m and 187.11 mS/m for 2 weeks, 4 weeks and 3 months, which, although higher, correlate reasonably well with those measured using the conductivity meter (141.07, 169.63 and 163.86 mS/m). One of the limitations with TDR is that due to the creation of an air gap during probe insertion, some of results could not be obtained.

In this case, the (point) measurements using TDR proved similar to those of the conductivity meter, which provided an average over the upper 10mm of the sample, and this was attributed to the lack of such an intensely local reaction observed in the Kaolin Clay.

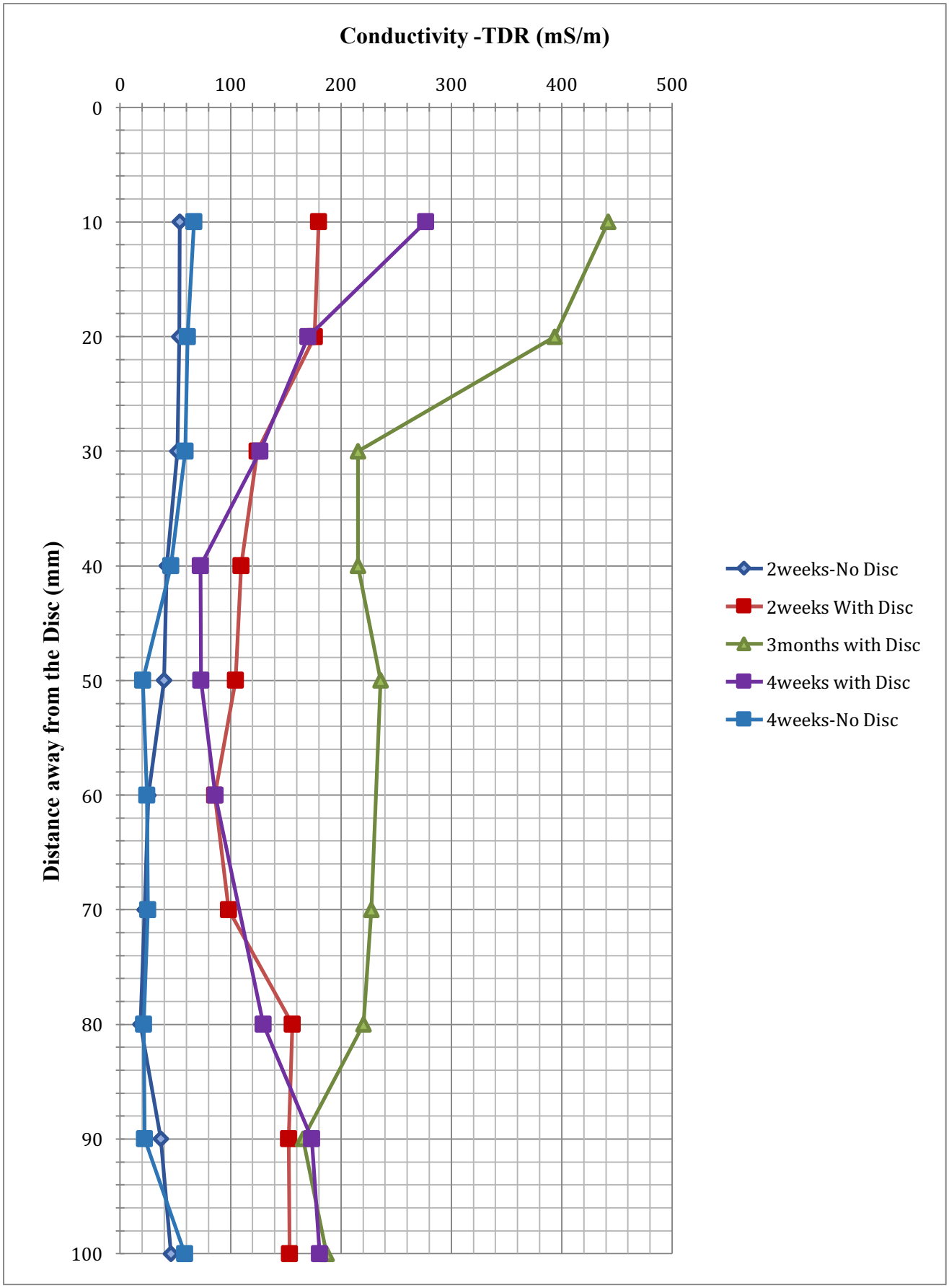

Figure 4.31 Conductivity measurements for Oxford Clay using TDR

4.3.4 Permittivity

Tables A27 and A28 and Figure A32 and A33 present the permittivity results for Kaolin Clay and Oxford Clay respectively obtained from TDR. The results in these tables are used only in GPRMax software, the values being measured at the same time as conductivity was measured by TDR. As was the case for the conductivity measurement, there was only one possibility to measure the permittivity and hence replicability could not be assessed.

The permittivity of the Kaolin Clay was found to be generally higher than Oxford Clay (see Tables A27 and A28). This is particularly evident when the cast iron disc was used in the tests. Without the cast iron disc, the permittivity for the 2-week Kaolin Clay sample is marginally greater (32.85-34.83) than the 2-week values for Oxford Clay (31.44-33.56). Interestingly this trend reverses after 4 weeks with no disc: Kaolin Clay recording 31.09-33.38 and Oxford Clay recording 33.12-34.65. When the cast iron disc was involved, a singularly high value of permittivity was recorded at the anode for the 2-week Kaolin Clay sample (53.69), while the values otherwise ranged between 27.17 and 36.50 for Kaolin Clay. The equivalent 'with disc' results for Oxford Clay showed singularly low values of 9.04 and 9.46 (both possibly due to the creation of air gaps while testing) and two readings that could not be obtained for this same reason; otherwise the values ranged from 21.57 and 34.93.

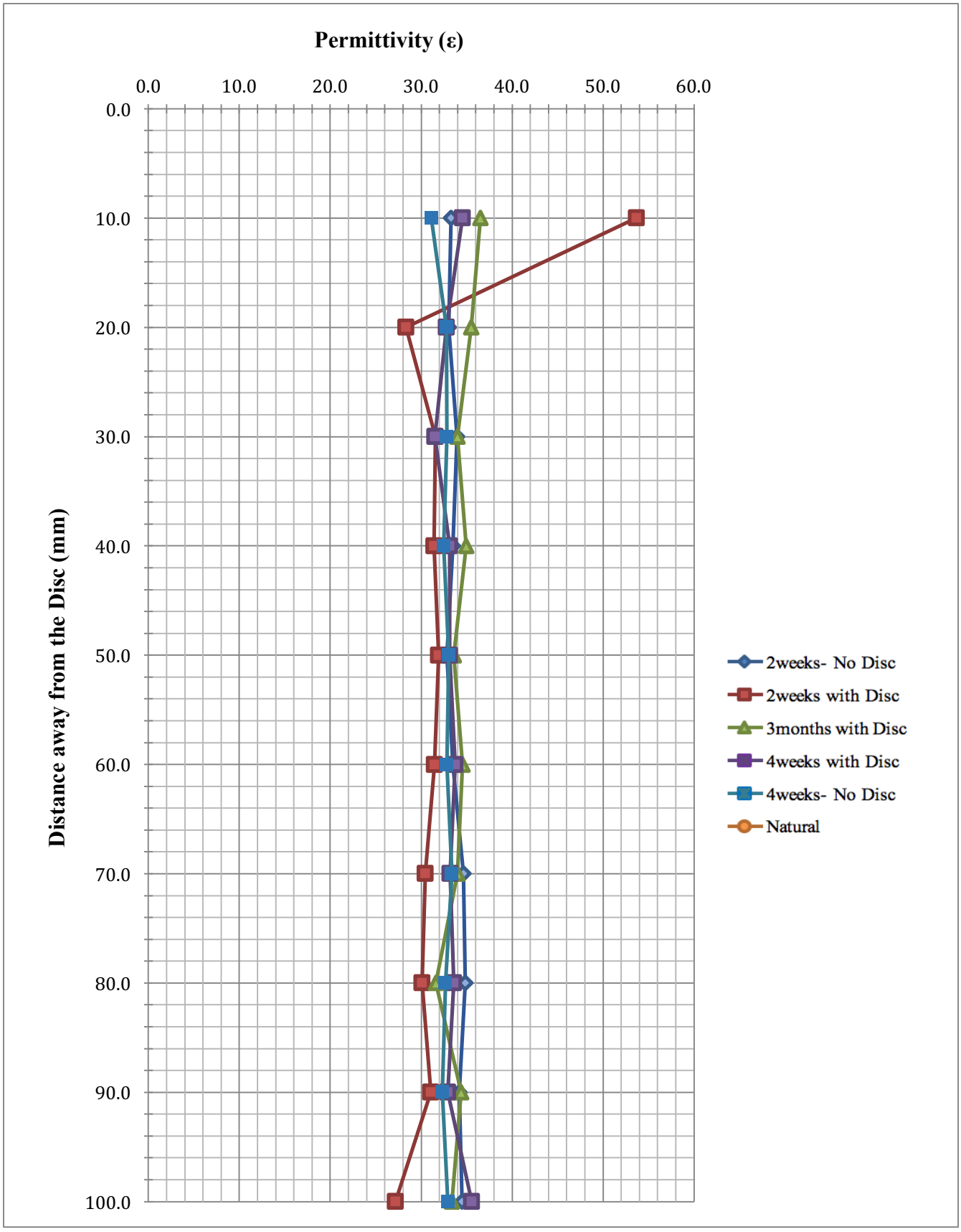

Figure 4.32 Permittivity measurements for Kaolin Clay using TDR

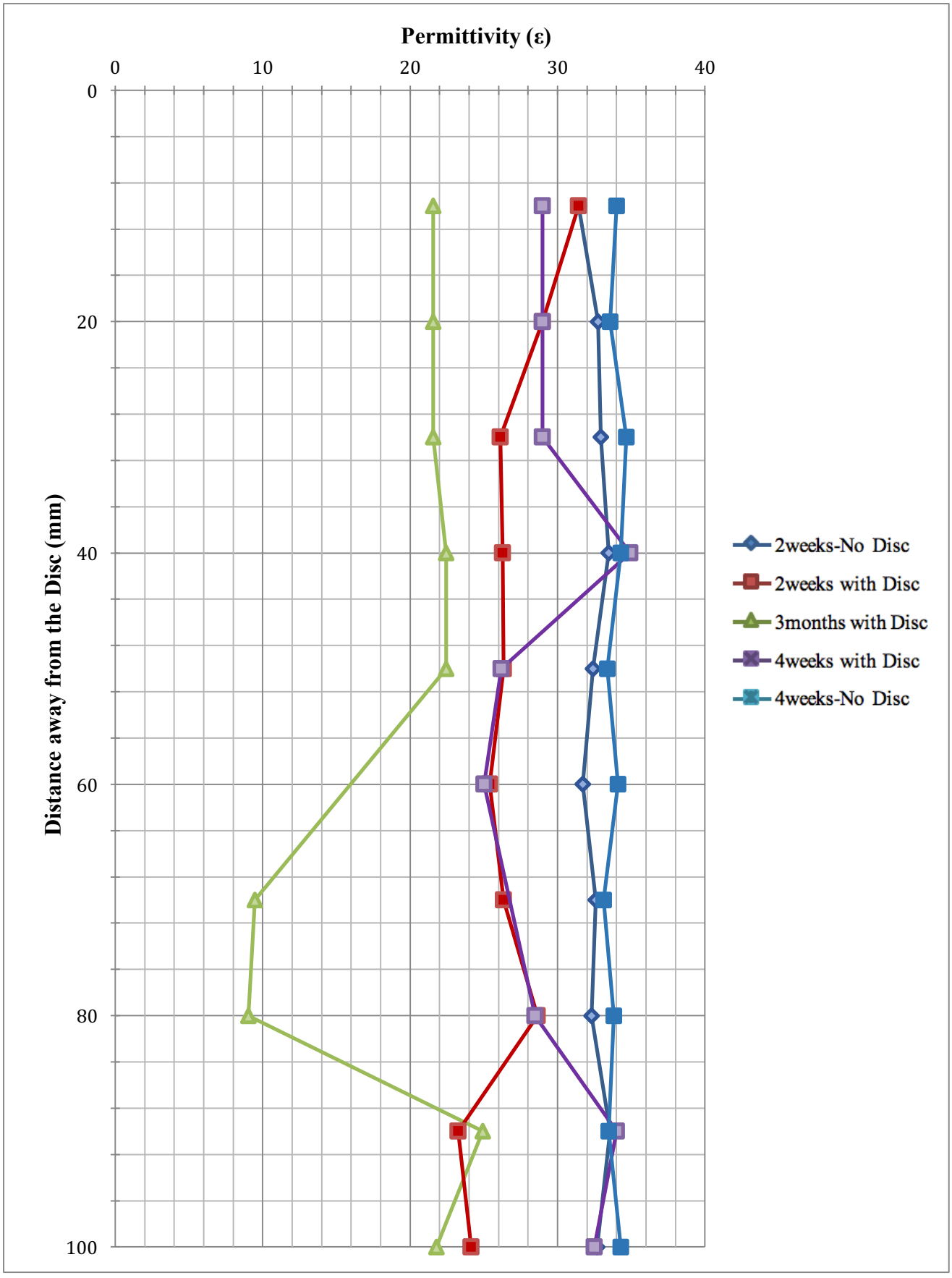

Figure 4.33 Permittivity measurements for Oxford Clay using TDR

4.4 Summary

This chapter presented the laboratory results that were measured based on the experimental methods described in methodology chapter. As electrokinetic treatment was used to speed up the corrosion process, the results were presented in two groups; the results for tests in which no cast iron disc was used, which show the effect of electrokinetics on Kaolin Clay and Oxford Clay samples alone, and the results for tests in which a cast iron disc was used in order to present the effects of iron degradation and ion migration into the clay samples.

The results showed that the electrokinetic treatment, which releases H^+ at the anode (creating an acid environment) and OH^- at cathode (creating an alkaline environment), has an effect on the pH profile throughout the clay specimens and influences the mobility and transport of cations in the clay. Kaolin Clay and Oxford Clay showed different behaviour under electrokinetic treatment, which is due to their mineralogy.

When the cast iron disc is involved, the iron ions migrate through the clay soil and substitute on cation exchange sites for lower valency ions. These ions are also involved in pH-dependent precipitation and complexation reactions. At the anode where there is corrosion of a cast iron disc, higher undrained shear strength was observed, along with greater pH decreases, and large conductivity increases (due to the far higher amount of iron ions). However, at the cathode the undrained shear strength was also high, with higher pH and conductivity increases (than the control specimens) due to the precipitation and dissolution.

The laboratory results are discussed in the next chapter.

CHAPTER FIVE

5.0 Discussion

5.1 Introduction

Cast iron pipes that are buried in clay soil can have direct contact with clay soil, which may be reactive and influence the cast iron pipe properties and durability. The chemical and physical properties of these soils can vary along the pipeline, and hence the degrees of aggressive environment could change over the length of the pipes. Corrosion of cast iron pipes may occur in the saturated zone of soil, where electrochemical oxidation of the cast iron is caused by contact with oxygenated water. Given sufficient time and oxygen, corrosion pitting occurs, releasing iron ions (termed Fe herein) into the clay and resulting in reactions with the clay minerals and/or the formation of iron oxide(s) and/or iron hydroxide(s) (termed herein iron oxyhydroxides, since the form is usually indiscernible) and aqueous salts in what is, in effect, a cathode-and-anode system (Section 2.17). The iron ions that react to form iron oxyhydroxides can be expected to be bound into the system, since iron oxyhydroxides have low solubility (albeit that the solubility is pH-dependent) and therefore localised effects might be expected. The transport of ions and solutes through the soil strongly influences the soil's conductivity. So, while the solubility and migration potential of released corrosion ions may be limited in range, the rate of corrosion increases as the electrical conductivity of the soil increases (Ekine & Emujakporue, 2010). The ions released by the corrosion of cast iron pipes contaminate the surrounding soil and elevate the iron/cation content, forming a diffuse plume around the corroding cast iron pipe. As mentioned previously (Section 2.17), the plume zone is where diffusion and migration of Fe occurs. This eventually modifies the chemical and physical properties of the soil and (depending on the pH of the soil at different points through the system, which itself is time-dependent) tends to decrease in influence away from the pipe as released ions form precipitates or complexes with the surrounding soil.

The levels of these interactions are different, and for clays will depend on the clay selectivity for interacting ions. Different clays have different selectivity for ions they can absorb or form complexes with (Yong et al., 1996), and this is usually dependent on the valency of the cation in the exchange sites for substitution (Mitchell & Soga, 2005), the cation exchange capacity and the reactive components contained. These interactions may include dissolution, precipitation, ion exchange, chemical incorporation and complexation. The process of iron pipe corrosion in soil is relatively slow, with a dynamic modification of the surrounding soil by the released ions. Using laboratory experimentation to establish realistic and reasonable rates of accelerating corrosion yields useful insights into the effect of aqueous chemistry on corrosion, notably the effects of pH, conductivity, Fe release, and iron oxyhydroxides development. Electrokinetic treatment, which accelerates the corrosion via forced ion migration and pH modification, is used to simulate conductivity modification around corroded iron pipes through the release of Fe and the interaction of these ions with the surrounding clay. This interaction changes the chemical properties of the clay, and can also modify the physical, electrical and mineralogical properties, thereby changing the clay's properties such as its Atterberg limits, strength, mineralogical composition, pH, and conductivity. For a better understanding of these interactions, a number of tests have been designed and these are explained in the methodology Chapter, see Sections 3.9, 3.10 and 3.11. To better identify and explain the geotechnical changes (undrained shear strength, moisture content and Atterberg limits) in clay soil, its geochemical properties (pH-dependent behaviour of Fe, sorption characteristic of ions, compositional analysis via XRF) and its geophysical properties (TDR) were also assessed.

The discussion chapter is structured into 5 sections:

1. Characterisation of preliminary material. It is necessary to discuss the potential for variability and error during the experimentation. These are discussed in this section. The section then discusses the implications of material properties and sample preparation.
2. Design of experiments and implications of electrokinetics. The changes in clay caused by the experimental design, and the implications of electrokinetic treatment, which increases the rate of corrosion and modifies the clay samples, are discussed in this section.
3. Clay modification. The two types of clays (Kaolin Clay and Oxford Clay) are examined after treatment over different time periods, and the modification of clay properties (geotechnical, geochemical and geophysical) are discussed in this section. In addition, the control samples (for both types of clay), where the electrokinetic treatment takes place without using a cast iron disc, are discussed and compared. Also, there is a section discussing the differences between the behaviour of these two types of clay soil over different time periods.
4. Assessment of the modification of the surrounding clay after the corrosion process. This section discusses the clay conductivity and permittivity modifications induced by corrosion, which are measured by using TDR. In addition, FDTD simulations, performed with GPRMax software to simulate the ability of GPR signals to detect buried cast iron pipes, are presented and discussed.
5. Key findings and summary. The key findings from the discussions are highlighted for both types of clay.

5.2 Characterisation of Preliminary Material

The potential for variability and error during testing and analyses are discussed in this section. The implications from the processes of preparing samples for the testing programme, extractions for analyses and assessment of composition are also discussed in this section.

5.2.1 Potential for Variability and Experimental Error

As in all scientific studies, it is necessary to evaluate the potential for error arising from the laboratory experimentation, analysis and assessment methods used. Repeatability and accuracy are particularly important for this study, due to the potential for variability imposed by the nature of the tests undertaken (e.g. chemical assessments). Kaolin Clay and Oxford Clay were used for sample preparation, and it was ensured that all material used was from a single batch (see Section 3.7), in order to minimise variability in prepared samples. Inherent heterogeneity was unavoidable, especially considering the sample preparation process. The Oxford Clay that was used for this research was from a previously-obtained batch, which was sealed in order to prevent any weathering and oxidation. The Kaolin Clay was procured from a company which supplied it sealed. Evaluations of the clay composition via XRF were undertaken on both types of raw material, and these are presented in Table 3.7. Concentrations of the evaluated components (Fe, Al, Si, Na, K, P, S, Ca, Mg and Mn) were repeatable and consistent for the replicated measurements.

Prior to making the samples, it was important to make sure that all equipment used for the tests is clean and acid washed to prevent any errors in results. This was done a couple of times. All the samples were produced in a same way in order to ensure repeatability of the results. The

water used in these tests was demineralised in order to avoid introduction of any other ions into the system.

For the chemical tests, it was important to ensure the consistency of samples used. For chemical tests such as pH and conductivity, crushed samples were required (see Section 3.10). These tests required sample extrusion and the use of representative samples (after crushing and mixing). Both pH and conductivity tests required air-dried soil, which was mixed with demineralised water after being dried. These tests were replicated (see Section 3.10.1) for each batch that generated 10 eluate fractions, which was necessary in order to evaluate consistency and repeatability of the chemical parameter measurements. Typically, pH tests generate 8-10 elute fractions, so the tests were replicated using these fractions. The results of the pH measurements show the trends were repeatable and comparable, i.e. pH development and conductivity trends were repeatable and comparable for the replicate fractions.

For the physical tests, it was equally important that the results were repeatable and comparable. It was important that physical tests (i.e. undrained shear strength, moisture content, Atterberg limits) were done on clay in its state immediately after treatment, i.e. it was not allowed to dry out. The physical tests were repeated to ensure repeatability and accuracy.

For geophysical tests such as TDR, conducted for permittivity and conductivity measurement, daily calibrations were carried out to prevent any errors (the range of data was different so it was important to calibrate), as it was not possible to repeat the tests due to the air gaps potentially occurring by inserting the probe into the sample.

As discussed earlier, this section presents the results of replicate test conducted to determine the accuracy and repeatability of this research study. Some tests, as shown in Table 5.1 and 5.2, were conducted on clay from 3 different layers (top, middle and bottom); in these tables

only the '3-month sample (with disc)' were used. Standard deviation and variance are calculated for all other samples (see Appendix A).

The cone penetration test was conducted at three different layer horizons (in each sample) and at different lateral points. This was conducted in the same manner as the main experiment was carried out (Section 3.11.1). The moisture content was recorded after the cone penetration tests had taken place for every point and depth. The moisture contents were reported for 3 readings and the mean (an average reading), the standard deviation and coefficient of variation (standard deviation divided by the mean or best estimate) were tabulated for each physical or chemical test, as shown in Tables 5.1 and 5.2. Chemical tests, such as pH, conductivity and iron (oxyhydroxides) content in the soil, are shown in Table 5.2. However, it was not possible to obtain geotechnical tests results in the same level of detail as conductivity and permittivity (obtained from TDR) due to the limitations explained in Section 3.12.1.

As demonstrated in Table 5.1, the standard deviation for the undrained shear strength lies within a small range between (0.050-0.115) for Kaolin Clay and Oxford Clay. Therefore, it can be concluded that the physical and chemical tests are repeatable, and therefore satisfactory. From the results, the effects of depth for Liquid limit and Plastic limit have not shown significant differences.

For the pH results in Table 5.2, it can be concluded that the distribution of ions due to the electrochemical effects (i.e. electrolysis, electroosmosis and electromigration processes) are uniform with depth and showed the effectiveness of the current distribution across the soil sample. The measured properties of treated soils are more uniform with depth, but have coefficients of variation of approximately 0.3%.

The undrained shear strength and Atterberg Limits values are the most variable parameters, while the water contents and geochemical results (pH, conductivity and iron content results)

are less variable. According to Baecher and Christian (2003), the variability among the laboratory measurements of effective friction angle is considerably less than that among in situ tests. First, greater care is usually taken with laboratory tests than with in situ tests, and second, the specimen quality for laboratory tests is almost always better than for in situ tests. Nevertheless, variation is expected even in well-controlled laboratory tests, and this is what is demonstrated here.

The consistency and repeatability of the obtained results, shown in the measurements, engendered confidence in the results obtained, so that they could be used for assessment of changes in properties in the main programme of tests.

Table 5.1 Results of geotechnical tests repeatability

Kaolin Clay													
	Distance away from anode (mm)	C_u (kPa)			w (%)			LL (%)			PL (%)		
		1	2	3	1	2	3	1	2	3	1	2	3
	0	74.4	74.3	74.4	45.1	45.1	45.4	69.2	69.2	69.2	26.4	26.3	26.5
	50	28.5	28.3	28.5	38.9	39.0	38.9	63.8	63.8	63.8	28.1	28.2	28.1
	100	35.2	35.1	35.1	44.9	44.9	44.9	60.7	60.3	61.0	28.4	28.4	28.4
Mean	**0**	74.3			45.2			69.17			26.36		
	50	28.4			38.93			63.77			28.14		
	100	35.13			44.9			60.66			28.41		
Standard deviation	**0**	0.0577			0.1732			0.015			0.015		
	50	0.1154			0.0577			0.019			0.019		
	100	0.0577			0			0.321			0.321		
Coefficient of variation	**0**	0.0033			0.033			0.000225			0.000225		
	50	0.0133			0.0033			0.000363			0.000366		
	100	0.0033			0			0.103225			0.103225		
Oxford Clay													
	Distance away from anode (mm)	C_u (kPa)			w (%)			LL (%)			PL (%)		
		1	2	3	1	2	3	1	2	3	1	2	3
	0	96.2	96.0	96.0	45.3	45.1	45.1	73.9	73.9	73.9	26.4	26.3	26.5
	50	77.6	77.6	77.7	35.6	35.9	35.4	69.2	69.3	69.2	28.1	28.2	28.1
	100	99.4	99.7	99.6	43.5	43.3	43.9	67.9	68.0	67.6	28.4	28.4	28.4
Mean	**0**	96.1			45.15			73.91			26.33		
	50	77.62			35.7			69.22			28.15		
	100	99.52			43.5			67.78			28.41		
Standard deviation	**0**	0.1154			0.1			0.026			0.110		
	50	0.0577			0.244			0.021			0.051		
	100	0.1527			0.282			0.177			0.011		
Coefficient of variation	**0**	0.0133			0.01			0.00072			0.012		
	50	0.0033			0.06			0.00048			0.002		
	100	0.0233			0.08			0.03152			0.0001		

Table 5.2 Results of geochemical test repeatability

Kaolin Clay										
	Distance away from anode (mm)	Iron content (%)			pH (%)			Conductivity (mS/m)		
		1	2	3	1	2	3	1	2	3
	0	9.58	9.57	9.58	3.13	3.20	3.10	189.34	189.35	189.35
	50	4.06	4.07	4.06	3.53	3.50	3.60	7.64	7.64	7.64
	100	2.30	2.30	2.30	12.94	12.94	12.94	175.44	175.44	175.44
Mean	**0**	9.57			3.1433			189.347		
	50	4.06			3.5433			7.64		
	100	2.3			12.94			175.44		
Standard deviation	**0**	0.0057			0.0513			0.0044		
	50	0.0057			0.0513			0.00		
	100	0.00			0.00			0.00		
Coefficient of variation	**0**	0.000033			0.0018			0.000025		
	50	0.000033			0.0018			0.00		
	100	0.00			0.00			0.00		
Oxford Clay										
	Distance away from anode (mm)	Iron content (%)			pH (%)			Conductivity (mS/m)		
		1	2	3	1	2	3	1	2	3
	0	32.98	32.99	32.97	2.72	2.71	2.73	429.00	430.00	429.00
	50	18.69	18.70	18.68	6.56	6.57	6.57	268.00	269.00	268.00
	100	6.07	6.07	6.07	11.31	11.31	11.31	163.86	163.86	163.86
Mean	**0**	32.98			2.7233			429.25		
	50	18.69			6.57			268.25		
	100	6.07			11.31			163.86		
Standard deviation	**0**	0.000100			0.000090			0.250000		
	50	0.000100			0.000025			0.300000		
	100	0.00			0.00			0.00		
Coefficient of variation	**0**	0.01			0.011			0.547		
	50	0.01			0.00			0.50		
	100	0.00			0.00			0.00		

5.2.2 Material Properties and Sample Preparation

The properties of the original raw materials, the sampling processes, and the constraints of sample preparation all provided an opportunity for contamination of the test specimens or extracted components. The Kaolin Clay used in testing was composed predominantly of Kaolin (74-80%), but also included montmorillonite, feldspar, mica and quartz (see Table 3.1). Compositional evaluations showed the structural dominance of silica and alumina (~85%) with a natural pH of 5.0 (see Table 3.5). The Oxford Clay used in this testing was composed of illite (~36% of the clay mineral content), smectite and kaolinite (see Table 3.2). The Oxford Clay also had a 5% organic content and a natural pH of 7.3.

The required amount of clay (see Section 3.7) was weighed and added to clean mixing bowls for mixing with demineralised water. The amount of water added was 5% more than the quantity required to achieve the test water content, calculated as being necessary in order to prevent any drying of the sample during mixing and packing making the specimens drier than the target value. The experience of previous researchers (such as Schmidt, 2007) and observations of mixing consistency were used to determine the mixing times; a suitable time of 20 minutes was selected and employed. The moisture content assessments were undertaken immediately after the completion of mixing, to ensure the desired initial moisture content had been reached. The moisture content assessments yielded a high accuracy of 99.8% (compared to the desired value), ensuring that samples where acceptably similar in terms of moisture content for each testing batch. This assurance was necessary to ensure the consistency of the corrosion process within samples.

As the slurry was poured into the experimental cell, with the help of a vibration plate any air voids created by the mixing process were expelled from the samples. This process was carried

out in a consistent way for each sample. For consolidation (see Section 3.7.1) of the samples, the required amount of load was applied consistently for samples for similar durations (as calculated to achieved the target testing conditions), in order to minimise errors and ensure consistency. This process was done with great care in order to replicate similar conditions for all samples. After consolidation and electrokinetic treatment, it was necessary to extrude the samples for further testing, such as TDR measurements (see Section 3.12.1). Non-reactive lubricant was applied on the internal wall of the cell to reduce friction during consolidation. This also helped during sample extrusion by preventing soil from sticking to the wall of the experimental cell. This was very useful and important, since the soil had to be sliced in layers without damage for use in chemical tests.

It should also be mentioned that the temperature effects which could influence evaporation from either samples or the water tank (supplying loading during consolidation) were considered, so the water level was constantly monitored in the water tank (by marking), to ensure minimal level changes, and during electrokinetic treatment the samples were always kept saturated at the top (anode) by utilising a water bath.

5.2.3 ICP Analysis

In addition to measurement of geochemical parameters required to inform discussions on clay modification by the released iron ions, limited extractions from the samples by different leaching processes were analysed using ICP-MS. The ICP analyses only provided information on ions that were particularly targeted, these being the ions that were released through the clay samples from the cast iron disc. However, the priority for the study was the precipitated ions, which influenced changes in the clay properties, in addition to the modification of chemical

parameters. As such, iron migration information was inferred from information provided by compositional analyses (XRF) of solid samples.

5.3 Justification for using Electrokinetics for the Corrosion Process

As explained in Section 2.7.1, in order to increase the rate of the corrosion process without changing the chemical conditions of clay and environmental conditions, an electrical voltage had to be applied (to a consolidated clay sample). Although some other options were available to use, the interest in these tests was on the effect of cast iron corrosion products (essentially iron ions) on clay soil and therefore introduction of other ions (from another source) had to be avoided. Also, it is difficult to relate the results to the real conditions occurring in situ if other ions are introduced. Therefore, alternative tests developed to analyse the corrosion properties of the metal were not usable to investigate the phenomenon of corrosivity in the environment of a cast iron pipe buried in clay.

In the case of buried pipelines, electrokinetic phenomena develop between different cathodic and anodic surface areas along the pipeline through the corrosion processes (graphitic corrosion). With the higher concentration of charged particles in some areas, ion movements take place inside the clay following the flow laws. As explained before (Section 2.7.1), differences in electrical potential between points on the surface of the metal (pipe) in contact with the soil may occur. In order to simulate the corrosion process, it was important to use a method which generates an electrical current (i.e. to induce migration of H^+ and OH^- towards the oppositely charged electrodes – Section 2.7.1).

Electromigration (Section 2.7) provided the basic technology for this set of tests, while the arguments for its use can be summarised as follows. Pipelines corrode normally along the pipe

surface, between areas which develop a galvanic cell. The result of the electric potential difference is the development of areas of oxidation and reduction, the moist soil acting as a conductor. These processes change the soil only very close to the surface. Use of an anode (oxidation) and a cathode (reduction) constructed from cast iron and placed on the two ends of a soil sample will enable larger amounts of affected soil to be obtained (Schmidt, 2007). The idea of this treatment was based on the inversion of cathodic protection (metal was oxidized at the anode, while the cathode was protected). Also, the electric field inside the clay helped to increase the migration of corrosion products (iron ions) into the clay. It was assumed that the corrosion products were migrated into the clay and thus the interaction zone was enlarged.

By reviewing other researchers' work, such as Schmidt (2007), who used the electrokinetic treatment in order to increase the rate of the corrosion process, there were some justifications made in support of this system. Schmidt used two cast iron discs, at the top and bottom of consolidated clay samples (Section 3.6.1), which were directly connected to the clay. The electric cables were connected via holes (for both discs – top and bottom) that were drilled in the cast iron disc. Also a water reservoir (or water bath) filled with deionized water was fitted at the top of the sample (anode side) to avoid the clay drying out by electroosmosis. It was observed that at the cathode side there was evidence of salt deposits, especially in the area in contact with the soil and around the drainage hole. It was mentioned that there were difficulties with removing the disc (at cathode side) due to the strongly cemented nature of these salt deposits. Schmidt used Oxford Clay, which has a mixture of clay minerals, for this treatment. Therefore, it was important to address this problem for this research – i.e. to prevent the precipitation of salts within the drainage pores in the disc causing clogging that prevented cathodic drainage during current injection – and it was solved using the method described in Section 3.6.3. Also the method used by Schmidt (2007) generates heat at the anode section and this tends also to make the soil dry, therefore to prevent this problem occurring the potential

difference across the system was limited while the water bath located at the anode section also served to keep the soil moist.

5.3.1 Electrokinetic Effects on the Experimental Process

The wide interest in the application of electrokinetic phenomena to site remediation started in the 1980s (Segall et al., 1980; Acar et al., 1990; Acar & Alshawabkeh, 1993). Most of the applications since then were based on laboratory data and only few papers describe in-situ applications (Lageman, 1993).

Corrosion in field is the same as the corrosion process in laboratory condition in terms of theory. As mentioned before, corrosion of cast iron is an electrochemical process, which involves oxidation (anodic) and reduction (cathodic) reactions on the metal surface (see Section 2.7.1). Throughout this process the metallic ions react with elements in the electrolyte to form other compounds such as rust (Makar et al., 2002). There are extra factors (explained below) that could affect the corrosion process in field conditions; these factors can be controlled in the laboratory and therefore the intensity of the corrosion process could vary. Generally, factors such as moisture content (e.g. acidity of rain or moisture from solution), conductivity and pH of soil, temperature, current density, depth of burial, oxygen (aeration), certain chemicals in soil (e.g. contaminants, bacteria or organic content of soil), soil corrosivity, soil porosity, and soil texture are the most important factors in corrosion process. Each of these factors has an important role in corrosion process of field condition.

Wagner & Traud (2002) advanced an electrochemical theory of corrosion, which describes iron corrosion as a coupled electrochemical reaction consisting of anodic metal oxidation and cathodic oxidant reduction. Iron materials corrode in a variety of aqueous environments. Iron

corrosion produces soluble metal ions in water at its initial stage and then the material ions develop into solid corrosion precipitates such as metal oxide and hydroxide. These cathodic reactions are electron transfer processes that occur at the metal surface, whereas anodic metal dissolution occurs as an ion transfer process across the interface. The anodic reaction of iron corrosion may occur only in the potential range more positive than its equilibrium potential and the cathodic reaction of oxidant reduction may occur only in the potential range more negative than its equilibrium potential. Also, corrosion in aqueous solution depends on acidity and basicity of solution (pH), i.e. additional to electrode potential. In the field condition, other solutes (other ions such as chloride and sulphides) may exist in aqueous solution and these may affect the corrosion-pH behaviour. The anodic dissolution of ions increases exponentially with the anodic electrode potential in acid solution. For iron in acid solution, where the hydrogen ion reduction causes the cathodic reaction of corrosion, the cathodic current increases exponentially with increasing cathode electrode potential in the more negative direction.

Corrosion, in the field, normally involves the transport of hydrated ions in the corrosion cell. Anions migrate from the cathodic reaction site to the anodic reaction site and cations migrate in the reverse direction. With the presence of a mass of corrosion rust on the iron surface, the ionic migration occurs through the rust precipitate, and the occluded solution directly in contact with metal under the rust may change its concentration of aggressive ions if the ions migrate selectivity across the rust. Iron hydroxides are anion selective in acidic solution and turn to be cation selective beyond a certain pH. In field conditions, the corrosion is often controlled by the oxygen diffusion towards the corroding metal surface, in which the corrosion potential is far more negative than the oxygen equilibrium. Also in field conditions the rate of corrosion decreases with an accumulation of the rust products, which prevent the inward diffusion of oxygen to the surface of the metal. In contrast, in laboratory conditions, using electrokinetic

conditions causes forcing of the cast iron corrosion by inserting hydrogen ions through electrolysis which are removed (i.e. transported towards the cathode) via electromigration, diffusion and electroosmostic processes, resulting in a low pH near anode area. Furthermore, in laboratory conditions (explained below), the alkali front moving towards the cast iron affects the solubility of the hydroxides and oxides, and also precipitation reactions. Therefore, it affects the pH sensitive charge on the clay, and thus the geophysical and geochemical behaviour of clay changes (explained in Section 2.7.1).

To simulate the process of cast iron corrosion under laboratory conditions, it was necessary to use an electrokinetic method to accelerate the rate of corrosion, as the process is slow in real time and would not be achievable within the timeframe of this research. Preliminary trials were used to find a suitable voltage and time (see Section 3.6.1). The electrokinetic treatment forced the migration of H^+ and OH^- ions from the anode and cathode respectively, therefore changing the pH locally. This anode-cathode reaction forced the corrosion of the cast iron disc at the anode, releasing Fe that migrated through the sample, with varying geochemical and geotechnical characteristics developing across the sample. Constant rehydration was maintained at the anode to compensate for dewatering (water moving from the anode to the cathode by electroosmosis) and thus prevent any drying out of the sample due to the treatment process.

In order to support and validate electrokinetic treatment effects on clay properties, the results from two other doctoral theses that utilised electrokinetic treatment (see Section 2.16) were taken into account. To assess the effects of migration of Fe on the clay properties, it was important to understand the effects of the electrokinetic treatment process on the clay properties. This was achieved by assessing the modification of test samples without a cast iron

disc to provide corrosion ions and using inert electrodes. This helped to produce a better understanding of the effects of the products of corrosion (iron oxyhydroxides and aqueous salts). In this research, the main effects (of concern) from the electrokinetic input were the pH, conductivity, undrained shear strength, moisture content and Atterberg limits of the tested clay.

In the anode-cathode system, a direct current is passed through a clay soil sample, which induces electromigration of cations and electroosmosis towards the cathode, and also potentially the electromigration of anions towards the anode. As mentioned previously, acidic conditions occur at the anode and alkalinic conditions are created at the cathode, which causes the dissolution of clay minerals, i.e. the minerals breaking down and releasing silica and/or alumina that react with available cations (via the same reaction at the bottom of the sample; see Figure 5.1).

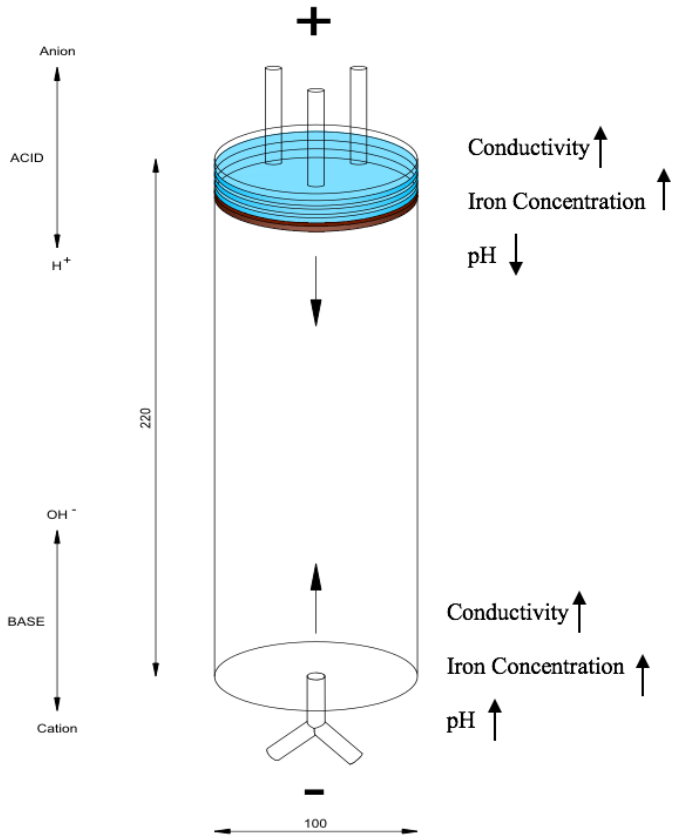

Figure 5.1 Effects of electrokinetic treatment on clay sample

One of the major factors that influences the mobility and transport of cations in soil is pH. The acid front tends to migrate towards the cathode and the alkaline front towards the anode by electromigration. The pH of treated samples for both soils showed that the acidic and alkaline conditions were generated (the pH for the samples ranged from around 3 at the anode side to 12 at the cathode; as also reported by Mitchell & Soga, 2005). It should be mentioned that since Kaolin Clay is naturally more acidic and has a much lower pH buffering capacity than Oxford Clay, more acidic initial conditions (lower pH) were observed at the anode for Kaolin Clay samples than the Oxford Clay samples at the early stages of the tests (2-4 weeks; see Section 4.3.2). This was influenced by time however, with further reductions in pH at the anode taking place during electrokinetic treatment, yielding an ultimately lower pH at the anode in the Oxford Clay after 3 months (2.72) than that observed in the Kaolin Clay (3.15).

At the top (anode) of the Oxford Clay samples, because of its mixed mineralogy and dominance of illite, high valency ions (i.e. aluminium, silicon, iron and magnesium – Al^{3+}, Si^{4+}, Fe^{2+} / Fe^{3+} and Mg^{2+}) would be expected to be released from the clay minerals in this low pH environment, along with Fe progressively being released from the cast iron disc. These released iron ions would substitute for lower-valency ions on the exchange sites of the clay, in addition to replacement of similar valency ions due to mass action, causing flocculation and an increase in both Plastic Limit and Liquid Limit (this can be seen in Figures 4.12 and 4.16). At the cathode, since OH^- is generated, the cations released from the clay and the disc, and transported through the system, combined with OH^- and other anions to form hydroxides and other salts. For Oxford Clay, high amounts of aluminium and silicon were found at the cathode (bottom of sample) along with a high amount of calcium. This can be explained in terms of the often reported (e.g. Liaki, 2006) 'lime stabilisation' reactions caused by dissolution of silica and alumina at high pH and formation of Calcium Silicate Hydrate (CSH), Calcium Aluminate Hydrate (CAH) and Hydrated Calcium Aluminosilicate (CASH) amorphous gels that

crystallise to stiffen or harden the clay. These amorphous gels were significantly visible in test samples after 3 months of electrokinetic treatment, and literally cemented the cathode electrodes to the bottom of test samples.

Conductivity was another factor that was affected by the electrokinetic process, due to the formation and movement of diffuse ions. In general, conductivity was raised greatly and progressively at the anode and decreased away from the anode (changing the pore fluid chemistry within the soil structure), with in many, but not all, cases a rise at the bottom samples (cathode) due to formation of salts and soluble precipitates. However, the patterns were distinctly different for the two clays. In the Kaolin Clay samples with no disc, the increased conductivity at the anode and cathode was attributed to the generation of H^+ and OH^- ions respectively, accompanied by lowered conductivity in the middle portion of the sample due to the relative insolubility of cations under these pH conditions. With a cast iron disc, there is the addition of Fe (iron ions) concentrations released from the disc and this progressively raised the conductivity near the anode. Near the cathode, the high pH led to a small amount of dissolution of the clay at 2- and 4-weeks and to a very considerable degree at 3-months, thus raising the conductivity. This was due to the dissolution of alumina and/or silica, i.e. from kaolin dissociation in the high pH environment around the cathode.

In the Oxford Clay samples, the conductivity increased to far higher levels. With no disc, the pattern was broadly similar to that of the Kaolin Clay with no disc, the raised conductivity at the anode being due to the concentration of H^+ ions, but added to by the dissolution and movement of ions from the clay at low pH (i.e. aluminium, silicon, iron and/or magnesium – Al^{3+}, $Si^{4+,}$ Fe^{2+} / Fe^{3+} and Mg^{2+}) as reported in the literature (Langmuir, 1997 & MacDonald, 1994). This latter effect might account for raised conductivity in the region from 20-40 mm

from the anode, although the values for conductivity for the Kaolin Clay at the anode and the cathode were higher than for the Oxford Clay when no cast iron disc was present. In the case of Kaolin Clay, which is stable at low pH (Kaolin Clay is stable under acid-weathering conditions), no significant quantity of ions from the clay minerals would be expected to be leached out at low pH. In Oxford Clay, dissolution of alumina and silica in a strong alkaline environment, which would then be followed by formation of CSH, CAH and/or CASH amorphous gels that crystallise, would be expected to add to the conductivity. However, when a disc was present in the Oxford Clay samples, the addition of Fe appears to have increased the conductivity greatly, and this effect occurs in the main body of the sample (especially at 3 months) as well as close to the anode and cathode. The chemical complexity of Oxford Clay influences the available ions, ion migration, and ultimately conductivity variably, in addition to factors such as high organic content (5%) which complexes cations.

The undrained shear strength of soil was increased at the anode and cathode ends of the samples as a result of the electrokinetic treatment. The changes in the shear strength and water content were more significant at the anode than at the cathode in general, other than for Oxford Clay after 3 months for tests with a cast iron disc (where the strength improvements were approximately similar). The increase in the undrained shear strength of both soils was due to the electrochemical hardening due to precipitation of ions and increased conductivity due to increased dissolved salts, which decreased the size of the diffuse double layer and brings particles closer together. Cementation reactions at the cathode can also influence the increase in shear strength (e.g. Liaki, 2006), alongside dewatering due to electroosmotic migration (although this general effect was prevented in these tests by the water feed to the anode). The possible causes of this cementation include clay dissociation, the products of which can complex with calcium and other cations to form cementations minerals (This was expected to happen in the case of Oxford Clay, as noted above) and precipitation of compounds such as

iron oxide and carbonates, which can cause cementing (Quigley, 1980). The results showed that the Oxford Clay had higher undrained shear strength (particularly in the main body of the samples and at the cathode, and especially after 3 months with a cast iron disc, Figure 4.4(b)) and that was attributed both to the higher amount of Fe, Ca^{2+} and other higher-valency ions which existed in it and were released at low pH near the anode, so that compound formation and cementation effects were stronger (notably near the cathode due to formation and crystallisation of CSH, CAH and/or CASH, as discussed above).

The evidence for the effects being due to chemical reactions is provided most evidently by comparing the data for Kaolin Clay at the anode in Figures 4.6 and 4.2(b): the water content is higher at the anode than in the main body of the sample (which in untreated soil would mean that the undrained shear strength would be lower) and yet the undrained shear strength is highest at the anode (74.4 kN/m^2). This same relationship can be seen in Oxford Clay by comparing Figure 4.8 and Figure 4.4(b). Also, due to precipitation and/or cementation near the cathode for the Oxford Clay tests with a cast iron disc, the undrained shear strength increased at the bottom of the sample – this can be clearly seen by comparing the data in the lower half of Figure 4.8 (Distance Away From Disc = 50-100 mm) with the results in Figure 4.4(b). Although not quite as clear, the same argument holds for Kaolin Clay when comparing Figures 4.2(a) and 4.2(b) with Figure 4.6, with the values at DAFD of 50-80 mm providing the strongest evidence.

The variation of the water content across the samples is presented in Figures 4.6 and 4.8, and Tables A5-A8. The water content generally increased towards the bottom of the samples (the cathode) as expected, since water was transported from the anode towards the cathode via electroosmosis (although it was influenced by the constant water head at the anode to prevent

drying), and this often resulted in a significant high 'spike' in water content at the cathode. Other researchers (e.g. Liaki, 2006; Tajudin, 2012; Ahmad et al. 2011) who used similar electrokinetic treatment on Kaolin Clay with a water feed at the anode also found high water contents at the anode and cathode (see Figure 5.2, reproduced from Ahmed et al., 2011). The term DW-DW in Figure 5.2 stands for distilled water feeds at the anode and cathode, which means that no extra ions were induced through the system (DW-DW is comparable to the results reported in this study where no cast iron disc was present).

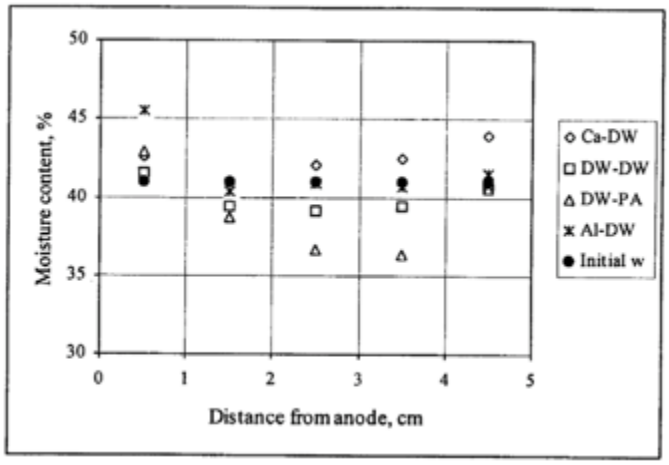

Figure 5.2 Water content at different segments of EK treated samples (Ahmad et al. 2011)

Atterberg limits were another factor that was affected through the electrokinetic treatment. The behaviour in terms of Liquid Limits was similar for Kaolin Clay and Oxford Clay. The Liquid Limit increased with time of treatment throughout the treated specimens with a cast iron disc and in each case exhibited a reducing trend towards the cathode (Figures 4.10 and 4.12), influenced by the pH (Figures 4.22 and 4.24). In all cases the Liquid limit increased at the anode, but the reducing trend towards the cathode meant that for the 2- and 4-week tests some of the values were lower than the natural (i.e. untreated) Liquid limit of the clays. For example,

the decreasing Liquid Limit in the 2- and 4-week samples for Kaolin Clay (a naturally acidic clay; Figure 4.12) under raised pH around the cathode is attributed to the clay modification, i.e. kaolin breaks down, while the increase in Liquid Limit near the anode in the presence of an acidic environment may be attributed to flocculation occurring due to the compression of the diffuse double layer, as there are more positive ions such as H^+ ions present. Additional higher-valency positive ions such as iron coming into the system from the anode and further thinning of the diffuse double layer via cation exchange of higher for lower valency ions causes the Liquid Limit to increase further. When the cast iron disc is involved, more iron ions are released through the system and iron ions would undergo lattice substitution, although in cases where lattice substitution for Al^{3+} due to mass action (i.e. concentration effects) there would be little effect on the diffuse double layer. These iron ions have low solubility and would be expected to preferentially precipitate in the more neutral conditions in the central portion of the samples.

The Plastic Limits of Kaolin Clay (Figure 4.14) and Oxford Clay (Figure 4.16) behaved differently. The Plastic Limit of Kaolin Clay initially increases (at 2 weeks) and then decreases with the time of treatment (with little change at 4 weeks, but a large reduction at 3 months). Nevertheless, when a cast iron disc is involved in the test the Plastic Limit of longest test (3-month sample) has a markedly higher value than the natural value. In contrast, the Plastic Limit for Oxford Clay generally increases with the time of the electrokinetic treatment, but only by a small amount and there is only a weak trend: an initial small rise (at 2 weeks) is followed by a further small rise (at 3 months) and significant scatter in the data with the most noticeable difference being in the region 30-50mm away from the anode (a uniformly high Plastic Limit at 3 months contrasts with values close to the natural value for the 2- and 4-week data). As Oxford Clay is a mixed clay with a natural pH of 7.3, it breaks down at low pH and releases ions such as Al, Si, Mg and Fe. The released Fe from the cvast iron disc will substitute on

cation exchange sites for lower valency ions and this will reduce the thickness of the diffuse double layer, therefore the Plastic Limit increases, yet this effect is not large as shown in Figure 4.16.

5.4 Clay Modification

The modification of Kaolin Clay and Oxford Clay was examined in geotechnical, geophysical and geochemical terms after the corrosion process. The results will now be discussed from a geotechnical point of view with supporting geophysical and geochemical results that were obtained from laboratory testing. It is important to remember that this research was designed to produce a better understanding of the effects of cast iron corrosion on clay soil (see Section 1.2), and specifically the release and migration of these corrosion products (as ions) into the clay soil using an electrokinetic treatment to observe the changes in the clays' physical and chemical properties. The electrokinetic effects have been discussed in Section 5.3. In this section the effects of iron ions (termed Fe herein) are assessed.

5.4.1 Kaolin Clay Batch – Geotechnical Evaluation

5.4.1.1 Results for Undrained Shear Strength

The three mechanisms associated with the electrochemical effects considered to cause an increase in undrained shear strength were dewatering, cation exchange and reaction product precipitation. From a design viewpoint, especially with cast iron corrosion, the key mechanisms causing an increase in undrained shear strength were cation exchange and precipitation, and these were validated using the Atterberg limits, pH, electrical conductivity and chemical compositional results.

The Fe, hence iron content, introduced into the clay samples had a significant influence on the undrained shear strength. The amount of iron in the Kaolin Clay prior to testing was 1.11% (see Table 3.7), which is relatively low (the equivalent value for Oxford Clay was 7.11%). The 2-week and 4-week samples without a cast iron disc showed only very small increases in the Fe concentrations (see Figure 4.18 and Table A14) – Kaolin Clay is stable at low pH near the anode (when a high concentration of H^+ is generated) and accordingly it was observed that the electrokinetic treatment did not significantly change the concentration of iron within the Kaolin Clay sample. In comparison, samples with a cast iron disc exhibited considerable changes over the same time period. Iron was released from the cast iron disc, with the highest amount of iron observed close to the disc (the anode) and the concentrations decreasing towards the bottom of the sample (towards the cathode). The Fe was moved through the sample as a result of electromigration such that increased levels were measured throughout the samples. The concentration of iron had the highest values, particularly in the central portion of the sample, after the longest time period (i.e. for the 3-month sample) – theoretical solubility of iron oxyhydroxides is lowest under neutral conditions, so the majority of the precipitation would occur here with time due to migration of any soluble iron ions (though see the comment on general low solubility) – thus confirming the expectation that the amount of iron introduced into the system increased as time passed. However, overlaid on this pattern is the fact that these iron ions were expected more generally to have low solubility, and hence a relatively limited migration potential due to electromigration through the sample, with a strong tendency to being precipitated close to the source at the anode. It is interesting that close to the bottom of the sample (the cathode), the concentration of iron also increased by a small amount, suggesting an effect caused by the high pH In this region. For example, these iron ions can also form complexes with other ions (e.g. disassociation of clay minerals and release of alumina and silica that complex with any available cation) where available, due to surface complexation

inherent in the properties of reactive iron oxyhydroxides, although it is expected that only limited iron ions will complex (and precipitate) in clays.

For the control samples, since no Fe was introduced into the system, the hydrogen ions caused changes in the pore chemistry in the clay-water electrolyte system and decreased the thickness of the diffuse double layer, which brought the particles closer together and resulted in a change in the soil physical and chemical parameters. This was supported by the pH values for the Kaolin Clay at the anode (Figure 4.22 and Table A18), which decreased from 5.50 to 4.01 for the 2-week sample to form an acidic environment. The pH range for both the 2- and 4-week samples without a cast iron disc was around or marginally below 4 in the vicinity of the anode and around 11.6 in the vicinity of the cathode, where the Kaolin Clay mineral breaks down and releases silica and alumina. The value of pH reduced marginally in the anode area (from 4.01 to 3.87) and increased marginally at the cathode area (from 11.47 to 11.60) with increasing electrokinetic treatment time (Table A18).

The behaviour of iron ions depends on the pH as the dissolution of clay mineral is dependent on the pH environment. When a cast iron disc was used, iron ions were released from the anode and this concentration increased over time (Figure 4.18). This had the effect of reducing further the pH at the anode (from around pH 4 to a value closer to 3, see Table A17), while the change in the pH value near the cathode was due to the strength of the alkaline environment showing an increase over time, being enhanced by the release of the iron ions into the system and precipitation of alkaline minerals at the cathode (little change over the 'no disc' cases after 2 weeks was followed by a small increase at 4 weeks and a large increase to 12.94 after 3 months; Table A17). Figure 4.22 indicates that the electrolysis process produced a large pH gradient across the soil sample due to the production of hydrogen and hydroxide ions at the anode and

cathode areas respectively for the 'no disc' cases, and that the release of more cations, through the system, contributes to creating more acidic and alkaline environments, this process being dependent on electrokinetic treatment time (as the duration of the process increased, the more acidic or alkaline the modified anodic and cathodic zones created in the sample became).

Interestingly, in the 2-week, 4-week and 3-month samples there was a secondary zone of effect of greater acidity in the middle of the sample around 50mm away from anode, this behaviour being the same for all three periods of treatment when a cast iron disc was used. This could be explained as occurring due to the meeting of the acidic and alkaline fronts, where migrating cations interact with OH^- and precipitate under neutral conditions (i.e. consuming hydroxide ions and lowering the pH, as shown in Figure 4.22). This localised pH anomaly may also be induced by a change in the clay charge (modification of the point of zero charge, which occurs at around pH 4.2) of the Kaolin Clay, but this will require further investigation to characterise effectively. Also, the sample that underwent the longest period of treatment, i.e. 3 months, had a noticeably more acidic environment in its middle and this correlated with far greater concentrations of iron being measured (see Figure 4.18) in the middle zone of the 3-month sample.

Considering the reactions that take place in Kaolin Clay when no cast iron disc was present, there are known effects on silica and alumina, both of which are present in significant proportions in the two clays tested (see Table 3.7) when the pH is changed (e.g. see Liaki, 2006). At low and high pH the Kaolin Clay has high ion solubility, whereas in the middle of the sample the solubility reduces. Brady & Walther (1989) reported that as the pH increases, so too does the concentration of the SiO^- groups, and consequently the reaction rate. Kaolin, being formed under acidic conditions, will become unstable under alkaline conditions,

dissociating through silica loss as silicic acid, with precipitation of gibbsite (Langmuir, 1997; Bauer et al., 2006). It is also reported by Huertas et al., (1998) that the dissolution rate of Kaolinite at pH 12 is one order of magnitude higher than in an acid solution. Under alkali attack, Kaolinite dissolution may thus occur to release silica and alumina. SiO^- and AlO^- would then tend to be transported towards the anode via electromigration and when it reached the acidic area (i.e. it meets the acid front) there could be changes in the physicochemical composition of the clay. However, with the precipitation of gibbsite $Al(OH)_3$ and relative insolubility of silicic acid ($H_2Si_2O_5$) formed from hydrated silica ions and water, complexation occurs locally, where any available cations exist in the pore solution. However, due to the limited availability of free cations in Kaolin Clay, there is a greater potential for migration of these ions through the test specimens as a consequence of electrokinetic treatment.

The conductivity graphs (see Figure 4.26) provide general support to these observations, showing high conductivity at the anode due to an excess of H^+ and Fe concentration (where a cast iron disc was used), and also high conductivity at the cathode with the dissolution of the clay mineral (especially at 3 months). As was discussed in Section 5.3.1, the electrokinetic treatment affected the control samples to a significant degree; yet when a cast iron disc was included in the system and Fe was released and migrated through the clay towards the cathode the effects were far greater. The soil conductivity was greatly increased at the anode, as discussed previously, but was also increased at the cathode via a time-dependent relationship (Figure 4.26) – a small increase for the 2- and 4-week samples was followed by a remarkably large increase at 3 months when the pH had reached its highest value (12.94; see Table A17) enhancing the clay mineral dissolution process and the iron concentrations were high in the main body of the sample (and showing a modest rise in the vicinity of the cathode; Figure 4.18). As referred to above, it is possible that other aqueous salts, such as those formed with

Al and Si, are present in the system at this time due to the rise from 11.93 (4 weeks) to 12.94 (3 months), thus contributing to the increase the conductivity at the anode and cathode.

The moisture content of the sample was another factor that is related to the undrained shear strength of the soil. The moisture content data showed higher values in the proximity of the anode in the Kaolin Clay attributed to the feed from the water bath. This test was designed based on an electrokinetic system in which there would be no water flows within the system caused by a hydraulic gradient and thus the difference in moisture contents at and between the electrodes could be attributed to the application of an electric field causing the movement of water and ions in the pore water between the electrodes under the electroosmosis and electromigration processes. From Figure 4.6, it can be seen that the moisture content values for the tests on Kaolin Clay with a cast iron disc were higher than for the samples without a disc at 2- and 4-weeks, and yet when the cast iron corrosion and Fe release into the system was greatest (at 3 months) the moisture content fell considerably throughout the sample. The reduction in thickness of the diffuse double layer, causing the clay particles to become more closely associated, accounts for this observation.

When considering undrained shear strength results, it is important to separate the results that show the effects of electrokinetic treatment without a cast iron disc from those that show the effects with a cast iron disc. This helps to develop a better understanding of the corrosion effect of the cast iron (i.e. iron ions) on clay behaviour. The results for undrained shear strength are generally higher when a cast iron disc is involved in the test (due to the iron release) than in a control test (without a cast iron disc), one immediate effect being that the diffuse double layer decreases and the undrained shear strength increases. However, the undrained shear strength is generally related to different factors such as iron release through the system combined with electrokinetic effects (pH and conductivity), causing cation exchange and precipitation reactions, and water content. In the vicinity of the anode, for all the durations tested, it could

be observed that the undrained shear strength was higher, even though the water content generally increased when a cast iron disc was used. This was attributed to the presence of iron, with oxides or hydroxides (expected to be usually in the form of Fe^{3+}) forming complexes, which bound metal cations very strongly. As the cast iron disc corroded and released iron ions through the Kaolin Clay, the soil near the disc had a higher strength; and, while the strength decreased away from the cast iron disc, at the bottom of the sample (cathode) the shear strength increased, attributed to Kaolin Clay disassociation and reaction of the released products with available metal cations and then re-precipitated to create a form of cementation.

Figure 5.3 presents the relationship between the undrained shear strength and water content for the treated Kaolin Clay samples with and without a cast iron disc. The data which lie above and/or to the right of the control line shows soil strengthening, i.e. due to chemical reactions, while the data below and/or lying to the left of the control relationship indicates weakening, in accordance with ideas presented by Rogers et al. (2003). Therefore, it can be proposed that the dotted arrows signify chemical improvement, while the solid arrows signify the opposite. The results presented here imply that data points that lie away from the control line, either above or below, may be attributed to chemical changes occurring due to changes in the diffuse double layer, while chemical reactions to create solid reaction products would throw the data points (far) above the control line (Rogers et al., 2003).

The circled points denote the data points adjacent to the anode, while the squared points denote data points close to the cathode. The first general observation is that all the points close to the cathode are markedly weaker than the anode points when a cast iron disc was used. Considering the graph in more detail, data for samples without a disc (2-weeks and 4-weeks) lie below the control line and show no clear trend of relative strength between the anode and cathode (at 2

weeks the strength at the cathode is marginally lower, while at 4 weeks the strengths are almost identical). This trend of a marginal reduction in strength might be caused simply as a result of electroosmosis causing a flushing of ions through the system (i.e. cation and anion movements within the soil prior to strong establishment of acid development (pH<4) at the anode) and a lack of replenishment (no ions introduced into the system from the inert electrodes and little clay mineral breakdown due to pH change, particularly at 2 weeks) since Kaolin Clay is relatively stable at low pH. A lower pH at the anode and a higher pH at the cathode at 4 weeks shows some strengthening from the low points at 2 weeks, with the data at the cathode being significantly closer to the control line.

In contrast, the measurements for the 2-weeks, 4-weeks and 3-month samples with a cast iron disc lie well above the control line and the value of undrained shear strength increases markedly with increasing time of treatment. Moreover, the movement through the graph is upward with respect to the control line. The cast iron disc (the source of iron ions) and the more extreme range of pH evidently cause the undrained shear strength to increase. In the 2-weeks and 4-weeks samples the stronger acid (pH<3) and base (pH>11.6) environments have developed and the shear strength has increased considerably. The increased iron content near the anode caused the greatest increase in undrained shear strength, for the reasons stated above while the reactions near the cathode described above account for the more modest strength increases. These chemical effects are shown to very markedly greater, i.e. the data points exist farther above the control line, for the 3-month sample.

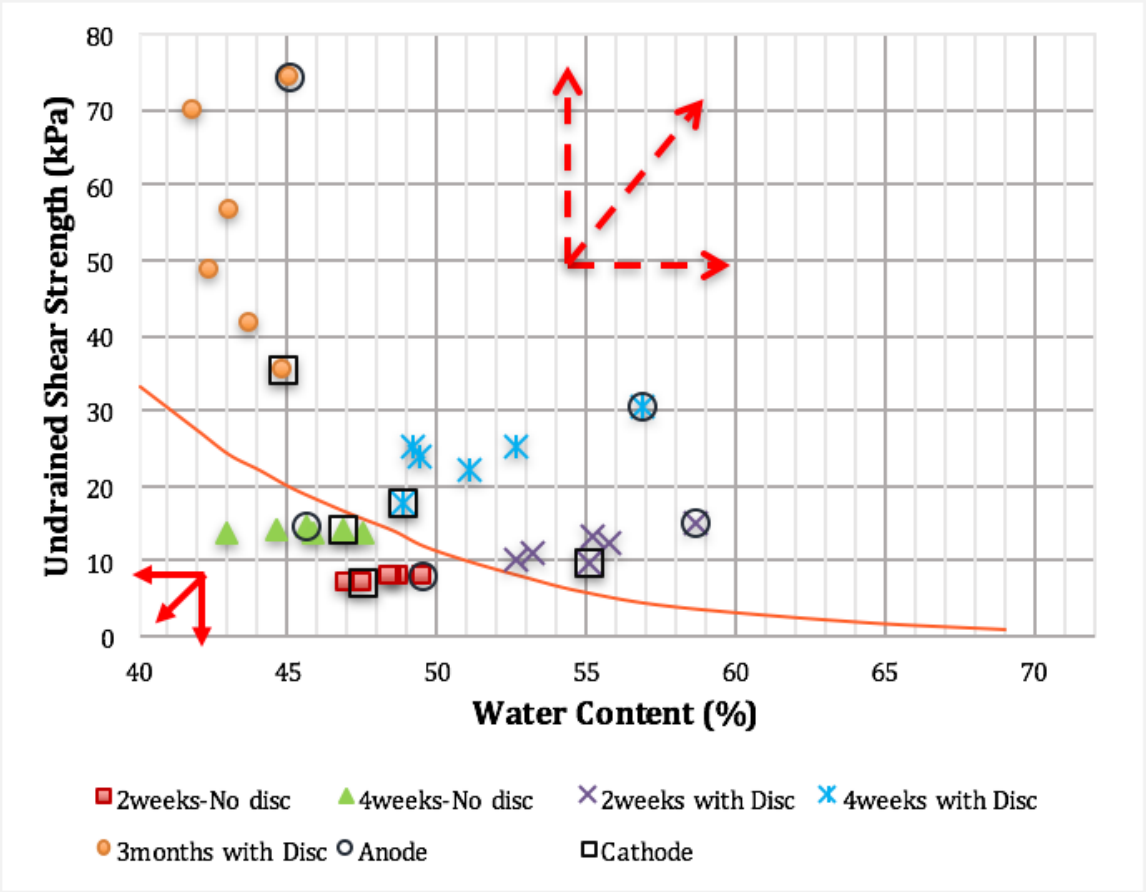

Figure 5.3 Variation of Soil undrained shear strength (kPa) with water content (%) for Kaolin Clay

5.4.1.2 Results for Atterberg Limits

The Kaolin Clay's Liquid and Plastic Limit results change due to electrokinetic treatment of the soil. It should be mentioned that consolidation alone does not affect the Atterberg limits, yet when the electrokinetic system is used the soil mineralogy and particle characteristics change.

Figure 4.10 shows the variation in Liquid Limits from the anode to the cathode when a cast iron disc was used in Kaolin Clay with different treatment times and hence degrees of

corrosion. The graph shows that the Liquid Limit decreased steadily from the highest values at the anode to the lowest value at the cathode. The values at the anode were markedly raised, whereas the Liquid Limit reduced below the natural value at the cathode for the 2- and 4-week samples. Only in the case of the 3-month sample was the Liquid Limit at the cathode increased above the natural value. This can be explained by the release of Fe from the anode into the sample in the presence of an acid environment (and hence H^+ ions also), which contributed to the effect of thinning the diffuse double layer (hence particle flocculation) via cation exchange of higher for lower valency ions (and/or mass action due to the high concentration of Fe and H^+) and raising the Liquid Limit. This effect became progressively greater as the treatment time increased. The Liquid Limit value decreased toward the cathode for Kaolin Clay soil, due to the opposite phenomenon occurring, i.e. the Liquid Limit falling as the pH rose. This indicated that the Liquid Limit decreased in a high pH environment.

Kaolin Clay is known to have a high pH sensitive surface charge (Boardman, 2004) and there is a greater cation exchange capacity in a higher pH environment. The high pH and low Liquid Limit values close to the cathode suggested that when the Fe ions moved towards the cathode, there would be $Fe(OH)_2$ precipitation, which would not dissolve (Loughnan,1969). The Fe concentration and pH both increased with treatment time and this caused an increase in Liquid Limit values close to the anode, as the graphs for the 3-month sample showed (Figures 4.10, 4.18 and 4.22).

Figure 4.14 illustrates the variation in Plastic Limit for Kaolin Clay samples with different treatment periods. The Plastic Limits evidently change due to physiochemical reactions caused by the electrokinetic stabilization process. The Kaolin Clay results were above the control value, there being a large rise in Plastic Limits above the natural value for the 2-week and 4-week tests and a smaller rise above the natural value for the 3-month sample. The 2-week sample, while exhibiting some variation between the anode and cathode, produced similar

values of Plastic Limit at the anode and cathode. The Plastic Limit increased marginally towards the cathode for the 4-weeks samples, and decreased locally around the anode at 3 months, but otherwise the raised Plastic Limits were approximately uniform throughout the treated samples. The lowering of the baseline from a high increase at 2- and 4-weeks to a more modest increase at 3 months might reflect a tendency for free ions to become bound into more stable cementitious products, thus reflecting also the raised undrained shear strengths at 3 months shown in Figure 4.2(b).

5.4.2 Oxford Clay Batch – Geotechnical Evaluation

5.4.2.1 Results for Undrained Shear Strength

The Oxford Clay behaved differently, due to its different mineralogy and organic content, as was explained in literature review (Chapter 2). This caused the corrosion products such as iron oxide and iron hydroxide to react differently (via ion exchange and/or complexation) from the way they did in the Kaolin Clay. The interaction process for the Kaolin Clay was explained in the previous section (see Section 5.4.1) and where appropriate the discussion for the Oxford Clay samples will refer to this. Oxford Clay is a very active soil, and it should be mentioned that it naturally has a high amount of iron (~7%; see tables 3.6 and 3.7) and, due to the 5% organic content, there is significant additional complexation, sorption and cation exchange taking place. As mentioned before (see Section 2.8.1.2), illites are defined as mica-like materials less than 2μm size and are structurally similar to muscovite, although they contain less K^+ and Al^{3+} and more Si^{4+} than muscovite, and they contain both Mg^{2+} and Fe.

There was no significant change in iron concentration in samples without a cast iron disc, but when a cast iron disc was used the amount of iron changed considerably (Figure 4.20). The amount of iron was highest in the 3-month sample (the longest test) and, as explained before, the iron released from the cast iron migrated towards the cathode causing the concentrations to be raised in the main body of the sample. The amount of iron was very high near the anode and the soil was relatively hard at 3 months (confirmed by the undrained shear strength results in Figure 4.4(b)), due to cementation and complexation. Because of dissolution of clay minerals near the cathode in a high pH environment and release of silica and/or alumina, which can produce CSH, CAH and/or CASH amorphous gels that crystallise (there being a sufficiently high CaO concentration for Ca^{2+} to be released in acidic conditions near the anode in this clay; see Tables 3.6 and 3.7), the Oxford Clay was very hard in this region as well due to the crystallisation and cementation reactions. This is also confirmed by Figure 4.4(b), but differs from the undrained shear strength profile for Kaolin Clay in the lower portion of the 3-month sample (Figure 4.2(b)) indicating that these cementitious reactions did not occur (probably due to the lack of Ca^{2+} in Kaolin Clay; see Tables 3.5 and 3.7).

Near the anode, the lowered pH caused ions to be released from the clay minerals (e.g. Ca^{2}+ and Al^{3+}) and, along with Fe released from the decomposing anode, these cations replaced metal ions of lower valency from the exchange sites on the clay. Moreover, the acid generated at the anode would be expected to dissolve precipitated salts in the clay. As the acid front progressively moves across the soil with time, this can be expected to keep the metal in solution until it is either precipitated at a neutral / higher pH close to the cathode or it is removed at the cathode (Mitchell & Soga, 2005). The pH values for Oxford Clay (Figure 4.24) showed the same trends as those for Kaolin Clay (Figure 4.22), ranging broadly between 3 and 12; however, the availability of more ions (i.e. as Oxford Clay is mixed-mineralogy clay, but also for the reasons stated immediately above) and the fact that it is less stable at lower pH than

Kaolinite (i.e. it breaks down at low pH and exhibits more ion solubility, whereas Kaolinite is more stable at low pH) served to enhance the effects caused by the lowered acidity at the anode and raised alkalinity at the cathode respectively. More specifically, as the clay minerals break down at low pH, silica acid was thought to be released, which is unstable and will complex readily following migration, while this picture is complicated further by the chemical complexity of Oxford Clay, which influences both the available ions and ion migration.

Near the cathode and the anode, the undrained shear strength was markedly higher than in the middle of the sample (for both tests – with disc and without disc, see Figures 4.4(a) and (b)). This was due to the electrochemical reactions described above, while the strength increase in the middle portion of the samples with a cast iron disc at 4 weeks (Figure 4.4(a)) and at 3 months (Figure 4.4(b)) was attributed to migration of Fe and other cations and precipitation of cementitious salts where the pH environment was closer to natural (Figure 4.24). The XRF data strengthen these arguments: for example, the high iron concentration (reaching 22.39% and 32.98%, Figure 4.20 and Table A15) near the anode at 4 weeks and 3 months, and raised alumina content near the cathode (measured at 9.75% by XRF) at 3 months.

As mentioned before, the undrained shear strength of a clay is also strongly influenced by its moisture content, which changed significantly in the Oxford Clay sample during the tests. The moisture contents of the Oxford Clay for the 2-weeks and 4-weeks samples (see Figure 4.8) was approximately the same, with raised values at the anode and the cathode respectively. The higher moisture content at the anode was due to the water bath (without which the moisture content would have been expected to fall), while at cathode it could be explained by the movement of (i.e. dragging force on) the cations causing water to be transported across the system due to electroosmosis. At 3-months, the moisture content, although still higher at the anode and cathode than in the central section of the sample, was markedly lower than the control value.

The samples were slightly stronger at the surface near the anode. The corrosion products such as iron oxide which have low solubility formed a thin, but stiff layer before they penetrated the clay. The material was also evidently stronger than the original clay after consolidation. At the other end, next to the cathode, the clay changed to a very stiff material with a crystalline structure, attributed to the dissolution of silica and alumina which caused the formation of CSH, CAH and/or CASH amorphous gels that crystallised and caused cementation to take place (this was observed at the end of tests, see later discussion), and this resulted in a very large strength increase. In the 3-month sample this crystalline structure near the cathode penetrated into the body of the clay sample.

Referring to the explanation given in Section 5.4.1.1 (Figure 5.3), the same procedure was carried out for the Oxford Clay samples and the result is plotted in Figure 5.4, i.e. to relate the variation of undrained shear strength to its water content for samples with and without a cast iron disc. The data without a cast iron disc for 2-weeks and 4-weeks lie below the control line, with the exception of data corresponding to measurements close to the anode that are on the control line. These results suggest that the short time period of these tests combined with the flushing of water through the system via electroosmosis using inert electrodes (i.e. no additional ions being introduced into the system) caused a reduction in the undrained shear strength of the treated soil, possibly due to thickening of the diffuse double layer as higher valency ions are caused to flow as a result of electrochemical effects, e.g. the H^+ ions released at the anode, by virtue of their high concentration, may replace exchangeable cations of higher valency on the clay. The data close to anode, with higher water contents, lie close to the control line, suggesting that this effect is countered at low pH values. The undrained shear strength measurements at 2-weeks and 4-weeks at the cathode show elevated undrained shear strengths relative to the majority of the sample, possibly suggesting that the dissolution of Oxford Clay minerals and release of Ca^{2+}, Mg^{2+}, Al^{3+}, Si^{4+} and Fe^{2+}, Fe^{3+} at low pH (though the data remain

above a pH of 5 in both cases), when migrated to the (high pH) cathode area, form complexes with the silica and alumina to create cementation reactions. However, the fact that this effect does not raise the data point above the control line in Figure 5.4 suggests that it is a weak, relative effect only – thus demonstrating the value of the graph.

The data points across the soil sample with a cast iron disc at 2-weeks lie mostly below the control line, with only the two points at and adjacent to the anode exhibiting an undrained shear strength above the control line. This replicates the effects shown with no disc and possibly suggests that the pH has not lowered sufficiently at the anode (the lowest value was 4.87) to bring about major changes. In contrast, the data points for 4-weeks sample all lie above the control line, which suggested that soil has strengthened throughout due to the chemical improvement induced by release of Fe from the cast iron disc and/or dissolution of ions from the clay at this time increment (the minimum pH reached in this test was 4.47). The strengthening of the soil throughout its length is attributed to the released Fe and/or other cations migrating through the soil and substituting for lower valency ions on the clay's cation exchange sites or replacing ions of similar valency due to 'mass action' (i.e. high concentration). The data for the 3-months sample with a cast iron disc lie well above the control line, which indicates that the undrained shear strength of the soil is due to more than the chemical changes occurring as a result of changes in diffuse double layer, i.e. that there is considerable strengthening due to reaction products forming by precipitation and/or cementitious gel formation and crystallisation. Interestingly, the strengths of the clay approaching the anode and the cathode are both markedly above those of the central portion of the sample, yet the water contents are highest at the two electrodes.

The undrained shear strength of Oxford Clay is higher than Kaolin Clay (comparing Figures 5.3 and 5.4), and this is attributed to the high quantity of Fe, Ca^{2}+ and other higher valency ions which exist naturally in the clay and are released at low pH near the anode. However, the

most striking difference concerns the uniformly-high strength profile for the 3-month test and the allied observation that the strength at the cathode at 3 months is higher than that at the anode. Figure 5.4 also makes clear the effect of the relatively large reduction in water content (i.e. the results lie well above the control line).

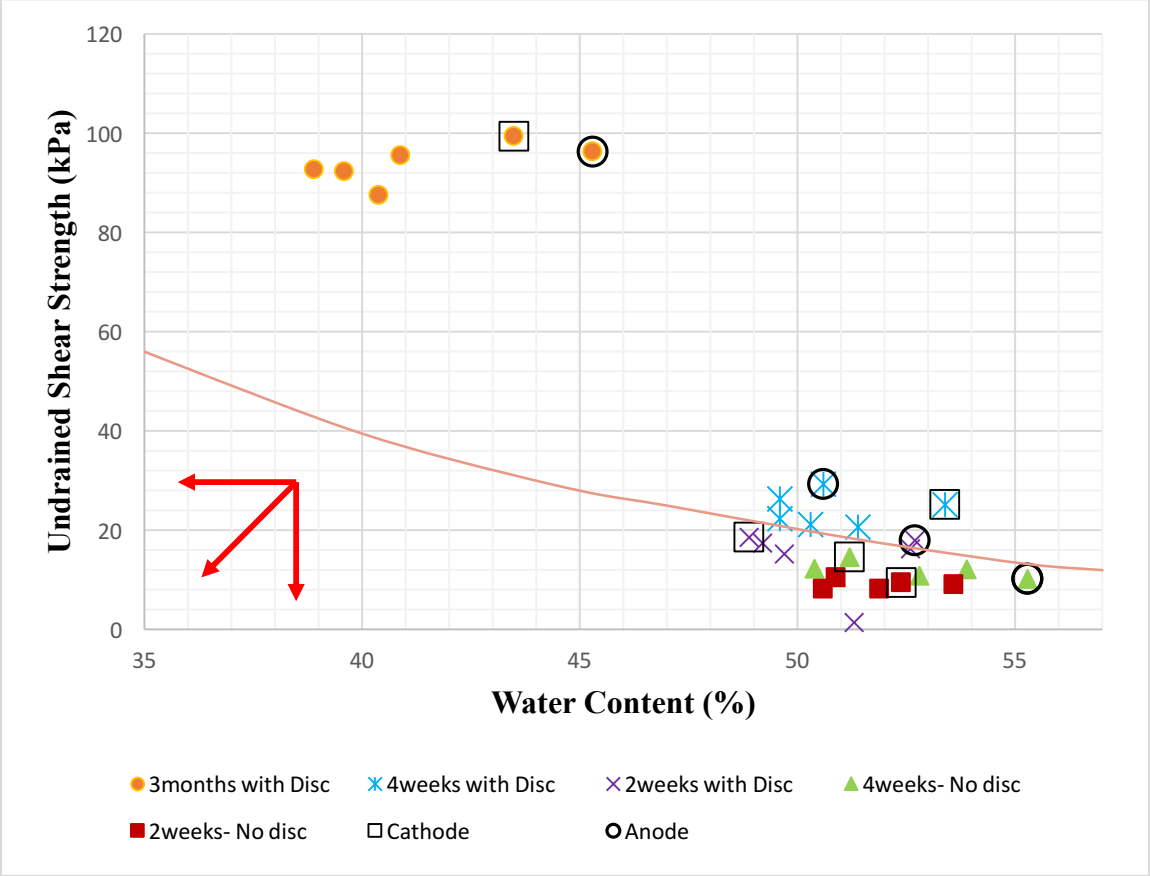

Figure 5.4 Variation of Undrained Shear Strength (kPa) with Water Content (%) for Oxford Clay

5.4.2.2 Results for Atterberg Limits

In order to verify the two mechanisms contributing to the increase in undrained shear strength, it is important to look at the results for the Atterberg limits. Changes in the Atterberg limits are related to the electrochemical process causing chemical stabilization through alterations made to the structure and fabric of the clay, modification to the clay mineralogy, and the type of exchangeable ions. According to Barker et al. (2004), the result of cation exchange is a considerable reduction in the thickness of the diffuse double layer. This allows closer contact between the clay platelets, which promotes edge-to-edge attraction, or flocculation, and results in changes in the soil workability, permeability, plasticity and swell properties. On the other hand, the precipitation of metal hydroxide can also be assessed by changes in the plasticity of the soil. This again is the result of changes in the thickness of the diffuse double layer coupled with crystallization over time to form a relatively strong and brittle fabric in the clay soil. Even though these two mechanisms have opposite effects in terms of the thickness of the diffuse double layer, interestingly both mechanisms result in an increase in shear strength. Thus testing the Atterberg limits is a useful diagnostic test to assess these mechanisms, which occur across the soil. This is especially useful when coupled with other tests dealing with water content, shear strength and other chemical features in order to confirm these phenomena.

Figure 4.12 presents the changes to the Liquid Limits for Oxford Clay in tests using a cast iron disc. The Liquid Limit measurements had a raised value at the anode and they decreased towards the cathode, due to the Fe released from the cast iron disc and ions released from the clay mineral at low pH near the anode causing thinning of the diffuse double layer via cation exchange of higher for lower valency ions. As additional ions came through the system as the treatment time increased, the Liquid Limit value increased. The Oxford Clay showed the same general behaviour regarding the Liquid Limit changes as the Kaolin Clay samples (Figure

4.10), although the data for the Kaolin Clay in the upper half of the samples are raised above the natural value at 2-weeks and the change between 4 weeks and 3 months is not as large.

Figure 4.16 illustrates the variations in Plastic Limit for different durations of treatment with a cast iron disc and shows a similar trend to that demonstrated by the Liquid Limits for Oxford Clay, i.e. values that are higher at the anode than at the cathode and values that increase progressively with time of treatment, although in almost all cases the Plastic Limits are raised above the natural value, the changes are relatively small and the patterns far less distinct. This pattern differs from that of the Kaolin Clay, which showed an approximately uniform pattern of Plastic Limit across the full sample, large rises above the natural for all three treatment durations and markedly lower values (though still raised) at 3-months than at 2-weeks and 4-weeks (Figure 4.14).

The trend showing the Plastic Limits for Oxford Clay increasing when the treatment time was longer mirrors the effect of the release of Fe and other cations being more extreme, i.e. the Fe concentration rises considerably to 3 months in the Oxford Clay samples (Figure 4.20) as does the conductivity (Figure 4.28). In general, therefore, the Plastic Limit distribution depends on several factors including the type of clay minerals and naturally-occurring salts, the pH gradient (Figure 4.24) and the release of certain ions (i.e. Al, Fe, Mg and Si) from the clay lattice and dissolved salts, and the introduction of Fe into the soil sample through corrosion of the cast iron disc. Bohn et al. (2001) support this argument, stating that a low pH of about pH<4.7 had caused multivalent cations of Al, Fe and Mg to be released from the degradation of clay minerals into pore fluid. (NB this value of pH is significant in relation to the discussion at the end of Section 5.4.2.1, where a pH of 4.47 showed a difference in behaviour than when the minimum pH was 4.87.) These multivalent cations, if substituted for cations of a lower valency in the clay mineral exchange sites, would cause thinning of the diffuse double layer. This argument therefore supports the theory that a combination of Fe released into the system and

release of multivalent cations from Oxford Clay mineral dissolution caused the effects shown in Figure 4.16.

5.4.3 Comparison between Kaolin Clay and Oxford Clay Samples

Kaolin Clay and Oxford Clay have different mineralogies, therefore their physical and chemical properties change differently when the Fe ions, and hence iron oxyhydroxides, are induced through the system. These changes could be expected to be correlated with the amount of iron concentration.

The most important factor in comparing these results is therefore the amount of iron released from the corrosion of the cast iron disc and transported through the clay system. Fe ions, which are multivalent cations (Fe^{2+} or Fe^{3+}), migrate in the soil samples due to the induced electric field from the anode to the cathode, either in the pore fluid or as complexes on the soil surface, and exist in varying concentrations both spatially (i.e. distance from the anode) and temporally (at 2-weeks, 4-weeks and 3-months). Hydrolysis reactions occur also at the anode and cathode, releasing H^+ and OH^- ions into the system (see Section 2.7.1). There is the potential for iron hydroxide ions ($FeOH^-$ or $Fe(OH^-)_2$) to form, and these would tend to migrate from the cathode to the anode. There is also the potential for iron oxide (FeO or Fe_2O_3), which have very low solubility, to complex. The migration of anions and cations leads to accumulation of ferrous ions close to, and progressively away from, the anode and iron hydroxide close to cathode.

The 3-month samples of Kaolin Clay and Oxford Clay (see Figures 5.5 and 5.6 respectively) show that the soil colour has been changed due to the iron migration through the system. This is due to iron oxyhydroxides precipitation and complexation. The zone of iron migration through the sample is noticeable. Furthermore, Figure 5.7 shows cementation at the cathode

(high pH) side of the 3-month sample of Oxford Clay, which is due to the dissolution of silica and alumina and the presence of released Calcium (confirmed by XRF), formation of Calcium Silicate Hydrate (CSH) and/or Calcium Aluminate Hydrate (CAH), and maybe also CASH, amorphous gels and their crystallisation.

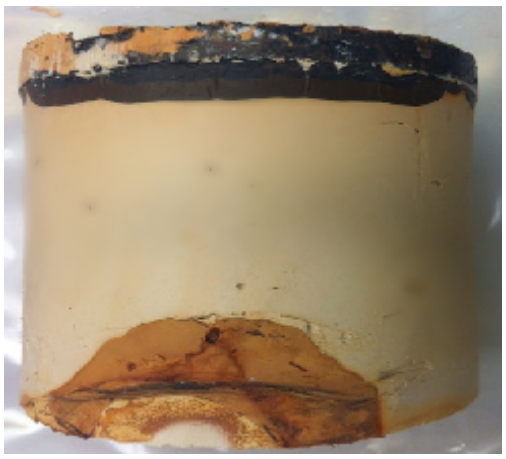

Figure 5.5 Kaolin Clay sample (3-months) **Figure 5.6 Oxford Clay sample (3-months)**

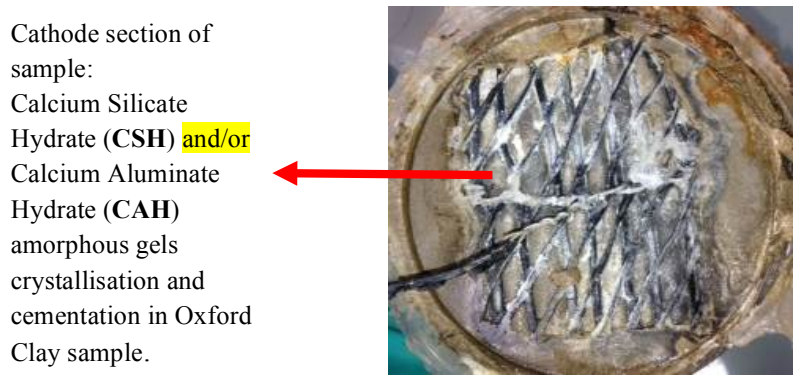

Figure 5.7 Cathode section of Oxford Clay 3-months sample

There is a high content of iron in Oxford Clay compared to Kaolin Clay (Tables 3.5 to 3.7), due to the mineralogy of the Oxford Clay soil, which is a relatively very active soil. The longest test (3-month sample) produced the largest values for the migration of Fe and formation (hence

concentration) of iron oxyhydroxides in the soil. Also, due to the precipitation of iron hydroxide close to cathode side and extending into the body of the sample of Kaolin Clay (see Figure 5.5), the amount of iron was increased for both types of soils, yet in different patterns (comparing Figures 4.18 and 4.20). These reactions were affected by the soil's pH, as the dissolution of clay minerals is dependent on the pH environment. A large pH gradient across the soil sample changed the chemistry of pore fluid, which led to alteration of the soil structure and, in some cases, alteration of the soil's mineralogy, especially close to the anode and cathode. The pH of both soils was changed such that it ranged from approximately 3 to 12 by electrokinetic treatment (see Figure 5.8). Both soils had the same behaviour in relation to the test without a cast iron disc. However, when a cast iron disc was involved in the test there was a 'jump' in the pH trend for Kaolin Clay samples at 2-weeks, 4-weeks and 3-months (e.g., this 'jump' occurred midway along the sample (50-60mm away from the anode) from a baseline of approximately 3.5-4.5 at 3-months in Figure 5.8); this trend was attributed to the meeting of acid and alkaline fronts where migrated H^+ and other cations from the anode interact with OH^- ions migrating away from the cathode. The 3-month sample of Oxford Clay was more acidic at the anode, due both to the high Fe release from the cast iron disc and also due to the increased potency of the hydrolysis reactions releasing H^+ ions with time of treatment (see Figure 5.8). The pH curve for the Oxford Clay sample, in contrast to the Kaolin Clay, showed a clear uniformly-rising trend with increasing distance from the disc. At 50mm away from the cast iron disc, the pH of Kaolin Clay drops to 3.53 (becomes more acidic) at an iron concentration of 4.06% (which increased from 1.80% to 4.06% between 4 weeks and 3 months; Table A13 and Figure 4.18), while at 70mm away from the disc the amount of Fe concentration increase to 4.59% which is associated with a significant incremental change in pH to 8.67. Developing highly acid and alkaline environments at the anode and cathode, respectively, equated with a significant increase in undrained shear strength (see Figure 5.8) and was accompanied by the

ions being available (ions' solubility) in the soil system. This corresponds to the idea that the corrosion was due to an electrochemical process, which converted metal substrates to oxides, hydroxides and aqueous salts within the cathode-anode system (Pritchard et al., 2013).

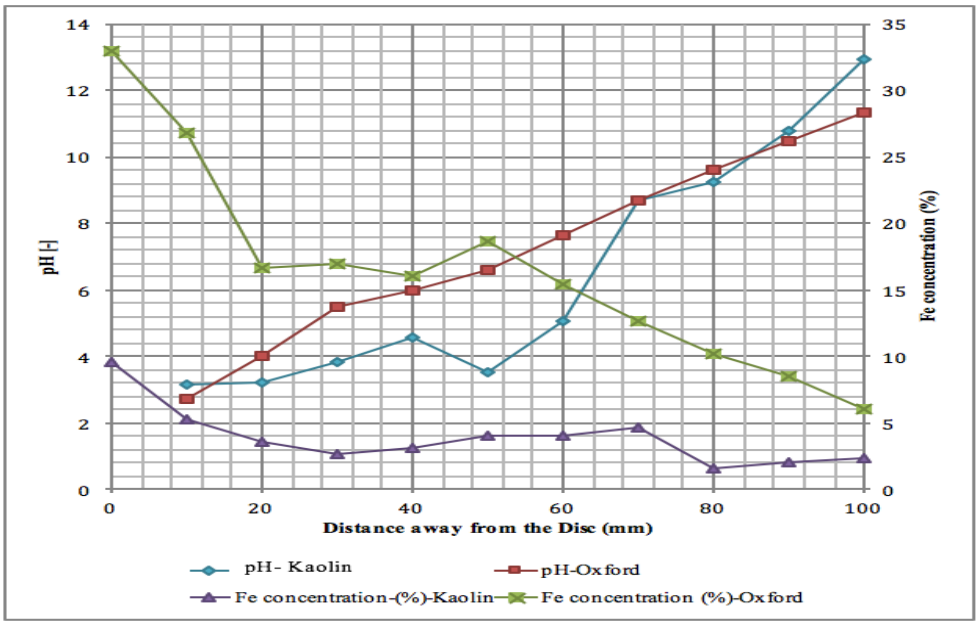

Figure 5.8 pH and iron concentration results of Kaolin Clay and Oxford Clay for 3-month samples

Also, the rate of corrosion increased with increases in the electrical conductivity of soil (as reported by Ekine & Emujakporue, 2010). Figure 5.9 presents the results for conductivity measurements of Kaolin Clay and Oxford Clay for the 3-month sample with a cast iron disc. The first major difference between these two types of clay is that the Oxford Clay has very high conductivity due to its more mixed mineralogy (hence soluble ion content). Both graphs show a similar trend: high conductivity at the anode, which was attributed to high H^+ and Fe concentrations, and also due to the solubility of ions at low pH in the case of Oxford Clay. Figure 5.9 also shows high conductivity at the cathode for the Kaolin Clay, which was

attributed to ion solubility at high pH in a clay that is relatively stable at low pH. The conductivity of Oxford Clay follows a similar trend to the iron concentration of Oxford Clay. It is therefore evident that the amount of iron released through the clay soil has direct relationship with soil conductivity. This trend is also evident in Figure 5.9 for the Kaolin Clay sample with the exception of the measurements at the cathode, where the Fe concentration remains relatively low (hence the attribution of the raised conductivity to clay mineral dissolution, stated above). However, the conductivity for Oxford Clay did not follow the same trend as that for Kaolin Clay, which can be attributed to three reasons: extent of Fe migration, precipitation of ions complexing with cations (a factor related to inherent solubility), and cementation and crystallisation at the cathode (see Figure 5.7).

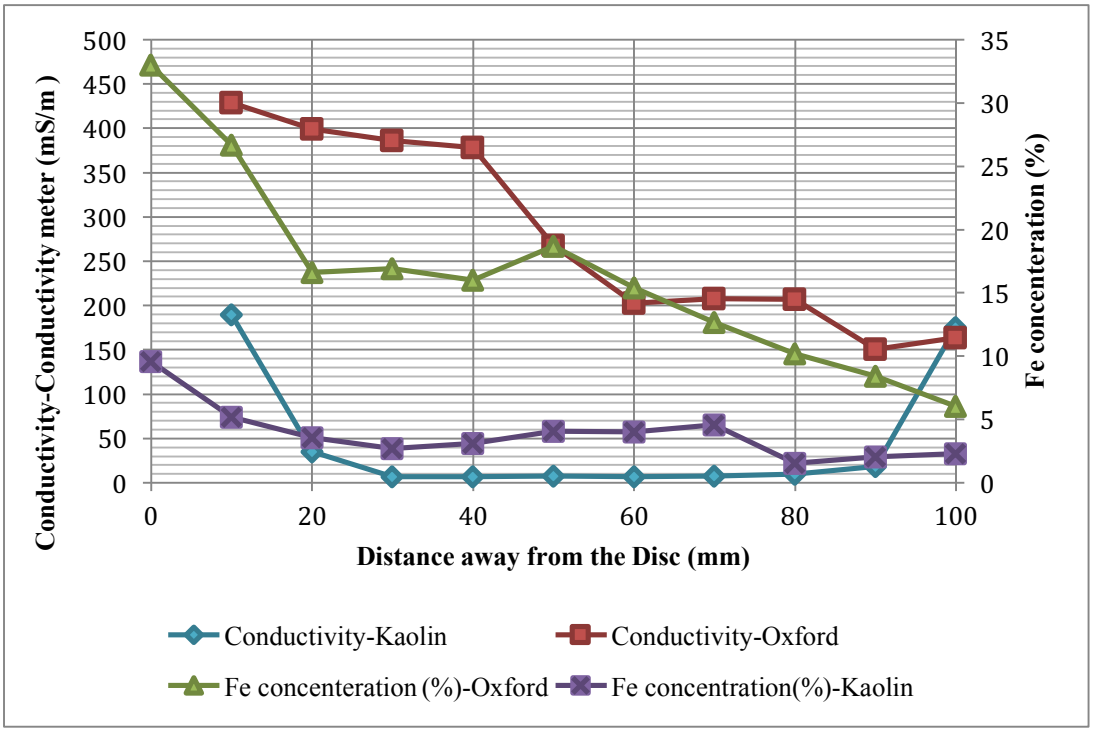

Figure 5.9 Conductivity and iron concentration results of Kaolin Clay and Oxford Clay for 3-months samples

The undrained shear strength of clay (see Figure 5.10) depends on factors such as cation exchange, salt precipitation and clay mineral dissolution and cementitious product formation and crystallisation, which cause changes in structure and mineralogy. The undrained shear strength of Oxford Clay was higher than that for Kaolin Clay, due to both higher concentrations of Fe (causing a greater, though similar, pattern of thinning of the diffuse double layer and salt precipitation than in the Kaolin Clay), but also higher availability of other cations to engage in these processes but also, importantly and evidently from Figure 5.10, a marked rise in undrained shear strength in the lower half of the sample, this being attributed to the CAH, CSH and/or CASH gel formation and crystallisation reactions describe earlier (calcium being available in Oxford Clay but not Kaolin Clay).

Generally, the results for the Oxford Clay compared with the Kaolin Clay showed that the Oxford Clay had been more affected by cast iron corrosion, and in turn causes enhanced Fe release (hence corrosion), and therefore failure of cast iron pipes would therefore be expected to be more likely in Oxford Clay than in Kaolin Clay, in spite of the fact that the Kaolin Clay was more acidic. The higher conductivity of the Oxford Clay relative to Kaolin Clay supports this argument, and would suggest that the clay also had higher corrosivity as a result of these features.

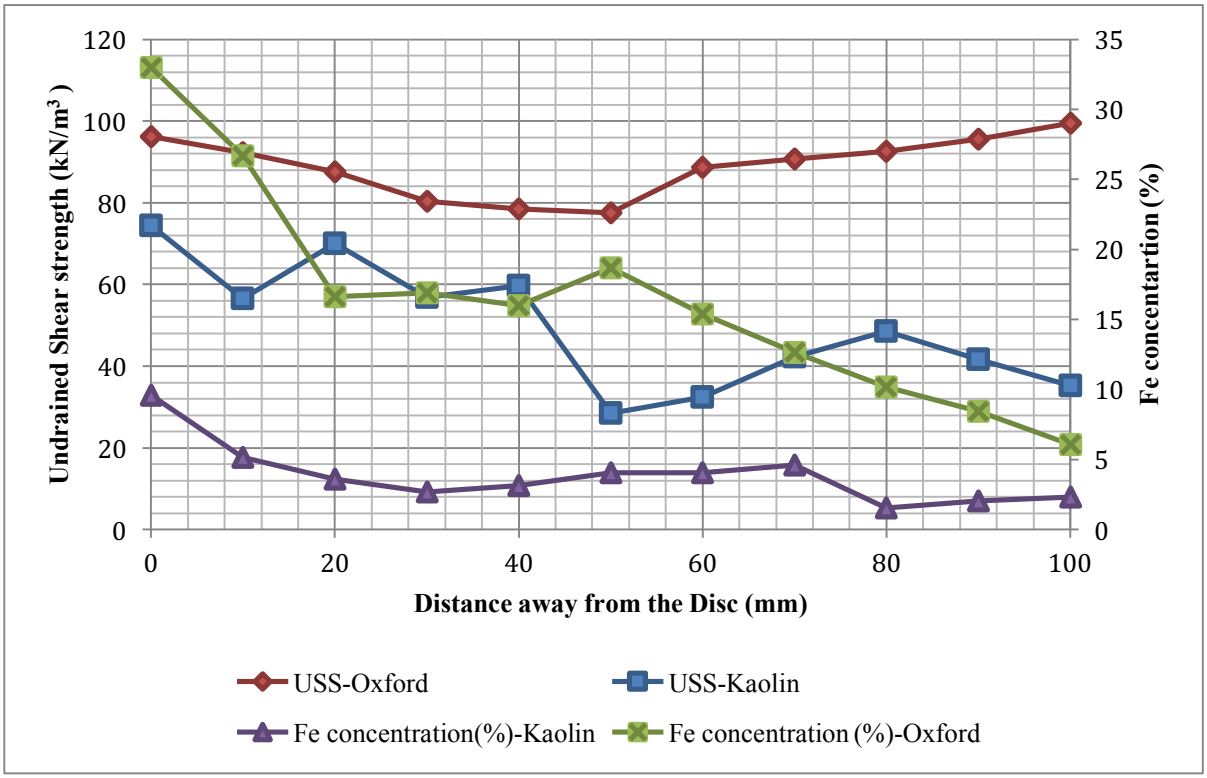

Figure 5.10 Undrained shear strength and iron concentration results of Kaolin and Oxford Clay for 3-months samples

5.5 Assessment of Corrosion Effects Through Simulation

As was discussed in the methodology chapter (see Section 3.12), it was not possible to use GPR on the samples due to their small dimensions. Therefore, the bulk conductivity (EC) and permittivity measurements of soil using TDR measurements (see Section 3.12.1) were used in FDTD simulations performed with GPRMax. The method used to create the simulations is explained in Section 3.13, while the values of conductivity and permittivity are given in Tables A29 to A32 in Appendix A.

Cast iron corrosion occurred due to the electrokinetic processes, replicating the electrochemical that occur naturally, and resulted in the formation of corrosion products (i.e. causing the release of Fe) and the transformation of the metal substrate, and causing iron oxyhydroxides and

aqueous salts to influence the clay. It is widely appreciated that cast iron pipes should be inspected and/or monitored in order to prevent failure and deterioration of the service provided by the network. However, excavation for inspection and monitoring is expensive; therefore, non-invasive assessment via geophysical techniques, such as GPR, could be carried out. FDTD simulations were used to simulate GPR signals to investigate buried iron pipes in clay soil in relation to the measured soil conductivity and other factors influencing clay modification induced by iron pipe corrosion (see Figure 5.11).

Figures 5.12 to 5.17 present the results of FDTD simulations performed with GPRMax. These simulations were created using the results of laboratory experimentation measurements (i.e. conductivity and permittivity results by TDR). The results of these simulations for Kaolin Clay and Oxford Clay were different, which was due to modification of the soil properties due to the corrosion and other reaction processes described earlier. Figures 5.12 to 5.14 present results for both control (no cast iron disc) and treated (with a cast iron disc) samples of Kaolin Clay and for different time periods. The pipe could be clearly observed by GPR at all the different points in the time period, which meant that the properties of the soil had not been modified in a way that prevented the pipe from being detected by GPR with a 700MHz antenna, and there was not much observable difference between the control and the sample affected by cast iron corrosion. A more detailed discussion is presented below.

For this research, it was important to understand the limitations and boundary levels beyond which pipes cannot be seen (i.e. those beyond which GPR would not detect the pipe) as a result of simulations. The most important factors are moisture content, which is the most influential factor a radar pulse will encounter and influences the depth of penetration of GPR signals – this in turn is influenced when the conductivity increases and the depth of penetration decreases due to the loss in signal strength at depth – while higher frequency signals do not penetrate as far as lower frequencies, but give better resolution. The composition of soil is another important

factor to consider in relation to signal penetration. Figure 5.11 presents the general influences on GPR for these tests, which vary depending on different environments, as well as operational factors.

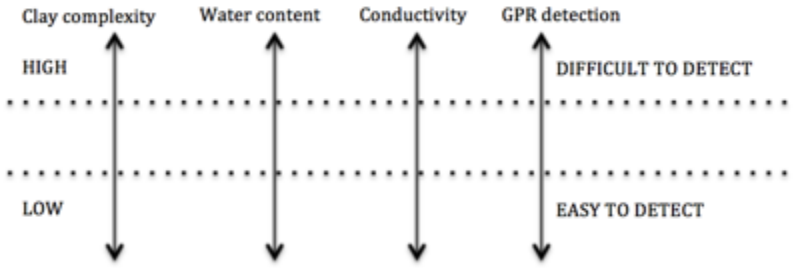

Figure 5.11 Factors affecting the pipe detection using GPR

5.5.1 Results of FDTD Simulation with GPRMax for Kaolin Clay

Figures 5.12 to 5.14 present results of FDTD simulations for both control and cast iron disc samples of Kaolin Clay for different time periods. The pipe could be clearly observed by GPR at all the different points in the time period, which meant that the properties of the soil had not been modified in a way that prevented the pipe from being detected by GPR, using a 700MHz antenna for the model with a simulated a pipe at 0.5m depth. It was concluded that there was no strongly discernible difference between the control and the sample affected by corrosion; the only hint at a difference concerns the lower parabolas in Figures 5.13(b) and 5.14. However, it should be recognised that detection of the pipe might change after a longer period of time as the corrosion process advances, as indicated by the weaker secondary reflections, and this might compromise the ability of the pipe to be detected under certain conditions. Nevertheless, these results do not suggest that detection in Kaolin Clay would be fatally compromised.

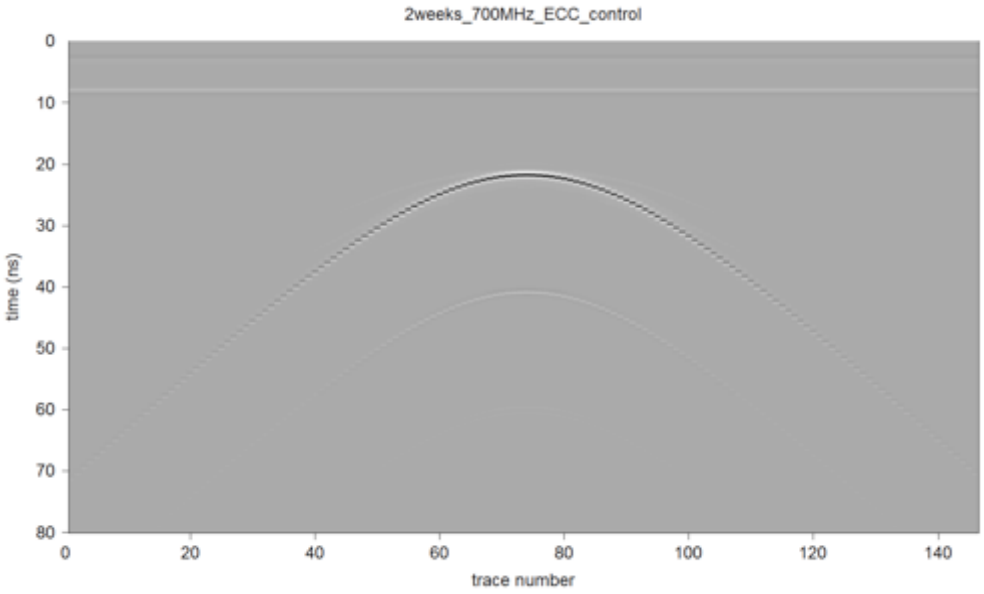

Figure 5.12 (a) FDTD simulation with GPRMax for GPR responses using measured test soil parameters for a 2-week Kaolin Clay sample without a cast iron disc

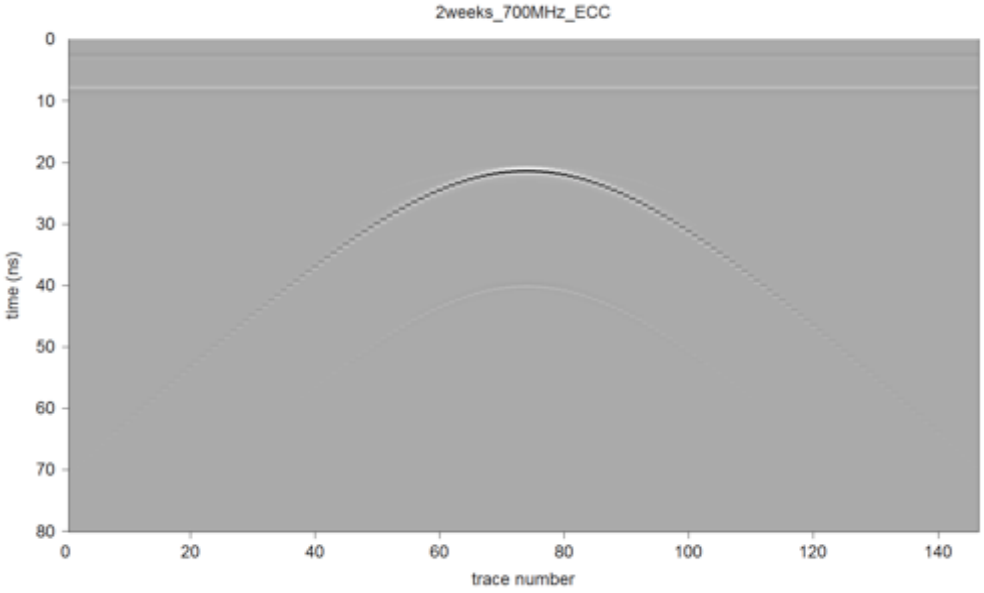

Figure 5.12 (b) FDTD simulation with GPRMax for GPR responses using measured test soil parameters for a 2-week Kaolin Clay sample with a cast iron disc

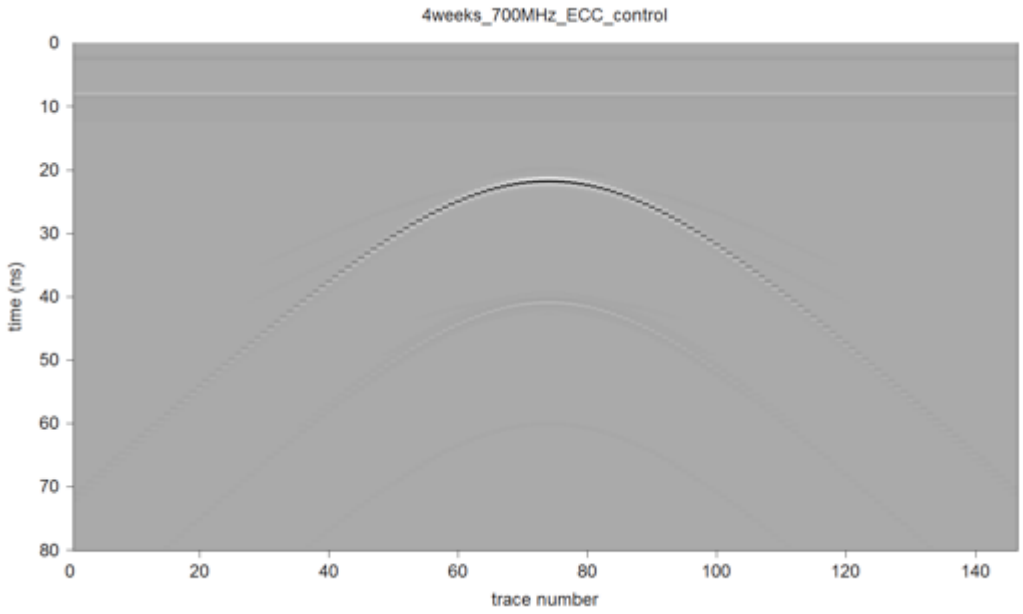

Figure 5.13 (a) FDTD simulation with GPRMax for GPR responses using measured test soil parameters for a 4-week Kaolin Clay sample without a cast iron disc

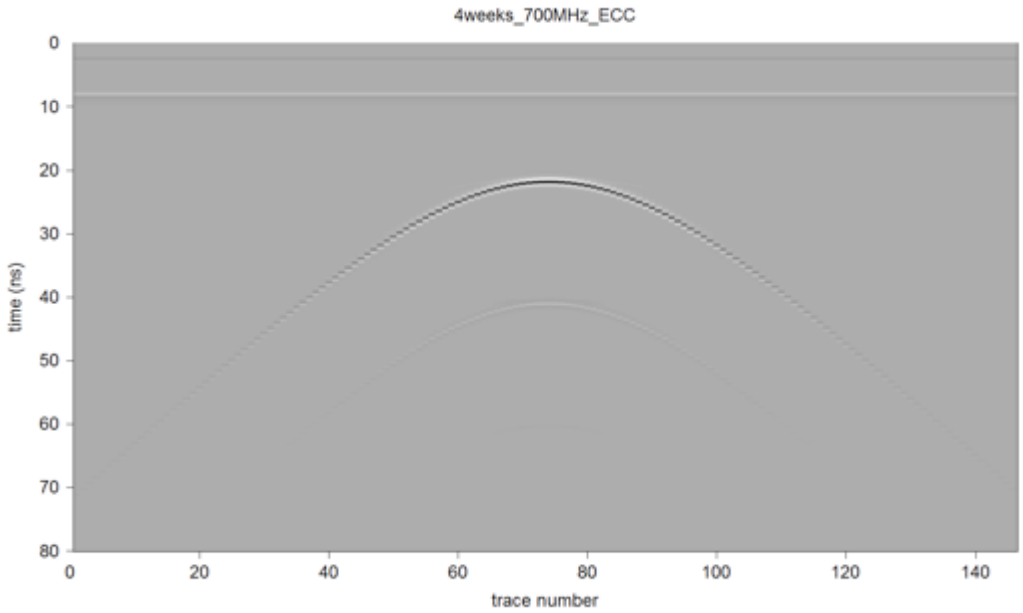

Figure 5.13 (b) FDTD simulation with GPRMax for GPR responses using measured test soil parameters for a 4-week Kaolin Clay sample with a cast iron disc

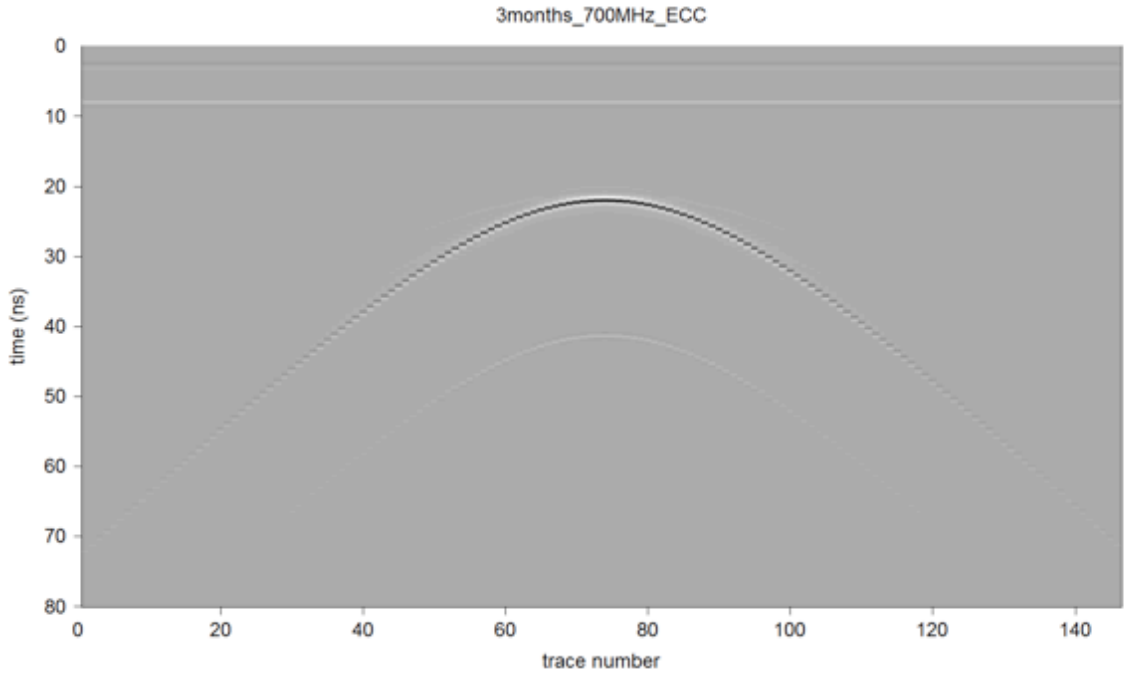

Figure 5.14 FDTD simulation with GPRMax for GPR responses using measured test soil parameters for a 3-month Kaolin Clay sample with a cast iron disc

5.5.2 Results of FDTD Simulation with GPRMax for Oxford Clay

The simulations for Oxford Clay showed different behaviours (see Figures 5.15 to 5.17). The results for the 2-weeks and 4-weeks control samples showed that the characteristics of the pipe were clearly detected by GPR. Although the treated samples (with a cast iron disc) for these two periods still permitted detection by the antenna, relative to the control samples the pipe resolution was not as distinct. The 3-month sample (Figure 5.17), using data for conductivity and permittivity for this sample, showed that GPR was unable to detect the pipe, and this was attributed to Oxford Clay modification due to the corrosion process. Since the major difference between the Kaolin Clay and Oxford Clay reactions to accelerated cast iron corrosion concerned the stabilisation reactions involving CAH, CSH and/or CASH, as noted above, then this aspect of ground modification in relation to GPR applications is worthy of further

investigation, although other features (such as the markedly raised Fe concentrations away from the cast iron pipe) might also influence.

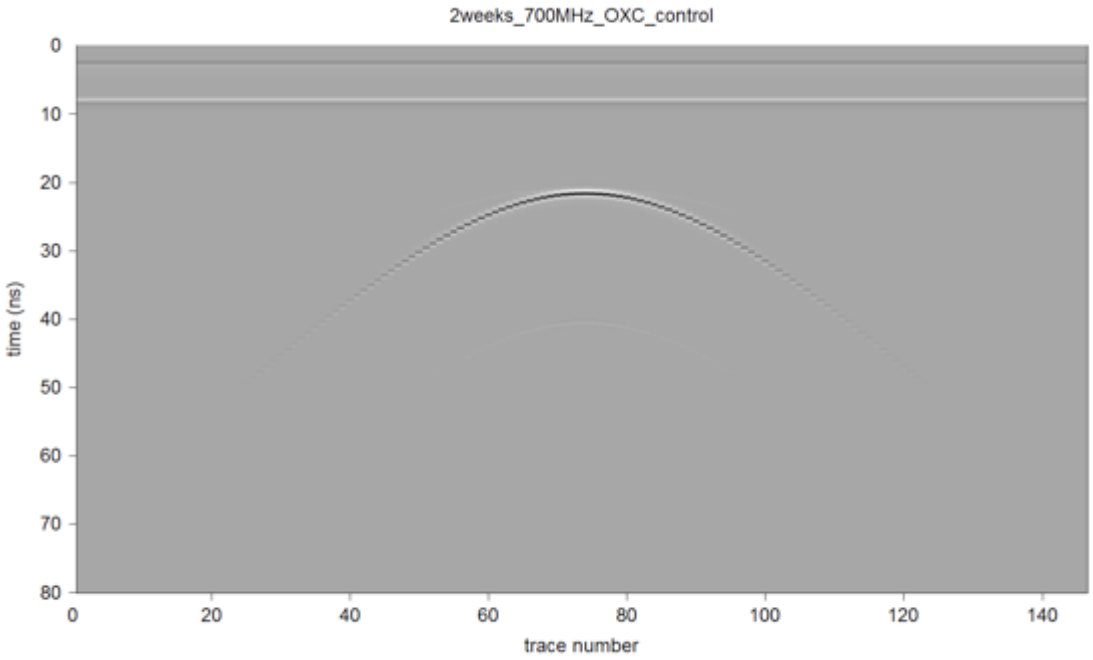

Figure 5.15 (a) FDTD simulation with GPRMax for GPR responses using measured test soil parameters for 2-week Oxford Clay sample without a cast iron disc

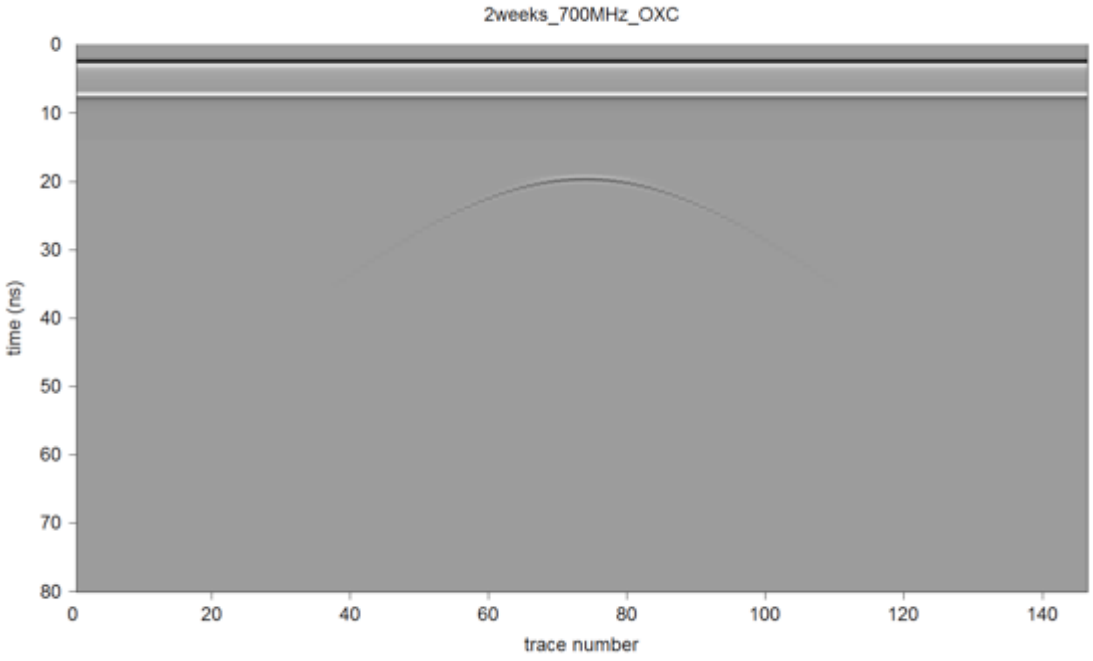

Figure 5.15 (b) FDTD simulation with GPRMax for GPR responses using measured test soil parameters for 2-week Oxford Clay sample with a cast iron disc

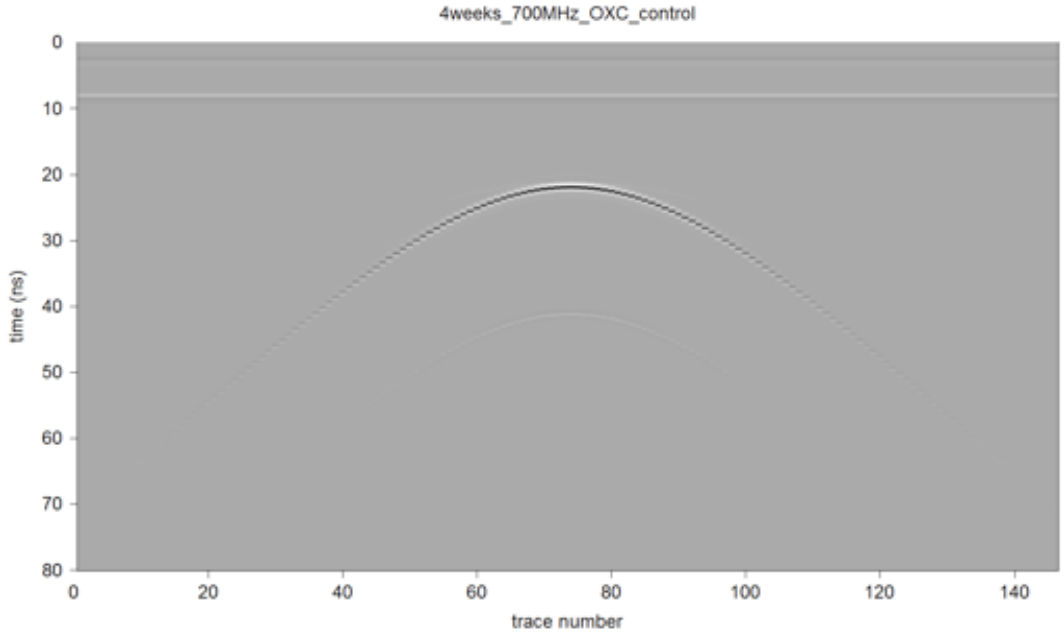

Figure 5.16 (a) FDTD simulation with GPRMax for GPR responses using measured test soil parameters for 4-week Oxford Clay sample without a cast iron disc

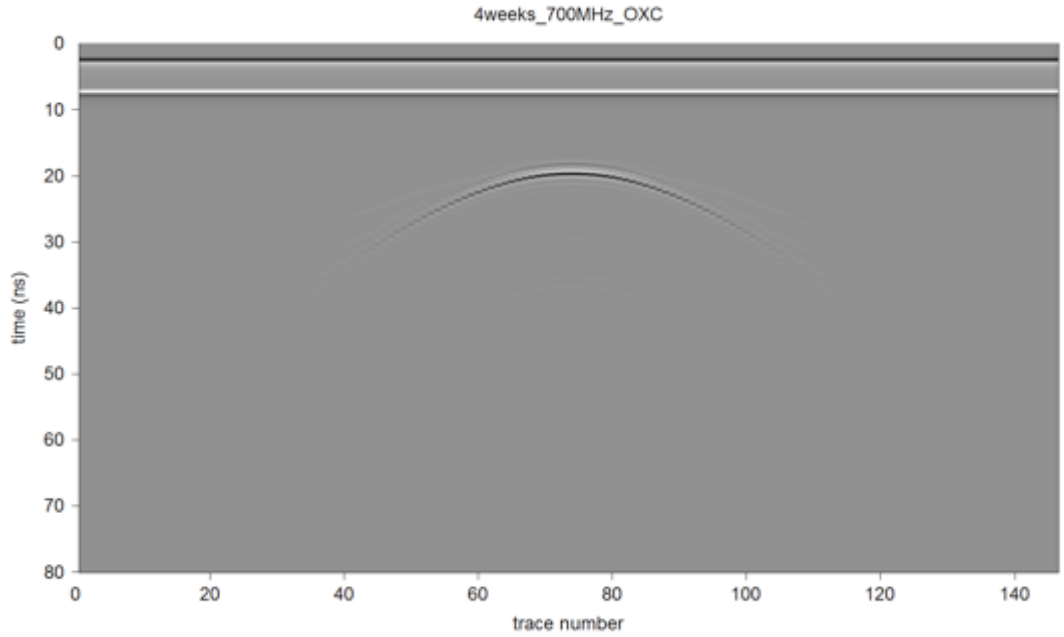

Figure 5.16 (b) FDTD simulation with GPRMax for GPR responses using measured test soil parameters for 4-week Oxford Clay sample with a cast iron disc

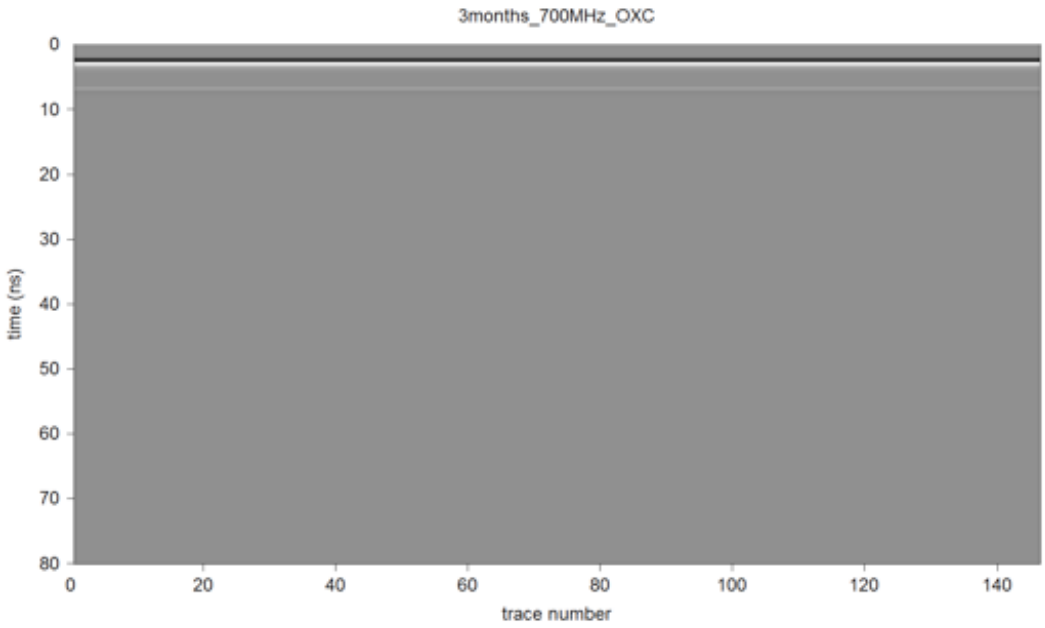

Figure 5.17 FDTD simulation with GPRMax for GPR responses using measured test soil parameters for 3-month Oxford Clay sample with a cast iron disc

5.6 Additional Results of FDTD Simulation with GPRMax for Kaolin and Oxford Clay

In order to discern the boundaries of these simulations (i.e. where the pipe disappears), additional simulation was required. Therefore, Figures 5.18 and 5.19 were plotted based on the TDR measurements for the cast iron disc samples to help estimate the conductivity and permittivity between two points, or beyond 3 months using very approximate extrapolations. It should be noted that this might not relate to values found in a real sample, but as only three measurements with three different times were available, there was no other option to estimate these values. Simulation of these data therefore gives estimations of conductivity and moisture content around the pipe where it will disappear / be detected. It should also be noted that these graphs and estimations are only valid for this test arrangement, i.e. they are extrapolations from the datasets obtained in the research and with different environmental conditions these simulation results may vary. Also, the geometry (location and size of the pipe) for these

simulations remains the same (i.e. as that stated in Section 3.13). Therefore, only the conductivity and permittivity parameters have been changed in the simulations.

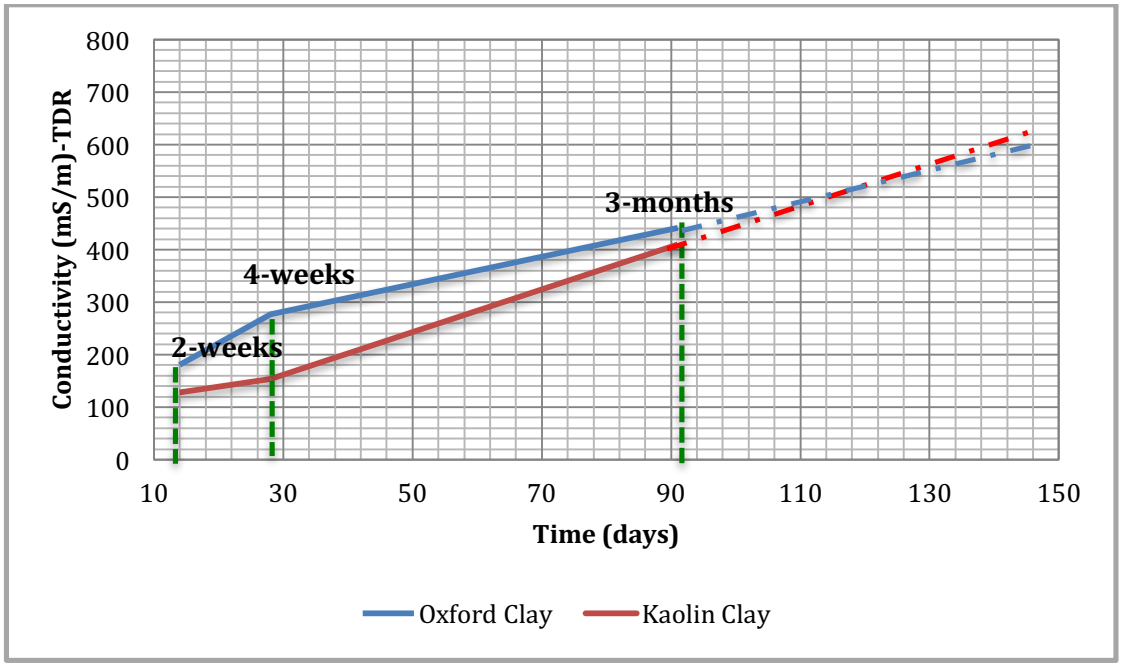

Figure 5.18 Conductivity extrapolations for Kaolin and Oxford Clay (using TDR data)

As explained in Section 2.12 permittivity and conductivity are the parameters used in the GPRMax programme. Therefore, it was important to know how permittivity and conductivity changed within the period tested (i.e. for the 2-weeks to 3-month samples with a cast iron disc), and to gain very approximate extrapolations beyond these ranges (for this exercise precision is neither needed, nor warranted). Figure 5.18 shows the conductivity results, and Figure 5.19 shows the permittivity results, extrapolated using the 2-weeks to 3-months range. The data used in these plots were the average TDR readings of the upper three layers (10mm-30mm away from the anode) and are reported in Tables A29 to A32.

For conductivity values in the additional simulations, values for times of treatment between 2 weeks and 3 months can be read from the solid lines in Figure 5.18, while values beyond 3

months were taken from the dashed extrapolation lines. Similarly, the values for permittivity can be drawn from Figure 5.19; the reasoning is discussed in relation to this graph hereafter. In order to choose the permittivity values for this further simulation, it was necessary to understand the patterns shown by the measured data, and hence where appropriate values for simulation lie. For example, the TDR measurements of permittivity for Oxford Clay yielded values between 31.44 (2-weeks samples) and 21.57 (3-month sample), where the GPR signals are not able to detect the pipe (as shown in Figure 5.17). Therefore, the permittivity value for further simulations should lie between 31.44 and 21.57. In contrast, for Kaolin Clay samples the measured permittivity values ranged between 28.32 (2-weeks sample) and 36.50 (3-month sample; neglecting the rogue value of 53.69) where pipe still can be detected. Therefore, a higher value of permittivity needs to be used for the simulations.

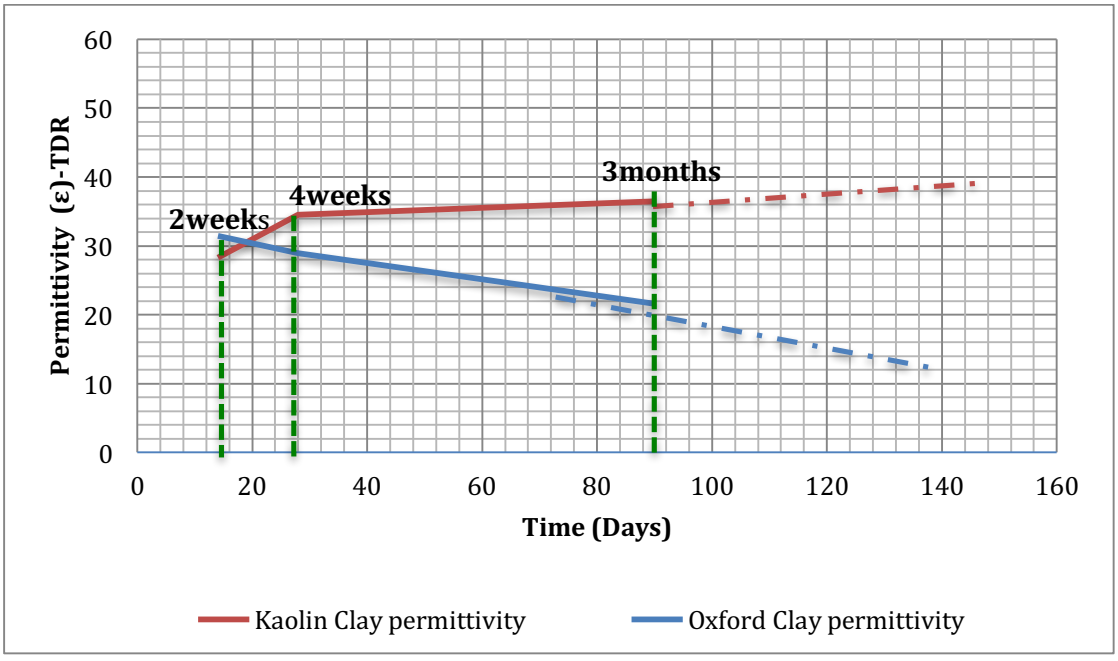

Figure 5.19 Permittivity extrapolations for Kaolin and Oxford Clay (using TDR data)

Moisture content is another important factor that is related to the signal attenuations. The moisture content for Kaolin Clay is higher than Oxford Clay during the testing (2-weeks to 3-months – see Figures 4.6 and 4.8, and Tables A5 to A8 in Appendix A) – and these values will have influenced the permittivity (and perhaps also conductivity) measurements made in the experiments. Although moisture content is not specifically input in the GPRMax simulations, the above point should be considered when interpreting these findings.

5.6.1 Kaolin Clay Samples - Additional Simulations

The Kaolin Clay simulation results show that the pipe is discernible for all simulations (from 2-weeks to 3-month samples – see Figures 5.12 to 5.14) and therefore further simulations needed to be considered for periods of treatment beyond 3 months (using the dashed lines in Figures 5.18 and 5.19 to provide the estimated values) in order to determine whether and when the pipe will 'disappear' in GPR tests. Table 5.3 shows the time, conductivity and permittivity values that were used for the simulations, while Figures 5.20 to 5.22 show the simulations using these values. For further simulation 20, 26 and 60 weeks were used. The conductivity values were chosen using Figure 5.18, but for permittivity it was not possible to choose a higher extrapolated value as it would not be realistic – values around 36-38 are approaching the maximum permittivity value of a fully saturated soil.

Table 5.3 Conductivity and permittivity values for Kaolin Clay used for additional simulations

Time	Distance away from Cast Iron Disc (mm)	Conductivity values mS/m	Permittivity values (ε)
20-weeks	10	609.5	36.97
	20	64.74	36.48
	30	27.85	35.01
26-weeks	10	701.32	37.50
	20	76.28	36.48
	30	32.31	35.01
60-weeks	10	950.50	40.50
	20	148.41	40.48
	30	129.25	37.01

Figures 5.20 to 5.22 present the results of the simulations, and in all figures the pipe can be detected. This means that the pipe might be detected no matter how long the process of corrosion took place in Kaolin Clay.

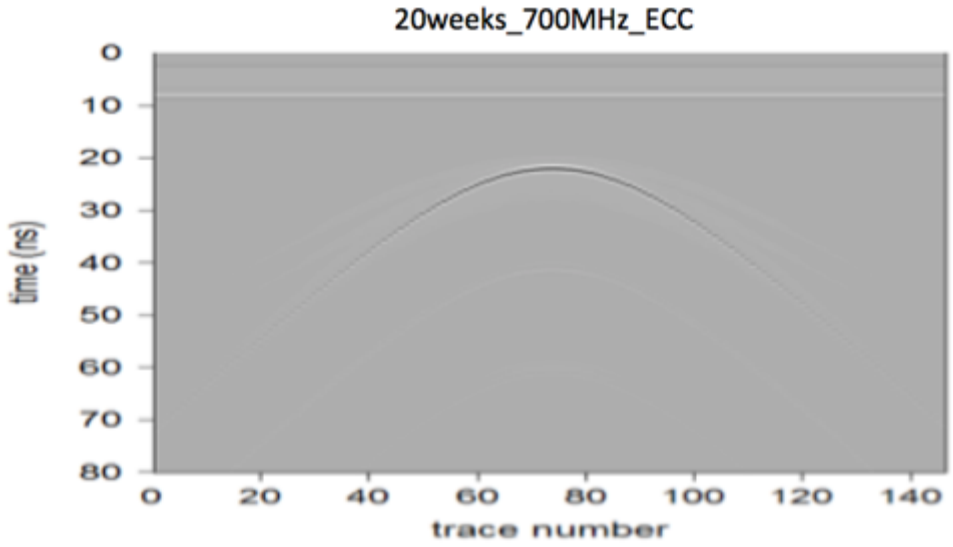

Figure 5.20 FDTD simulation with GPRMax for GPR responses using extrapolated test soil parameters for a 20-weeks Kaolin Clay sample with a cast iron disc

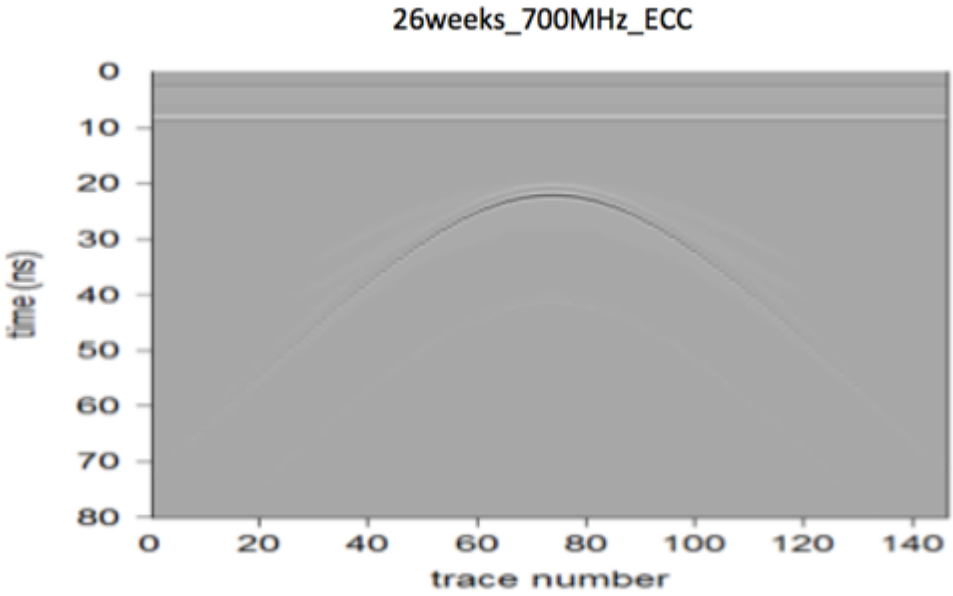

Figure 5.21 FDTD simulation with GPRMax for GPR responses using extrapolated test soil parameters for a 26-weeks Kaolin Clay sample with a cast iron disc

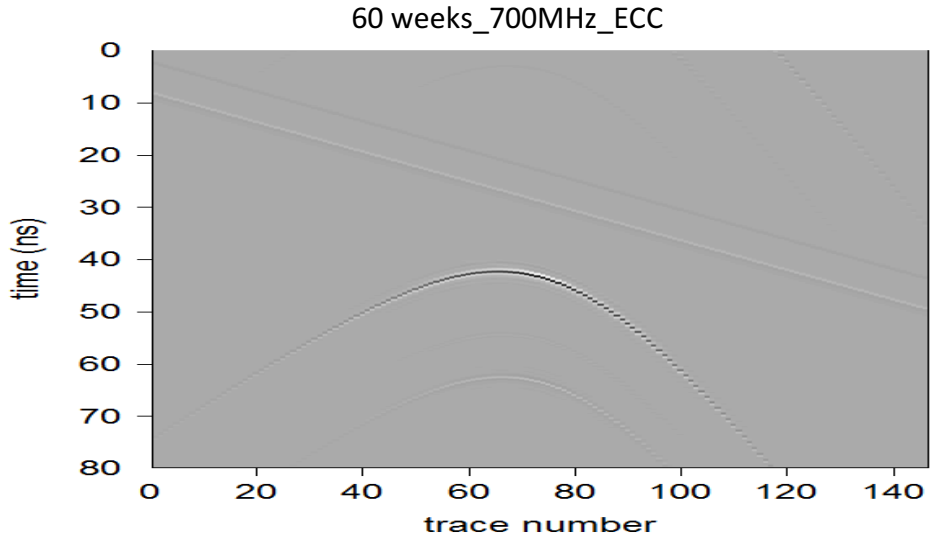

Figure 5.22 FDTD simulation with GPRMax for GPR responses using extrapolated test soil parameters for a 60-weeks Kaolin Clay sample with a cast iron disc

5.6.2 Oxford Clay Samples- Additional Simulations

Simulations for Oxford Clay showed that the pipe disappeared, i.e. could not be detected, for 3-month samples (Figure 5.17). Therefore, it was necessary to determine the time when the pipe disappeared (i.e. between the 4-weeks and 3-month samples). In order to do this, three additional simulations were used: 7, 9 and 10 weeks. It was expected that the pipe would start disappearing close to the values midway between the 4-weeks and 3-months sample on the basis of the previous results. Table 5.4 shows the time, conductivity and permittivity values used for the additional Oxford Clay simulations.

Table 5.4 Conductivity and permittivity value for Oxford Clay used for additional simulations

Time	Distance away from Cast Iron Disc (mm)	Conductivity values mS/m	Permittivity values (ε)
7-weeks	10	264.26	27.17
	20	136.34	27.42
	30	111.52	27.05
9-weeks	10	365.79	28.98
	20	160.23	27.62
	30	146.60	27.22
10-weeks	10	395.55	27.73
	20	132.11	24.77
	30	148.24	25.03

Figures 5.23 to 5.25 present the results of the simulation for Oxford Clay sample for 9, 10 and 7 weeks respectively and shows that the pipe could not be detected at 9 weeks, but was visible after 7 weeks.

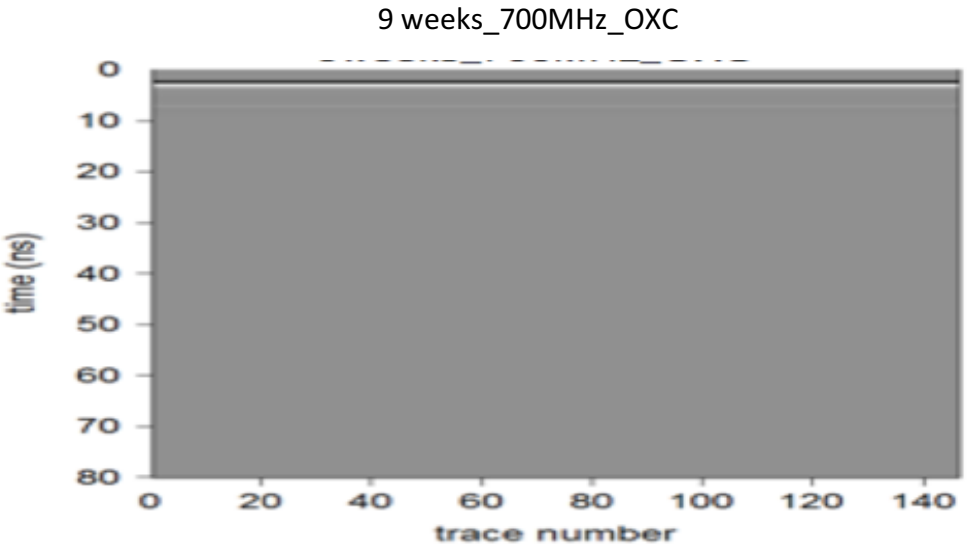

Figure 5.23 FDTD simulation with GPRMax for GPR responses using interpolated test soil parameters for a 9-weeks Oxford Clay sample with a cast iron disc

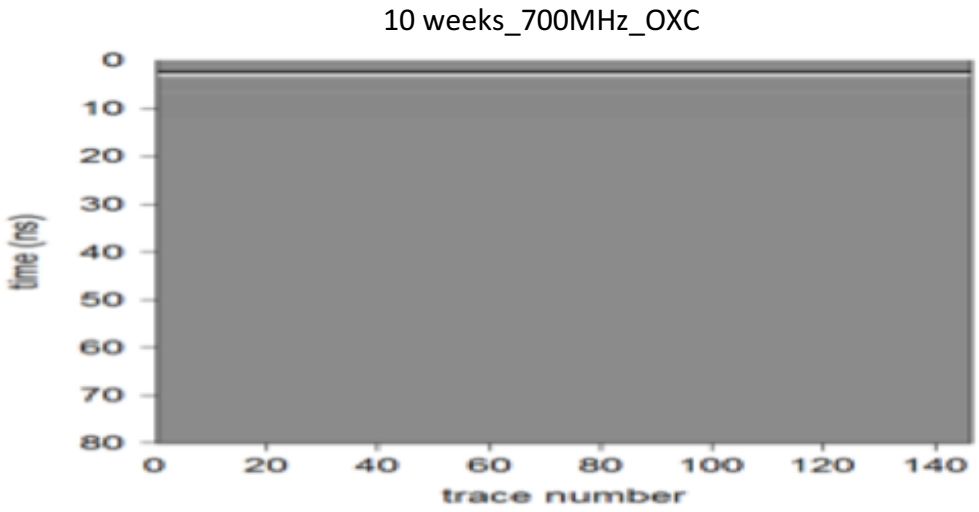

Figure 5.24 FDTD simulation with GPRMax for GPR responses using interpolated test soil parameters for a 10-weeks Oxford Clay sample with a cast iron disc

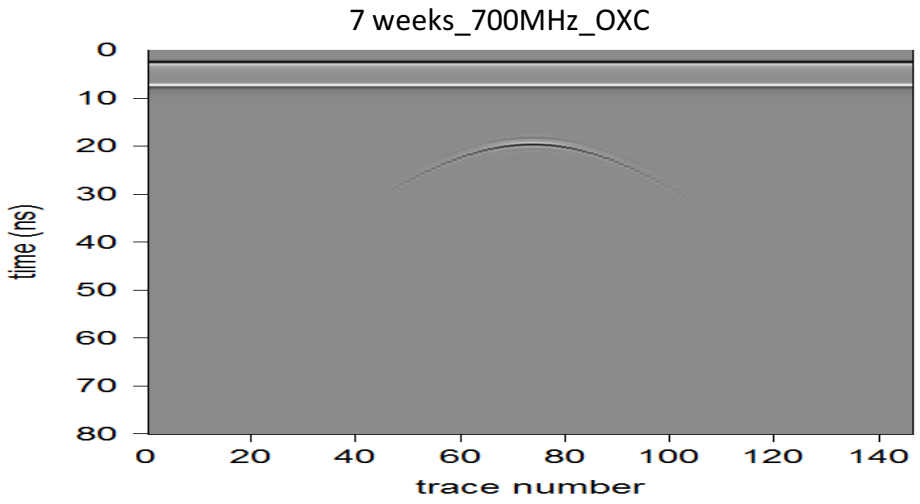

Figure 5.25 FDTD simulation with GPRMax for GPR responses using interpolated test soil parameters for a 7-weeks Oxford Clay sample with a cast iron disc

Permittivity is related to the water content more than conductivity. When soils are wet they show higher conductivity due to ions being free to move more easily. However, different soils have different ion contents and specific surface areas where ion exchange can take place. Kaolin Clay has a low specific surface area and therefore it does not reach very high levels of conductivity (even if it is very wet), whereas Oxford Clay has a far higher specific surface area and is more conductive than Kaolin Clay, even at lower water contents. From the simulations, it appears that even if the pipes corroded by a large amount and the conductivity immediately adjacent to the pipe is very high, the background conductivity of the soil matrix is much more important. In Kaolin Clay, conductivity is relatively low, even if it is very wet, and it appears that higher measurements of conductivity near the pipe are not enough to attenuate the signal to the point that the pipe becomes invisible (Figures 5.20 to 5.22).

More generally, if the soil is saturated and is not an expansive soil (e.g. Kaolin Clay, which lacks expansive clay mineral such as smectite) then the permittivity cannot go higher than a certain level, because permittivity increases with water content and the soil ceases to be a solid above a certain water content (the Liquid limit). Conversely the water content can go higher in

expansive soils, such as clay soils that contain smectite, although again only to a certain level, the limit in this case being 80 (this is the permittivity of free water at 20°C). Therefore, the measured value between 36-38 for Kaolin Clay probably represents the maximum permittivity value for this type of soil and the pipe will always be detectable using GPR. Table 5.5 presents the conductivity, permittivity and moisture content of soil conditions beyond which the pipe cannot be detected by GPR.

Table 5.5 Kaolin Clay and Oxford Clay Simulations Summary

Type of clay soil	Conductivity (mS/m)	Permittivity (ε)	Moisture content (%)	GPR simulations
Kaolin Clay	< 810	< 38.50	< 40.3	Pipe never disappears
Oxford Clay	~ 265	~ 27	~ 53	Between 7 and 9 weeks pipe starts to disappear

5.7 Summary

Corrosion of cast iron pipes has been a problem in the water industry since cast iron started to be used as a material for water distribution pipes (McNeill et al., 2001). The development of the corrosion process is dependent on the environmental conditions, which in the case of buried pipes means the properties of the surrounding soil. This research was designed using a method (see Chapter 3) that simulated the corrosion process and shows how the products of corrosion affect the geotechnical, geophysical and geochemical properties of clay soil. The most important aspect of these tests was to understand the chemical interactions which occur within the clay samples. Also, it was important to understand the electrokinetic effects on the clay properties in tests where no cast iron disc was included.

The electrokinetic treatment causes the release of H^+ ions at the anode and OH^- ions at the cathode, and therefore the development of an acid environment at the anode and alkaline environment at the cathode. Hence a pH gradient will be generated and it develops with the time of treatment. As the mineralogy changes under certain pH conditions, the clay mineralogy can break down and reaction products can be created, which in turn cause the clay's properties, such as undrained shear strength, Atterberg limits, pH and conductivity, to change.

When a cast iron disc is involved in the tests, for the Kaolin Clay sample, irons ions are released and are moved through the sample due to the electrokinetics – by electromigration. As iron oxyhydroxides have lowest solubility under neutral conditions, therefore precipitation would be expected to occur progressively away from the anode with time (as the pH is progressively lowered near the anode and the iron oxide concentration progressively increases), this being also reliant on the migration of soluble iron ions. Also, in the low pH environment near the anode, the Kaolin Clay is relatively stable and cation exchange on the clay exchange sites may be the only dominant clay reaction occurring – this causes the thickness of the diffuse double layer to decrease and brings the particles together, i.e. in closer association. Dissolution of the clay mineral at low pH is unlikely to occur because Kaolin Clay is naturally acidic and hence ion changes in the system near the anode would be restricted to release of chemical constituents from the Kaolin Clay at low pH. Moreover, due to the low solubility of iron oxyhydroxides generally and the greatest concentration of iron oxide close to the anode, most precipitation occurs in the upper layers of the Kaolin Clay samples close to the cast iron disc. Increasing the time of treatment (to 3 months) showed that the amount of iron oxide increased as time passed. At the cathode (high pH), as the Kaolin Clay is not stable in high pH conditions, the clay minerals dissociated and released silica and alumina, which complexed with available cations to form alkaline minerals. However, due to the lack of calcium in the Kaolin Clay, the classic

stabilisation reactions (involving CAH, CSH and/or CASH) failed to occur and the strength near the cathode remained relatively low compared with that at the anode.

In contrast in Oxford Clay, due to the mixed mineralogy, there was greater scope for significant complexation and cation exchange (due to the greater capacity of the clay's cation exchange sites). As the iron ions are released at the anode and, in low pH conditions in which Oxford Clay is relatively unstable, dissolution of Oxford Clay minerals occurs, the Fe and other cations will migrate towards the cathode and substitute on the cation exchange sites of the clay minerals for cations lower valency, or replace ions of similar valency due to 'mass action', which decreases the thickness of the diffuse double layer. At the cathode end of the Oxford Clay samples (i.e. at high pH) dissolution of silica and alumina, combined with release of calcium, can cause Calcium Silicate Hydrate (CSH) and/or Calcium Aluminate Hydrate (CAH), and maybe also Hydrated Calcium Aluminosilicate (CASH), amorphous gels to form and crystallise, creating cementation and considerable strength gain, while there is also scope for iron and other compounds to precipitate. These reactions will occur in samples without a cast iron disc, but to a far lesser degree.

Two different types of clay (i.e. Kaolin Clay and Oxford Clay) were used to identify the physical and chemical changes in clays having distinctly different mineralogy. It was found that the Kaolin Clay soil was less aggressive than the Oxford Clay soil, i.e. the corrosion activity was stronger in Oxford Clay, and this led to cementation, precipitation and complexation. After finishing the tests and cleaning the discs, the state of the cast iron disc that was used for 3-months sample (see Figure 5.26) also proved the aggressive behaviour of Oxford Clay – the disc used for the Oxford Clay sample obtained an uneven, pitted, surface whereas that for the Kaolin Clay sample, although obviously degraded, was far smoother. Essentially the Oxford Clay presented a much more aggressive environment due to its mixed mineralogy (including the more active smectite clay mineral) and the different ions released

and migrating through the soil. The changes to the clays were found not to greatly affect the ability of Ground Penetrating Radar to detect cast iron pipes in Kaolin Clay, but in Oxford Clay after approximately 7-8 weeks, when the changes in the clay had advanced (both in time and distance from the electrodes) in these (greatly) accelerated corrosion tests, it has been shown that Ground Penetrating Radar would be unable to detect buried cast iron pipes.

Further simulation indicated that for a clay soil such as Kaolin Clay, which is not an expansive soil and has a low specific surface area, and when it is saturated, GPR signals are not significantly attenuated and therefore the pipe can be detected while corrosion of the cast iron pipe advances. For soils that have different mineralogies and ion contents, and different specific surface areas, and in which ion exchange readily takes place (such as Oxford Clay), the result may vary.

Figure 5.26 Cast iron discs used for Oxford Clay (left side) and Kaolin Clay (right side)

CHAPTER SIX

6.0 Conclusion

6.1 Introduction

The corrosion of cast iron pipes buried directly in clay soils is one of the major challenges to the water industry of managing an ageing water distribution network in countries where cast iron features predominantly in the buried infrastructure. The corrosion occurs in the saturated zone of clay soil by electrochemical oxidation of the cast iron in contact with oxygenated water. The development of the corrosion process results in a galvanic cell being set up between the pipe (the anode) and the clay (a distributed cathode) and the pH change in this system causes iron ions to be released and corrosion products, such as iron oxide, iron hydroxide and aqueous salts, to form in the surrounding clay soil. These iron compounds are expected to have a low solubility and precipitate in the soil such that the concentration decreases away from the cast iron pipe. Moreover, excavation to prove the location, assess the state of buried cast iron pipes and monitor their degradation is both disruptive and expensive and hence remote surveying using geophysical techniques, notably ground penetrating radar (GPR), has been proposed to do this, although problems have been experienced in practice. It is important, therefore, to understand the influences on clay soils of cast iron degradation and their implications for GPR surveying.

The aim of this research was to gain a better understanding of how the ions released from cast iron corrosion in clay soils change the soil properties, and how the extent and degree of influence changes with time, and additionally to investigate the effect of these changes on the efficacy of GPR surveying. This was achieved by:

- Setting up controlled laboratory experiments to simulate and accelerate (using a weak electric field) the corrosion of cast iron in clay soil, and evaluate (at different stages of this corrosion) the geotechnical (undrained shear strength, moisture content and Atterberg limits), geophysical (permittivity) and geochemical (iron content, pH and conductivity) changes in two clay soils, a relatively pure clay of low activity (Kaolin Clay) and a clay with mixed mineralogy (Oxford Clay).
- Using the results (conductivity and permittivity) of the accelerated corrosion experiments in a FDTD simulation to investigate the ability of GPR techniques to detect the buried cast iron pipe.

In carrying out this research, it was important to understand the effect of the electrokinetic process itself (i.e. without any cast iron degradation) on the clays, and tests were therefore conducted using inert electrodes to provide control data.

The effects of electrochemical action on the two clay soils used in this research after two treatment periods (2 weeks and 4 weeks) without cast iron degradation were as follows:

- The electrokinetic treatment induced acidic conditions at the anode and alkalinic conditions at the cathode, and therefore induced a pH gradient across the clay samples, which influenced the solubility of the clay minerals and any salts contained within the clay. This effect increased with time.
- The electrokinetic process also changed the chemical composition of the pore fluid, and hence the electrical conductivity of the clays. This was more intense close to the anode and cathode, where the conductivity was raised, and the effect increased with time.
- The Atterberg limits changed in response to the above effects, and this also therefore varied with time of treatment.

- Although there was evidence of an initial reduction in the undrained shear strength, attributed to 'flushing' of ions through the system as a result of a water feed to the anode, small increases in the undrained shear strength were observed at 4 weeks. The strength increase was modest and approximately uniform in the Kaolin Clay, while the increase in strength in Oxford Clay occurred near the anode and the cathode. This increase in strength in both clays was attributed to a combination of cation substitution on the clay exchange sites, causing a reduction in the thickness of the diffuse double layer and closer association of the clay particles, and perhaps also some complexation of ions released by the pH changes and precipitation of salts. The latter reactions were more likely in the Oxford Clay (due to its constituent materials and poorer stability at low pH), while there was also possible evidence of clay mineral dissolution and CAH, CSH and/or CASH gel formation and crystallisation near the cathode in Oxford Clay at 4 weeks.

When a cast iron disc replaced the inert electrode used for the anode in the tests (i.e. there was a source of iron from the anode degradation), additional general changes were observed in the clay samples:

- Releasing iron ions into the system caused the pH to reduce further at the anode (the environment became more acid) and the pH to increase further at the cathode (excepting for the Oxford Clay sample at 3 months). This created the potential for greater dissolution of clay minerals.
- The concentration of Fe was greatly elevated at the anode and this increased with time, as did the concentration into the main body of the samples away from the anode due to electromigration.

- This pattern of pH change and Fe release (and in Oxford Clay particularly the release of other ions at low pH) and migration had a concomitant effect on the conductivity, which was greatly raised near the anode and raised near the cathode, with increases also experienced in the main body of the Oxford Clay samples, but not the Kaolin Clay samples (where the conductivity was lowered below the neutral value). It likewise influenced the Atterberg Limit measurements, the Liquid limit rising at the anode with an approximately linear reducing trend towards the cathode and the profiles translating upwards with treatment time, while the Plastic Limits showed an approximately uniform increase that varied with treatment time.
- The undrained shear strength of the clay samples increased in response to the above effects, due to a combination of cation exchange (and thinning of the diffuse double layer), salt precipitation and/or stabilisation reactions, dependent on the clay mineralogy.

6.2 Physical and Chemical Modification of Kaolin Clay

Releasing of iron ions (Fe), as a product of cast iron corrosion, caused the clay soil close to the cast iron disc to create a low pH (acidic) condition, lower than when no cast iron disc was used, and this lowered pH developed progressively with time. This was accompanied by a large concentration of iron oxide being detected at the anode (at all three time periods), and progressively away from the anode due to electromigration, with a marginally raised concentration in the body of the samples at 2 and 4 weeks, but a significantly raised concentration in all but the region close to the cathode at 3 months.

Since Kaolin Clay is naturally acidic and is relatively stable at low pH, cation exchange of higher valency ions (released from the Kaolin Clay's constituent materials, even if significant

clay mineral lattice breakdown does not occur) for lower valency ions on the clay exchange sites may be the only dominant clay reaction occurring – this causes the thickness of the diffuse double layer to decrease and causes the clay particles to become more closely associated. Moreover, due to the low solubility of iron oxyhydroxides generally and the greatest concentration of iron oxide being found close to the anode, most precipitation occurred in the upper layers of the Kaolin Clay samples close to the cast iron disc. Increasing the time of treatment (to 3 months) showed that the amount of iron increased as time passed. At the cathode (high pH), as the Kaolin Clay is not stable in high pH conditions, the clay minerals dissociated and released silica and alumina, which complexed with available cations to form alkaline minerals. However, due to the lack of calcium in the Kaolin Clay, the classic stabilisation reactions (involving CAH, CSH and/or CASH) fail to occur and the strength near the cathode remains relatively low compared with that at the anode.

Since water content strongly influences the undrained shear strength of clays, this relationship was explored in relation to the chemically-induced effects via a normalisation procedure (Figure 5.3) and demonstrated clearly that the raised strength measurements for all three periods when simulating cast iron corrosion were due to chemical modification in the clay system. Moreover, the greater effects at the anode than at the cathode are very clearly shown in Figure 5.3.

6.3 Physical and Chemical Modification of Oxford Clay

In contrast in Oxford Clay, due to its mixed mineralogy, the release of iron ions at the anode and the generation of low pH conditions, in which Oxford Clay is relatively unstable, the evidence suggests that dissolution of Oxford Clay minerals occurred, the Fe and other cations migrated towards the cathode and substituted on the cation exchange sites of the clay minerals

for cations lower valency, or replaced ions of similar valency due to 'mass action', which decreased the thickness of the diffuse double layer. As with Kaolin Clay, there was also evidence of considerable iron (and other metal) compound precipitation throughout the upper half of the sample at 3 months. In the lower half of the samples (where the pH was raised) at 2 weeks and 4 weeks, and especially at 3 months, there was evidence of dissolution of silica and alumina, which combined with release of calcium, caused amorphous gels of Calcium Silicate Hydrate, Calcium Aluminate Hydrate and/or Hydrated Calcium Aluminosilicate (it was not possible to distinguish between the reaction products) to form and crystallise, creating cementation and considerable strength gain.

As for Kaolin Clay, the relationship between water content and undrained shear strength was explored via normalisation (Figure 5.4) and similarly demonstrated clearly that the raised strength measurements at 4 weeks and 3 months when simulating cast iron corrosion were due to chemical modification in the clay system. However, in Oxford Clay the increased strength in the lower half of the samples, and especially at the cathode, was shown to shown to complement, and at 3 months exceed, the strength gains in the upper half of the samples, due to the stabilisation reactions. These chemical changes were demonstrated also in the photographs of the samples at the end of the tests.

These results demonstrated that the corrosion activity was stronger in Oxford Clay than Kaolin Clay, and this led to cementation as well as the cation exchange, complexation and precipitation reactions. The physical appearance of the cast iron discs at the end of the 3-month tests (see Figure 5.26) supported the argument that Oxford Clay is more aggressive to cast iron, the Oxford Clay disc exhibiting a highly uneven, pitted, surface whereas the Kaolin Clay disc, although obviously degraded, was far smoother. This was attributed to the Oxford Clay's mixed mineralogy (including the more active smectite clay mineral) and the different ions released and migrating through the soil.

6.4 Implications for Ground Penetrating Radar

The application of conductivity and permittivity measurements in FDTD simulations demonstrated that the chemically-induced changes to Kaolin Clay did not materially affect the ability of Ground Penetrating Radar to detect cast iron pipes. However, in Oxford Clay after approximately 7-8 weeks, when the chemically-induced changes in the clay had advanced (both in time and distance from the electrodes) in these accelerated corrosion tests, it was shown that Ground Penetrating Radar would be unable to detect buried cast iron pipes. Since the major difference in the chemically-induced changes between the two clays concerned the stabilisation reactions occurring in Oxford Clay, the poor performance of GPR in this soil type might be attributed to such reactions.

6.5 Further Work

This research was developed to gain a better understanding of the effects of cast iron corrosion products on clay properties with respect to time, and the implications of these changes on GPR performance. While an information database on this subject has been created for two types of clay and an understanding of chemical changes in these clays has been developed, further research is necessary to fully understand the mechanisms of these interactions with clays of different mineralogies. Moreover, the tests were designed to be carried out on small samples of clay, and it was thus not possible to do more detailed physical, chemical and geophysical analysis on the treated clays. The following suggestions for further work show only the ideas arising out of the work undertaken for this project.

- The tests can be repeated for different types of clay soil to gain a more extensive dataset and provide more support to the findings via a comparison of the chemical and physical

properties of the treated soil. These results might not be the same as those in field conditions, due to the conditions associated with the accelerated testing, but they would provide appropriate results to predict likely behaviour in the field conditions.

- Additional chemical analysis is strongly recommended, as the timeframe of this research, once initial developmental studies had been completed, did not make this opportunity possible. Iron solubility assessment is mentioned in Section 3.9.2. It is important to understand the behaviour of iron solubility conditions of the iron oxyhydroxides and the maximum amount of iron that could be sorbed by the clays of interest. Also, using ICP-MS analyses, which would be able to provide information on ions that were released through the clay samples from the cast iron disc and clay mineral alteration, would be helpful in developing this understanding.
- A programme of research should be carried out to provide evidence from field conditions (i.e. real cases) using the same physical, geophysical and chemical measurements, both to understand practical influences on the effects of cast iron corrosion products on clay soil and to compare the results with laboratory findings.
- A structured programme of laboratory tests should be carried out to determine the effect of cast iron corrosion without using the electrokinetic system and to compare the findings with results obtained from this research to understand the error that could possibility occur by using electrokinetics to accelerate corrosion.
- The approach of using electrokinetic experiments to accelerate corrosion could be extended by conducting longer experiments, by increasing the rate of acceleration (e.g. using a higher potential difference) and by exploring whether a rapid, cruder indicator test could be developed to highlight clays in which chemical alteration of the clay could lead to loss of detection ability using GPR surveying.

- Larger-scale samples should be treated in order to address the limitation of being unable to use GPR techniques while the corrosion of cast iron pipe occurs, i.e. to enable GPR reflection monitoring as the corrosion of cast iron pipe advances.

More generally, the creation of a comprehensive database of the results of chemical and geophysical testing could help to develop a better understanding of the clay-iron interaction mechanism. As civil engineers approaching this problem, it was not possible to delve deeply into soil chemistry reactions when devising practically-orientated experiments. This research achieved its purpose of determining the primary physical-chemical behaviour of soils due to cast iron pipe corrosion in clays, and its effect on GPR surveys, yet for some purposes (e.g. protection of buried iron artefacts) it is important to understand why these interactions take place, for which deeper soil chemistry knowledge is needed.

REFERENCES

Acar, Y. B. and Alshawabkeh, A. N. (1993) *Principles of Electrokinetic Remediation*. Environmental Science and Technology, 27 (13): 2638–2647.

Acar, Y.B., Gale, R.J. and Putnam, G. (1990) *Electrochemical Processing of Soils: Theory of pH Gradient Development by Diffusion and Linear Convection*. Journal of Environment Science and Health, 25, 687-714.

Adamson, L. G., Quigley, D.W., Ainsworth, H.R. and Chilingar, G.V. (1966) *Electrochemical Strengthening of Clayey Sandy Soils*. Engineering Geology, 1, (6): 451-459.

Ahmad, K., Taha, M.R. and Kassim, K.A. (2011) *Electrokinetic Treatment on a Tropical Residual Soil*. Proceedings of the Institution of Civil Engineers, Ground Improvement, 164: 3-13.

Alshawabkeh, A.N. and Sheahan, T.C. (2003) *Soft Soil Stabilisation by Ionic Injection under Electric Fields*. Ground Improvement, 7: 177-185.

Annan, A.P. (2008) *Electromagnetic Principles of Ground Penetrating Radar*. Ground Penetrating Radar Theory and Applications - Chapter 1. Oxford, UK: Elsevier. pp. 4-40.

Asavadorndeja, P. and Glawe, U. (2005) *Electrokinetic Strengthening of Soft Clay using the Anode Depolarization Method.* Bulletin of Engineering Environment, 64: 237-245.

ASTM (2008) *D4646–03 Standard Test Method for 24-h Batch-Type Measurement of Contaminant Sorption by Soils and Sediments*. ASTM Book of Standards Volume 11.

ASTM (2011) *D2487-11, Standard Practice for Classification of Soils for Engineering Purposes (Unified Soil Classification System)*. ASTM Book of Standards, 4.

Atanassova, R. and Kerestedjian, T. (2004) *Native Sulphur: A product of anthropogenic umaroles*. 32nd International Geological Congress, Florence, Abstracts, 633.

Atanassova, R., Kerestedjian, T. and Donchev, I. (2004) *Mineralogy and Remobilization Processes in the Weltz-Clinker Dump Site, Plovdiv Region, Bulgaria*. In: Pecchio, M. et al. (Editors) 8th International Congress for Applied Mineralogy ICAM, de Lindoia, Brazil, 387-389.

Atkinson, M. F. (2004*) Structural Foundations Manual for Low-rise Buildings*. 2nd Edition, Taylor & Francis, 67-68.

AWWA, American Water Works Association: http://www.awwa.org [Access May 2005]

Baecher, G.B. and Christian, J.T. (2003) *Reliability and Statistics in Geotechnical Engineering*. John Wiley and Sons, London and New York.

Baracos, A., Hurst W.D. and Legget, R.F. (1955) *Effects of Physical Environment on Cast Iron pipe.* National Research Council Canada, Division of Building Research. Ottawa.

Barker, J.E., Rogers, C.D.F., Boardman, D.I. and Peterson, J. (2004) *Electrokinetic Stabilization: An overview and case study*. Ground Improvement, 8: 47-58.

Batchelder, M., Mather, J.D. and Joseph, J.B. (2007) *The Stability of the Oxford Clay as a Mineral Liner for Landfill*. Water and Environment Journal, 12 (2): 92–97.

Bauer, A., Fiehn, B., Marquardt, C. M., Klein, M., Römer, J., Schäfer, T., Görtzen, A. and Kienzler, B. (2006) *Results on the Pu Diffusion in the Opalinus Clay*. In 6th EC FP-FUNMIG IP. Stockholm. 2nd Annual Workshop Proceedings: 231-237.

Bechtold, M., Huisman, J.A., Weihermüller, L. and Vereecken, H. (2010) *Accurate Determination of the Bulk Electrical Conductivity with the TDR100 Cable Tester*. Soil Science Society of America Journal, 74 (2): 495-501.

Benjamin, M. M., Sontheimer, H. and Leroy, P. (1996) *Corrosion of Iron and steel*. In Internal Corrosion of Water Distribution Systems. Cooperative Research Report. Denver, CO: American Water Works Association (AWWA) Research Foundation.

Bjerrum, L., Moum, J. and Eide, O. (1967) *Application of Electroosmosis to a Foundation problem in a Norwegian Quick Clay*. Geotechnique, 17: 214-235.

Boardman, D.I, Glendinning, S. and Rogers, C.D.F. (2004) *The Influences of Iron (III) and Lead (II) Contaminants on Lime-Stabilised Clay*. Geotechnique, 54 (7): 467-486.

Bohn, H.L., Brian, L.M. and George, A.O. (2001) *Soil Chemistry, 3rd Edition*. Wiley- Interscience, John Wiley & Sons, New York, 307.

Bonds, R.W., Lyle, M., Barnard, A., Horton, M. and Oliver, G.L. (2005) *Corrosion and Corrosion Control of Iron Pipe*: 75 years of research. Journal American Water Works Association (AWWA), 97 (6): 88-98

Bone, B.D., Barnard, L.H., Boardman, D.I., Carey, P.J., Hills, C.D., Jones, H.M., MacLeod, C.L. and Tyrer M. (2004b) *Review of Scientific Literature on the use of Stabilisation / Solidification for the Treatment of Contaminated Soils, Solid Wastes and Sludges.* Environment Agency, Science Report SC980003/SR2, www.environment- agency.gov.uk.

Bradford, S. (2000) *Practical Handbook of Corrosion Control in Soils; Pipelines, Tanks, Casings, Cable. Corrosion Series*. Edmonton, Canada: Casti Publishing Ltd.

Brady, P.V. and Walther, J.V. (1989) *Controls on Silicate Dissolution Rates in Neutral and Basic pH Solutions at 25 f.* Geochimica et Cosmochimica Acta, 53: 2823-2830.

Brady, P.V., Cygan, R.T. and Nagy, K.L. (1996) *Molecular Controls on Kaolinite Surface Charge*. Colloid Interface Science. 183: 356-364.

BSI (1990a) *Methods of Test for Soils for Civil Engineering Purposes:* Part 2: Classification Tests. BS1377. London: British Standards Institution.

BSI (1990b) *Methods of Test for Soils for Civil Engineering Purposes: Part 3: Chemical and Electro-Chemical Tests*. BS1377. British Standards Institution, London, UK.

BSI (1994) *Cast Iron. Designation of Microstructure of Graphite.* BS EN ISO 945, British Standards Institution, London, UK .

BSI (1997) *Founding – Grey Cast Iron.* BS EN 1561, British Standards Institution, London, UK.

BSI (1999) *Code of Practice for Site Investigations*. BS 5930. British Standards Institution, London, UK.

BSI (1999) *Code of Practice for Site Investigations*. BS 5930. British Standards Institution, London, UK.

BSI (2003) *Protection of Metallic Materials against Corrosion.* Corrosion Likelihood in Soils (Part I and II). BS EN 125901. British Standards Institution, London, UK.

Burland, J.B. (1990) *On the Compressibility and Shear Strength of Natural Clays*, Géotechnique, 40 (3): 329-378.

Campbell, J.E. (1990) *Dielectric Properties and Influence of Conductivity in Soils at One to Fifty Megahertz*. Soil Science Society of America Journal, 54 (2): 332-341.

Casagrande, A. (1948) *Classification and Identification of Soils*. Cambridge, MA: Harvard University.

Casagrande, L. (1949) *Electro-osmosis in soils,* Geotechnique, 1: 159-177.

Cassidy, N.J. (2007) *Frequency-Dependent Attenuation and Velocity Characteristics of Magnetically Lossy Materials.* In Proceedings of the Fourth International Workshop on Advanced Ground penetrating Radar. Naples, Italy, 27(29):142-146.

Cassidy, N.J. (2008) *Electrical and Magnetic Properties of Rocks, Soils and Fluids*. Ground Penetrating Radar Theory and Applications - Chapter 2. Oxford, UK: Elsevier. 41-72.

Cast Iron Pipe Research Association (1952) *Handbook of Cast Iron Pipe for Water, Gas, Sewage and Industrial Services*. Chicago Ill: Cast Iron Research Association.

Cast Iron Pipe Soil Institute (2006) *Cast Iron Soil Pipe and Fittings Handbook.* Hixon TN: Cast Iron Pipe Soil Institute.

Castiglione, P., Shouse, P.J. and Wraith, J.M. (2006) *Multiplexer Induced Interference on TDR Measurements of Electrical Conductivity*. Soil Science Society of America Journal, 70: 1453-1458.

CEN (2008) *The pH Dependent Leaching Test with Initial Acid or Base Addition CEN/TS 14429*. Brussels: European Committee for Standardisation CEN.

Ciullo, P. A. (1996) *Industrial Minerals and Their Uses* – A Handbook and Formulary. William Andrew Publishing, Noyes.

Cole, I.S. and Marney, D. (2012) *The Science of Pipe Corrosion*: A Review of the Literature on the Corrosion of Ferrous Metals in Soils. Corrosion Science. 56: 5-16.

Costello, S.B., Chapman, D.N., Rogers, C.D.F. and Metje, N. (2007*) Underground Asset Location and Condition Assessment Technologies*. Tunneling and Underground Space Technology 22, 524–542.

Cuardos, J. and Linarres, J.(1996) *Experimental Kinetic Study of Smectite-to-Illite Transformation*. Geochimica et Cosmochimica. Acta 60 (3):439-53.

Curioni, G. (2013) *Investigating the Seasonal Variability of Electromagnetic Soil Properties using Field Monitoring Data from Reflectometry probes.* PhD thesis, University of Birmingham, UK.

Dalton, F.N., Herkelrath, W.N., Rawlins, D.S. and Rhoades, J.D. (1984) *Time-Domain Reflectometry*: Simultaneous Measurement of Soil Water Content and Electrical Conductivity with a Single Probe. *Science*, 224 (4652): 989-990.

Daniels, D.J. (2004) *Ground Penetrating Radar*. 2nd ed.: The Institution of Electrical Engineering. London.UK.

Davis, J.L. and Annan, A.P. (1989) *Ground-Penetrating Radar for High-Resolution Mapping of Soil and Rock Stratigraphy*. Geophysical Prospecting, 37: 531-551.

Deer, W.A., Howie, R.A. and Zussman, J. (1992) *An Introduction to the Rock-forming Minerals.* New york. John Wiley and Sons.

Delaney, A.J. and Arcone, A. (1982) *Laboratory Measurements of Soil Electric Properties between 0.1 and 5 GHz.* U.S. Army CRREL Report. 82: 7-10.

Doolittle, J.A. and Collins, M.E. (1995) *Use of Soil Information to Determine Application of Ground Penetrating Radar*. Journal of Applied Geophysics, 33: 101-108.

Doyle, G., Seica, M.V. and Grabinsky, M.W.F. (2003) *The Role of Soil in the External Corrosion of Cast Iron Water Mains in Toronto, Canada*. Canada. Geotechnical. J. 40 225-236.

Drever, J. I. (1988) *The geochemistry of natural waters*. 2nd ed. Englewood Cliff, NJ: Prentice Hall, Inc.

Ekine, A.S. and Emujakporue, G.O. (2010) *Investigation of Corrosion of Buried oil Pipeline by Electrical Method*. Journal of Applied Sciences and Environmental Management, 14: 63-65.

Esrig, M.I. (1968) *Pore Pressure, Consolidation and Electrokinetics*. Journal of Soil Mechanics and Foundation Division, ASCE 94 (SM4), 899-922.

Esrig, M.I. and Gemeinhardt, J.P. (1967) *Electrokinetic Stabilisation of Illitic clay*. Journal of Soil Mechanics and Foundation Engineering, 93 (3): 109-128.

Evett, S.R. and Parkin, G. W. (2005) *Advances in Soil Water Content Sensing*: The Continuing Maturation of Technology and Theory. *Vadose Zone Journal*, 4 (2): 986- 991.

Faulkner, D.W.S. (2010) *Electrokinetics and Iron Precipitation for Ground Engineering and Metal Removal*. PhD thesis, University of Brighton, UK.

Ferre, P.A., Rudolph, D.L. and Kachanoski, R.G. (1996) *Spatial Averaging of Water Content by Time Domain Reflectometry:* Implications for twin rod probes with and without dielectric coatings. *Water Resources Research*, 32 (2): 271-279.

Freeman, S.R. (1999) *Graphitic Corrosion - Don't Forget about Buried Cast Iron Pipes*. Materials Performance, 38 (8): 68-69.

Geonor (2005a) *Test Equipment and Field Instrumentation Catalogue*. Geonor A/S, Oslo, Norway.

Geonor (2005b) *Instruction for use: Fall Cone Apparatus.* Part no. 200000, Geonor A/S, Oslo.

Giannopoulos, A. (1997) *The Investigation of Transmission-Line Matrix and Finite-Difference Time-Domain Methods for the Forward Problem of Ground Probing Radar.* PhD thesis, Department of Electronics, University of York, UK.

Giannopoulos, A. (2005) *Modelling Ground Penetrating Radar by Gprmax*. Construction and Building Materials,19: 755–762.

Giese, K. and Tiemann, R. (1975) *Determination of the Complex Permittivity from Thin- sample Time Domain Reflectometry Improved Analysis of the Step Response Waveform*. Advances in Molecular Relaxation Processes, 7 (1): 45-59.

Gillot, J.E. (1987) *Clay in Engineering Geology*. Developments in Geotechnical Engineering Vol.41, Elsevier Science publisher, Netherlands.

Goldberg, S. and Foster, H.S. (1990) *Flocculation of Reference Clays and Arid-zone Soil Clays*. Soil Science Socity of America Journal, 54: 714–718.

Grant, J.A. and Schultz, P.H. (1994) *Erosion of Ejecta at Meteor Crater: Constraints from ground-penetrating radar*. Proceedings, Fifth International Conference Ground-Penetrating Radar. Kitchner, Ontario, Canada, Waterloo Centre for Groundwater Research and the Canadian Geotechnical Society, 789- 803.

Greaves, R.J., Lesmes, D.P., Lee J.M. and Toksoz, M.N. (1996) *Velocity Variations and Water Content Estimated from Multi-offset, Ground-Penetrating Radar*. Geophysics, 61 (3): 683-695.

Grim, R.E. (1968) *Clay Mineralogy*, 2nd ed. McGraw-Hill, New York.

Gummow, R.A. and Wakelin, R.G. (1993*) A Summary of the Findings of recent Water Main Corrosion studies in Ontario*, Institute for Research in Construction (Publishers) Ottawa, Ontorio.

Gupta, S.K. and Gupta, B.K. (1979) *Critical soil-Moisture content in the Underground Corrosion of mild-steel.* Corrosion Science, 19: 171–178.

Hamnett, R. (1980) *A study of the Processes involved in the Electro-reclamation of Contaminated Soils*, Dissertation, University of Manchester, UK.

Hansbo, S. (1957) *A New Approach to the Determination of the Shear Strength of Clay by the Fall-Cone Test*. In Royal Swedish Geotechnical Institute Proceedings, 14.

Hao, T., Rogers, C.D.F., Metje, N., Chapman, D.N., Muggleton, J. M., Foo, K.Y., Wang, P., Pennock, S. R., Atkins, P.R., Swingler, S.G., Parker, J., Costello, S.B., Burrow, M.P.N., Anspach, J.H., Armitage, R.J., Cohn, A.G., Goddard, K., Lewin, P.L., Orlando, G., Redfern, M.A., Royal, A.C.D and Saul, A.J. (2012) *Condition Assessment of the Buried Utility Service Infrastructure*. Tunneling and Underground Space Technology, 28: 331-344.

Harbottle, M.J. (2003*) The use of Electrokinetics to Enhance the Degradation of Organic Contaminant in Soils*, PhD thesis, University of Oxford, UK.

Harry, M.J. (2009*) Hand book of Ground Penetrating Radar Theory and Applications*, 179-196.

Heimovaara, T.J. (1993) *Design of Triple-Wire Time-Domain Reflectometry Probes in Practice and Theory.* Soil Science Society of America Journal, 57 (6): 1410-1417.

Heimovaara, T.J., Focke, A.G., Bouten, W. and Verstraten, J.M. (1995) *Assessing Temporal Variations in Soil-water Composition with Time Domain Reflectometry.* Soil Science Society of America Journal, 59 (3): 689-698.

Herkelrath, W.N., Hamburg, S.P. and Murphy, F. (1991) *Automatic, Real-Time Monitoring of Soil Moisture in a Remote Field Area With Time Domain Reflectometry*. Water Resources Research, 27 (5): 857 864.

Hiemenz, P.C. (1977) *Principles of Colloid and Surface Chemistry*. Marcel Dekker, New York.

Huang, W.L., Long, M. and Pever, D.R. (1993) *An Experimentally Derived Kinetic Model for Smectite to Illite conversion and its use as Geothrmometer.* clays Minerals 41(2):162-77.

Hudak, P., Sadler, B. and Hunter, B. (1998) *Analyzing Underground Water-pipe breaks in Residual Soils.* Water Engineering Management, 145(12): 15-20.

Huertas, F.J., Chou, L. and Wollast, R. (1998) *Mechanism of Kaolinite Dissolution at Room Temperature and Pressure*: Part 1. Surface Speciation. Geochimica et Cosmochima Acta 62 (3): 417-431.

Huisman, J.A., Hubbard, S.S., Redman, J.D. and Annan, A.P. (2003) *Measuring Soil Water Content with Ground Penetrating Radar:* A Review. *Vadose Zone Journal*, 2 (4): 476- 491.

Huisman, J.A., Lin C.P., Weihermüller, L. and Vereecken, H. (2008) *Accuracy of Bulk Electrical Conductivity Measurements with Time Domain Reflectometry.* Vadose Zone Journal, 7 (2): 426-433.

Huisman, J.A., Sperl, C., Bouten, W. and Verstraten, J.M. (2001) *Soil Water Content Measurements at Different Scales: Accuracy of Time Domain Reflectometry and ground- penetrating radar*. Journal of Hydrology, 245: 48-58.

IAEA, International Atomic Energy Agency (2008) *Field Estimation of Soil Water Content.* A Practical Guide to Methods, Instrumentation and Sensor Technology. Vienna: IAEA.

Ingles, O.G., and Metcalf, J.B. (1972) *Soil Stabilization: Principles and Practice*. Butter worths, Sydney; London, 38.

Jack, T.R. and Wilmott, M.J. (2011) *Corrosion by Soils, Uhlig's Corrosion Handbook*, 3rd ed. RW Revie, John Wiley, New York, 333-349.

Jaganathan, A.P., Allouche, E.N. and Simicevic, N. (2010) *Numerical Modeling and Experimental Evaluation of a Time Domain UWB Technique for Soil void Detection*. Tunneling and Underground Space Technology, 25, 652–659.

Jakobs, J.W. and Hewes, F.W. (1987) *Underground Corrosion of Water Pipes.* in Calgary, Canada, Materials Performance, 26(5): 42-49.

Jason Consultants, LLC: www.jasonconsult.com [Accessed April 2009]

Jayasekera, S. and Hall, S. (2006) *Modification of the Properties of Salts Affected Soils using Electrochemical treatments.* Journal of Geotechnical and Geology Engineering.

Jones, S.B., Wraith, J.M. and Or, D. (2002) *Time Domain Reflectometry Measurement Principles and Applications.* Hydrological Processes, 16 (1): 141-153.

Kirmeyer, G.J., Richards, W. and Smith, C.D. (1994) *An Assessment of Water Distribution Systems and Associated Research Needs*. Denver, Colo. Research Foundation and American Water Works Association (AWWA).

Kleiner, Y. and Rajani, B. (2001b) *Comprehensive Review of Structural Deterioration of Water Mains: Statistical Models*, Urban Water, 3: 131-150.

Kleiner, Y. and Rajani, B. (2000) *Considering Time-Dependent Factors in the Statistical Prediction of Water Main Breaks*, Infrastructure Conference Proceedings, Baltimore, Maryland.

Koehl, S. (2000) *Grey Cast Iron Mains: Taking the Guesswork out of Replacement.* (IRC- NRC) Journal of Commerce: 6-8.

Koppenjan, S. (2008) *Ground Penetrating Radar Systems and Design. Ground Penetrating Radar Theory and Applications* - Chapter 3. Oxford, UK: Elsevier. pp. 73-97.

Kozisek, F. (1992) *Biogenic Value of Drinking water*. PhD thesis. Prague: National Institute of Public Health. Kreysa, G. and Schütze, M. (2008) *Dechema Corrosion Handbook* - Revised and Extended 2nd Edition. DECHEMA.

Lageman, R. (1993) *Electroreclamation.* Environmental Science Technology 27(13), 2648-2650.

Lamont-Black, J. and Weltman, A. (2010) *Electrokinetic Strengthening and Repair of Slopes.Technical Note,* Ground Engineering, April, 28-31.

Langmuir, D. (1997) *Aqueous Environmental Geochemistry*. Prentice Hall Inc., Upper Saddle River, NJ, USA.

LaQue, F.L. (1958) *The Corrosion Resistance of Ductile Irons*, Corrosion 14 485-492.

Lebron, I., Robinson, D.A., Goldberg, S. and Lesch, S.M. (2004), *The Dielectric Permittivity of Calcite and Arid zone Soils with Carbonate Minerals*. Soil Science Society of America Journal, 68:1549- 1559.

Liaki, C. (2006) *Physicochemical Study of Electrokinetically Treated Clay Soils using Carbon and Steel Electrodes*. PhD thesis, University of Birmingham, UK.

Liaki, C., Rogers, C.D.F. and Boardman, D.I. (2008) *Physicochemical Effects on Uncontaminated Kaolinite due to the Electrokinetic treatment using Inert Electrodes*. Journal of Environmental Health Science and Engineering Part A 43(8): 810–822.

Liaki, C., Rogers, C.D.F. and Boardman, D.I. (2010*) Physico-chemical Effects on Clay due to Electromigration using Stainless Steel Electrodes*. Journal of Applied Electrochemistry 40: 1225-1237.

Lide, D. R. (1995) *Handbook of chemistry and physics*. 76th edition. Boca Raton, FL: CRC Press.

Lin C.P., Chung, C.C., Huisman, J.A. and Tang, S.H. (2008) *Clarification and Calibration of Reflection Coefficient for Electrical Conductivity Measurement by Time Domain Reflectometry.* Soil Science Society of America Journal, 72 (4): 1033-1040.

Logan, K.H. (1947) *Corrosion by Soils*. Corrosion Handbook. Princeton, NJ: Electrochemical Society. pp. 446–481.

Logsdon, S.D. (2000) *Effect of Cable Length on Time Domain Reflectometry Calibration for High Surface Area Soils.* Soil Science Society of America Journal, 64: 54-61.

Logsdon, S.D. (2005) *Time Domain Reflectometry Range of Accuracy for High Surface Area Soils. Vadose Zone Journal*, 4: 1011-1019.

Logsdon, S.D. (2006) *Experimental Limitations of Time Domain Reflectometry Hardware for Dispersive Soils*. *Soil Science Society of America Journal*, 70: 537-540.

Loughnan, F. (1969) *Chemical Weathering of the Silicate Minerals*. New York: American Elsevier Publishing Company.

MacDonald, E. (1994) *Aspects of Competitive Adsorption and Precipitation of Heavy Metals by a Clay Soil*. Master of Engineering Thesis, McGill University, Montreal.

Makar, J. and Chagnon, N. (1999) *Inspecting Systems for Leaks, Pits, and Corrosion.* Journal American Water Works Association 91, 36.

Makar, J.M. and McDonald, S.E. (2007) *Mechanical Behavior of Spun-Cast Grey Iron Pipe*. *Journal of Materials in Civil Engineering*, 19 (10): 826-833

Makar, J.M. and Rajani, B.B. (2000) *Grey Cast - Iron Water Pipe Metallurgy*, *Journal of Materials in Civil Engineering*, 12 (3): 245-253.

Makar, J.M., Desnoyers, R. and McDonald, S.E. (2001) *Failure Modes and Mechanisms in Grey Cast Iron Pipe*. *Underground Infrastructure Research*: Municipal, Industrial and Environmental Applications Proceedings, Kitchener, Ontario, 1-10.

Makar, J.M., Rogge, R. and McDonald, S.E. (2002) *Circumferential Failure in Grey Cast Iron Pipes*. In Proceedings of the AWWA Infrastructure Conference, Chicago, 1-18.

Manoff, M. (1957) *Underground Corrosion,* National Bureau of Standards Circular 579, US Government Printing Office (Publishers), Washington DC.

May, H. M., Kinniburgh, D. G., HELMKE P.A. and Jackson, M. L. (1986) *Aqueous Dissolution, Solubilities and Thermodynamic Stabilities of common Aluminosilicate Clay Minerals Kaolinite and Smectites*. Geochim. Cosmochin. Acta 50:1667-77.

McNeill, J.D. (1980) *Electrical Conductivity of Soils and Rocks*. Mississauga, Canada: Geonics Ltd.

Melchers, R.E. (2011) *Modelling long-term Corrosion of Mild Steel in unpolluted Fresh and Sterile Seawaters.* Proc. 18th Intl. Corrosion Congress, Perth, Australia, 156.

Melchers, R.E. (2013) *Long-term Corrosion of Cast Irons and Steel in Marine and Atmospheric Environments*. Corrosion Science 68 : 186–194

Michael, T.B., Caruso, J., Smith, C.H., Schneider, R. (1998) *A New Perspective on Magnetic Field Sensing*. Sensors Magazine.

Milligan, V. (1995) *First Application of Electroosmosis to Improve Friction Pile Capacity-Three Decades Later*. Proceedings of the Institution of Civil Engineers, Geotechnical Engineering: 113 (2): 112–116.

Mirsal, I.A. (2004) *Soil Pollution – Origin, Monitoring and Remediation*. 2nd ed. Berlin, Germany: Springer Verlag.

Mitchell, J. K. and Soga, K. (2005) *Fundamentals of Soil Behavior*. 3rd ed. New York: John Wiley and Sons.

Moorman, B., Robinson, S. and Burgess, M. (2003) *Imaging Periglacial Conditions with Ground-Penetrating Radar*. Permafrost and Periglacial Processes, 14: 319–329.

Mordak, J. and Wheeler, J. (1988) *Deterioration of Asbestos Cement Water Mains*. In Final Report to the Department of the Environment. Wiltshire, UK: Water Research Center.

MTU, Mapping The Underworld: http://www.mappingtheunderworld.ac.uk/ [Accessed May 2013]

Mumpton, F. A. (1977) *Mineralogy and Geology of Natural Zeolites*. Reviews in Mineralogy Society of America.

Murray, J.N. and Moran, P.J. (1989) *Influence of Moisture on Corrosion of Pipeline Steel in Soils using in Situ Impedance Sspectroscopy*. Corrosion 45: 34–43.

Nagy, K.L., Blum, A.E. and. Lasaga, A.C. (1991) *Dissolution and Precipitation Kinetic of Kaolinite at 80°C and pH 3:the Dependence on Solution Saturation state*. American Journal of Science. 291(7): 649-86.

Nandy, A.K., Manjhi, J.K. and Roy, N.K. (2008) *Stream Sediment and Soil Samples by Microwave Digestion followed by ICP-MS Measurement*, Atomic Spectroscopy, 29: 115-123.

National Highway Institute (2009) *Report No. FHWA-NHI-09-087, Corrosion/ Degradation of Soil Reinforcements for Mechanically Stabilized Earth Walls and Reinforced Soil Slopes*, National Highway Institute, Washington.

Neal, A. (2004) *Ground-Penetrating Radar and its use in Sedimentology: Principles, Problems and Progress*. School of applied science, university of Worvehampton, UK, 66: 261-330.

Nicholas, D.M. and Ferguson, P.H. (2005) *Accurate Prediction of Cast Iron Watermain Performance using Linear Polarisation Resistance (LPR) Methodology*. In the proceedings of the New Zealand Water and Wastes Association. Conference, Auckland, NZ.

O'Day, D.K. (1989) *External Corrosion in Distribution Systems*, Journal American Water Works Association, 81(10): 44-52.

Ohsaki, Y. (1982) *Corrosion of Steel Piles Driven in Soil Deposits*, Soils and foundations 22 (3) 57-76.

Olhoeft, G.R. (2000) *Maximizing the Information Return from Ground Penetrating Radar*. Journal of Applied Geophysics, 43 (2-4): 175–187.

Ou, C.Y., Chien, S.C. and Wang, Y.G. (2009) *On the Enhancement of Electroosmotic soil Improvement by the Injection of Saline Solutions*. Applied Clay Science, 44, 130- 136.

Ouhadi, V.R., Yong, R.N. and Sedighi M. (2006) *Desorption Response and Degradation of Buffering Capacity of Bentonite Subjected to Heavy metal Contamination*. Engineering Geology, 85: 102 – 110.

Ozkan, S., Gale, R.J. and Seals, R.K. (1999) *Electrokinetic Stabilisation of Kaolinite by Injection of Al and PO_4 ions.* Ground improvement, 3: 135-144.

Paillat, T., Moreau, E., Grimoud, P.O. and Touchard, G. (2000) *Electrokinetic Phenomena in Porous Media Applied to Soil Decontamination*, IEEE Transaction on Dielectrics and Electrical Insulation, 7(5): 693-704.

Pennock, S.R., Abed, T.M., Curioni, G., Chapman, D.N., John, U.E. and Jenks C.H.J. (2014) *Investigation of Soil Contamination by Iron Pipe Corrosion and its Influence on GPR Detection.* In Proceedings of the 13th International Conference on Ground Penetrating Radar, Brussels, Belgium.

Pennock, S.R., Chapman, D.N., Rogers, C.D.F., Royal, A.C.D., Naji, A. and Redfern, M.A. (2010) *Effects of Iron Pipe Corrosion on GPR Detection*. the 13th International Conference on Ground Penetrating Radar, Lecce, Italy.1-5.

Petersen, R.B. and Melchers, R.E. (2012) *Long-term Corrosion of Cast iron Cement lined pipes*, Corrosion and Prevention, 23:1-12.

Pritchard, M., Craven, T., Mkandawire, T., Edmondson, A.S. and O'Neill, J.G. (2010) *A Comparison between Moringa Oleifera and Chemical Coagulants in the Purification of Drinking Water – An Alternative Sustainable Solution for Developing Countries*. Physic and Chemistry of the Earth, 35: 798-805.

Pritchard, O.G., Hallet, S.H. and Farewell, T. S. (2013) *Soil Corrosivity in the UK Impacts on Critical Infrastructure*. Infrastructure Transitions Research Consortium Working Paper Series. National Soil Resources Institute NSRI, Cranfield University, UK.

Pugh, R.C. (2002) *The Application of Eelectrokinetic Geosynthetic Materials to uses in the Construction Industry*. PhD Thesis, University of Newcastle upon Tyne, UK.

Quigley, R.M. (1980) *Geology, Mineralogy and Geochemistry of Canadian soft Soils: a Geotechnical Perspective*. Canadian Geotechnical Journal, 20: 288-298.

Rajani, B., Makar, J., McDonald, S., Zhan, C., Kuraoka, S., Jen, C.K. and Viens, M. (2000*) Investigation of Grey Cast Iron Water Mains to Develop a Methodology for Estimating Service Life*, American Water Works Association Research Foundation (Publishers), Denver, Colorado.

Rajani, B.B. and Kleiner, Y. (2001) *Comprehensive Review of Structural Deterioration of Water Mains*: *Physically based Models*. Urban Water, 3: 177–90.

Rajani, B.B. and Tesfamariam, S. (2004) *Uncoupled Axial, Flexural and Circumferential Pipe-soil Interaction Analyses of Partially Supported jointed Water Mains*. Canadian Geotechnical Journal, 41 (6): 997-1010.

Rajani, B.B., Zhan, C. and Kuraoka, S. (1996) *Pipe-Soil Interaction Analysis of Jointed Water Mains*. Canadian Geotechnical Journal, 33 (3): 393-404.

Rajani, K. and Ryden, B.E. (1992) *Measuring Aerial Soil Moisture Distribution with the TDR Method*. Geoderma, 52: 73-85.

Reeves, G.M., Sims, I. and Cripps, J.C. (2006) *Clay Materials Used in Construction*. Geological Society of London, UK, 108.

Reynaud, A. (2006) *Corrosion et Fontes*. (*Corrosion and Cast Iron*). Editions Techniques des Industries de la Fonderie.

Roberge, P.R. (2008) *Corrosion Engineering Principles and Practice*, Mc-Graw-Hill (Publishers), New York.

Robinson, D.A., Jones, S.B., Wraith, J.M., Or, D. and Friedman, S.P. (2003a) *A Review of Advances in*

Dielectric and Electrical Conductivity Measurement in Soils Using Time Domain Reflectometry. Vadose Zone Journal, 2 (4): 444-475.

Robinson, D.A., Schaap, M., Jones, S.B., Friedman, S.P. and Gardner, C.M.K. (2003b) *Considerations for Improving the Accuracy of Permittivity Measurement using Time Domain Reflectometry: Air-water Calibration, Effects of Cable Length*. Soil Science Society of America Journal, 67 (1): 62-70.

Robinson, S. (2006) *Issues in Conceptual Modelling for Simulation: Setting the Research Agenda*. Eds: S. Robinson, S. Taylor, S. Brailsford, and J. Garnett. Proceedings of the 2009 OR Society Simulation Workshop, Leamington Spa, UK.

Rogers, C.D.F., Hao, T., Costello, S.B., Burrow, M.P.N., Metje, N., Chapman, D.N., Parker, J., Armitage, R.J., Anspach, J.H., Muggleton, J.M., Foo, K.Y., Wang P., Pennock, S.R., Atkins, P.R., Swingler, S.G., Cohn, A.G., Goddard, K., Lewin, P.L., Orlando, G., Redfern, M.A, Royal, A.C.D. and Saul, A.J. (2012) *Condition Assessment of the Surface and Buried Infrastructure - A Proposal for Integration.* Tunnelling and Underground Space Technology, 28: 202-211.

Rogers, C.D.F., Liaki, C. and Boardman, D.I. (2003) *Advances in the Engineering of Lime Stabilised Clay Soils*. In Proceeding of International Conference on Problematic Soils, Nottingham, UK, July.

Romanoff, M. (1957) *Underground Corrosion,* National Bureau of Standards Circular 579, US Government Printing Office (Publishers), Washington DC.

Romanoff, M. (1962) *Corrosion of Steel Pilings in Soil*, National Bureau of Standards Monograph 58, U.S. Department of Commerce (Publishers), Washington, DC.

Saarenketo, T. (1998) *Electrical Properties of Water in Clay and Silty Soils*. Journal of Applied Geophysics, 40: 73-88.

Sachs S., Křepelová, A., Schmeide, K., Koban, A., Günther, A., Mibus, J., Brendler, V., Geipel, G. and Bernhard, G. (2007b) *Joint Project: Migration of Actinides in the System Clay, Humic Substance, Aquifer - Migration Behavior of Actinides (uranium, neptunium) in Clays: Characterization and*

quantification of the influence of humic substances. Wissenschaftlich-Technische Berichte, FZD-460, Forschungszentrum Dresden-Rossendorf, Dresden.

Sachs, S., Brendler, V. and Geipel, G. (2007a) *Uranium(VI) Complexation by Humic Acid under Neutral pH Conditions Studied by Laser-induced Fluorescence Spectroscopy*. Radiochim. 95:103-110.

Schifano, V. C. (2001) *Electrical Treatment of Clays*. PhD Thesis, University of Illinois, Urbana-Champaign.

Schmidt, A.M. (2007) *Physiochemical Changes in London Clay Adjacent to Cast Iron Pipes*. PhD Thesis, University of Birmingham, UK.

Schwertmann, U. (1991) *Solubility and Dissolution of Iron Oxides*. Plant and Soil, 130: 1–25.

Scott, D.A. (1977) *The Corrosion and Conservation of Iron* Materials from Trondheim, Norway, Department of Conservation, DKNVS Museet, Trondheim, Norway. Report, University College, Institute of Archaeology, Department of Conservation and Materials Science, University of London (unpublished internal report).

Segall, B.A., O'Bannon, C.E. and Matthias, J.A. (1980) *Electroosmosis Chemistry and Water Quality*. Journal of Geotechnical Engineering, 106(10): 1148-1152.

Shackelford, C.D. (1994) *Waste-Soil Interaction that alter Hydraulic Conductivity*, Hydraulic Conductivity and Waste Contaminant Transport in Soil, ASTM STP 1142, D.E. Daniel and S.J. Trautwein, Eds., American Society for Testing and Materials, Philadelphia

Shainberg, I. and Levy, G.J. (2005) *Salination Procecess*. Earth Systems and Environmental Sciences, from Encyclopedia of Soils in the Environment, 429-435.

Shaw, D.J. (1992) *Introduction to Colloidal and Surface Chemistry*. 4th Ed. Boston, MA: Butterworth-Heinemann.

Sibelco, Ltd: http://www.sibelco.com [Accessed March 2012]

Sing, R. (2011) *Applied Welding Engineering:* Processes, Codes, and Standards. Oxford, UK: Elsevier.

Snoswell, D.R.E. (2003) *The Influence of Surface Heterogeneity and Solution Composition on the Colloidal Stability of SiO_2 and TiO2 Dispersions.* PhD thesis Ian Wark Institute, University of South Australia.

Soderman, L.G. and Milligan, V. (1961) *Capacity of Friction Piles in Varied Clay Increased by Electroosmosis*. Proceedings Fifth International conference on Soil Mechanics and Foundation Engineering. Paris, (2):143–147.

Stangl, R., Buchan, G.D. and Loiskandl, W. (2009) *Field use and Calibration of a TDR-based Probe for Monitoring Water Content in a High-Clay Landslide Soil in Austria*. Geoderma, 150: 23-31.

Tajudin, S.A.A. (2012*) Electrokinetic Stabilization of Soft Clay*. PhD thesis, School of Civil Engineering, University of Birmingham, UK.

Tardy, Y. and Nahon, D. (1986) *Geochemistry of Laterites, Stability of Al-goethite, Al-hematite, and Fe^{+}-Kaolinite in Bauxites and Ferricretes: an Approach to the Mechanism of Concretion Formation*. American Journal of Science, 285: 865-903.

Thames Water Association of UK: http://www.thameswater.co.uk [Accessed May 2013]

Thomas, A.M., Chapman, D.N., Rogers, C.D.F., Metje, N., Atkins, P.R. and Lim, H.M. (2008) *Broadband Apparent Permittivity Measurement in Dispersive Soils Using Quarter*- Wavelength Analysis. Soil Science Society of America Journal, 72: 1401-1409.

Tomashov, N.D. (1966) *Theory of Corrosion and Protection of Metals*: The Science of Corrosion, Macmillan (Publishers), New York.

Topp, G.C. (2003) *State of the Art of Measuring Soil Water Content*. Hydrological Processes, 17: 2993-2996.

Topp, G.C., Davis, J.L. and Annan, A.P. (1980) *Electromagnetic Determination of Soil-Water Content: Measurements in Coaxial Transmission Lines*. Water Resources Research, 16 (3): 574-582.

Topp, G.C., Davis, J.L. and Annan, A.P. (2003) *The Early Development of TDR for Soil Measurements.* Vadose Zone Journal, 2: 492-499.

Uhlig, H.H. (1963) *Corrosion and Corrosion Control: An Introduction to Corrosion Science and Engineering.* 2nd Ed. John Wiley and Sons (Publisher), New York

Van Olphen, H. (1977) *An Introduction to Clay Colloid Chemistry* 2nd Ed. John Wiley and sons, New York.

Velde, B., and Vasseur, G. (1992) *Estimation of the Diagenetic Smectite to Illite Transformation in Time Temperature Space.* Am. Mineral, 77: 967-76.

Von Wolzogen Kuhr, C.A.H. and Van Der Vlugt, L.C. (1934) *Graphitization of Cast Iron as an Electrochemical Process in Anaerobic soils*, Water (den Haag), 18: 147-165 (in Dutch).

Wada, S.I. and Kakuto, Y. (1995) *Glycerol-extraction Refractometry for Determination of Gravimetric Water Content of Soil Sample*. Communication in Soil Science and Plant Analysis, 26: 1315-1322.

Wade, M.H. (1976) *Slope Stability by Electroosmosis*. Proceedings, 29th Canadian Geotechnical Conference, Vancouver B.C., Canada 10: 44–66.

Wagner, K. and Traud, Z. (2002) *Corrosion Sience.* Electrochemical society, 13.

Weast, R.C. (1972) *Handbook of Chemistry and Physics.*53rd Ed. Cleveland, OH: Chemical Rubber Company.

Weiler, K.W., Steenhuis, T.S., Boll, J. and Kung, K.J.S. (1998) *Comparison of Ground Penetrating Radar and Time-Domain Reflectometry as Soil Water Sensors.* Soil Science Society of America Journal, 62 (5): 1237-1239.

WSAA, Water Services Association of Australia: https://www.wsaa.asn.au [Accessed April 2008 and 2009]

Yeung, A.T. (2006) *Contaminant Extractability by Electrokinetics,* Environmental Engineering Science, 23 (1): 202 – 224.

Yong, R.N. and Mulligan, C.N. (2003) *Natural Attenuation of Contaminants in Soils.* Boca Raton, FL: Lewis Publishers.

Yong, R.N., Mohamed, A.M.O. and Warkentin, B.P. (1996) *Principles of Contaminant Transport in Soils.* New York: Elsevier.

Zhinkin, G.N. (1960) *Strengthening of Structural Bonds in Clay Soils as the Result of Electrochemical Stabilization*. Kolloidn. Zh. 1, Transl. Consultants Bureau, New York, 3-37.

Dallimore, S.R. and Davis, J.L. (1987) *Ground probing radar investigations of massive ground ice and near surface geology in continuous permafrost*. Geological Survey of Canada. 87 (1): 913-918.

Appendix A – Tabulated Results from the Experimental Measurements

Table A1 Undrained shear strength of Kaolin clay samples with disc

Kaolin Clay								
DAFD[1] (mm)	A (kN/m^2)	B (kN/m^2)	C (kN/m^2)	D (kN/m^2)	E (kN/m^2)	**2 weeks with Disc (Average)** (kN/m^2)	Variance	STD
0	14.5	14.5	14.4	14.5	14.5	**14.5**	0.0	0.0
10	13.3	13.2	13.3	13.3	13.3	**13.3**	0.0	0.0
20	12.2	12.3	12.3	12.2	12.1	**12.2**	0.0	0.1
30	12.4	12.4	12.8	12.2	12.3	**12.4**	0.0	0.2
40	12.6	12.5	12.6	12.5	12.6	**12.5**	0.0	0.0
50	12.4	12.4	12.4	12.4	12.3	**12.4**	0.0	0.0
60	12.8	12.7	12.7	12.7	12.7	**12.7**	0.0	0.0
70	14.9	14.8	14.9	14.9	14.9	**14.9**	0.0	0.0
80	11.1	11.2	11.2	11.2	11.2	**11.2**	0.0	0.0
90	10.1	10.1	10.1	10.1	10.1	**10.1**	0.0	0.0
100	9.8	9.8	9.8	9.9	9.8	**9.8**	0.0	0.0
						4 weeks with Disc (Average)		
0	30.5	30.4	30.5	30.9	30.6	**30.6**	0.0	0.2
10	25.1	25.1	25.2	25.2	25.2	**25.2**	0.0	0.1
20	22.3	22.2	22.2	22.2	22.2	**22.2**	0.0	0.0
30	25.8	25.3	25.8	25.8	25.7	**25.6**	0.0	0.2
40	23.1	23.1	23.1	23.0	23.1	**23.1**	0.0	0.0
50	24.1	24.1	24.1	24.1	24.1	**24.1**	0.0	0.0
60	23.7	23.7	23.7	23.7	23.7	**23.7**	0.0	0.0
70	23.7	23.6	23.6	23.7	23.6	**23.6**	0.0	0.0
80	23.9	23.8	23.8	23.8	23.8	**23.8**	0.0	0.0
90	25.1	25.1	25.1	25.1	25.1	**25.1**	0.0	0.0
100	17.7	17.7	17.7	17.7	17.7	**17.7**	0.0	0.0
						3 Months with Disc (Average)		
0	74.2	74.8	74.4	74.3	74.3	**74.4**	0.0	0.2
10	56.3	56.4	56.7	56.9	56.4	**56.6**	0.0	0.2
20	70.0	70.0	70.0	70.0	70.0	**70.0**	0.0	0.0
30	56.9	56.5	56.8	56.9	56.8	**56.8**	0.0	0.1
40	59.3	59.9	59.8	60.0	59.1	**59.6**	0.1	0.4
50	28.8	28.9	28.2	28.3	28.5	**28.5**	0.1	0.3

[1] DAFD stands for distance away from the disc (where anode generates).

60	32.7	32.8	32.3	32.0	32.0	**32.4**	0.1	0.3
70	42.9	42.1	42.3	42.0	42.0	**42.3**	0.1	0.3
80	48.8	48.5	48.6	48.2	48.7	**48.6**	0.0	0.2
90	41.8	41.9	41.3	41.8	41.2	**41.6**	0.1	0.3
100	35.3	35.7	35.2	35.1	35.1	**35.2**	0.0	0.2

Table A2 Undrained shear strength of Kaolin clay samples without disc

Kaolin Clay								
DAFD (mm)	A (kN/m^2)	B (kN/m^2)	C (kN/m^2)	D (kN/m^2)	E (kN/m^2)	**2 weeks-NO Disc (Average)** (kN/m^2)	Variance	STD
0	8.5	8.0	8.5	8.0	8.0	**8.2**	0.0	0.2
10	8.0	8.5	8.3	8.0	8.0	**8.1**	0.0	0.2
20	7.0	7.5	7.5	7.5	7.0	**7.3**	0.0	0.2
30	7.6	7.6	7.6	7.7	7.6	**7.6**	0.0	0.0
40	8.0	7.5	7.5	6.5	7.5	**7.4**	0.3	0.5
50	7.5	7.5	7.5	7.5	7.0	**7.4**	0.0	0.2
60	7.5	7.5	7.5	7.5	7.5	**7.5**	0.0	0.0
70	7.8	7.8	7.8	7.8	7.8	**7.8**	0.0	0.0
80	7.8	7.8	7.8	7.8	7.8	**7.80**	0.0	0.0
90	7.8	7.8	7.8	7.8	7.8	**7.8**	0.0	0.0
100	7.0	7.5	7.0	7.0	7.5	**7.2**	0.0	0.2
						4 weeks-NO Disc (Average)		
0	14.5	14.5	14.5	14.5	14.5	**14.5**	0.0	0.03
10	13.9	14.0	13.9	13.97	13.9	**13.9**	0.0	0.0
20	14.1	14.1	14.1	14.1	14.1	**14.1**	0.0	0.0
30	13.6	13.6	13.7	13.6	13.6	**13.6**	0.0	0.0
40	14.1	14.1	14.1	14.1	14.1	**14.1**	0.0	0.0
50	12.4	12.2	12.2	12.8	12.3	**12.4**	0.0	0.2
60	14.8	14.8	14.8	14.1	14.1	**14.5**	0.1	0.3
70	14.8	14.2	14.2	14.9	14.9	**14.6**	0.1	0.3
80	13.4	13.2	14.9	13.9	14.0	**13.9**	0.4	0.6
90	14.0	14.0	13.9	13.9	13.8	**13.9**	0.0	0.0
100	14.2	14.2	14.2	14.2	14.2	**14.2**	0.0	0.0

Table A3 Undrained shear strength of Oxford Clay samples with disc

Oxford Clay								
DAFD (mm)	A (kN/m^2)	B (kN/m^2)	C (kN/m^2)	D (kN/m^2)	E (kN/m^2)	**2 weeks with Disc (Average)** (kN/m^2)	Variance	STD
0	17.8	17.9	17.9	17.8	17.9	**17.9**	0.0	0.0
10	16.2	16.3	16.2	16.2	16.2	**16.3**	0.0	0.0
20	14.6	14.4	14.1	14.1	14.6	**14.4**	0.0	0.2
30	10.2	10.3	10.2	10.2	10.2	**10.3**	0.0	0.0
40	8.2	8.1	8.2	8.2	8.2	**8.2**	0.0	0.0
50	10.3	10.2	10.2	10.2	10.8	**10.4**	0.0	0.2
60	14.9	14.2	14.3	14.3	14.9	**14.5**	0.1	0.3
70	15.9	15.8	15.2	15.2	15.9	**15.6**	0.1	0.3
80	15.4	15.2	15.2	15.2	15.2	**15.3**	0.0	0.1
90	17.2	17.3	17.8	17.3	17.4	**17.4**	0.0	0.2
100	18.9	18.4	18.2	18.7	18.9	**18.6**	0.0	0.2
						4 weeks with Disc (Average)		
0	29.2	29.1	29.3	29.3	29.3	**29.3**	0.0	0.0
10	26.3	26.2	26.2	26.4	26.4	**26.3**	0.0	0.1
20	20.5	20.8	20.2	20.7	20.7	**20.6**	0.0	0.2
30	18.7	18.8	18.2	18.8	18.8	**18.7**	0.0	0.2
40	17.2	17.3	17.7	17.7	17.2	**17.4**	0.0	0.2
50	18.9	18.9	18.9	18.8	18.3	**18.8**	0.0	0.2
60	18.3	18.9	18.7	18.2	18.2	**18.5**	0.1	0.3
70	20.8	20.8	20.2	20.3	20.8	**20.6**	0.0	0.2
80	22.7	22.2	22.8	22.2	22.1	**22.4**	0.1	0.3
90	21.2	21.2	21.2	21.2	21.2	**21.2**	0.0	0.0
100	25.2	25.2	25.3	25.2	25.3	**25.2**	0.0	0.0
						3 Months with Disc (Average)		
0	96.0	96.7	96.0	96.0	96.6	**96.2**	0.1	0.3
10	90.6	99.6	90.1	90.3	90.9	**92.3**	0.0	0.2
20	87.6	87.9	87.1	87.7	87.6	**87.5**	0.0	0.2
30	80.0	80.0	80.6	80.8	80.5	**80.3**	0.1	0.3
40	78.9	78.8	78.3	78.0	78.6	**78.5**	0.1	0.3
50	77.7	77.8	77.6	77.0	77.9	**77.6**	0.1	0.3
60	88.8	88.5	88.6	88.7	88.9	**88.7**	0.0	0.1
70	90.9	90.9	90.8	90.6	90.6	**90.7**	0.0	0.1
80	92.9	92.1	92.7	92.6	92.9	**92.6**	0.1	0.3
90	95.1	95.6	95.6	95.6	95.9	**95.5**	0.0	0.2
100	99.6	99.7	99.7	99.1	99.1	**99.4**	0.1	0.3

Table A4 Undrained shear strength of Oxford Clay samples without disc

Oxford Clay								
DAFD (mm)	A (kN/m^2)	B (kN/m^2)	C (kN/m^2)	D (kN/m^2)	E (kN/m^2)	**2 weeks-NO Disc (Average)** (kN/m^2)	Variance	STD
0	10.4	10.0	10.1	10.5	10.3	**10.2**	0.0	0.2
10	9.0	9.1	9.1	9.1	9.0	**9.0**	0.0	0.0
20	8.4	8.0	8.0	8.4	8.4	**8.2**	0.0	0.2
30	7.5	7.7	7.1	7.6	7.4	**7.4**	0.0	0.2
40	7.3	7.4	7.2	7.1	7.3	**7.2**	0.0	0.1
50	6.0	6.5	6.4	6.4	6.2	**6.3**	0.0	0.2
60	5.5	5.4	5.6	5.7	5.4	**5.5**	0.0	0.1
70	6.3	6.5	6.5	6.5	6.4	**6.4**	0.0	0.0
80	7.1	7.2	7.3	7.3	7.3	**7.2**	0.0	0.0
90	8.4	8.0	8.4	8.1	8.0	**8.1**	0.0	0.2
100	9.4	9.4	9.5	9.5	9.4	**9.4**	0.0	0.0
						4 weeks-NO Disc (Average)		
0	12.1	12.5	12.1	12.1	12.4	**12.2**	0.0	0.2
10	11.2	11.2	11.2	11.2	11.3	**11.2**	0.0	0.0
20	10.8	10.8	10.8	10.9	10.9	**10.8**	0.0	0.0
30	8.6	8.5	8.4	8.6	8.4	**8.5**	0.0	0.1
40	8.6	8.6	8.6	8.6	8.7	**8.6**	0.0	0.0
50	7.3	7.4	7.4	7.2	7.2	**7.3**	0.0	0.1
60	7.3	7.0	7.3	7.3	7.0	**7.1**	0.0	0.1
70	8.0	8.0	8.1	8.0	8.0	**8.0**	0.0	0.0
80	10.5	10.5	10.5	10.6	10.5	**10.5**	0.0	0.0
90	12.4	12.6	12.1	12.0	12.6	**12.3**	0.0	0.2
100	14.6	14.7	14.6	14.7	14.7	**14.6**	0.0	0.0

Table A5 Moisture content of Kaolin Clay samples with disc

Kaolin Clay						
DAFD (mm)	Sample 1	Sample 2	Sample 3	**2 weeks with Disc (Average)** (%)	Variance	STD
10	59.2	58.6	58.9	**58.9**	0.2	0.5
20	55.1	55.5	55.2	**55.2**	0.0	0.2
30	55.8	55.8	55.8	**55.8**	0.0	0.0
40	54.5	54.2	54.9	**54.5**	0.1	0.3
50	52.4	52.8	52.3	**52.5**	0.0	0.2
60	53.2	53.2	53.4	**53.3**	0.0	0.0
70	54.0	53.2	52.9	**53.3**	0.3	0.5
80	53.0	53.6	53.1	**53.2**	0.1	0.3
90	53.0	52.5	52.5	**52.6**	0.0	0.2
100	55.0	54.9	54.9	**54.9**	0.1	0.3
				4 weeks with Disc (Average)		
10	56.9	56.9	56.9	**56.9**	0.0	0.0
20	52.7	52.8	52.7	**52.7**	0.0	0.0
30	51.1	51.0	51.2	**51.1**	0.0	0.0
40	50.2	50.3	50.0	**50.1**	0.0	0.1
50	50.4	50.5	50.4	**50.4**	0.0	0.0
60	50.9	50.9	51.9	**51.2**	0.3	0.5
70	50.9	51.1	50.3	**50.7**	0.1	0.4
80	49.4	49.4	49.4	**49.4**	0.0	0.0
90	49.2	49.2	49.2	**49.2**	0.0	0.0
100	48.9	48.9	48.9	**48.9**	0.0	0.0
				3 Months with Disc (Average)		
10	45.1	45.0	45.4	**45.1**	0.0	0.2
20	43.0	42.9	43.4	**43.1**	0.0	0.2
30	41.5	41.8	42.3	**41.8**	0.1	0.4
40	42.0	42.5	41.8	**42.1**	0.1	0.3
50	39.0	39.1	38.8	**38.9**	0.0	0.1
60	40.7	41.2	41.8	**41.2**	0.2	0.5
70	42.3	42.2	42.4	**42.3**	0.0	0.1
80	42.5	42.0	42.8	**42.4**	0.1	0.4
90	43.6	43.6	43.9	**43.7**	0.0	0.1
100	44.8	45.1	44.8	**44.8**	0.0	0.1

Table A6 Moisture content of Kaolin clay sample without disc

Kaolin Clay						
DAFD (mm)	Sample 1	Sample 2	Sample 3	**2 weeks-NO Disc (Average)** (%)	Variance	STD
10	49.2	49.3	49.3	**49.3**	0.1	0.4
20	48.8	48.7	48.5	**48.7**	0.0	0.1
30	47.0	47.0	47.0	**47.0**	0.0	0.0
40	45.8	46.0	45.7	**45.8**	0.0	0.1
50	44.4	44.4	44.8	**44.5**	0.0	0.2
60	45.7	45.8	45.5	**45.7**	0.0	0.1
70	46.9	46.9	46.9	**46.9**	0.0	0.0
80	48.6	48.7	48.2	**48.5**	0.0	0.2
90	48.6	48.3	48.2	**48.4**	0.0	0.1
100	47.8	47.8	47.8	**47.8**	0.0	0.0
				4 weeks-NO Disc (Average)		
10	45.7	45.7	45.6	**45.6**	0.0	0.0
20	43.2	42.9	42.9	**43.0**	0.0	0.1
30	44.6	44.8	44.5	**44.6**	0.0	0.1
40	44.8	45.0	44.9	**44.9**	0.0	0.1
50	45.1	45.1	45.0	**45.0**	0.0	0.0
60	45.5	45.9	45.4	**45.6**	0.0	0.2
70	45.4	45.5	45.7	**45.5**	0.0	0.1
80	47.6	47.2	47.8	**47.5**	0.0	0.2
90	45.8	46.0	45.9	**45.9**	0.0	0.1
100	46.9	47.0	46.8	**46.9**	0.0	0.0

Table A7 Moisture content of Oxford Clay samples with disc

Oxford Clay						
DAFD (mm)	Sample 1	Sample 2	Sample 3	**2 weeks with Disc (Average) (%)**	Variance	STD
10	52.9	52.9	52.4	**52.8**	0.1	0.3
20	52.3	52.9	52.7	**52.6**	0.1	0.3
30	51.0	51.0	51.8	**51.3**	0.2	0.4
40	50.5	50.3	51.0	**50.6**	0.1	0.3
50	50.8	50.4	50.4	**50.5**	0.0	0.2
60	50.9	50.3	50.6	**50.6**	0.0	0.3
70	50.9	51.0	50.9	**50.9**	0.0	0.0
80	49.8	49.4	49.9	**49.7**	0.0	0.2
90	49.1	49.2	49.3	**49.2**	0.0	0.1
100	48.9	49.0	48.7	**48.9**	0.0	0.1
				4 weeks with Disc (Average)		
10	50.5	50.5	50.4	**50.5**	0.0	0.0
20	49.5	49.5	49.6	**49.6**	0.0	0.0
30	51.3	51.8	51.2	**51.4**	0.0	0.3
40	52.9	52.2	52.2	**52.4**	0.1	0.3
50	53.9	54.0	54.4	**54.1**	0.0	0.2
60	52.2	52.2	52.2	**52.2**	0.0	0.0
70	50.2	50.8	51.2	**50.7**	0.2	0.4
80	49.3	49.8	49.7	**49.6**	0.0	0.2
90	50.8	50.0	50.0	**50.3**	0.2	0.4
100	53.7	53.7	53.7	**53.7**	0.0	0.2
				3 Months with Disc (Average)		
10	45.2	45.2	45.2	**45.2**	0.1	0.3
20	39.1	39.7	39.9	**39.6**	0.1	0.4
30	40.2	40.4	40.6	**40.4**	0.0	0.2
40	39.2	38.7	38.7	**38.9**	0.0	0.2
50	35.9	35.4	35.5	**35.6**	0.0	0.2
60	35.6	35.7	35.8	**35.7**	0.0	0.0
70	37.9	38.2	37.8	**38.0**	0.0	0.2
80	38.8	38.5	39.2	**38.9**	0.1	0.3
90	41.0	41.0	40.8	**40.9**	0.0	0.1
100	43.3	43.3	43.3	**43.3**	0.1	0.3

Table A8 Moisture content of Oxford Clay samples without disc

Oxford Clay						
DAFD (mm)	Sample 1	Sample 2	Sample 3	**2 weeks-NO Disc (Average)** (%)	Variance	STD
10	55.2	55.3	55.4	**55.3**	0.0	0.1
20	53.4	53.8	53.8	**53.6**	0.0	0.2
30	50.9	50.6	50.5	**50.6**	0.0	0.2
40	53.3	53.7	53.4	**53.4**	0.0	0.2
50	52.9	52.3	52.5	**52.6**	0.0	0.3
60	51.9	51.8	51.6	**51.8**	0.0	0.1
70	51.3	51.3	51.3	**51.3**	0.0	0.0
80	50.7	50.6	50.4	**50.6**	0.0	0.1
90	51.8	51.8	52.0	**51.9**	0.0	0.1
100	52.1	52.7	52.4	**52.4**	0.0	0.2
				4 weeks-NO Disc (Average) (%)		
10	53.7	54.7	53.7	**53.7**	0.0	0.2
20	55.8	55.1	55.3	**55.4**	0.1	0.3
30	52.4	52.8	53.1	**52.8**	0.1	0.3
40	52.5	52.5	52.5	**52.5**	0.0	0.0
50	52.0	52.5	52.1	**52.2**	0.0	0.2
60	50.7	50.8	50.2	**50.5**	0.1	0.3
70	50.6	50.7	50.4	**50.6**	0.0	0.1
80	50.6	51.1	50.9	**50.9**	0.0	0.2
90	50.3	50.2	50.7	**50.4**	0.0	0.2
100	51.0	51.2	51.3	**51.2**	0.0	0.1

Table A9 Liquid Limits of Kaolin clay samples with disc

Kaolin Clay						
DAFD (mm)	Sample 1	Sample 2	Sample 3	**2 weeks with Disc (Average)** (%)	Variance	STD
10	65.9	65.0	64.9	**64.9**	0.00	0.03
20	62.4	62.4	62.4	**62.3**	0.00	0.02
30	61.9	61.9	61.9	**61.9**	0.00	0.03
40	61.5	61.4	61.5	**61.5**	0.00	0.04
50	58.0	58.0	58.0	**58.0**	0.00	0.03
60	57.8	57.7	57.7	**57.7**	0.00	0.05
70	54.1	54.1	54.0	**54.1**	0.00	0.02
80	54.4	54.3	54.2	**54.3**	0.01	0.11
90	53.6	53.4	53.4	**53.4**	0.00	0.07
100	53.9	53.9	53.9	**53.9**	0.00	0.04
				4 weeks with Disc (Average)		
10	68.8	68.9	69.0	**68.9**	0.01	0.08
20	66.6	66.6	66.6	**66.6**	0.00	0.01
30	64.3	64.3	64.4	**64.3**	0.00	0.04
40	61.6	61.7	61.7	**61.7**	0.00	0.07
50	61.7	61.8	61.7	**61.7**	0.00	0.04
60	61.2	61.2	61.2	**61.2**	0.00	0.03
70	59.0	59.0	59.0	**59.1**	0.00	0.02
80	57.8	57.8	57.8	**57.8**	0.00	0.00
90	56.5	56.5	56.5	**56.5**	0.00	0.00
100	53.4	53.4	53.4	**53.4**	0.00	0.01
				3 Months with Disc (Average) (%)		
10	69.1	69.1	69.1	**69.1**	0.00	0.02
20	68.0	68.0	68.0	**68.0**	0.00	0.01
30	66.9	66.8	67.0	**66.9**	0.01	0.10
40	63.6	63.7	63.6	**63.6**	0.00	0.06
50	63.7	63.7	63.7	**63.7**	0.00	0.02
60	63.4	63.1	63.6	**63.4**	0.05	0.23
70	65.3	65.2	65.3	**65.2**	0.00	0.02
80	62.7	62.7	62.7	**62.7**	0.00	0.03
90	63.2	63.0	63.0	**63.0**	0.01	0.11
100	60.8	60.3	60.9	**60.7**	0.13	0.36

Table A10 Liquid Limits of Oxford Clay samples with disc

Oxford Clay						
DAFD (mm)	Sample 1	Sample 2	Sample 3	**2 weeks with Disc (Average)** (%)	Variance	STD
10	65.2	65.2	65.2	**65.2**	0.00	0.02
20	64.5	64.5	64.5	**64.5**	0.00	0.01
30	61.9	61.9	61.9	**61.9**	0.00	0.01
40	62.4	62.4	62.4	**62.4**	0.00	0.02
50	62.0	62.0	62.0	**62.0**	0.00	0.00
60	61.5	61.5	61.5	**61.5**	0.00	0.04
70	61.5	61.4	61.4	**61.4**	0.00	0.05
80	57.8	57.9	57.9	**57.8**	0.00	0.01
90	56.6	56.6	56.6	**56.6**	0.00	0.04
100	58.1	58.1	58.1	**58.1**	0.00	0.01
				4weeks with Disc (Average)		
10	69.3	69.3	69.3	**69.3**	0.00	0.03
20	68.4	68.4	68.4	**68.4**	0.00	0.04
30	67.4	67.3	67.3	**67.3**	0.00	0.04
40	69.5	69.5	69.5	**69.5**	0.00	0.02
50	65.8	65.8	65.8	**65.8**	0.00	0.03
60	66.3	66.2	66.3	**66.3**	0.00	0.06
70	65.9	65.8	65.9	**65.9**	0.00	0.05
80	65.2	65.1	65.2	**65.2**	0.00	0.07
90	63.7	63.7	63.7	**63.7**	0.00	0.04
100	63.2	63.2	63.2	**63.2**	0.00	0.01
				3 Months with Disc (Average)		
10	73.8	73.9	74.0	**73.9**	0.00	0.06
20	73.0	73.1	73.0	**73.1**	0.00	0.05
30	71.9	71.9	71.8	**71.8**	0.00	0.04
40	71.0	71.0	71.0	**71.0**	0.00	0.02
50	69.2	69.2	69.3	**69.2**	0.00	0.04
60	67.4	67.4	67.4	**67.5**	0.00	0.03
70	68.8	68.8	68.9	**68.8**	0.00	0.02
80	67.1	67.1	67.1	**67.1**	0.00	0.02
90	66.5	66.6	66.6	**66.6**	0.00	0.02
100	67.9	67.0	68.0	**67.6**	0.30	0.54

Table A11 Plastic Limits of Kaolin clay samples with disc

Kaolin Clay						
DAFD (mm)	Sample 1	Sample 2	Sample 3	**2 weeks with Disc (Average)** (%)	Variance	STD
10	34.2	34.2	34.2	**34.2**	0.00	0.02
20	32.4	32.5	32.4	**32.4**	0.00	0.02
30	32.3	32.2	32.3	**32.3**	0.00	0.02
40	34.8	34.7	34.8	**34.8**	0.00	0.02
50	34.3	34.3	34.3	**34.3**	0.00	0.02
60	33.7	33.7	33.7	**33.7**	0.00	0.03
70	35.4	35.5	35.6	**35.5**	0.01	0.08
80	34.4	34.3	34.3	**34.3**	0.00	0.02
90	34.7	34.9	34.8	**34.8**	0.00	0.07
100	34.5	34.5	34.2	**34.4**	0.03	0.16
				4 weeks with Disc (Average)		
10	32.9	33.0	32.8	**32.9**	0.01	0.07
20	35.0	35.1	35.1	**35.1**	0.00	0.06
30	33.8	33.9	33.8	**33.9**	0.00	0.07
40	33.5	33.5	33.5	**33.5**	0.00	0.01
50	33.8	33.3	33.4	**33.5**	0.07	0.27
60	34.4	34.1	34.2	**34.2**	0.02	0.14
70	35.3	35.3	35.3	**35.3**	0.00	0.01
80	35.0	35.1	35.0	**35.0**	0.00	0.02
90	37.6	37.3	37.0	**37.3**	0.07	0.27
100	35.6	35.5	35.6	**35.6**	0.00	0.02
				3 Months with Disc (Average)		
10	26.8	26.2	26.4	**26.3**	0.01	0.11
20	27.7	27.5	27.4	**27.6**	0.04	0.20
30	29.9	29.8	29.9	**29.8**	0.00	0.04
40	28.2	28.4	28.1	**28.2**	0.02	0.15
50	28.1	28.2	28.0	**28.1**	0.01	0.10
60	28.5	28.4	28.4	**28.4**	0.00	0.02
70	28.8	28.9	28.8	**28.8**	0.00	0.03
80	29.8	39.0	29.8	**29.9**	0.01	0.09
90	27.4	27.5	27.5	**27.5**	0.00	0.02
100	28.4	28.4	28.4	**28.4**	0.00	0.01

Table A12 Plastic Limits of Oxford Clay samples with disc

Oxford Clay						
DAFD (mm)	Sample 1	Sample 2	Sample 3	**2weeks with Disc (Average)** (%)	Variance	STD
10	36.8	36.8	36.2	**36.6**	0.14	0.38
20	36.8	36.9	36.9	**36.8**	0.00	0.01
30	35.5	35.5	35.4	**35.4**	0.00	0.01
40	35.0	35.0	35.0	**35.0**	0.00	0.01
50	35.6	35.6	35.6	**35.6**	0.00	0.01
60	36.2	36.2	36.2	**36.2**	0.00	0.02
70	36.9	36.3	36.8	**36.8**	0.00	0.01
80	35.4	35.4	35.4	**35.4**	0.00	0.02
90	36.0	35.9	35.9	**35.9**	0.00	0.02
100	35.6	35.6	35.6	**35.5**	0.00	0.02
				4weeks with Disc (Average)		
10	37.9	37.9	37.8	**37.8**	0.00	0.03
20	37.8	37.8	37.8	**37.8**	0.00	0.03
30	36.1	36.2	36.1	**36.1**	0.00	0.01
40	34.8	34.8	34.8	**34.8**	0.00	0.01
50	35.7	35.7	35.7	**35.7**	0.00	0.01
60	36.3	36.3	36.3	**36.3**	0.00	0.01
70	35.2	35.2	35.1	**35.1**	0.00	0.01
80	35	35.9	35.9	**35.9**	0.32	0.56
90	35.2	35.2	35.2	**35.2**	0.00	0.01
100	35.8	35.7	35.7	**35.7**	0.00	0.01
				3 Months with Disc (Average)		
10	37.8	37.8	37.1	**37.6**	0.14	0.38
20	37.3	37.1	37.1	**37.2**	0.02	0.13
30	37.3	37.2	37.4	**37.3**	0.01	0.09
40	37.2	37.3	37.1	**37.2**	0.01	0.08
50	36.9	36.9	36.8	**36.9**	0.00	0.06
60	35.7	35.7	35.9	**35.8**	0.02	0.13
70	35.6	35.5	35.5	**35.5**	0.01	0.08
80	36.9	36.9	36.9	**36.9**	0.00	0.01
90	35.9	35.9	35.9	**35.9**	0.00	0.02
100	36.8	36.9	36.8	**36.8**	0.00	0.02

Table A13 Iron concentration (%) in Kaolin clay samples with disc

Kaolin Clay						
DAFD (mm)	Sample 1	Sample 2	Sample 3	**2 weeks with Disc (Average)** (%)	Variance	STD
0	8.54	8.55	8.54	**8.54**	0.00	0.01
10	2.68	2.68	2.69	**2.68**	0.00	0.01
20	2.33	2.31	2.33	**2.32**	0.00	0.01
30	2.24	2.24	2.26	**2.25**	0.00	0.01
40	1.50	1.60	1.50	**1.53**	0.00	0.06
50	1.61	1.62	1.62	**1.62**	0.00	0.01
60	1.94	1.95	1.94	**1.94**	0.00	0.01
70	2.12	2.13	2.12	**2.12**	0.00	0.01
80	1.53	1.53	1.52	**1.53**	0.00	0.01
90	1.70	1.80	1.70	**1.73**	0.00	0.06
100	1.7	6.67	6.67	**1.7**	0.00	0.00
				4 weeks with Disc (Average)		
0	8.98	8.98	8.98	**8.98**	0.00	0.00
10	3.10	3.20	3.10	**3.13**	0.00	0.06
20	2.76	2.66	2.67	**2.70**	0.00	0.06
30	2.76	2.76	2.76	**2.76**	0.00	0.00
40	2.17	2.16	2.17	**2.17**	0.00	0.01
50	1.80	1.80	1.80	**1.80**	0.00	0.00
60	1.45	1.46	1.44	**1.45**	0.00	0.01
70	2.17	2.08	2.17	**2.14**	0.00	0.05
80	1.92	1.93	1.92	**1.92**	0.00	0.01
90	2.05	2.05	2.05	**2.05**	0.00	0.00
100	2.01	2.02	2.01	**2.06**	0.00	0.03
				3 Months with Disc (Average)		
0	9.58	9.57	9.58	**9.58**	0.00	0.01
10	5.00	5.30	5.20	**5.17**	0.02	0.15
20	3.60	3.59	3.59	**3.59**	0.00	0.01
30	2.76	2.68	2.67	**2.70**	0.00	0.05
40	3.13	3.13	3.13	**3.13**	0.00	0.00
50	4.06	4.07	4.06	**4.06**	0.00	0.01
60	4.04	4.04	4.04	**4.04**	0.00	0.00
70	4.59	4.60	4.59	**4.59**	0.00	0.01
80	1.55	1.56	1.55	**1.55**	0.00	0.01
90	2.06	2.06	2.06	**2.06**	0.00	0.00
100	2.30	2.30	2.30	**2.30**	0.00	0.00

Table A14 Iron concentration (%) in Kaolin clay samples without disc

Kaolin Clay						
DAFD (mm)	Sample 1	Sample 2	Sample 3	**2 weeks-No Disc (Average)** (%)	Variance	STD
0	1.39	1.40	1.36	**1.38**	0.00	0.02
10	1.36	1.36	1.36	**1.36**	0.00	0.00
20	1.34	1.34	1.34	**1.34**	0.00	0.00
30	1.34	1.33	1.34	**1.34**	0.00	0.01
40	1.30	1.31	1.29	**1.30**	0.00	0.01
50	1.27	1.26	1.26	**1.26**	0.00	0.01
60	1.28	1.27	1.27	**1.27**	0.00	0.01
70	1.24	1.24	1.26	**1.25**	0.00	0.01
80	1.27	1.28	1.28	**1.28**	0.00	0.01
90	1.32	1.33	1.33	**1.33**	0.00	0.01
100	1.34	1.34	1.35	**1.34**	0.00	0.01
				4 weeks –No Disc (Average)		
0	1.40	1.41	1.42	**1.41**	0.00	0.01
10	1.32	1.33	1.32	**1.32**	0.00	0.01
20	1.30	1.34	1.35	**1.33**	0.00	0.03
30	1.36	1.37	1.37	**1.37**	0.00	0.01
40	1.34	1.35	1.35	**1.35**	0.00	0.01
50	1.32	1.31	1.30	**1.31**	0.00	0.01
60	1.31	1.31	1.31	**1.31**	0.00	0.00
70	1.30	1.30	1.30	**1.30**	0.00	0.00
80	1.29	1.29	1.28	**1.29**	0.00	0.01
90	1.27	1.28	1.28	**1.28**	0.00	0.01
100	1.25	1.26	1.26	**1.26**	0.00	0.01

Table A15 Iron concentration (%) in Oxford Clay samples with disc

Oxford Clay						
DAFD (mm)	Sample 1	Sample 2	Sample 3	**2 weeks with Disc (Average)** (%)	Variance	STD
0	10.76	10.74	10.79	**10.76**	0.00	0.02
10	7.00	7.20	7.00	**7.07**	0.01	0.12
20	7.57	7.56	7.57	**7.57**	0.00	0.01
30	7.50	7.56	7.57	**7.54**	0.00	0.04
40	7.20	7.30	7.20	**7.23**	0.00	0.06
50	7.96	7.95	7.96	**7.96**	0.00	0.01
60	7.48	7.50	7.49	**7.49**	0.00	0.01
70	7.58	7.59	7.58	**7.58**	0.00	0.01
80	7.30	7.20	7.30	**7.27**	0.00	0.06
90	7.76	7.77	7.75	**7.76**	0.00	0.01
100	7.66	7.67	7.65	**7.66**	0.00	0.01
				4 weeks with Disc (Average)		
0	29.39	29.40	29.39	**29.39**	0.00	0.01
10	10.30	10.20	10.30	**10.27**	0.00	0.06
20	7.76	7.77	7.76	**7.76**	0.00	0.01
30	7.30	7.40	7.50	**7.40**	0.01	0.10
40	7.31	7.32	7.33	**7.32**	0.00	0.01
50	7.21	7.21	7.20	**7.21**	0.00	0.01
60	7.13	7.14	7.14	**7.14**	0.00	0.01
70	7.00	7.10	7.00	**7.03**	0.00	0.06
80	7.08	7.09	7.09	**7.09**	0.00	0.01
90	7.00	7.00	7.00	**7.00**	0.00	0.00
100	6.66	6.67	6.67	**6.67**	0.00	0.01
				3 Months with Disc (Average)		
0	32.98	32.99	32.97	**32.98**	0.00	0.01
10	26.71	26.70	26.70	**26.70**	0.00	0.01
20	16.63	16.62	16.63	**16.63**	0.00	0.01
30	16.91	16.90	16.91	**16.91**	0.00	0.01
40	16.00	15.90	16.10	**16.00**	0.01	0.10
50	18.69	18.70	18.68	**18.69**	0.00	0.01
60	15.40	15.30	15.50	**15.40**	0.01	0.10
70	12.70	12.60	12.70	**12.67**	0.00	0.06
80	10.10	10.20	10.20	**10.17**	0.00	0.06
90	8.43	8.42	8.43	**8.43**	0.00	0.01
100	6.08	6.07	6.07	**6.07**	0.00	0.01

Table A16 Iron concentration (%) in Oxford Clay samples without disc

Oxford Clay						
DAFD (mm)	Sample 1	Sample 2	Sample 3	**2 weeks- No Disc (Average)** (%)	Variance	STD
0	7.33	7.33	7.34	**7.33**	0.00	0.01
10	7.30	7.20	7.30	**7.27**	0.00	0.06
20	7.12	7.13	7.12	**7.12**	0.00	0.01
30	7.11	7.10	7.20	**7.14**	0.00	0.06
40	7.10	7.12	7.11	**7.11**	0.00	0.01
50	7.10	7.00	7.10	**7.07**	0.00	0.06
60	7.09	7.08	7.09	**7.09**	0.00	0.01
70	7.00	7.10	7.10	**7.07**	0.00	0.06
80	7.08	7.08	7.10	**7.09**	0.00	0.01
90	7.00	7.10	7.10	**7.07**	0.00	0.06
100	7.08	7.09	7.10	**7.09**	0.00	0.01
				4 weeks – No Disc (Average)		
0	7.36	7.37	7.35	**7.36**	0.00	0.01
10	7.31	7.32	7.33	**7.32**	0.00	0.01
20	7.10	7.20	7.15	**7.15**	0.00	0.05
30	7.11	7.12	7.11	**7.11**	0.00	0.01
40	7.20	6.90	7.10	**7.07**	0.02	0.15
50	7.00	7.10	7.20	**7.10**	0.01	0.10
60	7.00	7.10	7.20	**7.10**	0.01	0.10
70	7.08	7.09	7.10	**7.09**	0.00	0.01
80	7.10	6.90	7.20	**7.07**	0.02	0.15
90	7.08	7.09	7.09	**7.09**	0.00	0.01
100	7.00	7.10	7.10	**7.07**	0.00	0.06

Table A17 pH measurement of Kaolin clay samples with cast iron disc

Kaolin Clay						
DAFD (mm)	Sample 1	Sample 2	Sample 3	**2 weeks with Disc (Average)** [-]	Variance	STD
10	3.30	3.40	3.30	**3.33**	0.00	0.06
20	3.70	3.80	3.70	**3.73**	0.00	0.06
30	4.30	4.40	4.30	**4.33**	0.00	0.06
40	5.60	5.70	5.70	**5.67**	0.00	0.06
50	4.60	4.70	4.60	**4.63**	0.00	0.06
60	7.50	7.40	7.40	**7.43**	0.00	0.06
70	8.70	8.60	8.70	**8.67**	0.00	0.06
80	9.50	9.40	9.40	**9.43**	0.00	0.06
90	10.60	10.70	10.60	**10.63**	0.00	0.06
100	11.60	11.70	11.60	**11.63**	0.00	0.06
				4 weeks with Disc (Average)		
10	3.30	3.30	3.30	**3.30**	0.00	0.00
20	3.70	3.80	3.70	**3.73**	0.00	0.06
30	4.00	4.00	4.00	**4.00**	0.00	0.00
40	5.50	5.50	5.60	**5.53**	0.00	0.06
50	4.10	4.20	4.10	**4.13**	0.00	0.06
60	7.40	7.30	7.40	**7.37**	0.00	0.06
70	7.90	8.00	7.80	**7.90**	0.01	0.10
80	8.40	8.30	8.30	**8.33**	0.00	0.06
90	8.60	8.60	8.70	**8.63**	0.00	0.06
100	11.90	11.90	12.00	**11.93**	0.00	0.06
				3 Months with Disc (Average)		
10	3.15	3.15	3.15	**3.15**	0.00	0.06
20	3.20	3.30	3.20	**3.23**	0.00	0.06
30	3.80	3.80	3.90	**3.83**	0.00	0.06
40	4.60	4.50	4.60	**4.57**	0.00	0.06
50	3.50	3.50	3.60	**3.53**	0.00	0.06
60	5.00	5.10	5.00	**5.03**	0.00	0.06
70	8.70	8.60	8.70	**8.67**	0.00	0.06
80	9.20	9.30	9.20	**9.23**	0.00	0.06
90	10.80	10.80	10.80	**10.80**	0.00	0.00
100	12.94	12.94	12.94	**12.94**	0.00	0.00

Table A18 pH measurement of Kaolin clay samples without cast iron disc

Kaolin Clay						
DAFD (mm)	Sample 1	Sample 2	Sample 3	**2 weeks- No Disc (Average) [-]**	Variance	STD
10	4.01	4.01	4.01	**4.01**	0.00	0.00
20	5.23	5.21	5.23	**5.22**	0.00	0.01
30	5.73	5.72	5.70	**5.72**	0.00	0.02
40	6.10	6.20	6.10	**6.13**	0.00	0.06
50	7.20	7.30	7.30	**7.27**	0.00	0.06
60	8.40	8.40	8.30	**8.37**	0.00	0.06
70	8.70	8.60	8.60	**8.63**	0.00	0.06
80	9.10	9.20	9.10	**9.13**	0.00	0.06
90	10.00	10.10	10.10	**10.07**	0.00	0.06
100	11.50	11.40	11.50	**11.47**	0.00	0.06
				4 weeks – No Disc (Average)		
10	3.90	3.90	3.90	**3.87**	0.00	0.06
20	4.90	4.80	4.90	**4.87**	0.00	0.06
30	5.60	5.70	5.70	**5.67**	0.00	0.06
40	6.70	6.80	6.80	**6.77**	0.00	0.06
50	7.30	7.40	7.30	**7.33**	0.00	0.06
60	8.50	8.70	8.60	**8.60**	0.01	0.10
70	9.20	9.10	9.00	**9.10**	0.01	0.10
80	9.40	9.30	9.30	**9.33**	0.00	0.06
90	10.20	10.30	10.40	**10.30**	0.01	0.10
100	11.60	11.60	11.60	**11.60**	0.00	0.00

Table A19 pH measurement of Oxford Clay samples with cast iron disc

Oxford Clay						
DAFD (mm)	Sample 1	Sample 2	Sample 3	**2weeks with Disc (Average)** [-]	Variance	STD
10	4.90	4.80	4.90	**4.87**	0.00	0.06
20	5.60	5.70	5.70	**5.67**	0.00	0.06
30	6.50	6.40	6.50	**6.47**	0.00	0.06
40	7.60	7.70	7.70	**7.67**	0.00	0.06
50	7.90	8.00	7.90	**7.93**	0.00	0.06
60	8.50	8.50	8.50	**8.50**	0.00	0.00
70	9.60	9.70	9.60	**9.63**	0.00	0.06
80	10.40	10.50	10.50	**10.47**	0.00	0.06
90	11.20	11.30	11.20	**11.23**	0.00	0.06
100	12.14	12.20	12.13	**12.15**	0.00	0.06
				4weeks with Disc (Average)		
10	4.40	4.50	4.50	**4.47**	0.00	0.06
20	5.50	5.40	5.50	**5.47**	0.00	0.06
30	6.20	6.30	6.20	**6.23**	0.00	0.06
40	7.60	7.40	7.50	**7.50**	0.01	0.10
50	7.90	7.80	7.90	**7.87**	0.00	0.06
60	8.50	8.40	8.50	**8.47**	0.00	0.06
70	9.20	9.20	9.20	**9.20**	0.00	0.00
80	10.30	10.20	10.40	**10.30**	0.01	0.10
90	11.70	11.80	11.80	**11.77**	0.00	0.06
100	12.35	12.36	12.35	**12.35**	0.00	0.01
				3 Months with Disc (Average)		
10	2.72	2.73	2.71	**2.72**	0.00	0.01
20	4.00	3.99	3.99	**3.99**	0.00	0.01
30	5.46	5.45	5.47	**5.46**	0.00	0.01
40	5.99	5.98	5.98	**5.98**	0.00	0.01
50	6.56	6.55	6.57	**6.56**	0.00	0.01
60	7.63	7.63	7.62	**7.63**	0.00	0.01
70	8.65	8.66	8.66	**8.66**	0.00	0.01
80	9.60	9.61	9.59	**9.60**	0.00	0.01
90	10.49	10.48	10.50	**10.49**	0.00	0.01
100	11.31	11.30	11.31	**11.31**	0.00	0.01

Table A20 pH measurements of Oxford Clay samples without cast iron disc

Oxford Clay						
DAFD (mm)	Sample 1	Sample 2	Sample 3	**2weeks-No Disc (Average) [-]**	Variance	STD
10	5.70	5.60	5.70	**5.67**	0.00	0.06
20	6.20	6.20	6.10	**6.17**	0.08	0.06
30	6.90	6.90	6.90	**6.90**	0.16	0.00
40	7.30	7.30	7.30	**7.30**	0.05	0.00
50	8.50	8.40	8.50	**8.47**	0.41	0.06
60	9.40	9.30	9.40	**9.37**	0.25	0.06
70	10.10	10.20	10.10	**10.13**	0.18	0.06
80	11.40	11.50	11.40	**11.43**	0.51	0.06
90	11.90	11.80	11.70	**11.80**	0.05	0.10
100	12.00	12.10	11.90	**12.00**	0.02	0.10
				4weeks – No Disc (Average)		
10	5.50	5.40	5.50	**5.47**	0.00	0.06
20	6.60	6.70	6.80	**6.70**	0.01	0.10
30	7.30	7.40	7.30	**7.33**	0.00	0.06
40	7.90	8.00	7.80	**7.90**	0.01	0.10
50	8.70	8.60	8.50	**8.60**	0.01	0.10
60	9.80	9.70	9.90	**9.80**	0.01	0.10
70	11.30	11.40	11.30	**11.33**	0.00	0.06
80	11.80	11.80	11.70	**11.77**	0.00	0.06
90	12.00	11.90	12.10	**12.00**	0.01	0.10
100	12.20	12.10	12.20	**12.17**	0.00	0.06

Table A21 Conductivity measurements by conductivity meter for Kaolin clay with cast iron disc

Kaolin Clay						
DAFD (mm)	Sample 1	Sample 2	Sample 3	**2 weeks with Disc (Average)** (μS/m)	Variance	STD
10	114.20	114.20	114.20	**114.20**	0.00	0.01
20	13.90	13.91	13.92	**13.91**	0.00	0.01
30	4.82	4.81	4.83	**4.82**	0.00	0.01
40	4.14	4.14	4.14	**4.14**	0.00	0.00
50	4.10	4.10	4.11	**4.10**	0.00	0.01
60	5.06	5.07	5.05	**5.06**	0.00	0.01
70	1.67	1.68	1.67	**1.67**	0.00	0.01
80	3.15	3.15	3.16	**3.15**	0.00	0.01
90	29.68	29.68	29.68	**29.68**	0.00	0.00
100	56.12	56.12	56.12	**56.12**	0.00	0.00
				4 weeks with Disc (Average)		
10	147.3	147.2	147.2	**147.23**	0.00	0.05
20	51.20	51.21	51.20	**51.20**	0.00	0.01
30	27.00	27.00	27.00	**27.00**	0.00	0.00
40	25.60	25.50	25.60	**25.57**	0.00	0.06
50	25.70	25.70	25.70	**25.70**	0.00	0.00
60	25.50	25.50	25.40	**25.47**	0.00	0.06
70	25.10	25.10	25.10	**25.10**	0.00	0.00
80	26.20	26.30	26.20	**26.23**	0.00	0.06
90	43.70	43.70	43.60	**43.67**	0.00	0.06
100	58.04	58.04	58.04	**58.04**	0.00	0.00
				3 Months with Disc (Average)		
10	189.34	189.35	189.34	**189.34**	0.00	0.01
20	35.00	35.00	35.00	**35.00**	0.00	0.00
30	7.03	7.01	7.02	**7.02**	0.00	0.01
40	6.99	6.98	6.98	**6.98**	0.00	0.01
50	7.64	7.64	7.63	**7.64**	0.00	0.01
60	6.98	6.99	6.98	**6.98**	0.00	0.01
70	7.28	7.28	7.28	**7.28**	0.00	0.00
80	10.00	10.01	10.00	**10.00**	0.00	0.01
90	18.30	18.30	18.30	**18.30**	0.00	0.00
100	175.45	175.44	175.44	**175.44**	0.00	0.01

Table A22 Conductivity measurements by conductivity meter for Kaolin clay without cast iron disc

Kaolin Clay						
DAFD (mm)	Sample 1	Sample 2	Sample 3	**2weeks-No Disc (Average)** (μS/m)	Variance	STD
10	73.22	73.21	73.21	**73.21**	0.00	0.01
20	62.95	62.96	62.95	**62.95**	0.00	0.01
30	2.54	2.54	2.53	**2.54**	0.00	0.01
40	2.59	2.58	2.58	**2.58**	0.00	0.01
50	2.53	2.54	2.53	**2.53**	0.00	0.01
60	2.73	2.72	2.73	**2.73**	0.00	0.01
70	3.48	3.48	3.49	**3.48**	0.00	0.01
80	4.76	4.76	4.76	**4.76**	0.00	0.00
90	3.89	3.88	3.89	**3.89**	0.00	0.01
100	48.78	48.78	48.78	**48.78**	0.00	0.00
				4weeks –No Disc (Average)		
10	77.55	77.54	77.54	**77.54**	0.00	0.00
20	4.38	4.39	4.37	**4.38**	0.00	0.00
30	3.76	3.75	3.77	**3.76**	0.00	0.00
40	3.73	3.72	3.74	**3.73**	0.00	0.00
50	3.77	3.79	3.80	**3.79**	0.00	0.00
60	3.56	3.58	3.57	**3.57**	0.00	0.00
70	3.40	3.43	3.42	**3.42**	0.00	0.00
80	3.22	3.20	3.22	**3.21**	0.00	0.00
90	5.86	5.88	5.86	**5.87**	0.00	0.00
100	51.58	51.58	51.59	**51.58**	0.00	0.00

Table A23 Conductivity measurements by conductivity meter for Oxford Clay with cast iron disc

Oxford Clay						
DAFD (mm)	Sample 1	Sample 2	Sample 3	**2weeks with Disc (Average)** (µS/m)	Variance	STD
10	171.00	172.00	171.00	**171.33**	0.33	0.58
20	150.00	150.00	151.00	**150.30**	0.33	0.58
30	148.00	148.00	148.00	**148.00**	0.00	0.00
40	141.00	140.00	140.00	**140.33**	0.33	0.58
50	85.00	85.00	85.00	**85.33**	0.33	0.58
60	87.00	87.00	86.00	**86.67**	0.33	0.58
70	101.00	101.00	101.90	**101.63**	0.40	0.64
80	134.8	134.8	134.8	**134.8**	0.00	0.00
90	133.50	133.00	133.00	**133.17**	0.08	0.29
100	141.00	141.20	141.00	**141.07**	0.01	0.12
				4weeks with Disc (Average)		
10	253.10	253.20	253.20	**253.17**	0.00	0.06
20	160.00	160.20	160.00	**160.07**	0.01	0.12
30	145.00	145.00	144.80	**144.93**	0.01	0.12
40	110.00	111.00	110.00	**110.33**	0.33	0.58
50	50.00	50.00	50.00	**50.00**	0.00	0.00
60	65.80	65.70	65.80	**65.77**	0.00	0.06
70	64.50	64.50	64.66	**64.55**	0.01	0.09
80	103.50	103.50	103.50	**103.50**	0.00	0.00
90	159.40	159.50	159.50	**159.47**	0.00	0.06
100	169.60	169.60	169.70	**169.63**	0.00	0.06
				3 Months with Disc (Average)		
10	430.00	429.00	430.00	**429.00**	0.33	0.58
20	400.00	399.00	399.00	**399.00**	0.33	0.58
30	386.00	386.00	386.00	**386.00**	0.00	0.00
40	378.00	376.00	377.00	**378.00**	1.00	1.00
50	268.00	268.00	269.00	**268.00**	0.33	0.58
60	202.90	203.00	202.80	**202.90**	0.01	0.10
70	207.90	207.80	207.80	**207.80**	0.00	0.06
80	206.90	206.90	206.90	**206.90**	0.00	0.00
90	150.66	150.65	150.66	**150.66**	0.00	0.01
100	163.86	163.86	163.86	**163.86**	0.00	0.00

Table A24 Conductivity measurements by conductivity meter for Oxford Clay without cast iron disc

Oxford Clay						
DAFD (mm)	Sample 1	Sample 2	Sample 3	**2weeks-No Disc (Average)** (μS/m)	Variance	STD
10	45.00	46.00	45.00	**45.33**	0.33	0.58
20	37.00	37.00	38.00	**37.33**	0.33	0.58
30	23.00	23.00	23.00	**23.00**	0.00	0.00
40	22.00	21.00	21.00	**21.33**	0.33	0.58
50	19.00	20.00	19.00	**19.33**	0.33	0.58
60	18.00	18.00	17.00	**17.67**	0.33	0.58
70	17.00	17.00	15.90	**16.63**	0.40	0.64
80	17.00	17.00	17.00	**17.00**	0.00	0.00
90	19.50	19.00	19.00	**19.17**	0.08	0.29
100	23.00	23.20	23.00	**23.07**	0.01	0.12
				4weeks –No Disc (Average)		
10	63.50	63.00	63.00	**63.17**	0.08	0.29
20	55.00	55.40	55.00	**55.13**	0.05	0.23
30	40.00	40.00	40.00	**40.00**	0.00	0.00
40	36.00	36.00	36.20	**36.07**	0.01	0.12
50	19.00	19.00	19.00	**19.00**	0.00	0.00
60	20.00	20.00	20.00	**20.00**	0.00	0.00
70	21.00	21.30	21.00	**21.10**	0.03	0.17
80	20.00	20.00	20.30	**20.10**	0.03	0.17
90	20.00	20.00	20.50	**20.17**	0.08	0.29
100	42.00	42.00	42.00	**42.00**	0.00	0.00

Table A25 Conductivity measurements by TDR for Kaolin clay

Kaolin Clay					
DAFD (mm)	**2weeks with Disc (Average)** µS/m	**4weeks with Disc (Average)** µS/m	**3 Months with Disc (Average)** µS/m	**2weeks-No Disc (Average)** µS/m	**4weeks –No Disc (Average)** µS/m
10	127.40	154.15	409.50	85.33	87.27
20	41.50	19.90	64.84	48.33	50.20
30	15.00	13.64	22.93	7.53	8.40
40	14.90	13.46	13.75	5.00	8.23
50	14.50	13.41	4.99	4.93	8.83
60	14.60	13.31	0.00	4.70	8.77
70	14.20	14.45	6.86	6.17	8.50
80	15.40	34.28	1.75	6.63	13.27
90	11.60	34.79	11.59	4.43	26.73
100	67.00	69.00	333.90	61.43	74.77

Table A26 Conductivity measurements by TDR for Oxford Clay

Oxford Clay					
DAFD (mm)	**2weeks with Disc (Average)** µS/m	**4weeks with Disc (Average)** µS/m	**3 Months with Disc (Average)** µS/m	**2weeks-No Disc (Average)** µS/m	**4weeks –No Disc (Average)** µS/m
10	179.99	276.79	441.96	54.07	66.75
20	175.92	170.23	393.57	53.41	61.13
30	124.16	126.6	215.34	52	58.98
40	109.63	72.72	215.21	42.3	46.17
50	104.52	73.06	235.67	39.85	20.55
60	85.57	86.3	NA	25.61	24.2
70	98.35	NA[2]	227.69	22.05	24.9
80	155.91	129.8	220.29	18.36	21.36
90	152.65	173.47	165.44	36.75	22.16
100	153.32	180.82	187.11	46.06	58.51

[2] NA: Not Available.

Table A27 Permittivity measurements for Kaolin Clay using TDR

Kaolin Clay					
DAFD (mm)	**2weeks with Disc (Average)** (ε)	**4weeks with Disc (Average)** (ε)	**3 Months with Disc (Average)** (ε)	**2weeks-No Disc (Average)** (ε)	**4weeks –No Disc (Average)** (ε)
10	53.69	34.56	36.50	33.29	31.09
20	28.32	32.76	35.48	33.03	32.76
30	31.57	31.53	34.01	33.92	32.85
40	31.39	33.12	34.93	33.47	32.49
50	31.92	33.12	33.56	32.85	33.03
60	31.48	33.74	34.56	33.47	32.85
70	30.44	33.20	34.01	34.65	33.38
80	30.09	33.56	31.61	34.83	32.67
90	31.04	32.94	34.38	34.20	32.32
100	27.17	35.57	33.38	34.47	32.94

Table A28 Permittivity measurements for Oxford Clay using TDR

Oxford Clay					
DAFD (mm)	**2weeks with Disc (Average)** (ε)	**4weeks with Disc (Average)** (ε)	**3 Months with Disc (Average)** (ε)	**2weeks-No Disc (Average)** (ε)	**4weeks –No Disc (Average)** (ε)
10	31.44	28.97	21.57	31.44	34.01
20	28.97	28.97	21.57	32.76	33.56
30	26.11	28.97	21.57	32.94	34.65
40	26.27	34.93	22.44	33.47	34.29
50	26.35	26.19	22.44	32.40	33.38
60	25.41	25.02	NA	31.70	34.11
70	26.35	NA[3]	9.46	32.58	33.12
80	28.63	28.47	9.04	32.32	33.83
90	23.26	34.01	24.94	33.56	33.47
100	24.15	32.49	21.79	32.67	34.29

[3] NA: Not Available.

Table A29 Conductivity measurements for GPRMax Simulations using TDR for Kaolin Clay

Kaolin Clay					
DAFD (mm)	**2 weeks with Disc (Average)** mS/m	**4 weeks with Disc (Average)** mS/m	**3 months with Disc (Average)** mS/m	**2 weeks – No Disc (Average)** mS/m	**4 weeks – No Disc (Average)** mS/m
10	127.40	154.15	409.50	85.33	87.27
20	41.50	19.90	64.84	48.33	50.20
30	15.00	13.64	22.93	7.53	8.40
ave	**61.3**	**62.56**	**165.75**	**47.06**	**48.62**

Table A30 Conductivity measurements for GPRMax Simulations using TDR for Oxford Clay

Oxford Clay					
DAFD (mm)	**2weeks with Disc (Average)** mS/m	**4weeks with Disc (Average)** mS/m	**3 Months with Disc (Average)** mS/m	**2weeks-No Disc (Average)** mS/m	**4weeks –No Disc (Average)** mS/m
10	179.99	276.79	441.96	54.07	66.75
20	175.92	170.23	393.57	53.41	61.13
30	124.16	126.6	215.34	52	58.98
ave	**160.0**	**191.2**	**350.29**	**53.16**	**62.28**

Table A31 Permittivity measurements for GPRMax Simulations using TDR for Kaolin Clay

Kaolin Clay					
DAFD (mm)	**2 weeks with Disc (Average)** (ε)	**4 weeks with Disc (Average)** (ε)	**3 months with Disc (Average)** (ε)	**2 weeks – No Disc (Average)** (ε)	**4 weeks – No Disc (Average)** (ε)
10	53.69*	34.56	36.50	33.29	31.09
20	28.32	32.76	35.48	33.03	32.76
30	31.57	31.53	34.01	33.92	32.85
ave	**29.95**	**32.95**	**35.33**	**33.41**	**32.23**

Table A32 Permittivity measurements for GPRMax Simulations using TDR for Oxford Clay

Oxford Clay					
DAFD (mm)	**2 weeks with Disc (Average)** (ε)	**4 weeks with Disc (Average)** (ε)	**3 months with Disc (Average)** (ε)	**2 weeks – No Disc (Average)** (ε)	**4 weeks – No Disc (Average)** (ε)
10	31.44	28.97	21.57	31.44	34.01
20	28.97	28.97	21.57	32.76	33.56
30	26.11	28.97	21.57	32.94	34.65
ave	**28.84**	**28.97**	**21.57**	**32.38**	**34.07**